THÈSE DE DOCTORAT

Présentée à l'Université de Lille

Ecole Doctorale ENGSYS
Sciences de l'ingénierie et des systèmes
par Léa Rosselle

Development of biological models to test new treatments for chronic and infected wounds.

Développement de modèles biologiques pour tester de nouveaux traitements contre les plaies chroniques et infectées

Soutenue le 7 décembre 2021 devant le jury composé de

Prof. Jean-Luc CRACOWSKI	Rapporteur	CHU Grenoble Alpes
Prof. Tijani GHARBI	Rapporteur	Université de Franche-Comté
Prof. Rachel AUZELY-VELTY	Présidente du Jury	Université Grenoble Alpes
Dr. Anna-Rita CANTELMO	Examinatrice	Institut Pasteur de Lille
Prof. Sabine SZUNERITS	Directrice de thèse	Université de Lille
Dr. Nadia SKANDRANI	Co-encadrante de thèse	TissueAegis

ABSTRACT - Development of biological models to test new treatments for chronic and infected wounds.

OBJECTIVE: Development of a human wound infection model to analyse topical treatment effectiveness of novel wound dressings.

Skin processes excellent regeneration properties allowing its rapid healing upon dermal injury. If wounds fail to heal in an orderly and timely manner, chronic wounds (e.g. diabetic foot ulcers, venous leg ulcers, pressure ulcers, etc.) develop and their treatment remains a global challenge. In addition, these diseases might be accompanied by severe infections. While a myriad of topical therapies and dressings are available, very few have shown to be effective in promoting wound repair. The integration of nanomaterials into wound healing bandages combined with transdermal drug delivery are such innovative dressings for both wound healing and infection treatment. These approaches seem to be adapted to overcome current developments in local passive therapies that have shown nonsignificant efficacy. Efficiently testing is currently mainly conducted on animal models, which can limit direct transferability to humans and poses ethnic issues. Some of these limitations can be overcome by using ex vivo skin models obtained from leftover skin parts after esthetical surgery, as described in this work. The viability of the skin samples allows us to test treatments over a period of 7 days. The developed ex vivo human skin model proved promising in the context of bacteria colonized wounds by following skin structure impact, gene expression profile and bacteria colonization. It could be in addition used to indicate the performance of novel skin bandages such as near-infrared light activatable hydrogels, antibacterial peptide loaded photothermally active cryogels and photothermal activatable microneedles.

KEYWORD = *Ex vivo* skin model. Wound infection. Hydrogel. Cryogel. Photothermal.

RESUME - Développement de modèles biologiques pour tester de nouveaux traitements contre les plaies chroniques et infectées.

OBJECTIFS : Développement d'un modèle d'infection de plaie humaine pour analyser l'efficacité du traitement local de nouveaux pansements.

La peau possède d'excellentes propriétés de régénération qui lui permettent de cicatriser rapidement en cas de blessure. Si les plaies ne guérissent pas de manière ordonnée et spontanée, des plaies chroniques se développent et trouver un traitement efficace reste un défi mondial. Bien qu'il existe une myriade de thérapies et de pansements, très peu se sont avérés efficaces pour favoriser la guérison de ces plaies. Une nouvelle avancée consistant à intégrer des nanomatériaux dans des pansements cicatrisants combinée à l'administration transdermique de médicaments semble une solution innovante et encourageante. Actuellement, les études sont principalement menées sur des modèles animaux, ce qui peut limiter la transférabilité directe à l'homme et poser des problèmes éthiques. Certaines de ces limitations peuvent être surmontées en utilisant des modèles de peau ex vivo obtenus à partir de déchets hospitaliers provenant de chirurgie esthétique, comme décrit dans ce travail. La viabilité des échantillons de peau nous permet de tester les traitements sur une période de 7 jours. Le modèle de peau humaine ex vivo développé s'est avéré prometteur dans le contexte des plaies colonisées par des bactéries en suivant l'impact de la structure de la peau, le profil d'expression génétique et la colonisation des bactéries. Il pourrait alors être utilisé pour analyser les performances de nouveaux pansements tels que des hydrogels activables par la lumière proche infrarouge, des cryogels photothermiquement actifs et des micro-aiguilles activables par photothermie.

MOTS CLÉS : Modèle de peau ex vivo. Infection de la plaie. Hydrogel. Cryogel. Photothermie.

ACKNOWLEDGEMENTS

Hugo. It has been a pleasure working with you and sharing conversations and good times. Also many thanks to the TissueAegis team in Paris.

Thanks to IRI's staff for your good mood and your involvement in making the building more friendly (and safe).

Thanks to Yuanyuan Miao, despite the ups and downs of the thesis, spending this Phd together has given me a huge support.

A special thanks to my family and friends for their constant support during all these years. I felt all your love and support in good and bad times.

Finally, thank you to my partner Pierre-Julien for your presence, your support and your patience. You make me full of confidence every day.

LIST OF ABBREVIATIONS

- 5 -

3D	Three Dimensions
Abs	Absorbance
AMP	adenosine monophosphate
ATCC	American Type Culture Collection
BGL	Blood Glucose Level
BHI	Brain Heart Infusion
BuMA	Butyl MethAcrylate
C57BL/6	C57 black 6
°C	Degree Celsius
cDNA	complementary Deoxyribonucleic acid
CFU	Colony Forming Unit
CG	Cryogel
CO2	Carbon dioxide
DA	Diels−Alder
DAPI	4',6'-diamidino-2-phenylindole
DMEM	Dulbecco's Modified Eagle Medium
DMSO	Dimethylsulfoxyde
DNA	Deoxyribonucleic acid
DNase I	Desoxyribonuclease I
E. coli	*Escherichia coli*
EPS	Extracellular PolySaccharide
FBS	Fetal Bovin Serum
FITC	Fluorescein IsoThioCyanate
FuMA	Furfuryl MethAcrylate
GFP	Green fluorescent protein
GFP-HDFCs	GFP-human dermal fibroblasts cells
GO	Graphene Oxide
H&E	Hematoxylin & Eosin
HPLC	High Performance Liquid Chromatography
HSP	Heat Shock Protein
IC50	half maximal Inhibition Concentration
IFN	Interferon
IL	Interleukin
IU	International Unit
K	Keratin
KHz	KiloHertz
LB	Luria-Bertani
MIC	Minimum Inhibitory Concentration
MN	Microneedle
MoS_2	Molybdenum Disulfide
MRSA	Methicillin-resistant S. aureus

MW	Molecular weight
NaCl	Chlorure de sodium
NCS	Newborn Calf Serum
NIPAM	N-isopropylacrylamide
NIR	Near infrared
NP	Nanoparticule
OD	Optical Density
P. aeruginosa	*Pseudomonas Aeruginosa*
PBS	Phosphate buffer Saline
PCR	Polymerase Chain Reaction
PEG	Polyethylene glycol
PEGDA	Polyethylene glycol diacrylate
PEGDMA	Poly(ethylene glycol) dimethacrylate
PEGMEMA	Poly(ethylene glycol) methyl ether methacrylate
PeVs	Platelet extraVesicules
PNIPAM	Poly(N-isopropylacrylamide)
PTT	Photothermal therapy
PVA	Polyvinyl alcohol
qPCR	quantitative Polymerase Chain Reaction
RNA	Ribonucleic acid
rGO	reduced Graphene Oxide
S. aureus	*Staphylococcus aureus*
SC	Stratum corneum
S. epidermis	*Staphylococcus epidermis*
SEM	Scanning electron microscopy
TNF	Tumor Necrosis Factor
TDD	Transdermal drug delivery
UV	Ultra-violet
W	Watt

OBJECTIVES

This thesis is dedicated to the development of models of studies and new innovative materials for chronic wound therapy. Different fields of research such as chemical synthesis and material characterization, biological studies will be combined. The thesis manuscript is organized into four chapters.

Chapter 1 is an introduction into chronic wound disease with a focus on current and advanced management of this disease. The use of hydrogels and cryogels are detailed as well as the use of advanced photothermal and drug delivery technologies. These techniques are both necessary to improve wound healing and eradicate infections. In a second part, the problems posed when we need to develop a model of chronic wound or infected wound are presented.

Chapter 2 describes the design and evaluation of the *ex vivo* models developed in our lab in order to study wound infection and wound re-epithelialization. The culture of skin explants allows us to investigate several parameters such histological structures, gene expression and bacterial bioburden.

Chapter 3 outlines the application of ex vivo models by presenting a skin irritancy test under heating by laser irradiation, the use of topical therapeutics for wound healing and the application of antibiotics into infected wound model. The ex vivo model offers a wide range of study possibilities which is very valuable in the context of chronic wounds requiring the development of combined therapy.

Chapter 4 describes two innovative dressings using cryogel, a polymeric material, combine with nanomaterials for photothermal therapy and drug release of antibacterial agents. Both the characterization, drug release profile and ex vivo evaluation are presented.

Chapter 5 summarizes the results and presents some perspectives on the work.

TABLE OF CONTENTS

CHAPTER 1 : INTRODUCTION

1.1 Chronic wounds - medical context

It is estimated that 1-2% of the population in developing countries will experience a chronic wound in their lifetime.[1-2] This represents a significant health and economic burden for our society and global wound care expenditures amount ranges from \$28.1 billion to \$96.8 billion annually.[3-4] A chronic wound is defined as a wound that does not heal in an orderly and spontaneous manner due to an incomplete and uncoordinated healing process[5] and when the healing process is longer than eight weeks.[6] Chronic wounds may have individual combinations of causes making it unlikely that a common cure will be found for all patients. For the patient, non-healing wounds cause numerous discomforts. Indeed, the wound can be painful, cause itching, have an unpleasant smell, release fluid, limit mobility and cause a lack of sleep.[2] Together with these physiological symptoms, the long recovery, the restrictive treatment and the embarrassment of social situations cause psychological disorders and have a strong impact on the quality of life of the patient.[7] Depending on the severity of the wound, the patient may be treated at home or require hospitalization.[8] In both cases, the medical staff needs specialized training in order to properly adapt the care and support the patient psychologically. Some complications can also occur such as infection[9], without treatments germs may spread and lead to septicaemia, amputation[10] or can also lead to the death of the patient.[11]

Multiple factors can affect the wound healing and cause improper and impaired tissue repair : oxygenation, infection, age, nutrition, diabetes, obesity, etc.[12] Persons aged older than 60 years are the most affected population.[13] Indeed, the aging of the skin causes dysfunctions in the healing mechanisms. Poorly healing wounds are more common on the feet or lower legs and often result from circulation problems or diabetes. All chronic wounds are unique but often occur in patients with underlying disorders, such as chronic mechanical pressure, arterial or venous insufficiency, diabetes or burns.[2] These similarities in pathogenesis have made it possible to divide them into groups such as venous leg ulcers, diabetic foot ulcers and pressure ulcers (**Figure 1.1**).[14] Knowledge of pathology allows us to adapt the treatment to optimize healing. For example, in the case of a diabetic foot ulcer, the healing problem is often due to ischemia, so it is necessary to restore circulation in the extremity of the limb, whereas a venous leg ulcer is often caused by hypertension in the vein, so the treatment applied is compression.[15]
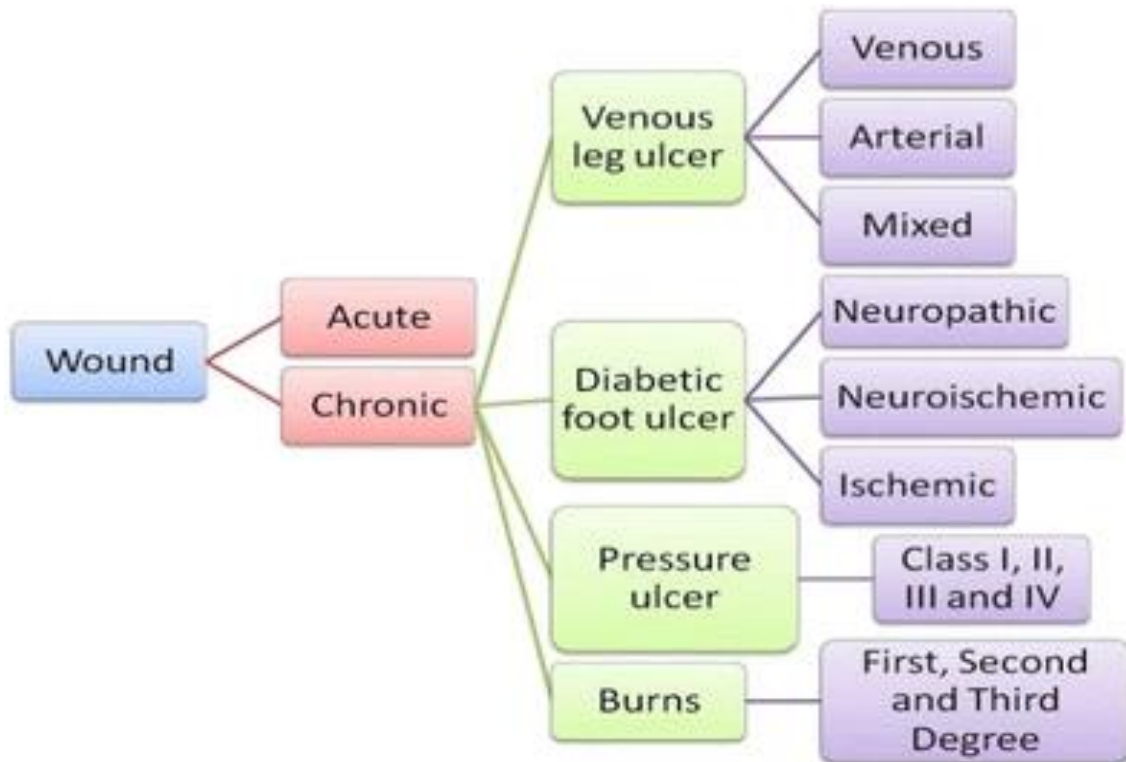
***Figure 1.1 :** Different types of chronic wound.[adapted from Ref. [16]]*

Wound management combines wound assessment with the selection of an effective treatment.[17] It is the cumulative process of observation, data collection and evaluation. As all wounds have different causes, aspects and stages, the diagnosis of the wound must be accurate and well done to provide the most appropriate treatment to the patient.[10,18] The assessment should start by establishment of the thorough patient history followed by the physical examination of the wound. An accurate description of the wound's evolution must be made to allow for proper patient follow-up. Standardized methods were developed to allow clinicians to monitor the wound condition. For instance, the three major classifications methods of Diabetic foot ulcers are compared in **Table 1.1**.[19]

Table 1.1 : *Major classification methods for ulceration evaluation. [adapted from Ref.[19]]*

Major classification methods.

	Wagner-Meggitt	**University of Texas**	**PEDIS**
Grade 0	Pain only, no open ulcer	Pre-ulceration	
Grade 1	Superficial ulcer	Superficial wound	Skin intact, no infection or loss of sensation
Grade 2	Deep ulcer	Wound penetrating to tendon or capsule	Superficial ulcer with infection at the surface and loss of sensation
Grade 3	Deep ulceration with osteomyelitis	Wound penetrating to bone or joint	Ulcer reaching the fascia, muscle, and tendon, fasciitis and septic arthritis likely
Grade 4	Localized Gangrene		Ulcer depth reaching the bone or joint, SIRS
Grade 5	Extensive Gangrene, Amputation likely		
References	[13,16,17]	[18]	[19]

Due to the prolonged opening of the skin, the presence of persistent infection is frequently observed in chronic wounds. The wound is always and rapidly colonized by common microbiota of the skin.[4] Several levels of germs are observed one the wound and it is important to well evaluate to identify if it's a normal colonization or an infection (**Figure 1.2**).[20]
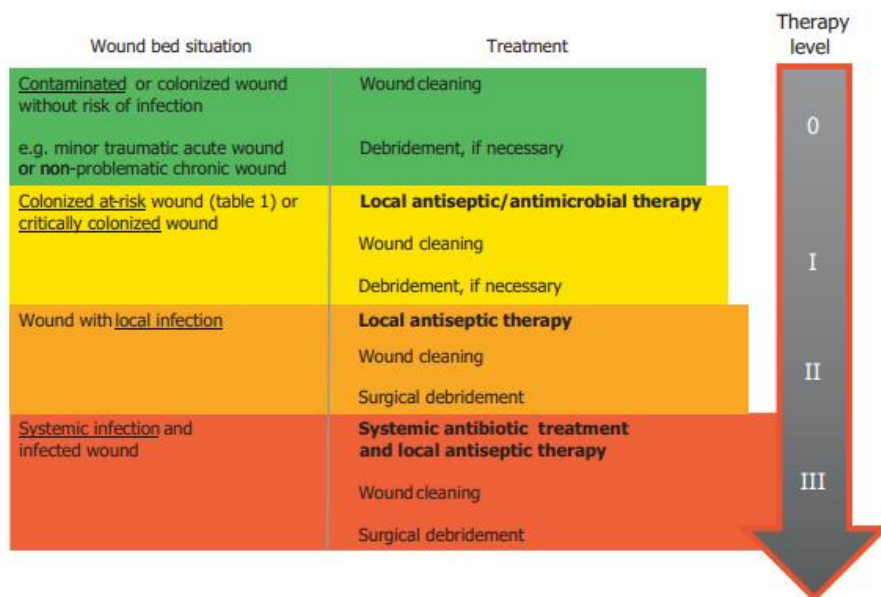
Figure 1.2: *Therapeutic steps for antimicrobial wound treatment. [adapted from Ref.[20]]*

Without treatment, wound infections quickly lead to sepsis and death of the patient. Therefore, diagnosis must be made fast. The identification of local infection in a chronic wound can be carried out in the first line by the presence of clinical signs and symptoms of infection.[21] The classic local inflammatory signs of an infection are: redness, heat, pain, purulent discharge, associated or not with general signs (fever or chills, feeling of general malaise).[22] Unfortunately, sometimes the only sign of infection in wounds may be the delayed healing that makes the diagnosis uncertain. Clinical criteria from various guidelines have been used to define infection in chronic wounds.[21-24] A clinical experience showed that with a trained eye biofilm can be visualized in chronic wounds because its appearance is quite different from slough wound[25] confirming the necessity of care personal education. In the second intention, a wound culture can be done to evaluate the microorganism's presence in the wound bed and quantification. The two steps for wound cultures are the acquisition of a specimen from the wound (wound tissue, needle-aspiration wound fluid or swab sampling) and the laboratory procedures : grow, identify and quantify the microorganisms.[21] This procedure can be used when the infection isn't clinically obvious. As bacteria are always present on the wound, wound culture has been challenged over the years as to its effectiveness.[26]

For the good management of the patient's wound, the tissue types and the texture of the wound may be determined. The different type of tissues can easily be remembered by colours[16,21] :

- Red wounds are typically a clean and granular wound
- Yellow wounds correspond to devitalized tissue of sloughy wound
- Black wounds contain necrotic tissue

Mix of tissue types can be present on the same wound (**Figure 1.3**).[27]

During the assessment of the wound, the clinician identifies tissue types within the wound and determines the percentage of each tissue. This informs the stage of wound healing in order to administer the appropriate treatment throughout the healing.

Figure 1.3 : Two examples of chronic wound healing. A. Healing of Diabetic foot-heel ulcer. LEFT: Before debridement, showing necrotic material covering most of the wound bed. MIDDLE: applying semi-occlusive moist wound care with physiologic saline solution: wound defect has become filled with pink granulation tissue, epithelialization occurs from the wound edges. RIGHT: Wound closure achieved by meshed partial thickness skin grafting with a ratio of 1.5 to 1. B. Healing of Venous leg ulcer. LEFT: Venous leg ulcer with presence of slough on wound bed. MIDDLE LEFT: The same patient after 4 weeks of every other day application of a hyaluronic acid pad and daily compression bandaging. MIDDLE RIGHT: Ulcer almost healed with preservation of perilesional skin. RIGHT: Complete healing after 3 months.[adapted from Ref.[28]]

1.1.1 Wound treatment

The first step in treatment is preparation of the wound bed. It involves the debridement of the wound, the exudate management, and the resolution of bacterial imbalance.[29] Next, the clinician must select the most appropriate dressing to protect the wound and provide an optimal environment for healing. The concept of wound bed preparation has evolved from many years to provide a great approach to removing barriers to natural healing and enhancing the effects of therapies.[30] This part is very important for the proper wound care and should not be forgotten despite the new advanced therapies. As a first step, the wound should be cleansed with a low toxicity solution. This step removes the least adherent contaminants from the wound surface by choosing methods that minimize chemical and mechanical trauma to the wound tissue.

Then, debridement of non-viable or foreign materials is performed. This step includes the removal of host necrotic tissue, adherent dressing material, multiple organism-related biofilm, or slough, exudate, and debris on the surface of the wound.[21] The goal of this step is to promote active healing. Several types of debridement are available depending on the kind of tissue (**Table 1.2**).[18] For instance, an infected tissue may be removed more efficiently by a mechanical debridement such as Sharp or surgical, whereas slough can be removed with enzymatic debridement.

Table 1.2 : Types of debridement.[adapted from Ref.[18]]

Sharp—At the bedside (using scalpel or curette)

Surgical—In the operating theatre

Autolytic—Facilitation of the body's own mechanism of debridement with appropriate dressings

Biological—Larval (maggot) therapy

Enzymatic—Not widely used; pawpaw (papaya) or banana skin used in developing countries

Mechanical—Wet-to-dry dressings (not widely used in the UK)

Wound care has become increasingly important given the rise in chronic wounds and the morbidity associated with them. The variety of wound types has resulted in a wide range of wound care products, which are still being improved with new products. The purpose of the various treatments is to protect the healing wound from infection and also to promote the healing process. Unfortunately, one type of wound care has not been conclusively shown to accelerate healing more than another, increasing the challenges that clinicians face in managing and treating acute and chronic wounds. Wound care products include dressings, pharmaceutical agents such as antibiotics or growth factors that can be delivered directly to the wound through different systems but also more advanced therapies such as physical stimulation or cell therapies. and emerging technologies to achieve better wound healing are explored in this section.

After wound debridement, an efficient dressing must be selected. Dressings are medical devices. They are defined as wound covering. Through the ages, there have been wound dressings of all shapes, sizes, colors, and origins.[31] The traditional wound dressing is well known as a cotton bandage or a gauze which have the property to absorb a big part of the moisture containing the wound. A broad range of polymers in the form of films, foams, and gels have been produced, which can provide an optimum condition in the wound healing process. The ideal dressing should achieve rapid healing at reasonable cost with minimal inconvenience to the patient. Several criteria are necessary to evaluate a good dressing. As describe in the review of Mukhopadhyay *et al.*, the most important criteria for a good dressing are [32].

- Ease of application
- Comfortable to remove
- Bio-adhesiveness to the wound surface
- Sufficient water vapour permeability
- Easily sterilised
- Protection against microorganism
- Elasticity and high mechanical strength
- Compatibility with topical therapeutic agents
- Optimum oxygen permeability
- Biodegradability
- Non-toxic and non-antigenic property
- Maintains moist environment around the wound (prevention of dehydration)
- Long shelf life
- Cost-effective and cosmetically acceptable
- Removes excess exudates but prevents saturation to the outer surface.

A dressing is selected according to the type, depth, location, size and texture of the wound but also according to its state of bacterial colonization, the clinical conditions of the patient and the cause. The use of the various dressings has been mainly summarized to help healthcare professionals prescribe the most suitable dressings for wound care (**Table 1.3**).[33-38] At this time, no ideal dressing exists

Table 1.3 : Classes of wound dressings and skin replacements currently available.[adapted from Ref. [33]]

TABLE 7.3. Classes of Wound Dressings and Skin Replacements Currently Available.

Class	Composition	Characteristics/function	Commercial examples
Gauze	Woven cotton fibers	Permeable with desiccation; debridement; painful removal	Curity®
Calcium-alginates	Seaweed polymer that forms a gel when absorbs fluid	Absorbs exudate; nonadherent; nonirritating; requires a cover dressing (permeable)	Algisorb,® Sorbsan®
Impregnated gauzes	Fine mesh fabric (silicone, nylon) with dermal porcine collagens	Nonadherent; semipermeable	Biobrane II®
Films	Plastic (polyurethane); semipermeable	Allows water vapor permeation; adhesive	Opsite,® Tegaderm®
Foams	Hydrophilic (wound side) and hydrophobic (outer side); semipermeable	Necrotic/exudative wounds	Lyofoam,® Allevyn®
Hydrogels	Water (96%) and polymer (polyethyleneoxide)	Aqueous environment; requires secondary dressing; no adherence; not recommended if infection is present; semipermeable	Vigilon,® Aquasorb®
Hydrocolloids	Hydrophilic colloidal particles and adhesive	Absorbs fluid; necrotic tissue autolysis; little adherence; occlusive	Duoderm,® Intrasite®
Absorptive powders and pastes	Starch copolymers, hydrocolloidal particles	Absorbs exudate; used as a filler; good for deep wounds	Geliperm,® Duoderm granules®
Silicone	Silicone sheets	Sheet induces a localized electromagnetic field; decreases scar formation?	Sil-K®
Mechanical vacuum	Vacuum, sponge, plastic film	Sponge conforms to wound and vacuum removes edema fluid; stimulation of repair?	VAC® device
Dermal matrix replacements	Acellular matrix	Permeable; increased stimulation of repair?	Alloderm® (human, dermis), SIS® (porcine, small bowel submucosa), Integra® (bovine collagen, GAG, and silicone epidermal-type layer)
Dermal living replacements	Absorbable matrix populated with fibroblasts	Permeable; increased stimulation of repair?	Dermagraft®
Skin living replacement	Bovine collagen matrix populated with human fibroblasts with an outer layer of human keratinocytes	Impermeable; increased stimulation of repair?	Apligraf® (FDA approved 6/98)

A multitude of brands within each class are available, and only a few examples are listed. Recently, skin replacements have become available. Although expensive, they have great potential clinical usefulness. No particular brands are recommended in any class.

Source: Data partially taken from Feedar JA. Clinical management of chronic wounds. In: McCulloch JM, Kloth LC, Feedar JA, eds. Wound Healing Alternatives in Management. Philadelphia: Davis, 1995:137–185.

In order to select the most suitable dressing, many guidelines and charts are available in each country and hospital.[10,39-49] An example of the wound dressing selection chart of the National Health Service (NHS) of the United Kingdom (UK) is shown in **Figure 1.4**.[41] The different types of tissue are presented and the dressings corresponding to the appropriate care are associated.

WOUND DRESSING SELECTION CHART

South Tees Hospitals **NHS**
NHS Foundation Trust

These are suggested dressings – please refer to the Formulary for further guidance.

	Aims of Care	Exudate	Consider using		Special Notes
			Primary dressing	Secondary dressing	
Necrotic	Debride eschar and promote moisture balance N.B. DO NOT debride hard, black necrosis on heels or ischaemic limbs. Refer to appropriate specialist.	Low	**Hydrocolloid** – Duoderm Thin **Hydrogel** – Kerralite Cool or Flaminal Hydro **Honey** – MediHoney Wound gel or HCS	**Film** – C-View Film / C-View Post-Op or Mepitel Film if skin is friable	A holistic assessment is essential before choosing a wound dressing. Inappropriate care can lead to delayed wound healing for patients and unnecessarily high costs for the healthcare provider.
		Moderate	**Honey** – Algivon Plus	**Super Absorbent** – Kliniderm, Kerramax Care or Sorbion Sana	
Sloughy	De-slough and provide healthy bed for granulation; promote moisture balance.	Low	**Hydrogel** – Kerralite Cool or Flaminal Hydro	**Film** – C-View Film / C-View Post-Op or Mepitel Film if skin is friable	ALWAYS use the most appropriate primary dressing (in contact with the wound and to the size of the wound) and only use a secondary dressing when necessary.
		Moderate	**Iodine** – Iodoflex **Alginate** – Sorbsan, Flaminal Forte **Hydrofiber** – Aquacel Extra or Foam **Alginate** – Urgosorb **Foam** – Mepilex XT	**Foam** – Mepilex Border or Mepilex XT, Urgotul Absorb Border	Protect peri-wound skin if necessary to prevent excoriation.
		High	**Gelling Fibre** – Kytocel	**Super Absorbent** – Kliniderm, Kerramax Care or Sorbion Sana	Frequency of dressing change depends on level of exudate. **Always dress as appropriate.**
Granulating	Provide healthy bed for epithelialisation and promote moisture balance.	Low	**Low / non-adherent dressing** Atrauman, Urgotul, Mepitel One	**Film** – C-View Film / C-View Post-Op or Mepitel Film if skin is friable	Skin tears – apply non-adherent dressing and leave for 7 days.
		Moderate	**Foam** – Mepilex Border or Mepilex XT, Urgotul Absorb Border	**Foam** – Mepilex Border or Mepilex XT, Urgotul Absorb Border	**Diabetic Foot** – please ensure patient under care of Diabetic Podiatrist. Povitulle may be used to protect the wound.
		High	**Alginate** – Sorbsan, Flaminal Forte **Hydrofiber** – Aquacel Extra or Foam	**Super Absorbent** – Kliniderm, Kerramax Care or Sorbion Sana	
Epithelialising	Promote epithelialisation and wound maturation.	Low	**Low / non-adherent dressing** Atraumen, Urgotul, Mepitel One	**Island Dressing** – C-View Post-Op	**Leg Ulcers / compression** A full leg ulcer assessment MUST be completed by a competent practitioner prior to application of compression.
		Moderate	**Foam** – Mepilex Border or Mepilex XT, Urgotul Absorb Border	**Foam** – Mepilex Border or Mepilex XT, Urgotul Absorb Border	
		High		**Super Absorbent** – Kliniderm, Kerramax Care or Sorbion Sana	
Infected	Manage infection and associated wound characteristics.	Low	**Non-Adherent** – Urgotul SSD	**Dressing Pad**	**ONLY** use antimicrobial dressings if the wound is confirmed as infected or critically colonised. Review treatment plan every two weeks, updating accordingly.
		Moderate	**Iodine** – Iodoflex **Alginate** – Flaminal Forte **Hydrofiber** – Aquacel AG + Extra	**Foam** – Mepilex Border or Mepilex XT, Urgotul Absorb Border	
		High	**Gelling Fibre** – Kytocel **Alginate** – Urgosorb Silver	**Super Absorbent** – Kliniderm, Kerramax Care or Sorbion Sana	

Figure 1.4 : *The wound dressing selection chart of the National Health Service (NHS) of the United Kingdom (UK).[adapted from Ref.[41]]*

In case of infection, a biofilm-structure embedding microorganisms develops rapidly on the wound and can reach deeper tissues quickly if the infection spreads.[14] For this reason, good management of the infection is essential but is extremely difficult to eradicate with conventional wound care products. Two kinds of treatment are available : dressings with antibacterial agents and systemic antibiotics administration.[50-51] In the two cases, the wound should always be cleaned regularly.[18] Despite the fact that a significant amount of research has been carried out in the area, no ideal treatment has been found.[55] There is no evidence that the use of local antiseptics or antibiotics or systemic antibiotic therapy is beneficial for the healing of a chronic infected wound.[22] Most effort have been conducted to boost the antimicrobial activity of a broad range of topically applied therapeutic agents but studies still are ongoing to improve wound healing process and its effectiveness.[52-59] In theory, topical application of antibacterial agents shows the most promising properties for local infection therapy. It allows the direct administration of a high quantity of antimicrobial target to the infected zone and gives the possibility of using other antibacterial agents that cannot be administered orally, especially to avoid the emergence of resistant bacteria conducted by systemic antibiotherapy.[55]

Another advantage of the local route rather than the systemic route is that the antibiotic has a big impact on the bacterial flora of the intestine mainly.[56-57] However, the topical application of antibiotics also acts on the microbiota of the skin, the resident bacteria being useful for healing and reducing infection by producing proteolytic enzymes. It would therefore be interesting to consider this decrease in the microbiota and its essential actions in order to add the right components to compensate for the loss of the microbiota.[58]

Another problem concerns the administration of antibiotics at low concentrations. Indeed, when microorganisms are organized in biofilms, the efficacy of an antibiotic requires much higher concentrations compared to bacteria in planktonic form.[59] If antibiotics are applied at sub-inhibitory concentrations, it has been shown that this strongly affects mutations, gene transfer and the ability of biofilms to form, which may result in the enhancement of certain virulence or resistance functions. Therefore, the effect of antibiotics is not limited to bactericidal or bacteriostatic action. In the presence of a sub-inhibitory concentration of antibiotics, the expressed genes are rather related to intracellular signaling with consequences on the collective behavior of bacterial populations, which supports the idea that in nature antibiotics that are secreted by many microorganisms act as signaling molecules.[60-62]

In general, when the degree of wound infection exceeds what can be controlled by local interventions, systemic antibiotics are warranted.[22,63] Medical recommendations are therefore quite weak on the treatment of infected wounds and depend on the knowledge and experience of the caregiver, not on evidence-based consensus. Some guidelines offer a selection of antibiotics to help physicians choose the most appropriate treatment.

1.1.2 Advanced therapy using hydrogels and cryogels

Remarkable progress has been made in the field of wound dressings. The design of new biocompatible materials has led to significant advances in the treatment of chronic wounds.[64-66] Various available compounds allow the development of dressings of different forms such as covering, injectable[67-68], adherent[69-70], antibacterial[71-73] and activatable[74-76] dressings as well as scaffolds[77-78], films[79-80], electrospun[81-82], nanomicelles[83-84], etc. The different materials are similar to those of already used dressings such as hydrogels or foams, but through various formulations and functionalizations, these materials have new properties. For example, Blacklow *et al*. have developed a hydrogel capable of reproducing a contraction mimicking wound healing in the embryo.[85] With the emergence of nanomedicine and nanotechnologies,

the incorporation of nanostructures in dressings is one of the research directions in the development of wound healing products.[86-87] The most developed has been the dressing incorporating silver particles, known for its antibacterial activity.[88-89] Much research has been conducted on the subject and dressings are currently available on the market. However, studies have shown a toxic effect of the silver particles which compromises its use for prolonged applications.[90-91] In wound healing, numerous studies have been performed on the incorporation of growth factors or other therapeutics agents in polymeric wound dressings as a reservoir for passive topical release.[92-95] Two advanced polymeric materials are presented in the following paragraphs: hydrogels and cryogels.

Hydrogels are one of the most highly utilized biocompatible polymers for wound healing treatment.[96-97] The network of cross-linked polymers gives hydrogels a solid appearance while being composed of a large amount of water.[98] The high water content allows for easy encapsulation of hydrophilic drugs and protection of bioactive therapeutics by reducing the risk of drug denaturation and aggregation.[99] Hydrogel allows for the passive and steady release of the drug over time and is considered as a controlled release drug delivery system. The ability to passively control the release allows the system to hold larger amounts of drug while maintaining a drug concentration in the blood within the therapeutic window, allowing the drug to be used for a longer period of time and more effectively and avoid the elevated plasma concentration of the drug that is outside of the therapeutic window which can result in side effects and reduce the effectiveness of the treatment. This material presents ideal properties for biomedical applications[100] :

- The highest absorption capacity (maximum equilibrium swelling) in saline.
- Desired rate of absorption (preferred particle size and porosity) depending on the application requirement.
- The highest absorbency under load (AUL).
- The lowest soluble content and residual monomer
- The lowest price.
- The highest durability and stability in the swelling environment and during the storage.
- The highest biodegradability without formation of toxic species following the degradation.
- pH-neutrality after swelling in water.
- Colorlessness and non-toxic → Biocompatibility
- Photo stability.

- Re-wetting capability (if required) the hydrogel has to be able to give back the imbibed solution or to maintain it; depending on the application requirement (e.g., in agricultural or hygienic applications).

- Stimuli-responsive (Temperature, pH…)

- Variable mechanical properties: flexible, robust, elastic, self-healing, etc

Clearly, it is impossible for a hydrogel sample to perform all of the above required functions simultaneously. In fact, synthetic components that achieve the maximum level of some of these characteristics will result in inefficiency of the others. Therefore, in practice, the production reaction variables must be optimized to achieve an appropriate balance between properties. For example, hygienic hydrogel products must have the highest absorption rate, lowest rewetting rate, and lowest residual monomer[101], and hydrogels used in drug delivery must be porous and pH or temperature responsive.[102]

Another polymeric material has been more and more at the forefront in various biomedical applications. This material is the cryogel.[103] While conventional hydrogel has been widely used for its properties of flexibility, moisture and porosity, cryogel, which is a type of hydrogel, has recently emerged as an alternative in biomedicine and especially drug delivery. The cryostructure offers continuous interconnected pores that allow for increased surface area and thus absorption capacity (**Figure 1.5**).[104-105] The spongy and elastic nature of cryogel offers new tuneable textures for dressings. Various shapes of cryogel are available depending on the application, such as sheets, beads, discs or microparticles. The porous structure enables it to be used in various applications including drug delivery system[106-107], scaffold for cells-therapy[108], tissue engineering[109] or entrapment and immobilization of bacteria cells for wound infection[110].
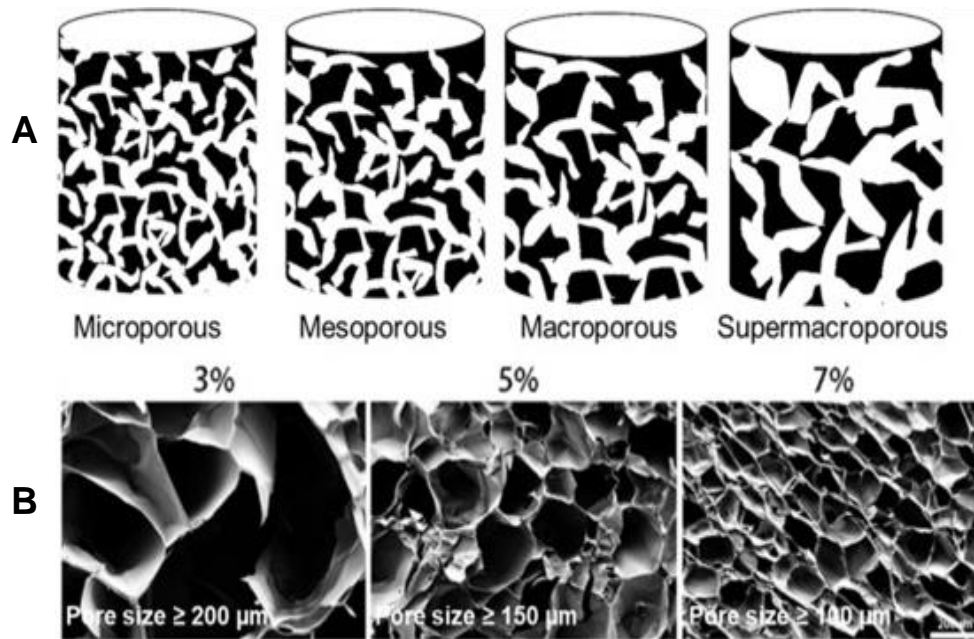
Figure 1.5 : *Cryogels can be fabricated in various porosity.* ***A.*** *Schematic representation showing the varying porosity of cryogels. Cryogels can be formed with porosity ranging from microporous to supermacroporous structures.* ***B.*** *Scanning electron microscopy (SEM) images of the cryogel with different concentrations showing different pore sizes. [adapted from Ref.[103]]*

In addition, cell and tissue-based therapies are currently exploited to repair or replace damaged tissue and improve biological function using healthy cells, optimized cells, stem cells, tissue-engineered substitutes, allografts or blood-derived products.[111-113] Nowadays, many cells are studied for wound healing. The most studied therapeutic cells or tissues are mesenchymal stem cells, platelet rich plasma, epidermal and dermal substitutes.[114] Despite the very promising interest in cellular therapies, clinical studies have established that the implanted cells undergo apoptosis and are eliminated by the body a few hours after injection.[115] Furthermore, although stem cell differentiation has been demonstrated in vitro, the evidence on implanted cells has not been clearly defined.[116] Thus, to promote the growth of implanted cells, it is necessary to associate a scaffold or a vehicle carrier to optimize the process.[117] The use of more complex structures such as skin substitutes have shown encouraging results in various clinical studies[118], but their mode of operation is still poorly understood. Several tissue-engineered skin substitutes are available on the market.[119]

1.1.3 Nanotechnological approaches for wound healing

Physical therapies have gained interest in wound management, leading to the development of new technologies and devices.[34] The physical system involves the transfer of

energy to the wound, which in turn results in observable and measurable changes in wound healing. Effective technologies proposed include electrical stimulation[120], low frequency ultrasound[121], mechanical stimulation[122], pulsed radiofrequency energy[123], shock waves[124], electromagnetics[125], photomodulation[126], oxygen-associated therapies[127], thermal stimulation, etc. The hypothesis of heat treatment for wound healing has emerged for many years. The first hypotheses that heat could improve healing appeared from the observation of hypothermia occuring during surgery.[128-129] With the anesthesia, the body temperature decreases to 35°C. It has been shown that this hypothermia leads to a slowing down of the healing of the post-surgical wound compared to patients who would have been kept at higher temperatures during the operation. In addition, hypothermia would favor infections.[130] This phenomenon would be due to the disruption of blood circulation during hypothermia.[131-133] Indeed, it causes vasoconstriction of the vessels which decreases blood flow. Since oxygenation of the wound is very important in the healing process, this would explain the significant impact. It has been demonstrated with in vitro studies, that hyperthermia would promotes wound healing process with increasing chemotaxis, phagocytosis, fibroblast proliferation,[134-135] lymphocytes immune response[136-138] as well as improvement of heat shock proteins expression which have been widely studied for their involvement in healthy healing.[139-143] Heat shock is a stress suffered by a living organism following an increase in temperature.[144] This stress results in the production of specific proteins to combat the negative effects of the temperature change and thus restore cellular homeostasis. The proteins involved are the heat shock proteins (HSP). These are chaperone proteins that play a role in protein folding, so they help the proteins to reach their conformation and then withdraw. It has also been observed that chaperone proteins help the immune system to detect injured cells by presenting pieces of protein on the cell surface.[145] The use of a dressing to heat the skin should be further investigated in order to establish satisfactory clinical results.[146-151] Several methods have been proposed, such as the use of a radiant[152], NIR irradiation[153-154] or photothermy[155-156]. The most advanced product is a novel bandaging system for warm up active wound therapy by topical radiant heating.[152, 157-158] This new dressing optimizes the wound environment by maintaining a body temperature of 36 to 37.5°C. This patch produces moist heat, providing a warm and moist wound environment.

Recently, a particular focus has been placed on the use of photothermal treatment (PTT).[159] Photothermal agents are able to convert light energy to heat under near infrared (NIR) irradiation. For instance, nanostructures with photothermal capability are graphene oxide, reduced graphene oxide, gold nanoparticles, molybdenum disulfide, copper sulfide, etc.[160-162]

It offers the possibility to adapt the temperature by modulating the concentration of photothermal agents in the dressing or by the modulation of stimulus intensity in order to choose the adequate temperature according to the target. Indeed, several studies have revealed the effect of temperature on wound healing.[163-165] It is believed that at temperatures between 41 and 43 °C there was activation of immune cells, between 45 and 50°C there is a selective effect on cancer cells, and above 50°C, the temperature has an effect on the integrity of the membranes of bacterial cells, which can therefore have a bacterial ablation effect during infection.[166] For the moment, studies on healing involving heat have mostly been validated in *in vitro* (cell culture) and *in vivo* trials but rarely in clinical conditions. Numerous pilot studies are available[167-172] but few large-scale studies have been conducted to date.[173] Furthermore, the only treatment available is the administration of radiant heat to monitor the wound environment but no research has been conducted on the application of heat to deeper tissues.

Applying medication to a chronic wound requires removal of the dressing, which exposes the wound to potential infection and causes great discomfort to the patient. New specialized dressings have been invented to release the medication in a controlled manner. This technology is known as transdermal drug delivery based on the therapeutics penetrating the stratum corneum, the outermost layer of skin.[174] Initially used as a new route for drug delivery, the extension of its use to chronic wounds has been mainly investigated due to the need of topical treatment.[166,175-176] Transdermal drug delivery (TDD) has received great interest as a method for noninvasive drug administration, with the objective of targeting the upper layers of the skin. Compared to oral administration systems, transdermal approaches have the advantage of overcoming first-pass metabolism of drugs in the gut and liver, improving the patient compliance and reducing side effects, and have proven to be of great therapeutic utility.[177] It avoids furthermore pain and safety issues associated with needle-based drug injections and burst release. To date, a transdermal based approach can deliver drugs with a short-half-life time more easily and eliminates frequent administrations to maintain constant drug delivery. Local cutaneous effects are achieved by dissolving or suspending the drug in an appropriate vehicle that is applied topically in the form of creams, ointments or in a patch. The main limitation of passive transdermal delivery is that only a handful of drugs can penetrate the skin passively.[178] From a physicochemical point of view, an ideal transdermal drug candidate has to meet a number of requirements such as high lipophilicity, low molecular weight (< 500 Dalton), sufficient solubility in water at pH 6 to 7.4 (e.g. $\approx$ 0.05 to 1 mg/mL if target delivery rate is in the mg range per day), and a suitable pKa (determines solubility of the un-ionized form at physiological pH).[179]

Today, the low permeability of the stratum corneum remains a barrier for water-soluble and high molecular weight molecules to transdermal administering via passive diffusion through the skin. For this purpose, several technologies have been proposed over the years to modify the properties of the stratum corneum.[180-182] The **Figure 1.6** summarizes the different technologies for enhancing transdermal drug delivery.[183-186] During the thesis, the photothermal enhancement strategy for drug delivery using nanomaterials was mainly explored.
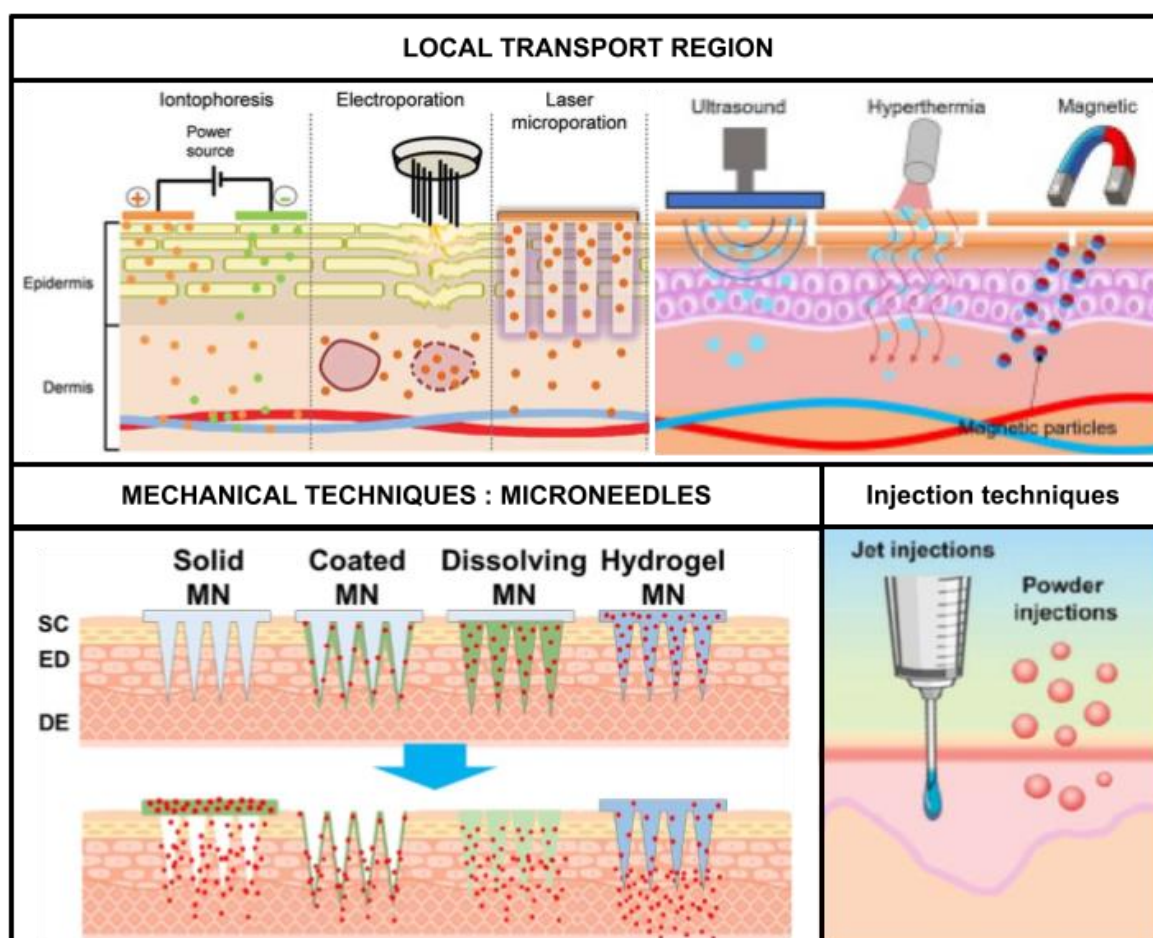
Figure 1.6 : *Different approaches towards subcutaneous drug delivery.[adapted from Ref.[185-188]]*

Despite considerable efforts that have been conducted on wound healing management development, wound healing complications remain a global burden with hundred thousands of deaths annually and a consequent financial part of health care. The rapid improvements over the last four millennia provide promising research areas in various fields such as optic physics, microfluidics, material sciences, nanoengineering, and stem cells biology. The development of novel smart dressings is consequently in progress to not only serve as a passive dressing to

cover wounds but also play an active role by dynamically contributing in healing. The combination of multiple properties obtained with the emergence of technologies, such as cell therapies, physical therapies and drug delivery systems, is leading to future wound care development that could significantly contribute to reducing morbidity and saving more lives.

1.2 Models for wounds study

Wound healing is an essential biological mechanism present in all multicellular organisms. From the restoration of the skin barrier to the complete regeneration of a limb, each species has its own mechanisms that allow species survival in case of external injuries.[187] This phenomenon has been largely studied over the years to understand better the complex physiological mechanisms involved in tissue repair. In this perspective, many different models have been developed both for understanding the tissue repair process and for testing pharmaceuticals and cosmetics products.[188]

A lot of different models mimicking the skin at cellular, histological, physiological levels are available. These models can be divided into two groups*: in vitro* and *in vivo* models with their own strengths and weaknesses (**Table 1.4**).[189] In a study, the model or rather the models have to be selected with care as no model can completely replicate clinical human wound healing. Obviously, human studies seem to be the most relevant way to determine the effectiveness of a wound treatment or to understand human repair processes[190] but they are often impractical because of ethical considerations and the replicability of the study.[191] Firstly, it is difficult to obtain a sufficient number of patients with similar wounds for a randomized trial. On the other hand, the wound measurements are limited as the main way to analyse the evolution of the healing is to make a histological study which requires frequent biopsies. Finally, to produce accurate results on wound healing, untreated or vehicle-treated control wounds have to be used. Therefore, the human model often remains impracticable for robust studies.[188]

Table 1.4 : *Advantages and limitations of different skin models for dermatological research.[adapted from Ref.[189]]*

Models	Advantages	Limitations
Mono-cellular (2D) [16-23, 32, 61, 62]	Defined conditions	Only one cell type
	Reproducibility	No 3D culture
	Cryo-preservation/Bank	Few parameters
	Cheap and very easy to use	Variability and no controlled parameters for primary cells
Co-culture (2D) [24-31, 62]	Cellular interactions	No 3D culture
	Reproducibility	Variability and no controlled parameters for primary cells
	Definite conditions	
	Cryo-preservation/Bank	
	Cheap and easy to use	
Organotypic models (3D) [11, 13, 34-53, 60-63]	3D structure	Large variability and no controlled parameters
	Many cellular type and interactions	No integration of nervous and vascular system
	Easy to use	No peeling
In vivo Animals [39, 54-56, 60]	Nearest to reality	Ethical problems for using living animals
	Integration of all parameters	Prohibited for cosmetics Differences with humans
		Difficulty to analysis for none invasive methods Expensive
		Requires intensive training and certification of staff
	Nearest to reality	Ethical problems and difficult administratively
	Integration of all parameters	Expensive
In vivo Humans	Easy for none invasive methods	
	No biological variability and dependency	Relevance according to reality with unknown parameters
	Control of all known parameters	
In virtuo models [57-59]	Probably integration of parameters impossible for other models	Numerous unknown data

The *in vitro* models are based on the culture cells that can be simple monolayer cell culture, a three-dimensional multicellular model with different types of cell combination or an organo-culture of skin explants.[189] The *in vivo* models have been mainly used in the case of chronic wounds study, both in biological understanding and treatment testing.[192] Animal models were developed with different species depending on the study purpose and are often used to complement findings from in vitro assays.[193] A careful selection of the species has to be done to have a relevant wound healing model according to the study purpose. Small mammals like rodents are frequently used due to their inexpensive cost, ease of handling and good knowledge of the species.[194] In fundamental studies, amphibians, especially salamander, have been widely used for scarless healing[195-197], drosophila and zebrafish are more used for live imaging[198-199] or genome wide screening studies[200] and embryos were largely studied for their contraction ability.[201-203] Pigs has been more used to identify new therapeutics toward the goal of accelerating wound repair.[204-206]

Therefore, wound healing models are essential to detect new biomarkers, study repair mechanisms and pathology and test the efficiency of new therapeutics. Unfortunately, no single

appropriate model is close enough to humans. The combination of different models is needed.[207] Nowadays, the model considered as the best available alternative to study complex cellular and molecular interaction involved in wound healing is animals. It is however often used after preliminary *in vitro* studies. The advantage of *in vitro* studies is that they can be conducted on human materials. Thus, human cells are widely available to study biological mechanisms and the reaction to some physical and chemical stimulation.[208] The possibility to use human skin explant is also a great opportunity to design studies on whole skin structure including all cell types of the skin and surrounding components.[189]

In order to successfully study wound biofilms, it was necessary to generate wound models in vitro and in vivo. Designing a biofilm in the laboratory has been a challenge for several decades.[209] The importance of reproducing the wound environment as closely as possible allows us to understand the mechanisms of formation and resistance of biofilms on the wound and also to test treatments against these biofilms. Knowing that most chronic wound treatments are dressings, models should be adapted to allow this study.The wound environment consists of the wound bed (skin) as a support, the supply of nutrients by the host and the secretion of exudates.[210] The choice of the biofilm support must consider this aspect. Firstly, the air-liquid interface condition is clearly essential for wound reproduction. Secondly, the wound nutrients are different from classic culture medium. The adaptation of the medium is important for the wound mimicking.

Several systems have been set up, both *in vitro* and *in vivo*. Techniques range from simple agar[211-215] to *in vivo* animal models[214-216]. These include continuous flow culture systems[217-219], collagen gel matrix containing biofilm aggregates with serum protein mimicking the wound bed of chronic wounds[220-224], ex vivo skin explants[225-228] and reconstructed human skin[229-231] to name a few (**Figure 1.7**).
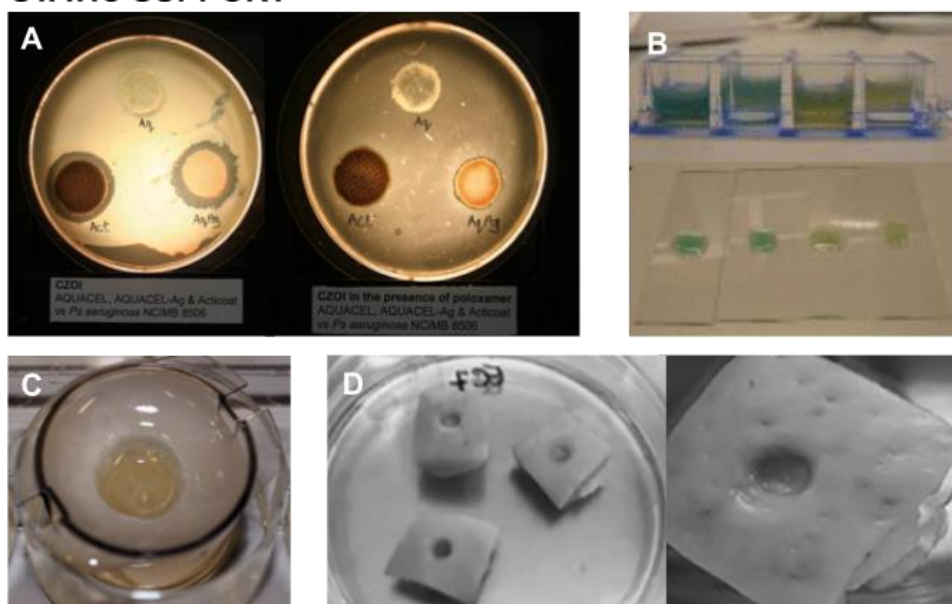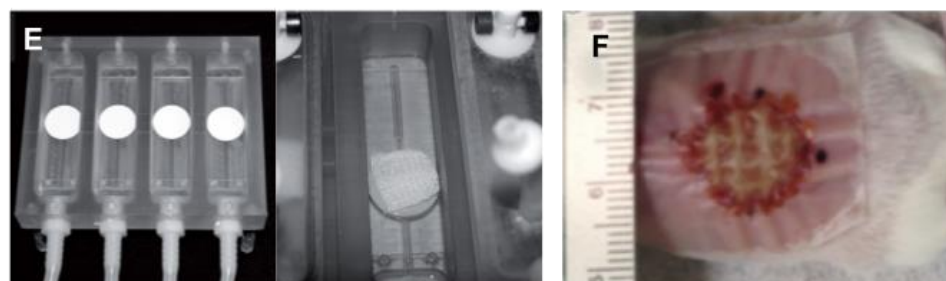
Figure 1.7 : *Examples of biofilm models on various surfaces. **A.** Culture of Pseudomonas aeruginosa and dressing efficiency assay by zone of inhibition measurement on Mueller–Hinton agar (Left) and on poloxamer gel (Right).[211] **B.** Side view of the 8-well culture slides where the wells contain collagen matrices with Pseudomonas aeruginosa (PAO1) biofilm (Top) and microscopic slides with matrices that were gently moved from the culture slide (Bottom).[220] **C.** Collagen wound model is designed to represent a grade 1B diabetic foot ulcer. The collagen matrix was situated in a tissue culture well insert in a 6-well plate that was bathed in media. A void was created in the model using a mold.[224] **D.** Porcine skin explant model of chronic wounds with Petri dish with solid TSB media (1.2% agar) containing three porcine skins after 24 h of incubation with bacteria (E. coli) (Left) and zoom on the wound in the middle a skin explant (Right).[227] **E.** Images of a colony-DFR reactor: absorbent pads glued onto glass microscope slides (Left); gauze dressing placed on top of the inoculated membrane (Right).[217] **F.** Chronic wound mouse model for polymicrobial biofilm infection. Surgical excision of the dermis can be performed on mice to create a full thickness wound. Bacteria are then inoculated directly onto the wound bed. An adhesive dressing is applied to prevent contractile healing, and help protect the wound from contaminants. Wound closure can be measured over time, and tissue can be removed to visualize the biofilm.[232] [adapted from Ref.[211,217,220,224,227,232]]*

All models mentioned above are prone to limitations in mimicking human-like conditions.[209] For *in vitro* models, the surface and media do not fully reflect the nutritional conditions and the culture temperature used to form and maintain the biofilm is mostly 37°C, the body temperature, while the wound bed temperature ranges between 31-35°C[233] and can vary between persons and body location. For in vivo models are expensive, difficult to standardize and sometimes failed to have a good transferability to humans.[210]

The models offer the possibility to make a mixed biofilm community. As Biofilms in chronic wounds are never composed of a single bacterial species, multi-pathogens models seem obvious to develop an effective treatment. Sun *et al*. were the first to develop a multi-species biofilm model called the Lubbock chronic wound infection model (**Figure 1.8**).[234] Several variants of this method have been then further proposed with different support.[232,235-236]

Invivo   Invitro
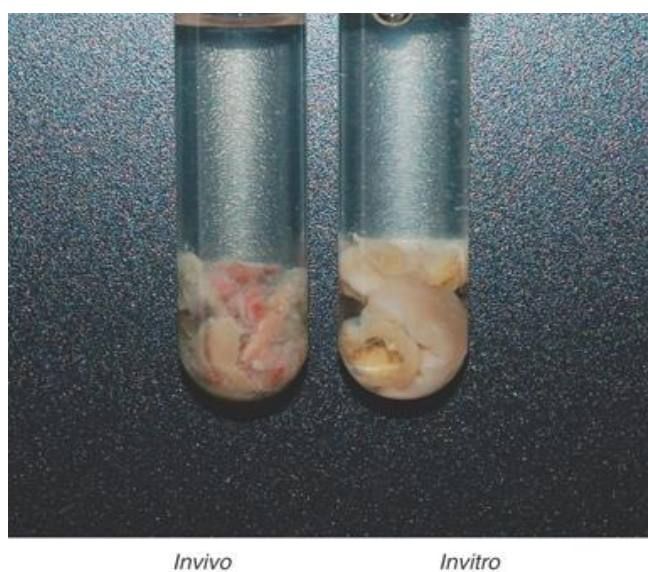
Figure 1.8 : Visual comparison of an actual debridement sample taken from chronic wound biofilm with the Lubbock chronic wound biofilm. This image compares a typical chronic wound biofilm on the left and the Lubbock chronic wound biofilm on the right showing the similarity in texture and consistency between the in vivo biofilms we typically recover and the in vitro model described in this manuscript.[adapted from Ref.[234]]

The majority of biofilm models have been established for aerobic pathogens, whereas we know that strict anaerobes are an important component of the wound microflora.[237] A few models capable of maintaining an anaerobic population are available. The maintenance of anaerobes can be achieved by creating an anaerobic environment on the top of the wound[238] or by integration of anaerobic bacteria into a multispecies biofilm to maintain it in an essentially

aerobic environment.[240] The study of biofilms is very complex because of the lack of consensus among the diversity of techniques and the difficulty to replicate clinical conditions. In addition, differences in sensitivity depending on the biofilm model may affect the result. Brackman *et al*. used a combination of models to study the association of a quorum sensing inhibitor, thus presenting several elements to confirm the hypotheses. Indeed, the antibacterial activity was evaluated on medical-grade silicone disks, a collagen matrix model, a reconstructed human skin model and an in vivo model. The concordance of the results makes this study very robust.[241]

In wound healing research, the concordance between results of in vitro and animal models with those observed in humans is only partial.[242] The concept of using human material as a preclinical model for wound-healing research and thus predetermined hypotheses should be explored. With these preliminary results, valid *in vitro* or animal models could be implemented for more in depth investigations not feasible with humans. *Ex vivo* skin samples from humans seem appropriate to replace experimental animals and cross the bridge of translational issues. As laboratory animals become increasingly limited[243], the need for alternative methods has led to the use of free tissue flaps. In particular, many efforts have been made to replace classic animal irritancy tests by skin explant models.[244-246] Thus, ex vivo skin models have been extensively exploited for toxicity testing of chemicals[247-249] or cosmetics[245,250] but also for studies of skin permeability[251-254], wound healing[255-257] and infections[258-259] both for treatment testing[260-263] and for fundamental studies[264-268].

Ex vivo skin samples are fairly easy to obtain. It consists of skin leftovers from cosmetic surgeries[269], initially considered as medical waste and intended for disposal. More than 900,000 abdominoplasty procedures, involving the removal of excess skin and fat from the mid and lower abdomen, are performed worldwide each year.[270] Thus, many materials may be available for skin studies. Other surgical procedures, such as lower body lift, thigh lift, arm lift, buttock lift, breast reduction, can provide many skin samples with a variety of skin parts.

Skin samples are collected right after surgery and should be used immediately or maximum 1-2 days after. This surgery's dependence is one of the constraints of the model as the availability of biological tissues is limited. In addition, there are legal requirements for the use of human samples. The approval and authorization of the French Ethics Committee (Comité de Protection de Personnes or CPP) and the French Ministry of Research and Higher Education are needed.[271]

Ex vivo models are also called skin explants, organ-cultured skin or skin organ. It is a small sample of skin that is cultured in an adequate medium. The explant has a 3D structure and contains all skin layers (stratum corneum, epidermis, dermis with extracellular matrix and hypodermis).[256] It is easier to obtain compared to reconstructed skin as it is used immediately after surgery or biopsies.[189] After the collect, decontamination, resizing and de-hypodermisation are performed to obtain the skin sample.[208] The piece of skin can be wounded for wound healing studies (**Figure 1.9**).[189,269] Samples are cultivated in an appropriate culture medium and can be studied over the course of a few days. Explants are usually used for 10-14 days maximum, depending on culture conditions. The culture is generally performed in an incubator at 37°C and 5% CO_2. The most common techniques used to characterise the models are histological stains and cellular assay like proliferation, apoptosis and cytotoxicity tests.[189] Indeed, several markers have been established for studying re-epithelialization and extracellular matrix remodeling. The recruitment and activation of immune cells to the site of the wound can also be visualized.
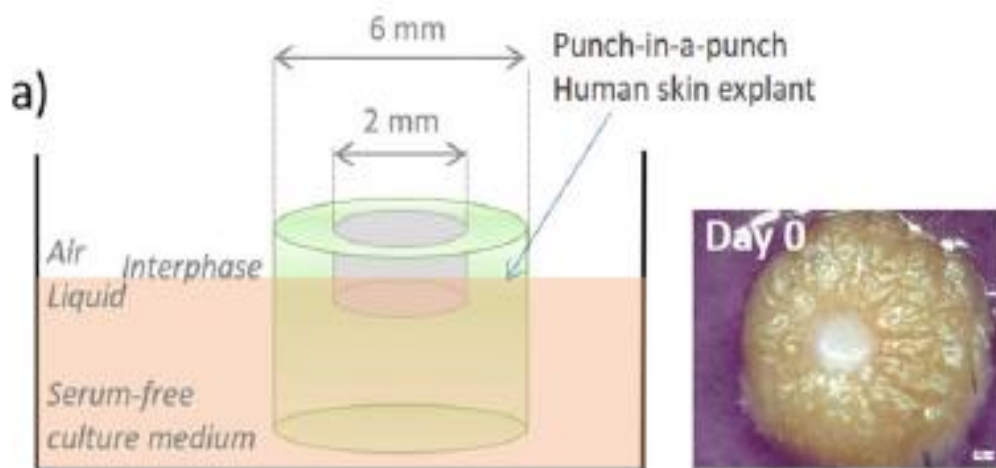
Figure 1.9 *: Human skin punch-in-a-punch ex vivo wound healing model. Left : Schematic illustration of the punch-in-a-punch ex vivo wound healing model. Firstly, a 2 mm inner biopsy punch is generated by gently punching into skin, penetrating the epidermis and the upper part of the dermis by clockwise rotation of the biopsy punch in order to create a wound. Forceps are used to pull up the skin punch and excise at the dermis level using scissors to create a central wound. Subsequently, the outer punch is prepared, using a 6 mm biopsy punch around the wound. Right : macroscopic image of skin explant, top view.[adapted from Ref.[208]]*

Obviously, the classic disadvantages of *in vitro* models are also observed in this model like the lack of innervation, circulation and immune systems, as well as the contraction and

tension of tissue is lacking.[188,272] The culture environment in a closed incubator at 37°C without light exposure. In addition, standardization and consistency of the model remain a challenge.[273] Skin explants are representative of the donor's age and lifestyle (sun exposure, injuries, care, allergies, medications, smoking or drug use); therefore, these variabilities must be accounted for in the experimental design.[189] Fortunately, the number of samples carried out with skin from a single donor allows for the inclusion of untreated or vehicle-treated controls and the implementation of additional analyses to produce accurate results.[274]

The *ex vivo* models offer the possibility to use healthy or disease skin, full thickness or separate layers of the skin, to be the interface between in vitro and in vivo studies and can also be grafted on living animals.[188-189,273] It is a time- and cost-efficient and a valuable model to study wound healing.[275] All kinds of cells are included and common communication mediators like cytokines or growth factors can be induced in the skin.[189] In addition, molecules can be added in the medium for special studies.

REFERENCES

1.   Sen, C. K.; Gordillo, G. M.; Roy, S.; Kirsner, R.; Lambert, L.; Hunt, T. K.; Gottrup, F.; Gurtner, G. C.; Longaker, M. T. Human Skin Wounds: A Major and Snowballing Threat to Public Health and the Economy. *Wound Repair Regen* **2009**, *17* (6), 763–771. https://doi.org/10.1111/j.1524-475X.2009.00543.x.

2.   Siddiqui, A. R.; Bernstein, J. M. Chronic Wound Infection: Facts and Controversies. *Clinics in Dermatology* **2010**, *28* (5), 519–526. https://doi.org/10.1016/j.clindermatol.2010.03.009.

3.   Posnett, J.; Gottrup, F.; Lundgren, H.; Saal, G. The Resource Impact of Wounds on Health-Care Providers in Europe. *J Wound Care* **2009**, *18* (4), 154–161. https://doi.org/10.12968/jowc.2009.18.4.41607.

4.   Sen, C. K. Human Wounds and Its Burden: An Updated Compendium of Estimates. *Advances in Wound Care* **2019**, *8* (2), 39–48. https://doi.org/10.1089/wound.2019.0946.

5.   Lazarus, G. S.; Cooper, D. M.; Knighton, D. R.; Margolis, D. J.; Pecoraro, R. E.; Rodeheaver, G.; Robson, M. C. Definitions and Guidelines for Assessment of Wounds and Evaluation of Healing. *Arch Dermatol* **1994**, *130* (4), 489–493. https://doi.org/10.1001/archderm.1994.01690040093015.

6.   Information, N. C. for B.; Pike, U. S. N. L. of M. 8600 R.; MD, B.; Usa, 20894. *Chronic Wounds: Overview*; Institute for Quality and Efficiency in Health Care (IQWiG), 2018.

7.   Moffatt, C.; Vowden, P.; Augustin, M.; Justiniano, A.; Lindholm, C.; Margolis, D.; Nelson, A. SENIOR EDITORIAL ADVISORS - EWMA. 20.

8.   Mahmoudi, M.; Gould, L. J. Opportunities and Challenges of the Management of Chronic Wounds: A Multidisciplinary Viewpoint. *CWCMR* **2020**, *7*, 27–36. https://doi.org/10.2147/CWCMR.S260136.

9.   Percival, S. L.; Hill, K. E.; Williams, D. W.; Hooper, S. J.; Thomas, D. W.; Costerton, J. W. A Review of the Scientific Evidence for Biofilms in Wounds. Wound Repair and Regeneration 2012, 20 (5), 647–657. https://doi.org/10.1111/j.1524-475X.2012.00836.x

10.   Apelqvist, J.; Bakker, K.; Houtum, W. H. van; Schaper, N. C. Practical Guidelines on the Management and Prevention of the Diabetic Foot. *Diabetes/Metabolism Research and Reviews* **2008**, *24* (S1), S181–S187. https://doi.org/10.1002/dmrr.848.

11.   Escandon, J.; Vivas, A. C.; Tang, J.; Rowland, K. J.; Kirsner, R. S. High Mortality in Patients with Chronic Wounds. *Wound Repair and Regeneration* **2011**, *19* (4), 526–528. https://doi.org/10.1111/j.1524-475X.2011.00699.x.

12.   Guo, S.; DiPietro, L. A. Factors Affecting Wound Healing. *J Dent Res* **2010**, *89* (3), 219–229. https://doi.org/10.1177/0022034509359125.

13.   Gould, L.; Abadir, P.; Brem, H.; Carter, M.; Conner-Kerr, T.; Davidson, J.; DiPietro, L.; Falanga, V.; Fife, C.; Gardner, S.; Grice, E.; Harmon, J.; Hazzard, W. R.; High, K. P.; Houghton, P.; Jacobson, N.; Kirsner, R. S.; Kovacs, E. J.; Margolis, D.; Horne, F. M.; Reed, M. J.; Sullivan, D. H.; Thom, S.; Tomic-Canic, M.; Walston, J.; Whitney, J. A.; Williams, J.; Zieman, S.; Schmader, K. Chronic Wound Repair and Healing in Older Adults: Current Status and Future Research. *J Am Geriatr Soc* **2015**, *63* (3), 427–438. https://doi.org/10.1111/jgs.13332.

14.   Frykberg, R. G.; Banks, J. Challenges in the Treatment of Chronic Wounds. *Advances in Wound Care* **2015**, *4* (9), 560–582. https://doi.org/10.1089/wound.2015.0635.

15.   Bjarnsholt, T.; Kirketerp-Møller, K.; Jensen, P. Ø.; Madsen, K. G.; Phipps, R.; Krogfelt, K.; Høiby, N.; Givskov, M. Why Chronic Wounds Will Not Heal: A Novel Hypothesis. *Wound Repair and Regeneration* **2008**, *16* (1), 2–10. https://doi.org/10.1111/j.1524-475X.2007.00283.x.

16.   Mukherjee, R.; Tewary, S.; Routray, A. Diagnostic and Prognostic Utility of Non-Invasive Multimodal Imaging in Chronic Wound Monitoring: A Systematic Review. *J Med Syst* **2017**, *41* (3), 46. https://doi.org/10.1007/s10916-016-0679-y.

17.   Vowden, K.; Vowden, P. Wound Dressings: Principles and Practice. *Surgery (Oxford)* **2017**, *35* (9), 489–494. https://doi.org/10.1016/j.mpsur.2017.06.005.

18.   Grey, J. E.; Enoch, S.; Harding, K. G. Wound Assessment. *BMJ* **2006**, *332* (7536), 285–288.

19.   Gianino, E.; Miller, C.; Gilmore, J. Smart Wound Dressings for Diabetic Chronic Wounds. *Bioengineering (Basel)* **2018**, *5* (3), 51. https://doi.org/10.3390/bioengineering5030051.

20.   Dissemond, J.; Assadian, O.; Gerber, V.; Kingsley, A.; Kramer, A.; Leaper, D. J.; Mosti, G.; Grzymala, A. P. de; Riepe, G.; Risse, A.; Romanelli, M.; Strohal, R.; Traber, J.; Vasel-Biergans, A.; Wild, T.; Eberlein, T. Classification of Wounds at Risk and Their Antimicrobial Treatment with Polihexanide: A Practice-Oriented Expert Recommendation. SPP 2011, 24 (5), 245–255. https://doi.org/10.1159/000327210.

21.   Baranoski, S.; Ayello, E. A. *Wound Care Essentials: Practice Principles*; Lippincott Williams & Wilkins, 2008.

22.   Prise en charge des infections cutanées bactériennes courantes. Annales de Dermatologie et de Vénéréologie 2019, 146 (10), 610–625. https://doi.org/10.1016/j.annder.2019.07.002.

23.   Dissemond, J.; Assadian, O.; Gerber, V.; Kingsley, A.; Kramer, A.; Leaper, D. J.; Mosti, G.; Grzymala, A. P. de; Riepe, G.; Risse, A.; Romanelli, M.; Strohal, R.; Traber, J.; Vasel-Biergans, A.; Wild, T.; Eberlein, T. Classification of Wounds at Risk and Their Antimicrobial Treatment with Polihexanide: A Practice-Oriented Expert Recommendation. SPP 2011, 24 (5), 245–255. https://doi.org/10.1159/000327210.

24.   Sibbald, R. G.; Woo, K.; Ayello, E. A. Increased Bacterial Burden and Infection: The Story of NERDS and STONES. *Advances in Skin & Wound Care* **2006**, *19* (8), 447–461.

25.   Hurlow, J.; Bowler, P. G. Clinical Experience with Wound Biofilm and Management: A Case Series. *Ostomy Wound Manage* **2009**, *55* (4), 38–49.

26.   Gardner, S. E.; Frantz, R. A.; Doebbeling, B. N. The Validity of the Clinical Signs and Symptoms Used to Identify Localized Chronic Wound Infection. *Wound Repair and Regeneration* **2001**, *9* (3), 178–186. https://doi.org/10.1046/j.1524-475x.2001.00178.x.

27.   Nichols, E. Describing a Wound: From Presentation to Healing. *Wound Essentials* **2015**, *10* (1), 56–61.

28.   Falanga, V. *Cutaneous Wound Healing*, Vincent Falanga.; Martin Dunitz: London, 2001.

29.   Schultz, G. S.; Sibbald, R. G.; Falanga, V.; Ayello, E. A.; Dowsett, C.; Harding, K.; Romanelli, M.; Stacey, M. C.; Teot, L.; Vanscheidt, W. Wound Bed Preparation: A Systematic Approach to Wound Management. Wound Repair and Regeneration 2003, 11 (s1), S1–S28. https://doi.org/10.1046/j.1524-475X.11.s2.1.x.

30.   Schultz, G. S.; Barillo, D. J.; Mozingo, D. W.; Chin, G. A. Wound Bed Preparation and a Brief History of TIME. *International Wound Journal* **2004**, *1* (1), 19–32. https://doi.org/10.1111/j.1742-481x.2004.00008.x.

31.   Müller, I. Theory and Practice of Wound Healing in the Past. In *Wound Healing and Skin Physiology*; Altmeyer, P., Hoffmann, K., el Gammal, S., Hutchinson, J., Eds.; Springer: Berlin, Heidelberg, 1995; pp 3–18. https://doi.org/10.1007/978-3-642-77882-7_1.

32.   Mukhopadhyay, A.; Sikka, M. P.; Midha, V. K. 14 - Speciality Dressings for Managing Difficult-to-Heal Wounds. In *Advanced Textiles for Wound Care (Second Edition)*; Rajendran, S., Ed.; The Textile Institute Book Series; Woodhead Publishing, 2019; pp 391–421. https://doi.org/10.1016/B978-0-08-102192-7.00014-X.

33.   Lorenz, H. P.; Longaker, M. T. Wounds: Biology, Pathology, and Management. In *Essential Practice of Surgery: Basic Science and Clinical Evidence*; Li, M., Norton, J. A., Bollinger, R. R., Chang, A. E., Lowry, S. F., Mulvihill, S. J., Pass, H. I., Thompson, R. W., Eds.; Springer: New York, NY, 2003; pp 77–88. https://doi.org/10.1007/0-387-22744-X_7.

34.   Boateng, J.; Catanzano, O. Advanced Therapeutic Dressings for Effective Wound Healing—A Review. *Journal of Pharmaceutical Sciences* **2015**, *104* (11), 3653–3680. https://doi.org/10.1002/jps.24610.

35.   Powers, J. G.; Morton, L. M.; Phillips, T. J. Dressings for Chronic Wounds. *Dermatologic Therapy* **2013**, *26* (3), 197–206. https://doi.org/10.1111/dth.12055.

36.   Dressings Indications and Recommended Uses. LEAFLET ON GOOD PRACTICE IN HEALTHCARE TECHNOLOGY USE. HAS Recommandations. 2011.

37.   Vowden, K.; Vowden, P. Wound Dressings: Principles and Practice. *Surgery (Oxford)* **2017**, *35* (9), 489–494. https://doi.org/10.1016/j.mpsur.2017.06.005.

38.   Rezvani Ghomi, E.; Khalili, S.; Nouri Khorasani, S.; Esmaeely Neisiany, R.; Ramakrishna, S. Wound Dressings: Current Advances and Future Directions. *Journal of Applied Polymer Science* **2019**, *136* (27), 47738. https://doi.org/10.1002/app.47738.

39.   Singh, N.; Armstrong, D. G.; Lipsky, B. A. Preventing Foot Ulcers in Patients With Diabetes. JAMA 2005, 293 (2), 217–228. https://doi.org/10.1001/jama.293.2.217.

40.   Frykberg, R. G.; Zgonis, T.; Armstrong, D. G.; Driver, V. R.; Giurini, J. M.; Kravitz, S. R.; Landsman, A. S.; Lavery, L. A.; Moore, J. C.; Schuberth, J. M.; Wukich, D. K.; Andersen, C.; Vanore, J. V. Diabetic Foot Disorders: A Clinical Practice Guideline (2006 Revision). *The Journal of Foot and Ankle Surgery* **2006**, *45* (5, Supplement), S1–S66. https://doi.org/10.1016/S1067-2516(07)60001-5.

41.   South Tees NHSFT Wound Dressing Chart. 2015.

42.   Malleret, M.; Tixier, D. Petit Missel du Traitement de la Plaie Chronique; Clermont-Ferrand, 2013; p 24.

43.   Vowden, K.; Vowden, P. Wound Dressings: Principles and Practice. *Surgery (Oxford)* **2017**, *35* (9), 489–494. https://doi.org/10.1016/j.mpsur.2017.06.005.

44.   Chronic Wound Care Guidelines. The Wound Healing Society 2017.

45.   Moore, Z.; Dowsett, C.; Smith, G.; Atkin, L.; Bain, M.; Lahmann, N. A.; Schultz, G. S.; Swanson, T.; Vowden, P.; Weir, D.; Zmuda, A.; Jaimes, H. TIME CDST: An Updated Tool to Address the Current Challenges in Wound Care. *J Wound Care* **2019**, *28* (3), 154–161. https://doi.org/10.12968/jowc.2019.28.3.154.

46.   Crumbley, D. R.; Kane, M. A. Development of an Evidence-Based Pressure Ulcer Program at the National Naval Medical Center: Nurses' Role in Risk Factor Assessment, Prevention, and Intervention Among Young Service Members Returning from OIF/OEF. *Nursing Clinics of North America* **2010**, *45* (2), 153–168. https://doi.org/10.1016/j.cnur.2010.02.009.

47.   Mölnlycke Health Care. Encompass Wound Dressing Selection Guide. European pressure ulcer advisory panel 2019.

48.   Pressure Injury Staging Guide. Shield HealthCare 2006.

49.   Scharnatta, C.; BcSN, R. Skin & Wound Care Products in SCHR. 30.

50.   Wu, H.; Moser, C.; Wang, H.-Z.; Høiby, N.; Song, Z.-J. Strategies for Combating Bacterial Biofilm Infections. *International Journal of Oral Science* **2015**, *7* (1), 1–7. https://doi.org/10.1038/ijos.2014.65.

51.   Benjamin A. Lipsky, Christopher Hoey, Topical Antimicrobial Therapy for Treating Chronic Wounds, Clinical Infectious Diseases, Volume 49, Issue 10, 15 November 2009, Pages 1541–1549, https://doi.org/10.1086/644732

52.   Håkansson, J.; Ringstad, L.; Umerska, A.; Johansson, J.; Andersson, T.; Boge, L.; Rozenbaum, R. T.; Sharma, P. K.; Tollbäck, P.; Björn, C.; Saulnier, P.; Mahlapuu, M. Characterization of the in Vitro, Ex Vivo, and in Vivo Efficacy of the Antimicrobial Peptide DPK-060 Used for Topical Treatment. *Front Cell Infect Microbiol* **2019**, *9*. https://doi.org/10.3389/fcimb.2019.00174.

53.   Brackman, G.; Garcia-Fernandez, M. J.; Lenoir, J.; De Meyer, L.; Remon, J.-P.; De Beer, T.; Concheiro, A.; Alvarez-Lorenzo, C.; Coenye, T. Dressings Loaded with Cyclodextrin–Hamamelitannin Complexes Increase Staphylococcus Aureus Susceptibility Toward Antibiotics Both in Single as Well as in Mixed Biofilm Communities. *Macromolecular Bioscience* **2016**, *16* (6), 859–869. https://doi.org/10.1002/mabi.201500437.

54.   Chen, H.; Lan, G.; Ran, L.; Xiao, Y.; Yu, K.; Lu, B.; Dai, F.; Wu, D.; Lu, F. A Novel Wound Dressing Based on a Konjac Glucomannan/Silver Nanoparticle Composite Sponge Effectively Kills Bacteria and Accelerates Wound Healing. *Carbohydrate Polymers* **2018**, *183*, 70–80. https://doi.org/10.1016/j.carbpol.2017.11.029.

55.   Howell-Jones, R. S.; Wilson, M. J.; Hill, K. E.; Howard, A. J.; Price, P. E.; Thomas, D. W. A Review of the Microbiology, Antibiotic Usage and Resistance in Chronic Skin Wounds. *J Antimicrob Chemother* **2005**, *55* (2), 143–149. https://doi.org/10.1093/jac/dkh513.

56.   Zhou, Y.; Li, Y.; Zhang, L.; Wu, Z.; Huang, Y.; Yan, H.; Zhong, J.; Wang, L.-J.; Abdullah, H. M.; Wang, H. H. Antibiotic Administration Routes and Oral Exposure to Antibiotic Resistant Bacteria as Key Drivers for Gut Microbiota Disruption and Resistome in Poultry. *Frontiers in Microbiology* **2020**, *11*, 1319. https://doi.org/10.3389/fmicb.2020.01319.

57.   Tirelle, P.; Breton, J.; Riou, G.; Déchelotte, P.; Coëffier, M.; Ribet, D. Comparison of Different Modes of Antibiotic Delivery on Gut Microbiota Depletion Efficiency and Body Composition in Mouse. *BMC Microbiology* **2020**, *20* (1), 340. https://doi.org/10.1186/s12866-020-02018-9.

58.   Percival, S. L.; Emanuel, C.; Cutting, K. F.; Williams, D. W. Microbiology of the Skin and the Role of Biofilms in Infection. *International Wound Journal* **2012**, *9* (1), 14–32. https://doi.org/10.1111/j.1742-481X.2011.00836.x.

59.   Stewart, P. S.; William Costerton, J. Antibiotic Resistance of Bacteria in Biofilms. *The Lancet* **2001**, *358* (9276), 135–138. https://doi.org/10.1016/S0140-6736(01)05321-1.

60.   Laureti, L.; Matic, I.; Gutierrez, A. Bacterial Responses and Genome Instability Induced by Subinhibitory Concentrations of Antibiotics. *Antibiotics (Basel)* **2013**, *2* (1), 100–114. https://doi.org/10.3390/antibiotics2010100.

61.   Vasilchenko, A. S.; Rogozhin, E. A. Sub-Inhibitory Effects of Antimicrobial Peptides. *Front. Microbiol.* **2019**, *10*. https://doi.org/10.3389/fmicb.2019.01160.

62.   Zhanel, G. G.; Hoban, D. J.; Harding, G. K. Subinhibitory Antimicrobial Concentrations: A Review of in Vitro and in Vivo Data. *Can J Infect Dis* **1992**, *3* (4), 193–201.

63.   Hernandez, R. The Use of Systemic Antibiotics in the Treatment of Chronic Wounds. *Dermatologic Therapy* **2006**, *19* (6), 326–337. https://doi.org/10.1111/j.1529-8019.2006.00091.x.

64.   Kamoun, E. A.; Kenawy, E.-R. S.; Chen, X. A Review on Polymeric Hydrogel Membranes for Wound Dressing Applications: PVA-Based Hydrogel Dressings. *Journal of Advanced Research* **2017**, *8* (3), 217–233. https://doi.org/10.1016/j.jare.2017.01.005.

65.   Boateng, J.; Catanzano, O. Advanced Therapeutic Dressings for Effective Wound Healing—A Review. *Journal of Pharmaceutical Sciences* **2015**, *104* (11), 3653–3680. https://doi.org/10.1002/jps.24610.

66.   Moura, L. I. F.; Dias, A. M. A.; Carvalho, E.; de Sousa, H. C. Recent Advances on the Development of Wound Dressings for Diabetic Foot Ulcer Treatment—A Review. *Acta Biomaterialia* **2013**, *9* (7), 7093–7114. https://doi.org/10.1016/j.actbio.2013.03.033.

67.   Chen, H.; Cheng, R.; Zhao, X.; Zhang, Y.; Tam, A.; Yan, Y.; Shen, H.; Zhang, Y. S.; Qi, J.; Feng, Y.; Liu, L.; Pan, G.; Cui, W.; Deng, L. An Injectable Self-Healing Coordinative Hydrogel with Antibacterial and Angiogenic Properties for Diabetic Skin Wound Repair. *NPG Asia Materials* **2019**, *11* (1), 3. https://doi.org/10.1038/s41427-018-0103-9.

68.   Deng, Y.; Ren, J.; Chen, G.; Li, G.; Wu, X.; Wang, G.; Gu, G.; Li, J. Injectable in Situ Cross-Linking Chitosan-Hyaluronic Acid Based Hydrogels for Abdominal Tissue Regeneration. *Scientific Reports* **2017**, *7* (1), 2699. https://doi.org/10.1038/s41598-017-02962-z.

69.   Qu, J.; Zhao, X.; Liang, Y.; Zhang, T.; Ma, P. X.; Guo, B. Antibacterial Adhesive Injectable Hydrogels with Rapid Self-Healing, Extensibility and Compressibility as Wound Dressing for Joints Skin Wound Healing. *Biomaterials* **2018**, *183*, 185–199. https://doi.org/10.1016/j.biomaterials.2018.08.044.

70.   Gupta, S.; Webster, T. J.; Sinha, A. Evolution of PVA Gels Prepared without Crosslinking Agents as a Cell Adhesive Surface. *Journal of Materials Science: Materials in Medicine* **2011**, *22* (7), 1763–1772. https://doi.org/10.1007/s10856-011-4343-2.

71.   Das Ghatak, P.; Mathew-Steiner, S. S.; Pandey, P.; Roy, S.; Sen, C. K. A Surfactant Polymer Dressing Potentiates Antimicrobial Efficacy in Biofilm Disruption. *Scientific Reports* **2018**, *8* (1), 1–9. https://doi.org/10.1038/s41598-018-19175-7.

72.   Anjum, S.; Arora, A.; Alam, M. S.; Gupta, B. Development of Antimicrobial and Scar Preventive Chitosan Hydrogel Wound Dressings. *International Journal of Pharmaceutics* **2016**, *508* (1), 92–101. https://doi.org/10.1016/j.ijpharm.2016.05.013.

73.   Romić, M. D.; Klarić, M. Š.; Lovrić, J.; Pepić, I.; Cetina-Čižmek, B.; Filipović-Grčić, J.; Hafner, A. Melatonin-Loaded Chitosan/Pluronic® F127 Microspheres as in Situ Forming

Hydrogel: An Innovative Antimicrobial Wound Dressing. *European Journal of Pharmaceutics and Biopharmaceutics* **2016**, *107*, 67–79. https://doi.org/10.1016/j.ejpb.2016.06.013.

74.   Kim, H.; Izadjoo, M. Antimicrobial Activity of a Bioelectric Dressing Using an in Vitro Wound Pathogen Colony Drip-Flow Reactor Biofilm Model. *Journal of Wound Care* **2016**. https://doi.org/10.12968/jowc.2016.25.Sup7.S47.

75.   Zhao, X.; Wu, H.; Guo, B.; Dong, R.; Qiu, Y.; Ma, P. X. Antibacterial Anti-Oxidant Electroactive Injectable Hydrogel as Self-Healing Wound Dressing with Hemostasis and Adhesiveness for Cutaneous Wound Healing. *Biomaterials* **2017**, *122*, 34–47. https://doi.org/10.1016/j.biomaterials.2017.01.011.

76.   Ashrafi, M.; Novak-Frazer, L.; Morris, J.; Baguneid, M.; Rautemaa-Richardson, R.; Bayat, A. Electrical Stimulation Disrupts Biofilms in a Human Wound Model and Reveals the Potential for Monitoring Treatment Response with Volatile Biomarkers. *Wound Repair and Regeneration* **2019**, *27* (1), 5–18. https://doi.org/10.1111/wrr.12679.

77.   Van Vlierberghe, S.; Dubruel, P.; Schacht, E. Biopolymer-Based Hydrogels As Scaffolds for Tissue Engineering Applications: A Review. *Biomacromolecules* **2011**, *12* (5), 1387–1408. https://doi.org/10.1021/bm200083n.

78.   Miguel, S. P.; Figueira, D. R.; Simões, D.; Ribeiro, M. P.; Coutinho, P.; Ferreira, P.; Correia, I. J. Electrospun Polymeric Nanofibres as Wound Dressings: A Review. *Colloids and Surfaces B: Biointerfaces* **2018**, *169*, 60–71. https://doi.org/10.1016/j.colsurfb.2018.05.011.

79.   Ahmed, A.; Mandal, U.; Taher, M.; Susanti, D.; Jaffri, J. PVA-PEG Physically Cross-Linked Hydrogel Film as a Wound Dressing: Experimental Design and Optimization. *Pharmaceutical Development and Technology* **2017**, *23*, 1–25. https://doi.org/10.1080/10837450.2017.1295067.

80.   Superabsorbent Crosslinked Carboxymethyl Cellulose-PEG Hydrogels for Potential Wound Dressing Applications. *International Journal of Biological Macromolecules* **2018**, *106*, 1218–1234. https://doi.org/10.1016/j.ijbiomac.2017.08.124.

81.   Shirazaki, P.; Varshosaz, J.; Kharazi, A. Z. Electrospun Gelatin/Poly(Glycerol Sebacate) Membrane with Controlled Release of Antibiotics for Wound Dressing. *Adv Biomed Res* **2017**, *6*. https://doi.org/10.4103/abr.abr_197_16.

82.   Hodgkinson, T.; Yuan, X.-F.; Bayat, A. Electrospun Silk Fibroin Fiber Diameter Influences in Vitro Dermal Fibroblast Behavior and Promotes Healing of Ex Vivo Wound Models. *Journal of Tissue Engineering* **2014**, *5*, 204173141455166. https://doi.org/10.1177/2041731414551661.

83.   Patel, M.; Nakaji-Hirabayashi, T.; Matsumura, K. Effect of Dual-Drug-Releasing Micelle–Hydrogel Composite on Wound Healing in Vivo in Full-Thickness Excision Wound Rat Model. *Journal of Biomedical Materials Research Part A* **2019**, *107* (5), 1094–1106. https://doi.org/10.1002/jbm.a.36639.

84.   Bahadoran, M.; Shamloo, A.; Nokoorani, Y. D. Development of a Polyvinyl Alcohol/Sodium Alginate Hydrogel-Based Scaffold Incorporating BFGF-Encapsulated Microspheres for Accelerated Wound Healing. *Scientific Reports* **2020**, *10* (1), 7342. https://doi.org/10.1038/s41598-020-64480-9.

85.   Blacklow, S. O.; Li, J.; Freedman, B. R.; Zeidi, M.; Chen, C.; Mooney, D. J. Bioinspired Mechanically Active Adhesive Dressings to Accelerate Wound Closure. *Science Advances* 2019, *5* (7), eaaw3963. https://doi.org/10.1126/sciadv.aaw3963.

86.   A Novel Wound Dressing Based on Ag/Graphene Polymer Hydrogel: Effectively Kill Bacteria and Accelerate Wound Healing - Fan - 2014 - Advanced Functional Materials - Wiley Online Library.

87.   Zwitterionic Nanocomposite Hydrogels as Effective Wound Dressings - Journal of Materials Chemistry B (RSC Publishing).

88.   Wilkinson, H. N.; Iveson, S.; Catherall, P.; Hardman, M. J. A Novel Silver Bioactive Glass Elicits Antimicrobial Efficacy Against Pseudomonas Aeruginosa and Staphylococcus Aureus in an Ex Vivo Skin Wound Biofilm Model. *Front. Microbiol.* **2018**, *9*. https://doi.org/10.3389/fmicb.2018.01450.

89.   You, C.; Li, Q.; Wang, X.; Wu, P.; Ho, J. K.; Jin, R.; Zhang, L.; Shao, H.; Han, C. Silver Nanoparticle Loaded Collagen/Chitosan Scaffolds Promote Wound Healing via Regulating Fibroblast Migration and Macrophage Activation. *Sci Rep* **2017**, *7* (1), 1–11. https://doi.org/10.1038/s41598-017-10481-0.

90.   Brouillard, C.; Bursztejn, A.-C.; Latarche, C.; Cuny, J.-F.; Truchetet, F.; Goullé, J.-P.; Schmutz, J.-L. Silver Absorption and Toxicity Evaluation of Silver Wound Dressings in 40 Patients with Chronic Wounds. *Journal of the European Academy of Dermatology and Venereology* **2018**, *32* (12), 2295–2299. https://doi.org/10.1111/jdv.15055.

91.   Percival, S. L.; Slone, W.; Linton, S.; Okel, T.; Corum, L.; Thomas, J. G. The Antimicrobial Efficacy of a Silver Alginate Dressing against a Broad Spectrum of Clinically Relevant Wound Isolates. *International Wound Journal* **2011**, *8* (3), 237–243. https://doi.org/10.1111/j.1742-481X.2011.00774.x.

92.   Shamloo, A.; Sarmadi, M.; Aghababaie, Z.; Vossoughi, M. Accelerated Full-Thickness Wound Healing via Sustained BFGF Delivery Based on a PVA/Chitosan/Gelatin Hydrogel Incorporating PCL Microspheres. *International Journal of Pharmaceutics* **2018**, *537* (1), 278–289. https://doi.org/10.1016/j.ijpharm.2017.12.045.

93.   Hsieh, H.-T.; Chang, H.-M.; Lin, W.-J.; Hsu, Y.-T.; Mai, F.-D. Poly-Methyl Methacrylate/Polyvinyl Alcohol Copolymer Agents Applied on Diabetic Wound Dressing. *Sci Rep* **2017**, *7* (1), 9531. https://doi.org/10.1038/s41598-017-10193-5.

94.   Liu, H.; Wang, C.; Li, C.; Qin, Y.; Wang, Z.; Yang, F.; Li, Z.; Wang, J. A Functional Chitosan-Based Hydrogel as a Wound Dressing and Drug Delivery System in the Treatment of Wound Healing. *RSC Adv.* **2018**, *8* (14), 7533–7549. https://doi.org/10.1039/C7RA13510F.

95.   Chen, H.; Guo, L.; Wicks, J.; Ling, C.; Zhao, X.; Yan, Y.; Qi, J.; Cui, W.; Deng, L. Quickly Promoting Angiogenesis by Using a DFO-Loaded Photo-Crosslinked Gelatin Hydrogel for Diabetic Skin Regeneration. *J. Mater. Chem. B* **2016**, *4* (21), 3770–3781. https://doi.org/10.1039/C6TB00065G.

96.   Kamoun, E. A.; Kenawy, E.-R. S.; Chen, X. A Review on Polymeric Hydrogel Membranes for Wound Dressing Applications: PVA-Based Hydrogel Dressings. *Journal of Advanced Research* **2017**, *8* (3), 217–233. https://doi.org/10.1016/j.jare.2017.01.005.

97.   Tavakoli, S.; Klar, A. S. Advanced Hydrogels as Wound Dressings. *Biomolecules* **2020**, *10* (8), 1169. https://doi.org/10.3390/biom10081169.

98.   Li, J.; Mooney, D. J. Designing Hydrogels for Controlled Drug Delivery. *Nature Reviews Materials* **2016**, *1* (12), 16071. https://doi.org/10.1038/natrevmats.2016.71.

99.   Gupta, P.; Vermani, K.; Garg, S. Hydrogels: From Controlled Release to PH-Responsive Drug Delivery. *Drug Discovery Today* **2002**, *7* (10), 569–579. https://doi.org/10.1016/S1359-6446(02)02255-9.

100.   Ahmed, E. M. Hydrogel: Preparation, Characterization, and Applications: A Review. *Journal   of   Advanced   Research*   **2015**,   *6*   (2),   105–121. https://doi.org/10.1016/j.jare.2013.07.006.

101.   Haque, Md. O.; Mondal, Md. I. H. Cellulose-Based Hydrogel for Personal Hygiene Applications. In *Cellulose-Based Superabsorbent Hydrogels*; Mondal, Md. I. H., Ed.; Polymers and Polymeric Composites: A Reference Series; Springer International Publishing: Cham, 2019; pp 1339–1359. https://doi.org/10.1007/978-3-319-77830-3_44.

102.   Sood, N.; Bhardwaj, A.; Mehta, S.; Mehta, A. Stimuli-Responsive Hydrogels in Drug Delivery   and   Tissue   Engineering.   *Drug   Deliv*   **2016**,   *23*   (3),   758–780. https://doi.org/10.3109/10717544.2014.940091.

103.   Shiekh, P. A.; Andrabi, S. M.; Singh, A.; Majumder, S.; Kumar, A. Designing Cryogels through Cryostructuring of Polymeric Matrices for Biomedical Applications. *European Polymer Journal* **2021**, *144*, 110234. https://doi.org/10.1016/j.eurpolymj.2020.110234.

104.   Gun'ko, V. M.; Savina, I. N.; Mikhalovsky, S. V. Cryogels: Morphological, Structural and Adsorption Characterisation. *Advances in Colloid and Interface Science* **2013**, *187–188*, 1–46. https://doi.org/10.1016/j.cis.2012.11.001.

105.   Tao, J.; Hu, Y.; Wang, S.; Zhang, J.; Liu, X.; Gou, Z.; Cheng, H.; Liu, Q.; Zhang, Q.; You, S.; Gou, M. A 3D-Engineered Porous Conduit for Peripheral Nerve Repair. *Sci Rep* **2017**, *7* (1), 46038. https://doi.org/10.1038/srep46038.

106.   de Lima, G. G.; Traon, F.; Moal, E.; Canillas, M.; Rodriguez, M. A.; McCarthy, H. O.; Dunne, N.; Devine, D. M.; Nugent, M. J. D. Composite Cryogels for Dual Drug Delivery and Enhanced Mechanical Properties. *Polymer Composites* **2018**, *39* (S1), E210–E220. https://doi.org/10.1002/pc.24450.

107.   Liu, J.; Fan, X.; Tao, Y.; Deng, C.; Yu, K.; Zhang, W.; Deng, L.; Xiong, W. Two-Step Freezing Polymerization Method for Efficient Synthesis of High-Performance Stimuli-Responsive Hydrogels. *ACS Omega* **2020**, *5* (11), 5921–5930. https://doi.org/10.1021/acsomega.9b04224.

108.   Koshy, S. T.; Ferrante, T. C.; Lewin, S. A.; Mooney, D. J. Injectable, Porous, and Cell-Responsive Gelatin Cryogels. *Biomaterials* **2014**, *35* (8), 2477–2487. https://doi.org/10.1016/j.biomaterials.2013.11.044.

109.   Hixon, K. R.; Lu, T.; Sell, S. A. A Comprehensive Review of Cryogels and Their Roles in Tissue Engineering Applications. *Acta Biomaterialia* **2017**, *62*, 29–41. https://doi.org/10.1016/j.actbio.2017.08.033.

110.   Lozinsky, V. I.; Faleev, N. G.; Zubov, A. L.; Ruvinov, S. B.; Antonova, T. V.; Vainerman, E. S.; Belikov, V. M.; Rogozhin, S. V. Use of PVA-Cryogel Entrapped Citrobacter Intermedius Cells for Continuous Production of 3-Fluoro-L-Tyrosine. *Biotechnol Lett* **1989**, *11* (1), 43–48. https://doi.org/10.1007/BF01026784.

111.   You, H.-J.; Han, S.-K. Cell Therapy for Wound Healing. *J Korean Med Sci* **2014**, *29* (3), 311–319. https://doi.org/10.3346/jkms.2014.29.3.311.

112.   Gibbons, G. W. Grafix®, a Cryopreserved Placental Membrane, for the Treatment of Chronic/Stalled Wounds. *Adv Wound Care (New Rochelle)* **2015**, *4* (9), 534–544. https://doi.org/10.1089/wound.2015.0647.

113.   Kosaric, N.; Kiwanuka, H.; Gurtner, G. C. Stem Cell Therapies for Wound Healing. *Expert Opinion on Biological Therapy* **2019**, *19* (6), 575–585. https://doi.org/10.1080/14712598.2019.1596257.

114.   Piaggesi, A.; Läuchli, S.; Bassetto, F.; Biedermann, T.; Marques, A.; Najafi, B.; Palla, I.; Scarpa, C.; Seimetz, D.; Triulzi, I.; Turchetti, G.; Vaggelas, A. EWMA Document: Advanced Therapies in Wound Management: Cell and Tissue Based Therapies, Physical and Bio-Physical Therapies Smart and IT Based Technologies. *J Wound Care* **2018**, *27(6), Suppl6*.

115.   Fu, Y.; Sui, B.; Xiang, L.; Yan, X.; Wu, D.; Shi, S.; Hu, X. Emerging Understanding of Apoptosis in Mediating Mesenchymal Stem Cell Therapy. *Cell Death Dis* **2021**, *12* (6), 1–12. https://doi.org/10.1038/s41419-021-03883-6.

116.   Lim, J. M.; Lee, M.; Lee, E. J.; Gong, S. P.; Lee, S. T. Stem Cell Engineering: Limitation, Alternatives, and Insight. *Annals of the New York Academy of Sciences* **2011**, *1229* (1), 89–98. https://doi.org/10.1111/j.1749-6632.2011.06093.x.

117.   Milan, P. B.; Lotfibakhshaiesh, N.; Joghataie, M. T.; Ai, J.; Pazouki, A.; Kaplan, D. L.; Kargozar, S.; Amini, N.; Hamblin, M. R.; Mozafari, M.; Samadikuchaksaraei, A. Accelerated Wound Healing in a Diabetic Rat Model Using Decellularized Dermal Matrix and Human Umbilical Cord Perivascular Cells. *Acta Biomaterialia* **2016**, *45*, 234–246. https://doi.org/10.1016/j.actbio.2016.08.053.

118.   Yoon, D.; Cho, Y. S.; Joo, S. Y.; Seo, C. H.; Cho, Y. S. A Clinical Trial with a Novel Collagen Dermal Substitute for Wound Healing in Burn Patients. *Biomater. Sci.* **2020**, *8* (3), 823–829. https://doi.org/10.1039/C9BM01209E.

119.   Vig, K.; Chaudhari, A.; Tripathi, S.; Dixit, S.; Sahu, R.; Pillai, S.; Dennis, V.; Singh, S. Advances in Skin Regeneration Using Tissue Engineering. *IJMS* **2017**, *18* (4), 789. https://doi.org/10.3390/ijms18040789.

120.   Petrofsky, J. S.; Lawson, D.; Berk, L.; Suh, H. Enhanced Healing of Diabetic Foot Ulcers Using Local Heat and Electrical Stimulation for 30 Min Three Times per Week. *J Diabetes* **2010**, *2* (1), 41–46. https://doi.org/10.1111/j.1753-0407.2009.00058.x.

121.   Alkahtani, S. A.; Kunwar, P. S.; Jalilifar, M.; Rashidi, S.; Yadollahpour, A. Ultrasound-Based Techniques as Alternative Treatments for Chronic Wounds: A Comprehensive Review of Clinical Applications. *Cureus* *9* (12), e1952. https://doi.org/10.7759/cureus.1952.

122.   McCallon, S. K. Negative-Pressure Wound Therapy. In *Wound Healing Evidence-Based Management, 4e*; McCulloch, J. M., Kloth, L. C., Eds.; McGraw-Hill Education: New York, NY, 2010.

123.   Kadry, A. M. The Clinical Efficacy of Pulsed Radio Frequency Energy on Chronic Wound Healing. *International Journal of PharmTech Research* **2016**, 8.

124.   Wang, C.-J.; Kuo, Y.-R.; Wu, R.-W.; Liu, R.-T.; Hsu, C.-S.; Wang, F.-S.; Yang, K. D. Extracorporeal Shockwave Treatment for Chronic Diabetic Foot Ulcers. *Journal of Surgical Research* **2009**, *152* (1), 96–103. https://doi.org/10.1016/j.jss.2008.01.026.

125.   Callaghan, M. J.; Chang, E. I.; Seiser, N.; Aarabi, S.; Ghali, S.; Kinnucan, E. R.; Simon, B. J.; Gurtner, G. C. Pulsed Electromagnetic Fields Accelerate Normal and Diabetic Wound Healing by Increasing Endogenous FGF-2 Release. *Plast Reconstr Surg* **2008**, *121* (1), 130–141. https://doi.org/10.1097/01.prs.0000293761.27219.84.

126.   Kuffler, D. P. Photobiomodulation in Promoting Wound Healing: A Review. *Regen Med* **2016**, *11* (1), 107–122. https://doi.org/10.2217/rme.15.82.

127.   Abidia, A.; Laden, G.; Kuhan, G.; Johnson, B. F.; Wilkinson, A. R.; Renwick, P. M.; Masson, E. A.; McCollum, P. T. The Role of Hyperbaric Oxygen Therapy in Ischaemic Diabetic Lower Extremity Ulcers: A Double-Blind Randomised-Controlled Trial. European Journal of Vascular and Endovascular Surgery 2003, 25 (6), 513–518. https://doi.org/10.1053/ejvs.2002.1911.

128.   Melling, A. C.; Ali, B.; Scott, E. M.; Leaper, D. J. Effects of Preoperative Warming on the Incidence of Wound Infection after Clean Surgery: A Randomised Controlled Trial. *The Lancet* **2001**, *358* (9285), 876–880. https://doi.org/10.1016/S0140-6736(01)06071-8.

129.   Kurz, A.; Sessler, D. I.; Lenhardt, R. Perioperative Normothermia to Reduce the Incidence of Surgical-Wound Infection and Shorten Hospitalization. *http://dx.doi.org.ressources-electroniques.univ-lille.fr/10.1056/NEJM199605093341901* **2009**. https://doi.org/10.1056/NEJM199605093341901.

130. Sheffield, C. W.; Sessler, D. I.; Hopf, H. W.; Schroeder, M.; Moayeri, A.; Hunt, T. K.; West, J. M. Centrally and Locally Mediated Thermoregulatory Responses Alter Subcutaneous Oxygen Tension. *Wound Repair and Regeneration* **1996**, *4* (3), 339–345. https://doi.org/10.1046/j.1524-475X.1996.40310.x.

131. Rabkin, J. M.; Hunt, T. K. Local Heat Increases Blood Flow and Oxygen Tension in Wounds. *Archives of Surgery* **1987**, *122* (2), 221–225. https://doi.org/10.1001/archsurg.1987.01400140103014.

132. Ikeda, T.; Tayefeh, F.; Sessler, D. I.; Kurz, A.; Plattner, O.; Petschnigg, B.; Hopf, H. W.; West, J. Local Radiant Heating Increases Subcutaneous Oxygen Tension. *The American Journal of Surgery* **1998**, *175* (1), 33–37. https://doi.org/10.1016/S0002-9610(97)00237-7.

133. Bornmyr, S.; Svensson, H.; Lilja, B.; Sundkvist, G. Skin Temperature Changes and Changes in Skin Blood Flow Monitored with Laser Doppler Flowmetry and Imaging: A Methodological Study in Normal Humans. *Clinical Physiology* **1997**, *17* (1), 71–81. https://doi.org/10.1046/j.1365-2281.1997.01313.x.

134. Xia, Z.; Sato, A.; Hughes, M. A.; Cherry, G. W. Stimulation of Fibroblast Growth in Vitro by Intermittent Radiant Warming. *Wound Repair and Regeneration* **2000**, *8* (2), 138–144. https://doi.org/10.1046/j.1524-475x.2000.00138.x.

135. Hiragami, F.; Motoda, H.; Takezawa, T.; Takabayashi, C.; Inoue, S.; Wakatake, Y.; Kano, Y. Heat Shock-Induced Three-Dimensional-Like Proliferation of Normal Human Fibroblasts Mediated by Pressed Silk. *Int J Mol Sci* **2009**, *10* (11), 4963–4976. https://doi.org/10.3390/ijms10114963.

136. Watts, A. M. I.; Tyler, M. P. H.; Perry, M. E.; Roberts, A. H. N.; McGrouther, D. A. Burn Depth and Its Histological Measurement. *Burns* **2001**, *27* (2), 154–160. https://doi.org/10.1016/S0305-4179(00)00079-6.

137. Rosenspire, A. J.; Kindzelskii, A. L.; Petty, H. R. Cutting Edge: Fever-Associated Temperatures Enhance Neutrophil Responses to Lipopolysaccharide: A Potential Mechanism Involving Cell Metabolism. *Journal of Immunology* **2002**, *169* (10), 5396–5400. https://doi.org/10.4049/JIMMUNOL.169.10.5396.

138. Evans, S. S.; Repasky, E. A.; Fisher, D. T. Fever and the Thermal Regulation of Immunity: The Immune System Feels the Heat. *Nat Rev Immunol* **2015**, *15* (6), 335–349. https://doi.org/10.1038/nri3843.

139. Scieglinska, D.; Krawczyk, Z.; Sojka, D. R.; Gogler-Pigłowska, A. Heat Shock Proteins in the Physiology and Pathophysiology of Epidermal Keratinocytes. *Cell Stress and Chaperones* **2019**, *24* (6), 1027–1044. https://doi.org/10.1007/s12192-019-01044-5.

140. Bhatia, A.; O'Brien, K.; Guo, J.; Lincoln, V.; Kajiwara, C.; Chen, M.; Woodley, D. T.; Udono, H.; Li, W. Extracellular and Non-Chaperone Function of Heat Shock Protein−90α Is Required for Skin Wound Healing. *Journal of Investigative Dermatology* **2018**, *138* (2), 423–433. https://doi.org/10.1016/j.jid.2017.08.043.

141.   Bellaye, P.-S.; Burgy, O.; Causse, S.; Garrido, C.; Bonniaud, P. Heat Shock Proteins in Fibrosis and Wound Healing: Good or Evil? *Pharmacology & Therapeutics* **2014**, *143* (2), 119–132. https://doi.org/10.1016/j.pharmthera.2014.02.009.

142.   Singh, K.; Agrawal, N. K.; Gupta, S. K.; Mohan, G.; Chaturvedi, S.; Singh, K. Decreased Expression of Heat Shock Proteins May Lead to Compromised Wound Healing in Type 2 Diabetes Mellitus Patients. *Journal of Diabetes and its Complications* **2015**, *29* (4), 578–588. https://doi.org/10.1016/j.jdiacomp.2015.01.007.

143.   Identification of the Critical Therapeutic Entity in Secreted Hsp90α That Promotes Wound Healing in Newly Re-Standardized Healthy and Diabetic Pig Models.

144.   Lindquist, S. THE HEAT-SHOCK RESPONSE. *Annu Rev Biochem.* **1986**, 44. https://doi.org/10.1146/annurev.bi.55.070186.005443.

145.   Tsan, M.-F.; Gao, B. Heat Shock Proteins and Immune System. *Journal of Leukocyte Biology* **2009**, *85* (6), 905–910. https://doi.org/10.1189/jlb.0109005.

146.   Guo, J.; Chang, C.; Li, W. The Role of Secreted Heat Shock Protein-90 (Hsp90) in Wound Healing - How Could It Shape Future Therapeutics? *Expert Rev Proteomics* **2017**, *14* (8), 665–675. https://doi.org/10.1080/14789450.2017.1355244.

147.   Schieke, S. M.; Schroeder, P.; Krutmann, J. Cutaneous Effects of Infrared Radiation: From Clinical Observations to Molecular Response Mechanisms. *Photodermatology, Photoimmunology & Photomedicine* **2003**, *19* (5), 228–234. https://doi.org/10.1034/j.1600-0781.2003.00054.x.

148.   Wang, C.-Y.; Tsai, S.-C.; Yu, M.-C.; Lin, Y.-F.; Chen, C.-C.; Chang, P.-C. Light-Emitting Diode Irradiation Promotes Donor Site Wound Healing of the Free Gingival Graft. *Journal of Periodontology* **2015**, *86* (5), 674–681. https://doi.org/10.1902/jop.2015.140580.

149.   Bhatia, A.; O'Brien, K.; Chen, M.; Wong, A.; Garner, W.; Woodley, D. T.; Li, W. Dual Therapeutic Functions of F-5 Fragment in Burn Wounds: Preventing Wound Progression and Promoting Wound Healing in Pigs. *Molecular Therapy - Methods & Clinical Development* **2016**, *3.* https://doi.org/10.1038/mtm.2016.41.

150.   Lee, J. H.; Jekal, S. J.; Kwon, P. S. The Effect of 630nm Light Emitting Diode (LED) Irradiation on Dermal Wound Healing. *Physiotherapy* **2015**, *101*, e847. https://doi.org/10.1016/j.physio.2015.03.1667.

151.   Souil, E.; Capon, A.; Mordon, S.; Dinh-Xuan, A. T.; Polla, B. S.; Bachelet, M. Treatment with 815-Nm Diode Laser Induces Long-Lasting Expression of 72-KDa Heat Shock Protein in Normal Rat Skin. *British Journal of Dermatology* **2001**, *144* (2), 260–266. https://doi.org/10.1046/j.1365-2133.2001.04010.x.

152.   Khan, A. A.; Banwell, P. E.; Bakker, M. C.; Gillespie, P. G.; McGrouther, D. A.; Roberts, A. H. Topical Radiant Heating in Wound Healing: An Experimental Study in a Donor Site Wound Model. *Int Wound J* **2004**, *1* (4), 233–240. https://doi.org/10.1111/j.1742-4801.2004.00065.x.

153. Yadav, A.; Gupta, A. Noninvasive Red and Near-Infrared Wavelength-Induced Photobiomodulation: Promoting Impaired Cutaneous Wound Healing. *Photodermatology, Photoimmunology & Photomedicine* **2017**, *33* (1), 4–13. https://doi.org/10.1111/phpp.12282.

154. Sowa, M. G.; Kuo, W.-C.; Ko, A. C.; Armstrong, D. G. Review of Near-Infrared Methods for Wound Assessment. *JBO* **2016**, *21* (9), 091304. https://doi.org/10.1117/1.JBO.21.9.091304.

155. Zhao, X.; Liang, Y.; Huang, Y.; He, J.; Han, Y.; Guo, B. Physical Double-Network Hydrogel Adhesives with Rapid Shape Adaptability, Fast Self-Healing, Antioxidant and NIR/PH Stimulus-Responsiveness for Multidrug-Resistant Bacterial Infection and Removable Wound Dressing. Advanced Functional Materials 2020, 30 (17), 1910748. https://doi.org/10.1002/adfm.201910748.

156. Sheng, L.; Zhang, Z.; Zhang, Y.; Wang, E.; Ma, B.; Xu, Q.; Ma, L.; Zhang, M.; Pei, G.; Chang, J. A Novel "Hot Spring"-Mimetic Hydrogel with Excellent Angiogenic Properties for Chronic Wound Healing. *Biomaterials* **2021**, *264*, 120414. https://doi.org/10.1016/j.biomaterials.2020.120414.

157. Sun, Z.; Yue, J.; Zhang, Q. Local Warming Therapy for Treating Chronic Wounds. *Cochrane Database Syst Rev* **2017**, *2017* (7), CD011728. https://doi.org/10.1002/14651858.CD011728.pub2.

158. Yue, J.; Zhang, S.; Sun, Q.; Sun, Z.; Wang, X.; Golianu, B.; Lu, Y.; Zhang, Q. Local Warming Therapy for Treating Chronic Wounds. *Medicine (Baltimore)* **2018**, *97* (12), e9931. https://doi.org/10.1097/MD.0000000000009931.

159. Pattani, V. P.; Tunnell, J. W. Nanoparticle-Mediated Photothermal Therapy: A Comparative Study of Heating for Different Particle Types. *Lasers in Surgery and Medicine* **2012**, *44* (8), 675–684. https://doi.org/10.1002/lsm.22072.

160. Chen, J.; Ning, C.; Zhou, Z.; Yu, P.; Zhu, Y.; Tan, G.; Mao, C. Nanomaterials as Photothermal Therapeutic Agents. *Progress in Materials Science* **2019**, *99*, 1–26. https://doi.org/10.1016/j.pmatsci.2018.07.005.

161. Yin, W.; Yan, L.; Yu, J.; Tian, G.; Zhou, L.; Zheng, X.; Zhang, X.; Yong, Y.; Li, J.; Gu, Z.; Zhao, Y. High-Throughput Synthesis of Single-Layer MoS2 Nanosheets as a Near-Infrared Photothermal-Triggered Drug Delivery for Effective Cancer Therapy. *ACS Nano* **2014**, *8* (7), 6922–6933. https://doi.org/10.1021/nn501647j.

162. Teodorescu, F.; Quéniat, G.; Foulon, C.; Lecoeur, M.; Barras, A.; Boulahneche, S.; Medjram, M. S.; Hubert, T.; Abderrahmani, A.; Boukherroub, R.; Szunerits, S. Transdermal Skin Patch Based on Reduced Graphene Oxide: A New Approach for Photothermal Triggered Permeation of Ondansetron across Porcine Skin. *Journal of Controlled Release* **2017**, *245* (Supplement C), 137–146. https://doi.org/10.1016/j.jconrel.2016.11.029.

163. Whitney, J. D.; Wickline, M. M. Treating Chronic and Acute Wounds with Warming: Review of the Science and Practice Implications. *Journal of WOCN* **2003**, *30* (4), 199–209. https://doi.org/10.1067/mjw.2003.134.

164. Capon, A.; Mordon, S. Can Thermal Lasers Promote Skin Wound Healing?: *American Journal of Clinical Dermatology* **2003**, *4* (1), 1–12. https://doi.org/10.2165/00128071-200304010-00001.

165. Tao, B.; Lin, C.; Deng, Y.; Yuan, Z.; Shen, X.; Chen, M.; He, Y.; Peng, Z.; Hu, Y.; Cai, K. Copper-Nanoparticle-Embedded Hydrogel for Killing Bacteria and Promoting Wound Healing with Photothermal Therapy. *J. Mater. Chem. B* **2019**, *7* (15), 2534–2548. https://doi.org/10.1039/C8TB03272F.

166. Zhang, X.; Tan, B.; Wu, Y.; Zhang, M.; Liao, J. A Review on Hydrogels with Photothermal Effect in Wound Healing and Bone Tissue Engineering. *Polymers* **2021**, *13* (13), 2100. https://doi.org/10.3390/polym13132100.

167. Thomas, D. R.; Diebold, M. R.; Eggemeyer, L. M. A Controlled, Randomized, Comparative Study of a Radiant Heat Bandage on the Healing of Stage 3–4 Pressure Ulcers: A Pilot Study. *Journal of the American Medical Directors Association* **2005**, *6* (1), 46–49. https://doi.org/10.1016/j.jamda.2004.12.007.

168. Kloth, L. C.; Berman, J. E.; Nett, M.; Papanek, P. E.; Dumit-Minkel, S. A Randomized Controlled Clinical Trial to Evaluate the Effects of Noncontact Normothermic Wound Therapy on Chronic Full-Thickness Pressure Ulcers: *Advances in Skin & Wound Care* **2002**, *15* (6), 270–276. https://doi.org/10.1097/00129334-200211000-00008.

169. Ellis, S. L.; Finn, P.; Noone, M.; Leaper, D. J. Eradication of Methicillin-Resistant Staphylococcus Aureus from Pressure Sores Using Warming Therapy. *https://home.liebertpub.com/sur* **2004**. https://doi.org/10.1089/109629603764655281.

170. Petrofsky, J. S.; Lawson, D.; Suh, H. J.; Rossi, C.; Zapata, K.; Broadwell, E.; Littleton, L. The Influence of Local Versus Global Heat on the Healing of Chronic Wounds in Patients with Diabetes. *https://home.liebertpub.com/dia* **2007**. https://doi.org/10.1089/dia.2007.0231.

171. Khan, A. A.; Banwell, P. E.; Bakker, M. C.; Gillespie, P. G.; McGrouther, D. A.; Roberts, A. H. Topical Radiant Heating in Wound Healing: An Experimental Study in a Donor Site Wound Model. *Int Wound J* **2004**, *1* (4), 233–240. https://doi.org/10.1111/j.1742-4801.2004.00065.x.

172. Whitney, J. D.; Salvadalena, G.; Higa, L.; Mich, M. Treatment of Pressure Ulcers with Noncontact Normothermic Wound Therapy: Healing and Warming Effects. *Journal of Wound Ostomy & Continence Nursing* **2001**, *28* (5), 244–252.

173. Scott, E. M.; Leaper, D. J.; Clark, M.; Kelly, P. J. Effects of Warming Therapy on Pressure Ulcers—a Randomized Trial. *AORN Journal* **2001**, *73* (5), 921–938. https://doi.org/10.1016/S0001-2092(06)61744-4.

174. Alkilani, A. Z.; McCrudden, M. T. C.; Donnelly, R. F. Transdermal Drug Delivery: Innovative Pharmaceutical Developments Based on Disruption of the Barrier Properties of the Stratum Corneum. *Pharmaceutics* **2015**, *7* (4), 438–470. https://doi.org/10.3390/pharmaceutics7040438.

175.   Boateng, J. S.; Matthews, K. H.; Stevens, H. N. E.; Eccleston, G. M. Wound Healing Dressings and Drug Delivery Systems: A Review. *Journal of Pharmaceutical Sciences* **2008**, *97* (8), 2892–2923. https://doi.org/10.1002/jps.21210.

176.   Contardi, M.; Kossyvaki, D.; Picone, P.; Summa, M.; Guo, X.; Heredia-Guerrero, J. A.; Giacomazza, D.; Carzino, R.; Goldoni, L.; Scoponi, G.; Rancan, F.; Bertorelli, R.; Di Carlo, M.; Athanassiou, A.; Bayer, I. S. Electrospun Polyvinylpyrrolidone (PVP) Hydrogels Containing Hydroxycinnamic Acid Derivatives as Potential Wound Dressings. *Chemical Engineering Journal* **2021**, *409*, 128144. https://doi.org/10.1016/j.cej.2020.128144.

177.   Prausnitz, M. R.; Langer, R. Transdermal Drug Delivery. *Nat Biotechnol* **2008**, *26* (11), 1261–1268. https://doi.org/10.1038/nbt.1504.

178.   Pastore, M. N.; Kalia, Y. N.; Horstmann, M.; Roberts, M. S. Transdermal Patches: History, Development and Pharmacology. *Br J Pharmacol* **2015**, *172* (9), 2179–2209. https://doi.org/10.1111/bph.13059.

179.   Jijie, R.; Barras, A.; Boukherroub, R.; Szunerits, S. Nanomaterials for Transdermal Drug Delivery: Beyond the State of the Art of Liposomal Structures. *J. Mater. Chem. B* **2017**, *5* (44), 8653–8675. https://doi.org/10.1039/C7TB02529G.

180.   Szunerits, S.; Boukherroub, R. Heat: A Highly Efficient Skin Enhancer for Transdermal Drug Delivery. *Front Bioeng Biotechnol* **2018**, *6*. https://doi.org/10.3389/fbioe.2018.00015.

181.   Waghule, T.; Singhvi, G.; Dubey, S. K.; Pandey, M. M.; Gupta, G.; Singh, M.; Dua, K. Microneedles: A Smart Approach and Increasing Potential for Transdermal Drug Delivery System. *Biomedicine & Pharmacotherapy* **2019**, *109*, 1249–1258. https://doi.org/10.1016/j.biopha.2018.10.078.

182.   Ramadan, S.; Guo, L.; Li, Y.; Yan, B.; Lu, W. Hollow Copper Sulfide Nanoparticle-Mediated Transdermal Drug Delivery. *Small* **2012**, *8* (20), 3143–3150. https://doi.org/10.1002/smll.201200783.

183.   Singhal, M.; Lapteva, M.; Kalia, Y. N. Formulation Challenges for 21st Century Topical and Transdermal Delivery Systems. *Expert Opinion on Drug Delivery* **2017**, *14* (6), 705–708. https://doi.org/10.1080/17425247.2017.1311320.

184.   Byrne, J.; Huang, H.-W.; McRae, J. C.; Babaee, S.; Soltani, A.; Becker, S. L.; Traverso, G. Devices for Drug Delivery in the Gastrointestinal Tract: A Review of Systems Physically Interacting with the Mucosa for Enhanced Delivery. *Advanced Drug Delivery Reviews* **2021**, *177*, 113926. https://doi.org/10.1016/j.addr.2021.113926.

185.   Jung, J. H.; Jin, S. G. Microneedle for Transdermal Drug Delivery: Current Trends and Fabrication. *J. Pharm. Investig.* **2021**, *51* (5), 503–517. https://doi.org/10.1007/s40005-021-00512-4.

186   Saratov State University; Ermakov, A. V.; Lengert, E. V.; Saratov State University; Venig, S. B.; Saratov State University. Nanomedicine and Drug Delivery Strategies for

Theranostics Applications. *ISUNSSP* **2020**, *20* (2), 116–124. https://doi.org/10.18500/1817-3020-2020-20-2-116-124.

187.   Gurtner, G. C.; Werner, S.; Barrandon, Y.; Longaker, M. T. Wound Repair and Regeneration. *Nature* **2008**, *453* (7193), 314–321. https://doi.org/10.1038/nature07039.

188.   Sami, D. G.; Heiba, H. H.; Abdellatif, A. Wound Healing Models: A Systematic Review of Animal and Non-Animal Models. *Wound Medicine* **2019**, *24* (1), 8–17. https://doi.org/10.1016/j.wndm.2018.12.001.

189.   Lebonvallet, N.; Jeanmaire, C.; Danoux, L.; Sibille, P.; Pauly, G.; Misery, L. The Evolution and Use of Skin Explants: Potential and Limitations for Dermatological Research. *Eur J Dermatol* **2010**, *20* (6), 671–684. https://doi.org/10.1684/ejd.2010.1054.

190.   Wilhelm, K.-P.; Wilhelm, D.; Bielfeldt, S. Models of Wound Healing: An Emphasis on Clinical Studies. *Skin Research and Technology* **2017**, *23* (1), 3–12. https://doi.org/10.1111/srt.12317.

191.   Darwin, E.; Tomic-Canic, M. Healing Chronic Wounds: Current Challenges and Potential Solutions. *Curr Dermatol Rep* **2018**, *7* (4), 296–302. https://doi.org/10.1007/s13671-018-0239-4.

192.   Grada, A.; Mervis, J.; Falanga, V. Research Techniques Made Simple: Animal Models of Wound Healing. Journal of Investigative Dermatology 2018, 138 (10), 2095-2105.e1. https://doi.org/10.1016/j.jid.2018.08.005.

193.   Trøstrup, H.; Thomsen, K.; Calum, H.; Hoiby, N.; Moser, C. Animal Models of Chronic Wound Care: The Application of Biofilms in Clinical Research. *CWCMR* **2016**, *Volume 3*, 123–132. https://doi.org/10.2147/CWCMR.S84361.

194.   Zomer, H. D.; Trentin, A. G. Skin Wound Healing in Humans and Mice: Challenges in Translational Research. Journal of Dermatological Science 2018, 90 (1), 3–12. https://doi.org/10.1016/j.jdermsci.2017.12.009.

195.   Godwin, J. W.; Rosenthal, N. Scar-Free Wound Healing and Regeneration in Amphibians: Immunological Influences on Regenerative Success. *Differentiation* **2014**, *87* (1), 66–75. https://doi.org/10.1016/j.diff.2014.02.002.

196.   Denis, J.-F.; Lévesque, M.; Tran, S. D.; Camarda, A.-J.; Roy, S. Axolotl as a Model to Study Scarless Wound Healing in Vertebrates: Role of the Transforming Growth Factor Beta Signaling Pathway. *Adv Wound Care (New Rochelle)* **2013**, *2* (5), 250–260. https://doi.org/10.1089/wound.2012.0371.

197.   Lévesque, M.; Villiard, É.; Roy, S. Skin Wound Healing in Axolotls: A Scarless Process. *Journal of Experimental Zoology Part B: Molecular and Developmental Evolution* **2010**, *314B* (8), 684–697. https://doi.org/10.1002/jez.b.21371.

198.   Ducuing, A.; Vincent, S. The Actin Cable Is Dispensable in Directing Dorsal Closure Dynamics but Neutralizes Mechanical Stress to Prevent Scarring in the Drosophila Embryo. *Nat Cell Biol* **2016**, *18* (11), 1149–1160. https://doi.org/10.1038/ncb3421.

199.   Noishiki, C.; Yuge, S.; Ando, K.; Wakayama, Y.; Mochizuki, N.; Ogawa, R.; Fukuhara, S. Live Imaging of Angiogenesis during Cutaneous Wound Healing in Adult Zebrafish. *Angiogenesis* **2019**, *22* (2), 341–354. https://doi.org/10.1007/s10456-018-09660-y.

200.   Álvarez-Fernández, C.; Tamirisa, S.; Prada, F.; Chernomoretz, A.; Podhajcer, O.; Blanco, E.; Martín-Blanco, E. Identification and Functional Analysis of Healing Regulators in Drosophila.   *PLOS   Genetics   **2015**,   *11*   (2),   e1004965. https://doi.org/10.1371/journal.pgen.1004965.

201.   Walmsley, G. G.; Hu, M. S.; Hong, W. X.; Maan, Z. N.; Lorenz, H. P.; Longaker, M. T. A Mouse Fetal Skin Model of Scarless Wound Repair. *J Vis Exp* **2015**, No. 95, 52297. https://doi.org/10.3791/52297.

202.   Stanisstreet, M.; Wakely, J.; England, M. A. Scanning Electron Microscopy of Wound Healing in Xenopus and Chicken Embryos. 14.

203.   Blacklow, S. O.; Li, J.; Freedman, B. R.; Zeidi, M.; Chen, C.; Mooney, D. J. Bioinspired Mechanically Active Adhesive Dressings to Accelerate Wound Closure. Science Advances 2019, 5 (7), eaaw3963. https://doi.org/10.1126/sciadv.aaw3963.

204.   Shevchenko, R. V.; Santin, M. Pre-Clinical Evaluation of Soybean-Based Wound Dressings and Dermal Substitute Formulations in Pig Healing and Non-Healing in Vivo Models. Burns & Trauma 2014, 2 (4). https://doi.org/10.4103/2321-3868.143624.

205.   Alvarez, O. M.; Mertz, P. M.; Eaglstein, W. H. The Effect of Occlusive Dressings on Collagen Synthesis and Re-Epithelialization in Superficial Wounds. *Journal of Surgical Research* **1983**, *35* (2), 142–148. https://doi.org/10.1016/0022-4804(83)90136-1.

206.   Zhang, X.; Yao, D.; Zhao, W.; Zhang, R.; Yu, B.; Ma, G.; Li, Y.; Hao, D.; Xu, F.-J. Engineering Platelet-Rich Plasma Based Dual-Network Hydrogel as a Bioactive Wound Dressing with Potential Clinical Translational Value. *Advanced Functional Materials* **2021**, *31* (8), 2009258. https://doi.org/10.1002/adfm.202009258.

207.   Hsieh, H.-T.; Chang, H.-M.; Lin, W.-J.; Hsu, Y.-T.; Mai, F.-D. Poly-Methyl Methacrylate/Polyvinyl Alcohol Copolymer Agents Applied on Diabetic Wound Dressing. *Sci Rep* **2017**, *7* (1), 9531. https://doi.org/10.1038/s41598-017-10193-5.

208.   *Molecular Dermatology: Methods and Protocols*; Botchkareva, N. V., Westgate, G. E., Eds.; Methods in Molecular Biology; Springer US: New York, NY, 2020; Vol. 2154. https://doi.org/10.1007/978-1-0716-0648-3.

209.   Azeredo, J.; Azevedo, N. F.; Briandet, R.; Cerca, N.; Coenye, T.; Costa, A. R.; Desvaux, M.; Di Bonaventura, G.; Hébraud, M.; Jaglic, Z.; Kačániová, M.; Knøchel, S.; Lourenço, A.; Mergulhão, F.; Meyer, R. L.; Nychas, G.; Simões, M.; Tresse, O.; Sternberg, C.

Critical Review on Biofilm Methods. *Critical Reviews in Microbiology* **2017**, *43* (3), 313–351. https://doi.org/10.1080/1040841X.2016.1208146.

210. Brackman, G.; Coenye, T. In Vitro and In Vivo Biofilm Wound Models and Their Application. In *Advances in Microbiology, Infectious Diseases and Public Health: Volume 1*; Donelli, G., Ed.; Advances in Experimental Medicine and Biology; Springer International Publishing: Cham, **2016**; pp 15–32. https://doi.org/10.1007/5584_2015_5002.

211. Percival, S. L.; Bowler, P. G.; Dolman, J. Antimicrobial Activity of Silver-Containing Dressings on Wound Microorganisms Using an in Vitro Biofilm Model. *International Wound Journal* **2007**, *4* (2), 186–191. https://doi.org/10.1111/j.1742-481X.2007.00296.x.

212. Clutterbuck, A. L.; Cochrane, C. A.; Dolman, J.; Percival, S. L. Evaluating Antibiotics for Use in Medicine Using a Poloxamer Biofilm Model. *Ann Clin Microbiol Antimicrob* **2007**, *6*, 2. https://doi.org/10.1186/1476-0711-6-2.

213. Percival, S. L.; Slone, W.; Linton, S.; Okel, T.; Corum, L.; Thomas, J. G. The Antimicrobial Efficacy of a Silver Alginate Dressing against a Broad Spectrum of Clinically Relevant Wound Isolates. *International Wound Journal* **2011**, *8* (3), 237–243. https://doi.org/10.1111/j.1742-481X.2011.00774.x.

214. Dai, T.; Kharkwal, G. B.; Tanaka, M.; Huang, Y.-Y.; Bil de Arce, V. J.; Hamblin, M. R. Animal Models of External Traumatic Wound Infections. *Virulence* **2011**, *2* (4), 296–315. https://doi.org/10.4161/viru.2.4.16840.

215. Dhall, S.; Do, D.; Garcia, M.; Wijesinghe, D. S.; Brandon, A.; Kim, J.; Sanchez, A.; Lyubovitsky, J.; Gallagher, S.; Nothnagel, E. A.; Chalfant, C. E.; Patel, R. P.; Schiller, N.; Martins-Green, M. A Novel Model of Chronic Wounds: Importance of Redox Imbalance and Biofilm-Forming Bacteria for Establishment of Chronicity. *PLOS ONE* **2014**, *9* (10), e109848. https://doi.org/10.1371/journal.pone.0109848.

216. Fila, G.; Kasimova, K.; Arenas, Y.; Nakonieczna, J.; Grinholc, M.; Bielawski, K. P.; Lilge, L. Murine Model Imitating Chronic Wound Infections for Evaluation of Antimicrobial Photodynamic Therapy Efficacy. *Front. Microbiol.* **2016**, *7*. https://doi.org/10.3389/fmicb.2016.01258.

217. Lipp, C.; Kirker, K.; Agostinho, A.; James, G.; Stewart, P. Testing Wound Dressings Using an in Vitro Wound Model. *J Wound Care* **2010**, *19* (6), 220–226.

218. Hill, K. E.; Malic, S.; McKee, R.; Rennison, T.; Harding, K. G.; Williams, D. W.; Thomas, D. W. An in Vitro Model of Chronic Wound Biofilms to Test Wound Dressings and Assess Antimicrobial Susceptibilities. *Journal of Antimicrobial Chemotherapy* **2010**, *65* (6), 1195–1206. https://doi.org/10.1093/jac/dkq105.

219. Kim, H.; Izadjoo, M. Antimicrobial Activity of a Bioelectric Dressing Using an in Vitro Wound Pathogen Colony Drip-Flow Reactor Biofilm Model. *Journal of Wound Care* **2016**. https://doi.org/10.12968/jowc.2016.25.Sup7.S47.

220. Werthén, M.; Henriksson, L.; Jensen, P. Ø.; Sternberg, C.; Givskov, M.; Bjarnsholt, T. An in Vitro Model of Bacterial Infections in Wounds and Other Soft Tissues. *APMIS* **2010**, *118* (2), 156–164. https://doi.org/10.1111/j.1600-0463.2009.02580.x.

221. Hakonen, B.; Lönnberg, L. K.; Larkö, E.; Blom, K. A Novel Qualitative and Quantitative Biofilm Assay Based on 3D Soft Tissue. *Int J Biomater* **2014**, *2014*, 768136. https://doi.org/10.1155/2014/768136.

222. Mineo, A.; Suzuki, R.; Kuroyanagi, Y. Development of an Artificial Dermis Composed of Hyaluronic Acid and Collagen. *Journal of Biomaterials Science, Polymer Edition* **2013**, *24* (6), 726–740. https://doi.org/10.1080/09205063.2012.708190.

223. Koide, M.; Osaki, K.; Konishi, J.; Oyamada, K.; Katakura, T.; Takahashi, A.; Yoshizato, K. A New Type of Biomaterial for Artificial Skin: Dehydrothermally Cross-Linked Composites of Fibrillar and Denatured Collagens. *Journal of Biomedical Materials Research* **1993**, *27* (1), 79–87. https://doi.org/10.1002/jbm.820270111.

224. Price, B. L.; Lovering, A. M.; Bowling, F. L.; Dobson, C. B. Development of a Novel Collagen Wound Model To Simulate the Activity and Distribution of Antimicrobials in Soft Tissue during Diabetic Foot Infection. *Antimicrobial Agents and Chemotherapy* **2016**, *60* (11), 6880–6889. https://doi.org/10.1128/AAC.01064-16.

225. Steinstraesser, L.; Sorkin, M.; Niederbichler, A. D.; Becerikli, M.; Stupka, J.; Daigeler, A.; Kesting, M. R.; Stricker, I.; Jacobsen, F.; Schulte, M. A Novel Human Skin Chamber Model to Study Wound Infection Ex Vivo. *Arch Dermatol Res* **2010**, *302* (5), 357–365. https://doi.org/10.1007/s00403-009-1009-8.

226. Schaudinn, C.; Dittmann, C.; Jurisch, J.; Laue, M.; Günday-Türeli, N.; Blume-Peytavi, U.; Vogt, A.; Rancan, F. Development, Standardization and Testing of a Bacterial Wound Infection Model Based on Ex Vivo Human Skin. *PLOS ONE* **2017**, *12* (11), e0186946. https://doi.org/10.1371/journal.pone.0186946.

227. Milho, C.; Andrade, M.; Vilas Boas, D.; Alves, D.; Sillankorva, S. Antimicrobial Assessment of Phage Therapy Using a Porcine Model of Biofilm Infection. *International Journal of Pharmaceutics* **2019**, *557*, 112–123. https://doi.org/10.1016/j.ijpharm.2018.12.004.

228. Ashrafi, M.; Novak-Frazer, L.; Morris, J.; Baguneid, M.; Rautemaa-Richardson, R.; Bayat, A. Electrical Stimulation Disrupts Biofilms in a Human Wound Model and Reveals the Potential for Monitoring Treatment Response with Volatile Biomarkers. *Wound Repair and Regeneration* **2019**, *27* (1), 5–18. https://doi.org/10.1111/wrr.12679.

229. Kim, P. Y.; Kim, Y.-S.; Koo, I. G.; Jung, J. C.; Kim, G. J.; Choi, M. Y.; Yu, Z.; Collins, G. J. Bacterial Inactivation of Wound Infection in a Human Skin Model by Liquid-Phase Discharge Plasma. *PLOS ONE* **2011**, *6* (8), e24104. https://doi.org/10.1371/journal.pone.0024104.

230. Shepherd, J.; Sarker, P.; Rimmer, S.; Swanson, L.; MacNeil, S.; Douglas, I. Hyperbranched Poly(NIPAM) Polymers Modified with Antibiotics for the Reduction of

Bacterial Burden in Infected Human Tissue Engineered Skin. *Biomaterials* **2011**, *32* (1), 258–267. https://doi.org/10.1016/j.biomaterials.2010.08.084.

231.   Haisma, E. M.; Rietveld, M. H.; Breij, A. de; Dissel, J. T. van; Ghalbzouri, A. E.; Nibbering, P. H. Inflammatory and Antimicrobial Responses to Methicillin-Resistant Staphylococcus Aureus in an In Vitro Wound Infection Model. *PLOS ONE* **2013**, *8* (12), e82800. https://doi.org/10.1371/journal.pone.0082800.

232.   Gabrilska, R. A.; Rumbaugh, K. P. Biofilm Models of Polymicrobial Infection. *Future Microbiol* **2015**, *10* (12), 1997–2015. https://doi.org/10.2217/fmb.15.109.

233.   Dini, V.; Salvo, P.; Janowska, A.; Di Francesco, F.; Barbini, A.; Romanelli, M. Correlation Between Wound Temperature Obtained With an Infrared Camera and Clinical Wound Bed Score in Venous Leg Ulcers. *Wounds* **2015**, *27* (10), 274–278.

234.   Sun, Y.; Dowd, S. E.; Smith, E.; Rhoads, D. D.; Wolcott, R. D. In Vitro Multispecies Lubbock Chronic Wound Biofilm Model. *Wound Repair and Regeneration* **2008**, *16* (6), 805–813. https://doi.org/10.1111/j.1524-475X.2008.00434.x.

235.   Dalton, T.; Dowd, S. E.; Wolcott, R. D.; Sun, Y.; Watters, C.; Griswold, J. A.; Rumbaugh, K. P. An In Vivo Polymicrobial Biofilm Wound Infection Model to Study Interspecies Interactions. *PLOS ONE* **2011**, *6* (11), e27317. https://doi.org/10.1371/journal.pone.0027317.

236.   Kucera, J.; Sojka, M.; Pavlik, V.; Szuszkiewicz, K.; Velebny, V.; Klein, P. Multispecies Biofilm in an Artificial Wound Bed—A Novel Model for in Vitro Assessment of Solid Antimicrobial Dressings. *Journal of Microbiological Methods* **2014**, *103*, 18–24. https://doi.org/10.1016/j.mimet.2014.05.008.

237.   Percival, S. L.; Hill, K. E.; Williams, D. W.; Hooper, S. J.; Thomas, D. W.; Costerton, J. W. A Review of the Scientific Evidence for Biofilms in Wounds. *Wound Repair and Regeneration* **2012**, *20* (5), 647–657. https://doi.org/10.1111/j.1524-475X.2012.00836.x.

238.   Maboni, G.; Davenport, R.; Sessford, K.; Baiker, K.; Jensen, T. K.; Blanchard, A. M.; Wattegedera, S.; Entrican, G.; Tötemeyer, S. A Novel 3D Skin Explant Model to Study Anaerobic Bacterial Infection. *Front Cell Infect Microbiol* **2017**, *7*, 404. https://doi.org/10.3389/fcimb.2017.00404.

240.   Sun, Y.; Smith, E.; Wolcott, R.; Dowd, S. e. Propagation of Anaerobic Bacteria within an Aerobic Multi-Species Chronic Wound Biofilm Model. *J Wound Care* **2009**, *18* (10), 426–431. https://doi.org/10.12968/jowc.2009.18.10.44604.

241.   Brackman, G.; Cos, P.; Maes, L.; Nelis, H. J.; Coenye, T. Quorum Sensing Inhibitors Increase the Susceptibility of Bacterial Biofilms to Antibiotics In Vitro and In Vivo. *Antimicrobial Agents and Chemotherapy* **2011**, *55* (6), 2655–2661. https://doi.org/10.1128/AAC.00045-11.

242.   Gordillo, G. M.; Bernatchez, S. F.; Diegelmann, R.; Di Pietro, L. A.; Eriksson, E.; Hinz, B.; Hopf, H. W.; Kirsner, R.; Liu, P.; Parnell, L. K. S.; Sandusky, G. E.; Sen, C. K.; Tomic-

Canic, M.; Volk, S. W.; Baird, A. Preclinical Models of Wound Healing: Is Man the Model? Proceedings of the Wound Healing Society Symposium. *Adv Wound Care (New Rochelle)* **2013**, *2* (1), 1–4. https://doi.org/10.1089/wound.2012.0367.

243.   *Report of Statistical Information on the Use of Animals for Scientific Purposes*; COMMISSION STAFF WORKING DOCUMENT; European commission: Brussels, 2018.

244.   Ex Vivo Model of Human Skin (HOSEC) as Alternative to Animal Use for Cosmetic Tests. *Procedia Engineering* **2015**, *110*, 67–73. https://doi.org/10.1016/j.proeng.2015.07.011.

245.   Matarrese, P.; Beauchef, G.; Peno-Mazzarino, L.; Lati, E.; Fitoussi, R.; Vié, K. Assessment of an Ex Vivo Irritation Test Performed on Human Skin Explants and Comparison of Its Results with Those of a 24-/48-h Human Patch Test for the Evaluation of Cosmetics. *Toxicology in Vitro* **2021**, *70*, 105030. https://doi.org/10.1016/j.tiv.2020.105030.

246.   Skin Organ Culture for the Study of Skin Irritancy. *Toxicology in Vitro* **1990**, *4* (4–5), 293–301. https://doi.org/10.1016/0887-2333(90)90067-4.

247.   Reus, A. A.; Usta, M.; Krul, C. A. M. The Use of Ex Vivo Human Skin Tissue for Genotoxity Testing. *Toxicology and Applied Pharmacology* **2012**, *261* (2), 154–163. https://doi.org/10.1016/j.taap.2012.03.019.

248.   Patatian, A.; Delestre-Delacour, C.; Percoco, G.; Ramdani, Y.; Di Giovanni, M.; Peno-Mazzarino, L.; Bader, Th.; Bénard, M.; Driouich, A.; Lati, E.; Benech, P.; Follet-Gueye, M. L. Skin Biological Responses to Urban Pollution in an Ex Vivo Model. *Toxicology Letters* **2021**, *348*, 85–96. https://doi.org/10.1016/j.toxlet.2021.05.003.

249.   Hwang, J.; Jeong, H.; Lee, N.; Hur, S.; Lee, N.; Han, J. J.; Jang, H. W.; Choi, W. K.; Nam, K. T.; Lim, K.-M. Ex Vivo Live Full-Thickness Porcine Skin Model as a Versatile In Vitro Testing Method for Skin Barrier Research. *International Journal of Molecular Sciences* **2021**, *22* (2), 657. https://doi.org/10.3390/ijms22020657.

250.   Gasser, P.; Lati, E.; Peno-Mazzarino, L.; Bouzoud, D.; Allegaert, L.; Bernaert, H. Cocoa Polyphenols and Their Influence on Parameters Involved in Ex Vivo Skin Restructuring. *International Journal of Cosmetic Science* **2008**, *30* (5), 339–345. https://doi.org/10.1111/j.1468-2494.2008.00457.x.

251.   Schmook, F. P.; Meingassner, J. G.; Billich, A. Comparison of Human Skin or Epidermis Models with Human and Animal Skin in In-Vitro Percutaneous Absorption. *International Journal of Pharmaceutics* **2001**, *215* (1), 51–56. https://doi.org/10.1016/S0378-5173(00)00665-7.

252.   Danso, M. O.; Berkers, T.; Mieremet, A.; Hausil, F.; Bouwstra, J. A. An Ex Vivo Human Skin Model for Studying Skin Barrier Repair. *Experimental Dermatology* **2015**, *24* (1), 48–54. https://doi.org/10.1111/exd.12579.

253.   Dennerlein, K.; Kiesewetter, F.; Kilo, S.; Jäger, T.; Göen, T.; Korinth, G.; Drexler, H. Dermal Absorption and Skin Damage Following Hydrofluoric Acid Exposure in an Ex Vivo

Human Skin Model. *Toxicology Letters* **2016**, *248*, 25–33. https://doi.org/10.1016/j.toxlet.2016.02.015.

254.   Infante, V. H. P.; Maia Campos, P. M. B. G.; Calixto, L. S.; Darvin, M. E.; Kröger, M.; Schanzer, S.; Lohan, S. B.; Lademann, J.; Meinke, M. C. Influence of Physical–Mechanical Properties on SPF in Sunscreen Formulations on Ex Vivo and in Vivo Skin. *International Journal of Pharmaceutics* **2021**, *598*, 120262. https://doi.org/10.1016/j.ijpharm.2021.120262.

255.   Hofmann, E.; Fink, J.; Eberl, A.; Prugger, E.-M.; Kolb, D.; Luze, H.; Schwingenschuh, S.; Birngruber, T.; Magnes, C.; Mautner, S. I.; Kamolz, L.-P.; Kotzbeck, P. A Novel Human Ex Vivo Skin Model to Study Early Local Responses to Burn Injuries. *Sci Rep* **2021**, *11* (1), 364. https://doi.org/10.1038/s41598-020-79683-3.

256.   Xu, W.; Hong, S. J.; Jia, S.; Zhao, Y.; Galiano, R. D.; Mustoe, T. A. Application of a Partial-Thickness Human *Ex Vivo* Skin Culture Model in Cutaneous Wound Healing Study. *Laboratory Investigation* **2012**, *92* (4), 584–599. https://doi.org/10.1038/labinvest.2011.184.

257.   Kratz, G. Modeling of Wound Healing Processes in Human Skin Using Tissue Culture. *Microscopy Research and Technique* **1998**, *42* (5), 345–350. https://doi.org/10.1002/(SICI)1097-0029(19980901)42:5<345::AID-JEMT5>3.0.CO;2-O.

258.   Boekema, B. K. H. L.; Vlig, M.; Guijt, D.; Hijnen, K.; Hofmann, S.; Smits, P.; Sobota, A.; Veldhuizen, E. M. van; Bruggeman, P.; Middelkoop, E. A New Flexible DBD Device for Treating Infected Wounds:In Vitro and ex Vivo evaluation and Comparison with a RF Argon Plasma Jet. *J. Phys. D: Appl. Phys.* **2015**, *49* (4), 044001. https://doi.org/10.1088/0022-3727/49/4/044001.

259.   Corzo-León, D. E.; Munro, C. A.; MacCallum, D. M. An Ex Vivo Human Skin Model to Study Superficial Fungal Infections. *Front. Microbiol.* **2019**, *10*. https://doi.org/10.3389/fmicb.2019.01172.

260.   Yoon, D. J.; Fregoso, D. R.; Nguyen, D.; Chen, V.; Strbo, N.; Fuentes, J. J.; Tomic-Canic, M.; Crawford, R.; Pastar, I.; Isseroff, R. R. A Tractable, Simplified Ex Vivo Human Skin Model of Wound Infection. *Wound Repair and Regeneration* **2019**, *0* (0). https://doi.org/10.1111/wrr.12712.

261.   Wilkinson, H. N.; Longhorne, F. L.; Roberts, E. R.; Brownhill, V. R.; Hardman, M. J. Cellular Benefits of Single-Use Negative Pressure Wound Therapy Demonstrated in a Novel Ex Vivo Human Skin Wound Model. *Wound Repair and Regeneration* **2021**, *29* (2), 298–305. https://doi.org/10.1111/wrr.12888.

262.   Neil, J. E.; Brown, M. B.; Williams, A. C. Human Skin Explant Model for the Investigation of Topical Therapeutics. *Sci Rep* **2020**, *10* (1), 21192. https://doi.org/10.1038/s41598-020-78292-4.

263.   Cho, H.; Won, C. H.; Chang, S. E.; Lee, M. W.; Park, and G.-H. Usefulness and Limitations of Skin Explants to Assess Laser Treatment. *Medical Lasers* **2013**, *2* (2), 58–63. https://doi.org/10.25289/ML.2013.2.2.58.

264. Companjen, A. R.; van der Wel, L. I.; Wei, L.; Laman, J. D.; Prens, E. P. A Modified Ex Vivo Skin Organ Culture System for Functional Studies. *Archives of Dermatological Research* **2001**, *293* (4), 184–190. https://doi.org/10.1007/s004030100219.

265. Moll, I.; Houdek, P.; Schäfer, S.; Nuber, U.; Moll, R. Diversity of Desmosomal Proteins in Regenerating Epidermis: Immunohistochemical Study Using a Human Skin Organ Culture Model. *Archives of Dermatological Research* **1999**, *291* (7–8), 437–446. https://doi.org/10.1007/s004030050435.

266. Bhora, F. Y.; Dunkin, B. J.; Batzri, S.; Aly, H. M.; Bass, B. L.; Sidawy, A. N.; Harmon, J. W. Effect of Growth Factors on Cell Proliferation and Epithelialization in Human Skin. *Journal of Surgical Research* **1995**, *59* (2), 236–244. https://doi.org/10.1006/jsre.1995.1160.

267. Onuma, H.; Mastui, C.; Morohashi, M. Quantitative Analysis of the Proliferation of Epidermal Cells Using a Human Skin Organ Culture System and the Effect of DbcAMP Using Markers of Proliferation (BrdU, Ki-67, PCNA). *Archives of Dermatological Research* **2001**, *293* (3), 133–138. https://doi.org/10.1007/s004030000195.

268. Han, Y.-P.; Tuan, T.-L.; Wu, H.; Hughes, M.; Garner, W. L. TNF-α Stimulates Activation of pro-MMP2 in Human Skin through NF-KB Mediated Induction of MT1-MMP. *J Cell Sci* **2001**, *114* (Pt 1), 131–139.

269. Ashrafi, M.; Hague, A.; Baguneid, M.; Alonso-Rasgado, T.; Bayat, A. Wound Healing and Cutaneous Scarring Models of the Human Skin. In *Skin Tissue Models for Regenerative Medicine*; Elsevier, 2018; pp 201–221. https://doi.org/10.1016/B978-0-12-810545-0.00009-7.

270. Plastic Surgery Statistics | Global Plastic Surgery Statistics https://www.isaps.org/medical-professionals/isaps-global-statistics/ (accessed 2021 -05 -28).

271. Activités réglementées concernant les échantillons biologiques humains destinés à la recherche //www.enseignementsup-recherche.gouv.fr/cid93150/activites-reglementees-concernant-les-echantillons-biologiques-humains-destines-a-la-recherche.html (accessed 2021 -09 -01).

272. Ud-Din, S.; Bayat, A. Non-Animal Models of Wound Healing in Cutaneous Repair: In Silico, in Vitro, Ex Vivo, and in Vivo Models of Wounds and Scars in Human Skin. *Wound Repair and Regeneration* **2017**, *25* (2), 164–176. https://doi.org/10.1111/wrr.12513.

273. Ansell, D. M.; Holden, K. A.; Hardman, M. J. Animal Models of Wound Repair: Are They Cutting It? *Experimental Dermatology* **2012**, *21* (8), 581–585. https://doi.org/10.1111/j.1600-0625.2012.01540.x.

274. Pastar, I.; Liang, L.; Sawaya, A. P.; Wikramanayake, T. C.; Glinos, G. D.; Drakulich, S.; Chen, V.; Stojadinovic, O.; Davis, S. C.; Tomic-Canic, M. Preclinical Models for Wound-Healing Studies. In *Skin Tissue Models for Regenerative Medicine*; Elsevier, 2018; pp 223–253. https://doi.org/10.1016/B978-0-12-810545-0.00010-3.

275. Mendoza-Garcia, J.; Sebastian, A.; Alonso-Rasgado, T.; Bayat, A. Optimization of an Ex Vivo Wound Healing Model in the Adult Human Skin: Functional Evaluation Using

Photodynamic Therapy. *Wound Repair and Regeneration* **2015**, *23* (5), 685–702. https://doi.org/10.1111/wrr.12325.

CHAPTER 2 : IMPLEMENTATION OF *EX VIVO* SKIN MODELS

2.1 SKIN WOUND INFECTION MODEL

Complex wounds such as diabetic foot ulcers represent a major challenge for the clinicians and wound care specialists.[1] Despite all the recent advances in the increased understanding of the molecular causes of failed healing,[2] multifaceted soft-tissue defects can overwhelm the regenerative capacity of skin and render the human body significantly vulnerable to infections. In infected wounds, bacteria, initially in low numbers, start colonizing different layers of the skin. When infections penetrate deep into tissues such as bone, or when they reach a tissue that has inadequate circulation, they can become difficult to treat and may become chronic infections. The most common types of bacteria that can affect the skin are *Pseudomonas aeruginosa* (*P. aeruginosa*) or *Staphylococcus aureus* (*S. aureus*)[3] with methicillin-resistant *S. aureus* being one of the most common bacteria causing more than half of all community-associated skin and soft tissue infections. While various wound dressings and antibacterial agents are available for the treatment for infected wounds, very few have shown substantial evidence in stimulating significant tissue repair.[4]

One of the prerequisites to test novel approaches is the access to meaningful model systems. The majority of research on wound infections is conducted on animal models.[5-7] Unfortunately, the transferability of these studies to humans is limited. Despite the great progress in translational research, wound healing mechanisms, as well as skin morphology, immunology and genetics, are too different between species.[8] For instance, the mice model, which is the most used model due to the accessibility, the great knowledge and the cost effectiveness, shows contractions promoted by the panniculus carnosus, a healing mechanism which is absent in human skin repair. These differences limit their usability as a model to realistically mimic wound infections in humans and thus confirm the efficiency of a new treatment.

Human *ex vivo* models allow us to rapidly and properly interpret findings and translate them to medicine. The use of leftovers from esthetic surgery, initially considered as medical waste and intended for disposal, is a great opportunity to develop a human model without ethics issues. Indeed, more than 900.000 abdominosplaties, consisting of the removal of excess skin and fat from the middle and lower abdomen, are carried out each year in the world.[9] Other surgeries like low body lift, thigh lift, arm lift, buttock lift, breast reduction can provide many skin samples with skin part diversity. Moreover, many efforts have been made to replace dermal toxicity testing of chemicals in the animal and *ex vivo* human skin models start to replace these models for many skin studies like wound repair[10-11] and infected wound.[12-15]

Some companies propose patented full-skin *ex vivo* culture systems to perform dermatological testing. By presenting an air-liquid interface, the system allows the application of creams, ointments, liquid substances as well as bandages and dressings or physical stimulus on the horny layer as against to cell culture systems that only allow the use of soluble substances in the culture medium and the absence of stratum corneum.[16] Genoskin, a French company located in Toulouse, developed an optimized culture to keep skin samples alive for 7 days in multi-well testing kits. It provides a new generation of human skin models and assays for reproducible and safety testing both for industry and research projects.[17] The availability of ready-to-use and easy-to-handle samples provide us with an excellent solution for testing the response of human skin to our products prior to clinical evaluation

In this chapter, the development of an *ex vivo* infected wound skin model is described and discussed in more detail to underline the major limitations of the model with the aim of assessing the ultimate applicability of these models for new treatments of complex wounds.

2.1.1 Wound healing in Hyposkin® model

To confirm that the culture conditions of the Hyposkin® model wounded and without infection (**Figure 2.1A**) are suitable for wound healing study, an histological evaluation of the wound was performed.
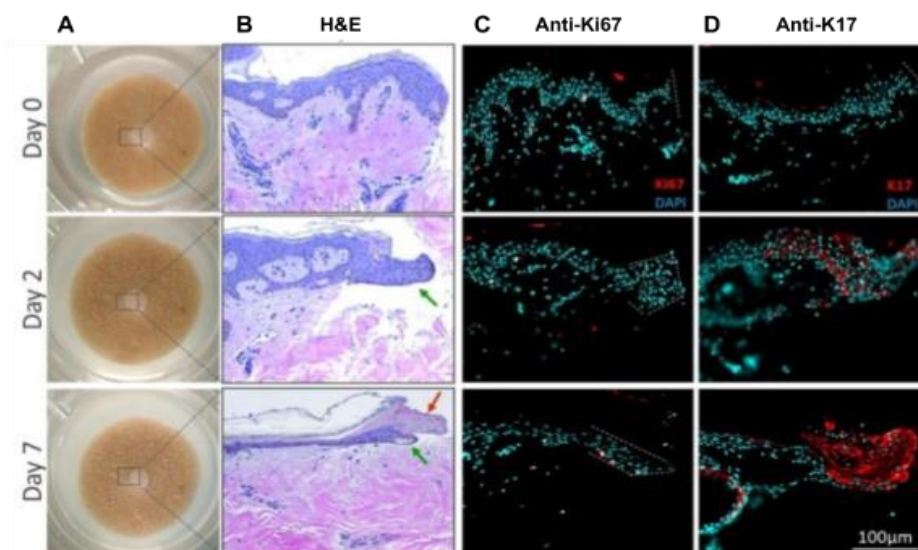

Figure 2.1 : *Analysis of wounded hyposkin® model. Time Course visualisation of wound healing was performed with different techniques. **A**. Macroscopic images of wounded biopsy. **B**. Hematoxylin & Eosin staining. **C-D**. Immunofluorescence staining with Ki67 and K17.*[18]

From H&E analysis, the clear cut of the wound edge is visible at day 0. On day 2, an epithelial tongue appeared and migrated until day 7 (**Figure 2.1B**). An immunofluorescence study was also performed to validate the cell activity at the edge of the wound. Markers of proliferation, Ki-67, and migration, K17, were used. The localization of the staining in the healing tongue confirms that the wound healing process is starting in the hyposkin® model (**Figure 2.1C-D**).

2.1.2 Efficient infection of human skin with *S. aureus*

The procedures employed to infect human skin tissues are summarized in **Figure 2.2**. Following human skin collection and injury, the wound area was infected with *Staphylococcus aureus* (*S. aureus*) by adding concentrated bacteria suspension on the top of the wound. Infection was performed for several days to allow the tissue colonization. After this incubation time, the tissue samples were harvested and subjected to different analyses, including bacterial counting, histological analysis, SEM and qPCR.
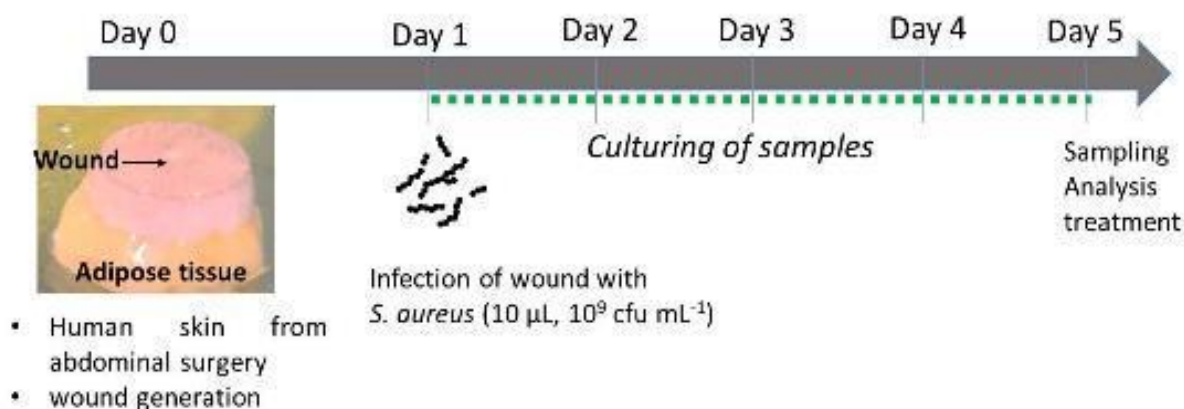

Figure 2.2: Experimental workflow of wound production and infection of Wounded Hyposkin® model: Representative image of the wound skin model, showing the superficial epidermis layer, the dermis, and the underneath adipose tissue. Arrow indicates the wound region. Wound skin models were collected at day 0 and freshly shipped. Bacterial infection was performed upon reception by dropping S. aureus solutions on the wound region and keeping the skin in culture medium without antibiotics at 37 °C for 5 days.

The infection of the skin samples with non-invasive *S. aureus* was followed by a visual inspection of the cultures showing changes in the color of the wound area as observed in **Figure**

2.3. On day 3, the wound area appeared yellow, one of the first indications of the installation of infection.
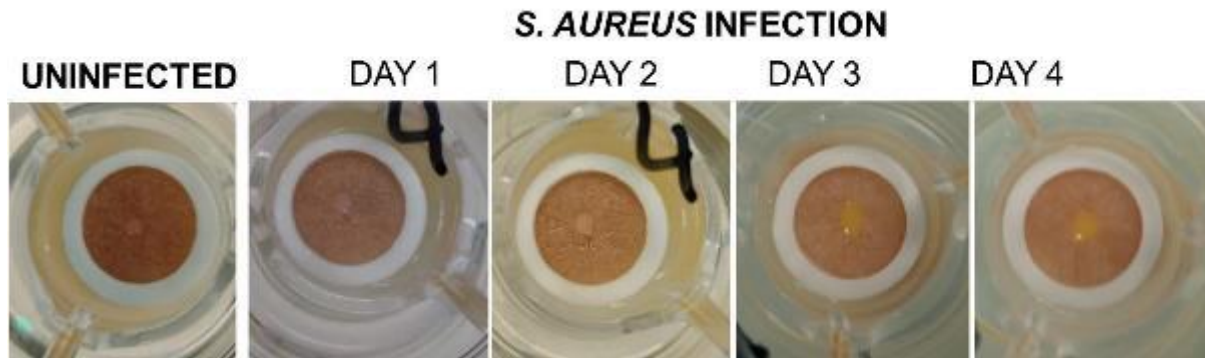

Figure 2.3: *Infection efficiency of S. aureus on ex vivo skin. Optical representative images of uninfected wound skin and wound skin infected with S. aureus (1×10^7 CFU) for one to four days.*

To quantify the infection, the number of viable bacteria in the skin tissue was determined overtime. After one day post-infection, using a bacterial stock solution of 1×10^9 CFU mL^{-1}, 1×10^7 CFU /g skin tissue were detected in 6 out of the 12 skin samples (**Figure 2.4A**), which increased to 1×10^8 CFU /g skin tissue after 3 days and up to almost 1×10^9 CFU /g skin tissue after 5 days (**Figure 2.4B**). Using a bacterial stock solution of 1×10^7 CFU mL^{-1}, we observed high variation in most of the infected skins. We therefore decided to use *S. aureus* solutions at the concentration of 1×10^9 CFU mL^{-1} over a time span of 5 days.
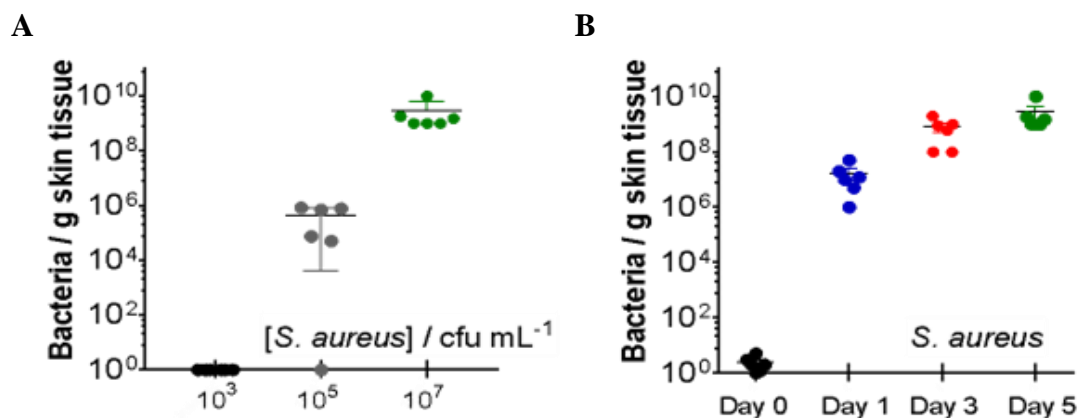

Figure 2.4: *Infection efficiency of S. aureus on ex vivo skin.* **A.** *Effect of the different S. aureus concentrations on bacterial counts per gram skin tissue after 5 days;* **B**. *Bacterial counts per gram skin tissue as determined from wound skin treated with S. aureus (1×10^7 CFU) at different time intervals. All the values are displayed as means ± SEM.*

2.1.3 Skin visualization of *S. aureus* infection in wound

A preliminary study was performed to allow us to identify the morphology, typical cocci shape, and the color of *S. aureus* in the tissue section. Indeed, it is important to know what to look for microscopically and be able to differentiate the bacteria structure from tissue structures. In **Figure 2.5,** we can see that a $60 \times$ magnification does not allow to distinguish the black purple balls group resting on the tissue surface. Bacteria are one third of the size of the surrounding epithelial cells and they appear in bacteria clusters in a matrix cloudy in accordance with the literature. [19-21] Depending on the fixation and processing, pictures may show the bacteria tightly adherent to the surface epithelium or pulled away slightly. In our infection model, we hoped for the penetration of bacteria through collagen fibers.
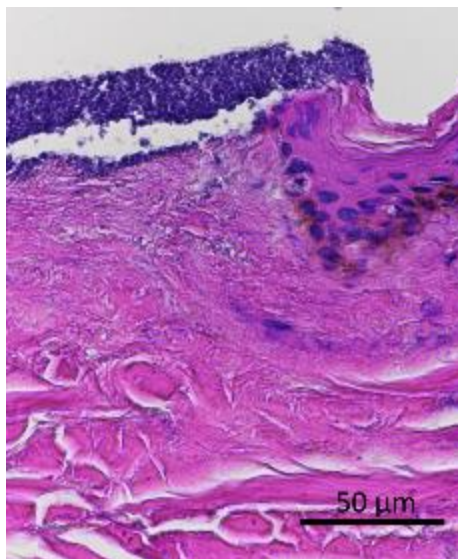

Figure 2.5: S. aureus Infection visualization with H&E staining. This sample was performed with a freezing skin inoculated with a large number of bacteria for 1 night to allow the building of S. aureus biofilm. The biofilm structure of S. aureus is well observed on the surface of the wound. Round bacteria are observed with magnificence of $60\times$.

In our model without infection, the wound structure and evolution may be well analyzed at first with the H&E staining. In **Figure 2.6A**, the 2 mm wound is viewed entirely at $4 \times$ magnification. The edge of the uninfected wound shows the wound healing process with the healing tong structure (**Figure 2.6B**). Furthermore, we can notice that the mechanical removal of the epidermis and a part of the dermis weakens the structure of the wound. The weakness of dermis (collagen fibers) induces the tissue dispersion during the fixation steps (**Figure 2.6C**).

This contrasts to the part beyond the edge of the wound where intact skin morphology was observed with the epidermis attached to the dermis (**Figure 2.6D**).
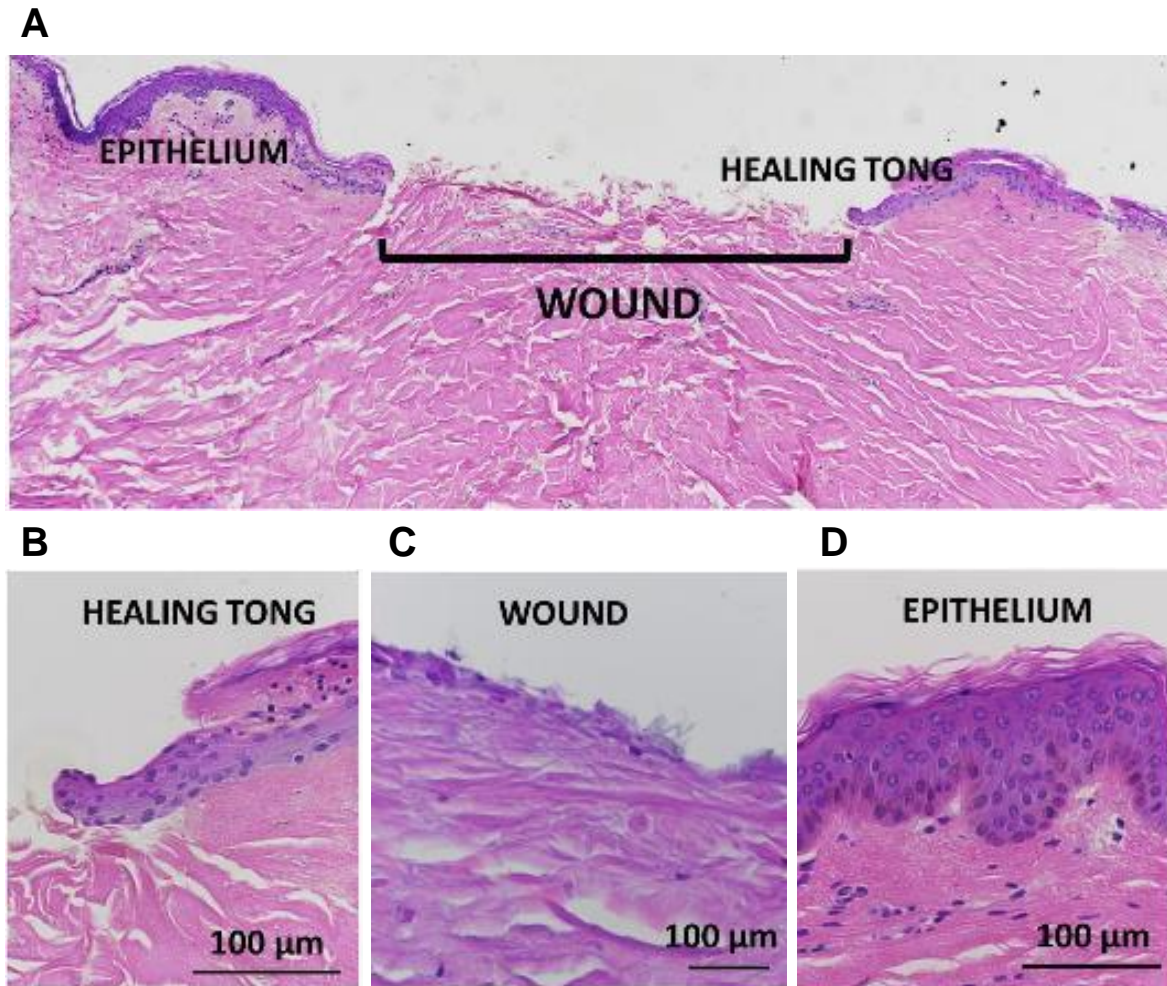

*Figure 2.6: Histological analysis of wound regions of the ex vivo skin model : H&E staining of wound not infected skin. **A**. Whole wound region. **B**. Zoom on Epithelium, with black purple staining of nucleus, light purple staining of cytoplasm and pink staining of collagen fibers. **C**. Zoom on the wound surface without epithelium. **D**. Zoom on the wound edge with the starting of the healing process with specific structure of healing tong.*

Following the wound structure analysis, bacteria colonization as well as the impact on skin morphology were analyzed. On the *ex vivo* infected skin, the presence of bacteria is clearly visible with the dark blue staining of small cocci-shape bacteria (**Figure 2.7**). Bacteria were detected on the surface of the wound (**Figure 2.7B**) but also deeper in the dermis (**Figure 2.7A**) confirming the bacteria penetration in collagen bundles. Moreover, they begin to colonize the area between the epidermis and the dermis (**Figure 2.7C**). *S. aureus* were detected up to 25-40 µm into the skin and a smaller amount was observed at 100 µm depth. This is not surprising as

the presence of oxygen at the skin surface enables the bacteria to have a higher growth rate compared to the lower part of the dermis.[22] Additionally, to the presence of bacteria, the skin structure shows infection related damage, like epidermis detachment and cell death in contrast with uninfected skin which show the intact and attached epidermis on the dermis.
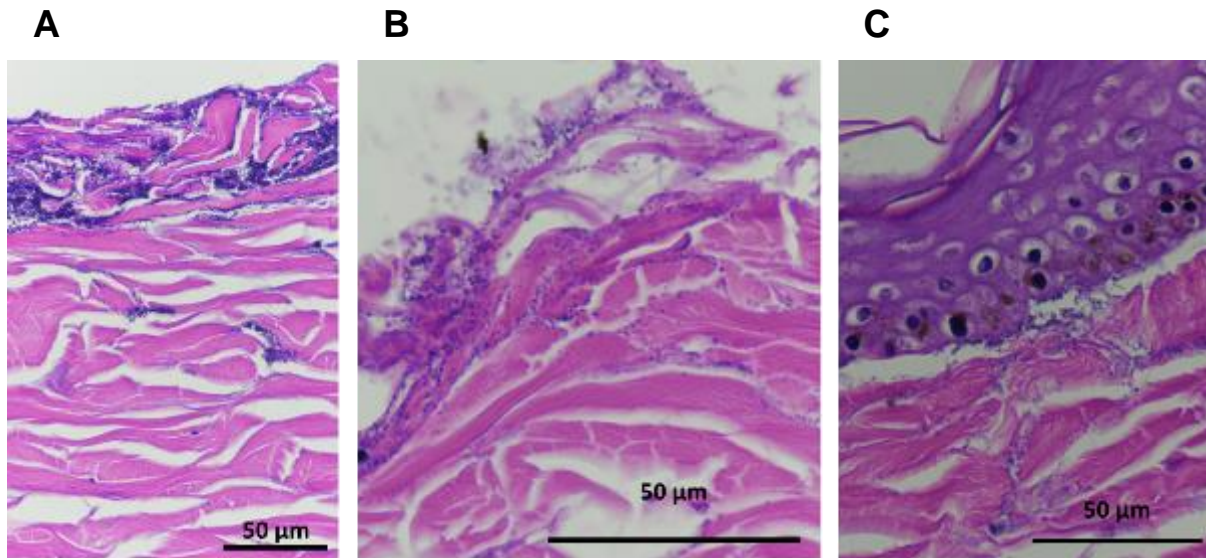

Figure 2.7: *Histological analysis of wound infected ex vivo skin with S. aureus (1× 10^7 CFU) for 5 days. H&E staining. **A**, **B**. colonization of the wound. **C**. penetration of the bacteria under the epithelium layer.*

The chosen complementary technique to confirm the presence of bacteria in the skin samples was the kit Thermo Scientific™ Richard-Allan Scientific™ Gram Stain (Tissue) to identify gram-positive and gram-negative bacteria in tissue sections:

- Gram-positive organisms stain blue to blue-black
- Gram-negative organisms stain red
- Tartrazine provides a yellow background stain

In **Figure 2.8,** examination of Gram-stained tissue sections revealed microcolonies attached to tissues. The dark purple color of small balls confirms the bacteria phenotypes of Gram-Positive *S. aureus* strain. Therefore, the previous results with H&E staining were confirmed by Gram Staining showing the presence of *S. aureus* in the upper skin layer and, to a lesser extent, into the dermis (**Figure 2.8**) (black, grey spots).
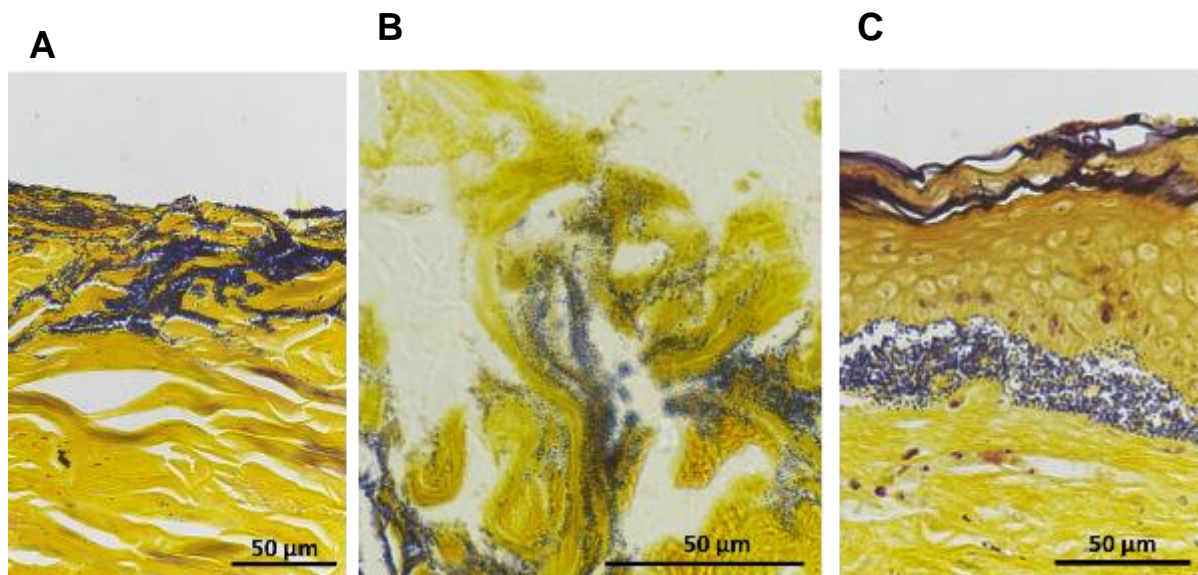
Figure 2.8: *Histological analysis of wound infected ex vivo skin with S. aureus (1× 10^7 CFU) for 5 days. Gram staining.* ***A****,* ***B****. colonization of the wound.* ***C****. penetration of the bacteria under the epithelium layer.*

Finding anti-bacteria antibodies for immunofluorescence remains a complex part as only a small number of specific anti-bacteria antibodies are available. For our study, an anti-*S. aureus* provided by BioRad was used. This antibody recognizes specific epitopes on the *S. aureus* membrane. Visualization of the specific interaction was achieved by further interaction with a fluorescent labeled secondary antibody, in our case Alexa 488, which can be excited at 490 nm and emits fluorescence in the green at 525 nm. Performing immunohistochemistry allows localization of the infection within the *S. aureus*-infected skin tissues.To assess antibody specificity, we first perform an immunofluorescence staining on *S. aureus* suspension fixed on a glass slide. As negative control, we used a suspension of *P. aeruginosa*. In **Figure 2.9**, fluorescence images show clearly the green labelling in *S. aureus* strain suspension and no bacteria detection in the *P. aeruginosa* strain suspension. This result underlines the specific interaction properties of anti-*S. aureus* antibodies. In addition, at higher magnification we can see that the fluorescent labelling is localised on membranes of bacteria indicating that the anti-*S. aureus* antibodies bind to the membrane pattern of *S. aureus*.
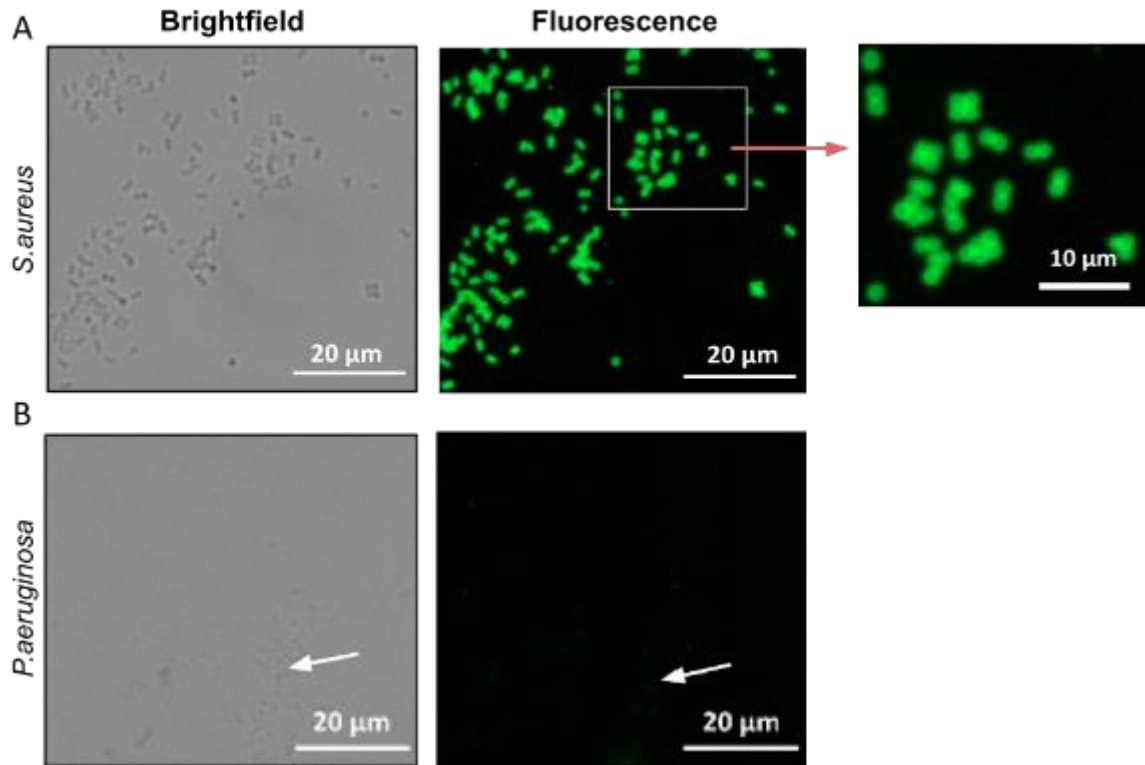
Figure 2.9: *Visualization of S. aureus with Immunofluorescence: Fluorescence images of a suspension of* **A.** *S. aureus (1× 10^7 CFU mL^{-1}) and* **B.** *P. aeruginosa (1× 10^7 CFU mL^{-1}) using an anti-S. aureus antibody revealed by a secondary antibody conjugated with Alexa 488 fluorophore.*

Immunostaining of slide-mounted tissue sections was performed with the same anti-*S. aureus* antibody and Alexa 488 fluorophore-conjugated secondary antibody. Counter-staining with DAPI was also performed to delineate the skin structure. It is important to notice that the skin exhibits endogenous fluorescence in the same wavelength range as the fluorophore. The stratum corneum shows a strong fluorescence signal under 490 nm light excitation and collagen fibers in deeper tissue layers show weak autofluorescence. Thus, this autofluorescence makes it easy to delineate skin borders. Nevertheless, the intensity is much lower than that obtained with specific antibody immunostaining. In consequence, the localization of the bacteria colonization becomes comfortable.

Fluorescence microscopy of the immunostaining sections of wounded skin produced images which agreed with those obtained using H&E and Gram staining. In comparison with the uninfected wound, the infected samples show a strong green fluorescence signal in the wounded part of the skin infected with *S. aureus* for 7 days, especially on the surface of the

wound. A clear colonization of the wound zone is visible with an infected layer depth of about 15-20 µm (**Figure 2.10**).

The presence of oxygen at the top of the skin apparently enabled the bacteria to achieve much higher growth rates than the bacteria in lower parts of the dermis. Although we focused on an infection with a single bacteria (*S. aureus*), most chronic wound infections have a polymicrobial nature, in which strict and facultative anaerobe bacteria dominate.[23]
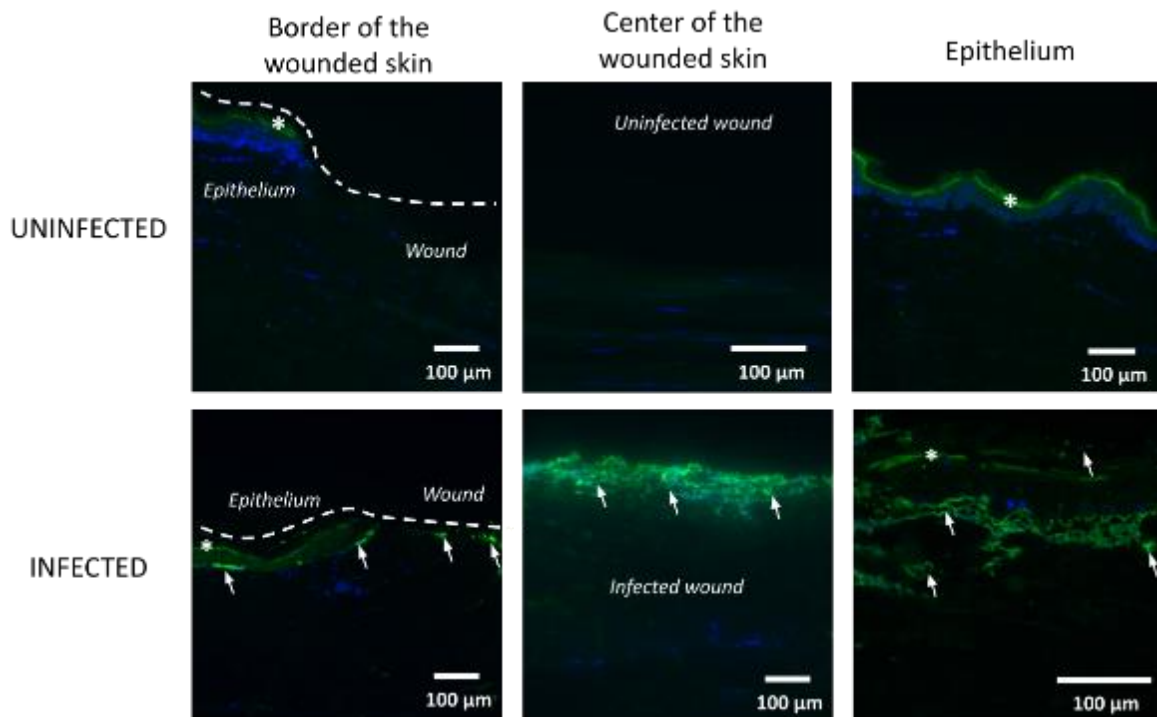
Figure 2.10: *Immunohistochemistry analysis of S. aureus infected wound skin samples (Green fluorescence: excitation 450 nm, emission 525 nm). A DAPI counterstaining was also performed. Dotted lines define the skin surface. Arrows show bacteria clusters. Stars spot the stratum corneum.*

SEM was used to verify the physical presence of viable bacteria within the wounds, the colonization location and the existence of complex biofilm structure. SEM imaging of vertically cut skin was performed both on our *S. aureus* infected wound model and a non-infected control. The fine structural organization of the epidermis and dermis were observed in both uninfected and infected samples. All skin layers were observed: plaque-like layers of the stratum corneum, compact structure of epidermis and the overall rearrangement of the dermal collagen network (**Figure 2.11**).

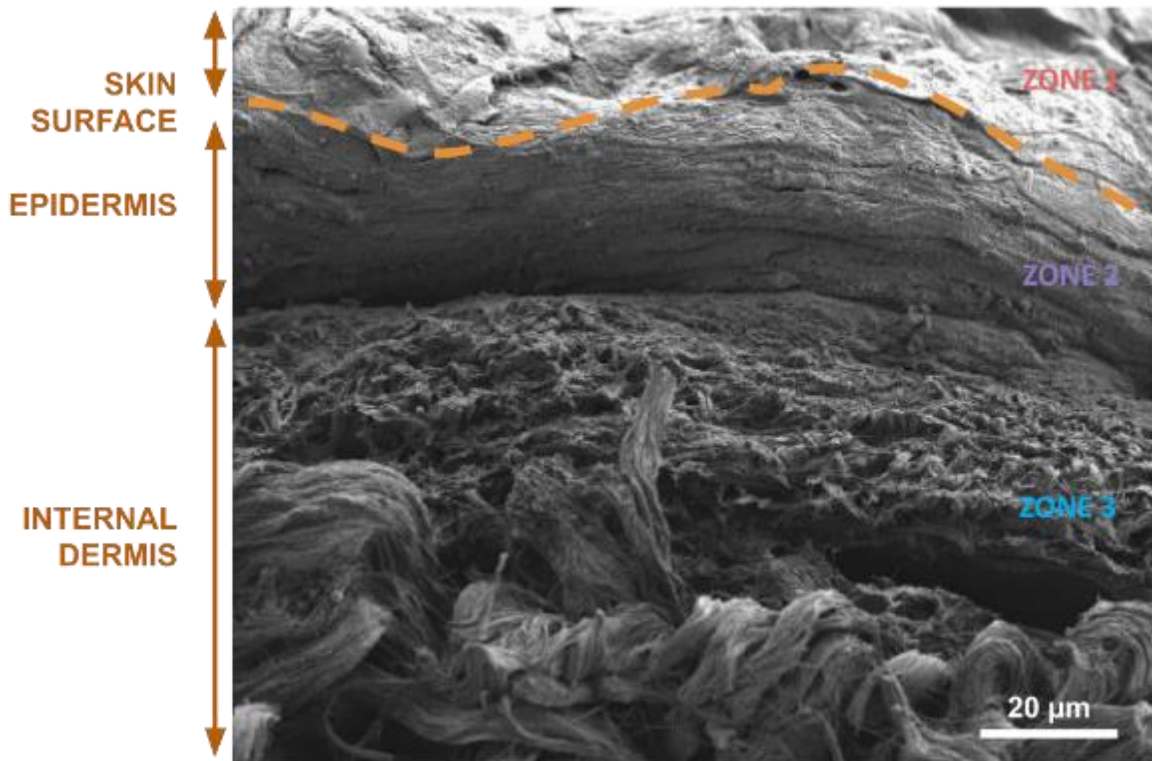***Figure 2.11****: Scanning electron microscopic image of the skin wound profile. The wounded skin samples were cultivated for 5 days in the genoskin medium. All skin layers are visible with SEM imaging: surface of the skin with plaque-like layers correspond to the stratum corneum (Zone 1), the epidermis layer appearing as a compact structure (Zone 2),a thick layer of fibrous connective tissue with a large amount of collagen fibers (Zone 3)*

Nevertheless, pictures of infected wounds (**Figure 2.12**) revealed some differences in skin morphology, especially with the presence of the aggregates of microcolonies of bacteria throughout the wound bed. A high number of bacteria was interwoven in collagen bundles and appeared physically attached to the collagen fibers. Furthermore, the higher magnification image shows the extracellular polysaccharide network (EPS matrix) surrounding the bacteria and confirms the biofilm conformation of bacteria in our model.[24]

The results comply with histologic analysis. Whilst large bacteria clusters can be observed in the uppermost layer of the skin, approximately at depths 20 µm, in the lowest layer no bacteria microcolony was observed. However, with the SEM we are able to distinguish single bacteria colonization in deeper tissue. This visualization clearly indicates that our model is capable of developing consistent wound biofilms. With the high efficiency, utility and versatility of SEM, it is possible to analyze the wound and visualize the bacterial biofilm. Provided that the preparation technique is appropriate, the potential for SEM to study bacteria and biofilms is wide-ranging.
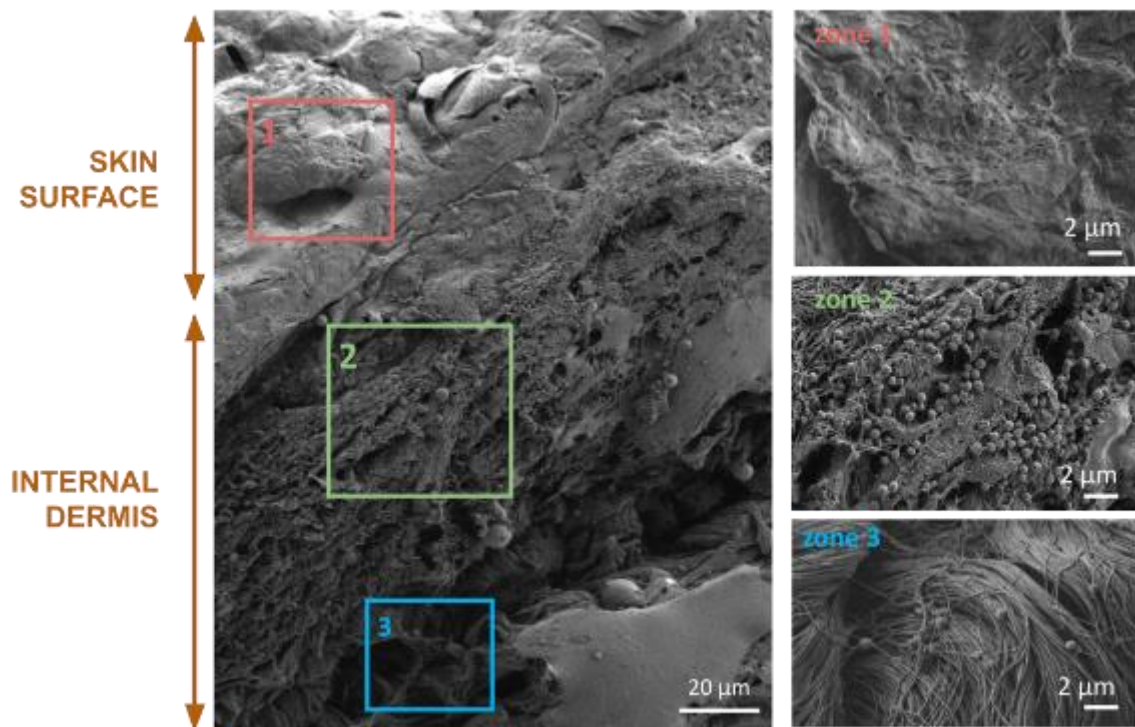
Figure 2.12: *Scanning electron microscopic image of the infected skin wound profile. The wounded and infected skin samples were fixed after 5 days of infection. All skin layers are visible on the picture: surface of the skin (Zone 1), collagen fibers containing cocci-shaped bacteria embedding in EPS matrix (Zone 2) and the deeper dermis with low amount of bacteria (Zone 3).*

2.1.4 Pre-inflammatory response to *S. aureus* infection

In order to verify whether the infected *ex vivo* skin model was still able to evoke an immune response, cytokine profiling was performed 5 days post-infection with Gram-positive *S. aureus*. In this study, the expression levels of the cytokines IL-6, IL-8, IL-1, TNFα, IFNα, IFNβ. The level of RNA expression can be detected by qPCR. As observed in **Figure 2.13**, we detected a significant increase in the expression levels of IL-6 after infection. The levels of IL-8 were also up-regulated, however they did not reach statistical significance. IL-8 is mainly produced by macrophages with its primary function being to induce chemotaxis of target cells, such as neutrophils and granulocytes.[25] The low level of IL-8 in response to the infection might indicate that no severe inflammation was installed in the skin.

We also determined the levels of IL-1 as indication of tissue damage and bacterial infection. A statistically significant increase was observed in wound skin infected for 5 days

with *S. aureus* **(Figure 2.13)**. In addition, significant induction of IFN-1α, IFN-β up and TNF-α to about 3-fold was observed after *S. aureus* infection **(Figure 2.13)**.
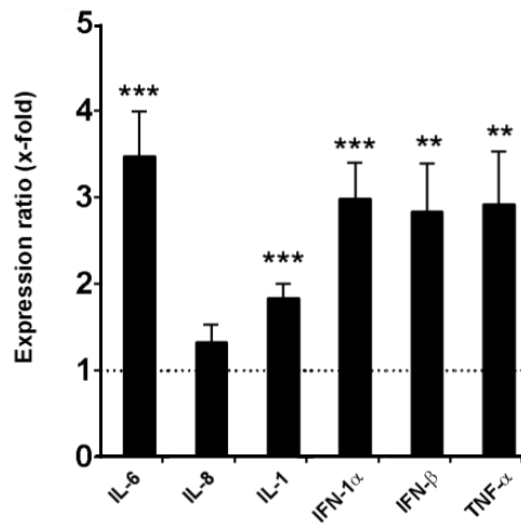
.

Figure 2.13: *Analysis of pro-inflammatory cytokines by qPCR on homogenate skin tissues. Tissue samples were harvested 5 days after infection with S. aureus. After homogenization, the expression profiles of the selected cytokines were determined by qPCR. Both groups were normalized to the uninfected control group. Dotted line: expression level in wound uninfected skins. Values are displayed as mean ±SEM (** p<0.01,*** p<0.001; **** p< P ≤ 0.0001 n=2-6).*

2.1.5 Infection with *P. aeruginosa*

In addition, our model is still limited to a single species of bacteria, namely *S. aureus*. Organisms such as *P. aeruginosa* and various anaerobic bacteria are also very common within chronic wound microbial flora.[12] It was useful to extend our investigation to other bacterial species, to deepen our understanding of the model's capabilities and shortcomings. *Pseudomonas aeruginosa* (*P. aeruginosa*), a Gram-negative opportunistic pathogen causing severe acute and chronic infections at different sites including skin burns and wounds, was chosen. For the first experiment, we proceed like *S. aureus* infection with 1×10^7 CFU for 5 days of incubation. By visual observation, the infection was rapidly visible on the surface of the skin with green pigment (**Figure 2.14A**). The infection spreads rapidly through the skin to contaminate the medium. During the collection, it appeared that the samples infected with *P. aeruginosa* were largely damaged. The epithelium took off from the dermis and the weight of the explant was 20% less than uninfected samples.
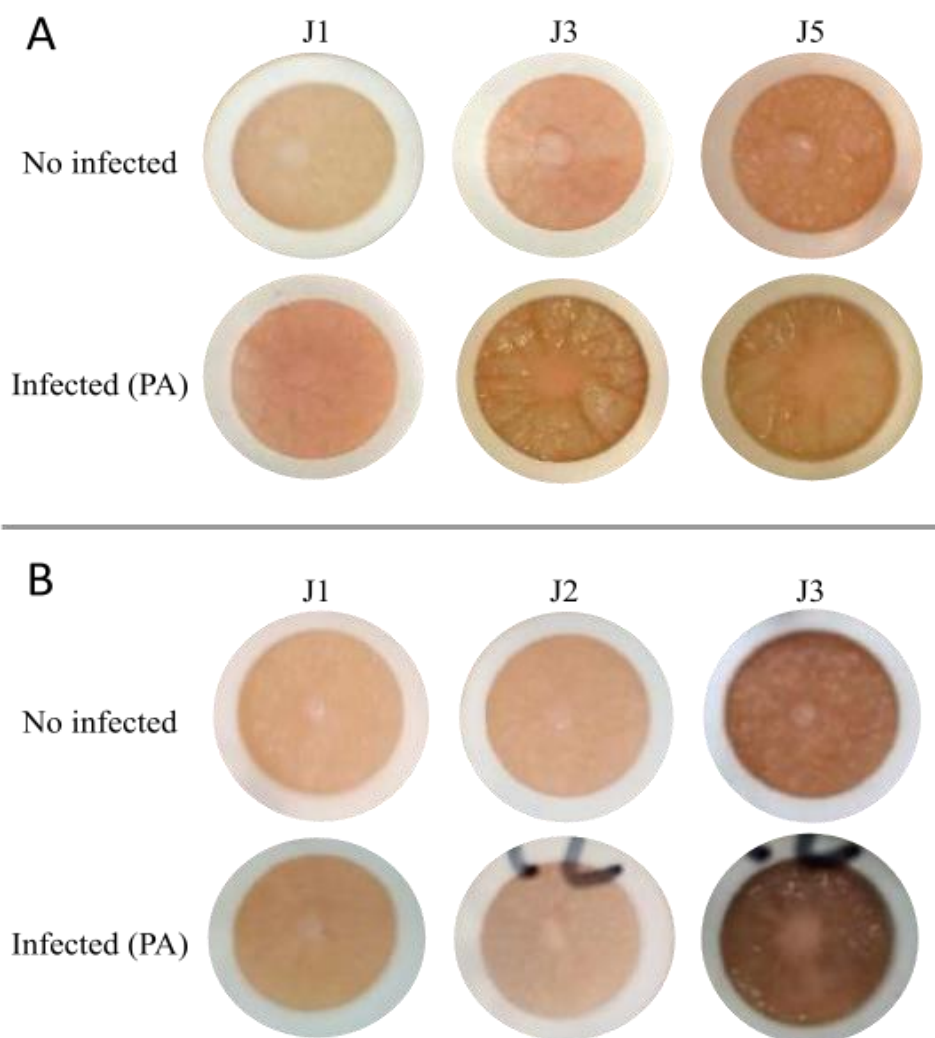
Figure 2.14*: P. aeruginosa infection of wounded skin. Optical representative images of uninfected wound skin and wound skin infected with P. aeruginosa. **A**. Infection with 1× 10^7 CFU for one to five days (First trial). **B**. Infection with 1× 10^4 CFU for one to three days (Second trial).*

For the second experiment, wounded skin explants were infected with low concentrated suspension of bacteria (1x10^4 CFU) for only 3 days. The macroscopic observation shows that the surface of the skin becomes green rapidly as the first experiment (**Figure 2.14B**). Bacteria pass through the skin and contaminate the culture medium. The wound edge becomes unclear indicating that the epithelium starts to unstick and skin explant starts to waste away after the 3 days infection. In correlation with macroscopic analysis, the bacteria quantification of infected skin shows rapid increase in growth of bacteria after 1 day (1×10^6 CFU /g skin tissue) and continue to expand rapidly until the third day (1×10^{10} CFU /g skin tissue) **(Figure 2.15).**

Figure 2.15: *Infection efficiency of P. aeruginosa on ex vivo skin.. Bacterial counts per gram skin tissue as determined from wound skin infected with P. aeruginosa (1× 10⁴ CFU) at different time intervals. All the values are displayed as means ± SEM*
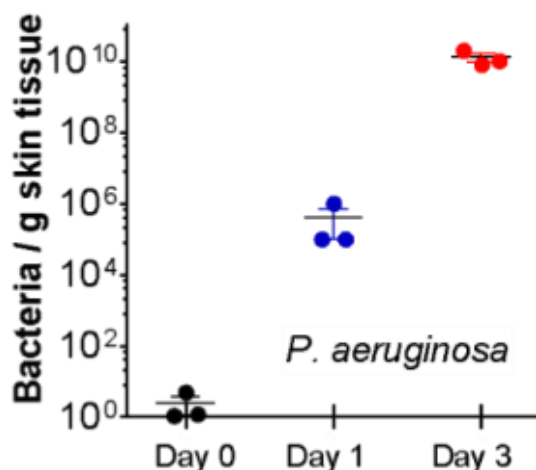
Our wound infection model with *P. aeruginosa* still has some limitations due to the non-viable skin sample after the infection. The optimization of the culture medium may be done by adding antibiotics to control the quick spreading of bacteria. As the virulence of *P. aeruginosa* is very strong, the reduction of bacteria concentration can also be considered.

In conclusion, an *ex vivo* human infected wound model as a valid alternative to the classical animal models was described. Hyposkin® model presents a convenient, ready to use and robust model in which *ex vivo* full thickness organ culture experiments may be performed. We showed that *S. aureus* strain adapted to induce detectable and consistent infection levels in the wound skins starting from 3 days post-infection up to one week. Interestingly, a lower bacterial stock solution led to high variation in most of the samples, suggesting that the development of an adequate microbial biofilm is necessary to induce a significant skin infection. When we used the invasive *P. aeruginosa* pathogen at the indicated concentration, we observed severe skin damage already after short bacterial exposure time. The complete destruction of the tissue architecture restricted the infection and prevented the subsequent inflammatory responses, limiting the use of this pathogen in our model. These evidences suggested that the microorganism strains, as well as the number of microorganisms applied and the length of the exposure time, should be carefully considered. Immunohistological analysis of *S. aureus* infected wounds showed significant bacteria colonization of the wound zone, with

an infected layer depth of about 15-20 µm. Except for the missing epidermis, we did not observe a deep skin damage, making this model relevant for the topical conditions. Scanning electron microscopy confirmed the presence of bacteria physically attached to the collagen fibers of the extracellular matrix. In addition, inoculation with *S. aureus* induced a pronounced inflammatory response characterized by increased expression levels of inflammatory cytokines, suggesting the viability of this model to investigate the effects of wound infections at transcriptional level. Overall, our model proved to generate a quantifiable bacterial infection and immune response. For future work, it would be interesting to investigate the biological interactions of the different bacteria biofilms with chronic wounds, as well as compare the effects of different antimicrobial agents.

The *ex vivo* model provides the opportunity to study the dynamics of infection and to test local treatments directly in humans. Despite the lack of the body environment, the human wound healing mechanisms and cell responses as well as the structure of the skin offered by this model give us a way to carry out a very informative first-line study. Genoskin, with its skin models suitable for many skin disorders, provides easy access to the complex skills of *ex vivo* explant culture. However, it has failed to be fully relevant for the study of infection and wound healing. Indeed, it is difficult to modulate the culture parameters to optimize our models. For example, the adaptation of the culture medium is essential to allow the implementation of a model with other bacterial strains as it would have been the case with *Pseudomonas aeruginosa*. Moreover, the implementation of a Polymicrobial model seems unfeasible if we cannot control all the conditions. In order to continue the development of models and to extend our knowledge, the establishment of our own explant culture is therefore an interesting prospect.

2.2 SKIN WOUND MODEL

The opportunity to collect skin from surgery is a great advance for research. Indeed, the experiment conducted on human materials allows us to rapidly and properly interpret findings and translate them to medicine. For this purpose, it is important to develop a professional relationship with clinics and hospitals that allow the use of skin explants. Then, it is needed to obtain the approval and authorization of the French Ministry of Research and Higher Education. Skin explants are collected right after surgery and transferred to the research lab. After the collect, decontamination, resizing and de-hypodermisation are performed to obtain

the skin samples. The large size of skin leftover makes it possible to obtain many samples. Thus, we can take samples at regular times during the 7 days in order to study the state of the sample over time. Before the resizing, the skin is wounded using a 2mm punch biopsy in order to obtain an open wound. Then, the culture is performed in a 24-well plate using the adequate culture medium. The study can be performed over the course of a few days, here we choose 7 days of culture. The culture is performed in an incubator at 37°C and 5% CO_2. Skin viability is mainly studied using microscopic techniques. The most used staining is hematoxylin & eosin staining. This stain allows visualization of different layers of the epidermis, dermis, and appendages. The changes created by the culture conditions can be easily observed.

In this chapter, the development of an *ex vivo* wound skin model is described and discussed in more detail to underline the major limitations of the model with the aim of assessing the ultimate applicability of these models for new treatments of complex wounds. The viability of skin in culture and the wound healing progression was investigated by Hematoxylin & eosin staining of skin sections.

2.2.1 Structure of the skin explant

The use of the *ex vivo* human model allows us to have a tissue that includes all the cell types as well as the appendages of the skin. Thus, with our model and H&E staining, we are able to distinguish the different layers of the skin (**Figure 2.16A**): the stratum corneum, the epidermis, the papillary dermis, the reticular dermis and the hypodermis containing the adipose tissue. It is also possible to differentiate cell types such as the different layers of keratinocytes, melanocytes with a characteristic brown color, and fibroblasts in the dermis (**Figure 2.16B**). For other cell types like immune resident cells, immunological staining is needed. The different structures of the dermis such as collagen fibers in different orientations, sebaceous glands (**Figure 2.16C**), sweat glands, blood capillaries and hair follicles can be discerned on the sections.[26]
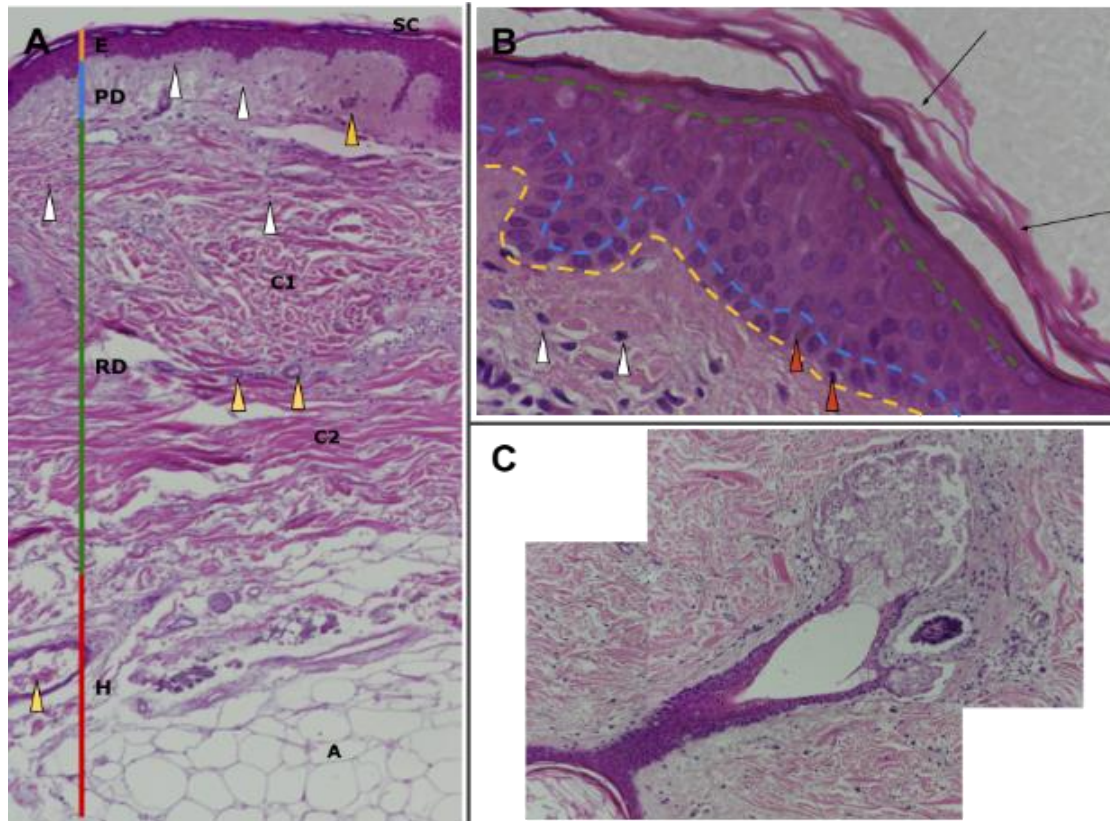
Figure 2.16 : *Histological Characterization of Ex Vivo Cultured Human Skin Explants.* ***A.*** *Low power displays of the full thickness skin including stratum corneum (SC), epidermis (E), papillary dermis (PD), reticular dermis (RD), containing collagen network in different orientation (C1, C2) with scattered fibroblasts (white triangle) as well as blood capillary (yellow triangle) and hypodermis (H) containing the adipose tissue (A).* ***B.*** *Zoom on keratinocyte layers with stratum corneum by irregular fiber structures (SC) and the basal keratinocyte layer (between yellow and green dotted lines) linked to the dermis at the level of the basement membrane (yellow dotted line). Fibroblasts (white triangles) and melanocytes (brown triangles).* ***C.*** *Sebaceous glands link to the hair follicle.*

As noticed in previous chapters, our skin samples come from different regions of the body. The use of leftovers from esthetic surgery can be obtained from abdominosplaties, low body lift, thigh lift, arm lift, buttock lift, breast reduction. During the thesis, three skin samples from three different donors so three different surgeries have been obtained. Skin samples from Genoskin arose from abdominal surgeries. The first collection of skin from the hospital of Lille was obtained from low body lift and the second from arm lift. The histological observation showed differences in skin organization, especially the number of keratinocyte layers of the epidermis (**Figure 2.17**). The papillary dermis also appears thicker in the abdominal samples than in limbs. It is considered that the abdominal region presents more preserved basal characteristics due to low exposure to external aggressors (UV radiation, pollution, etc.).

However, working on different types of skin allows us to explore more precisely the subtleties of this tissue and to have a broad knowledge of its properties. Moreover, the majority of chronic wounds are found on the lower limbs.
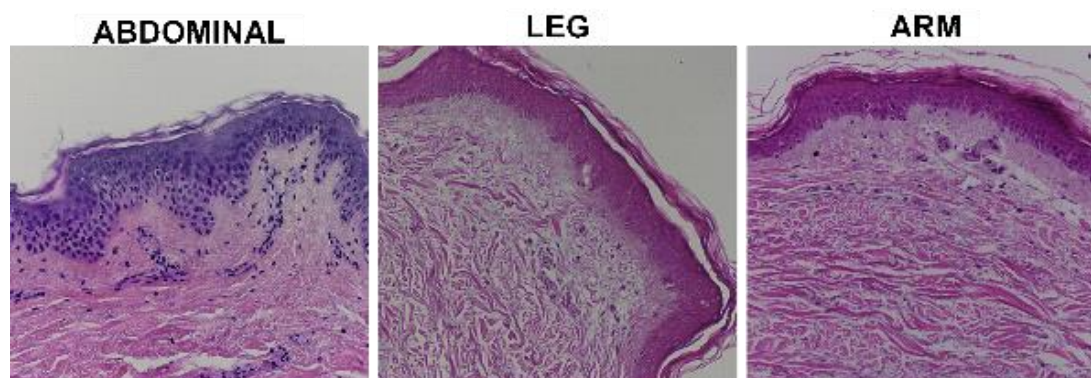

Figure 2.17 : *Histological Characterization of Ex Vivo Cultured Human Skin Explants from different regions of the body.*

To determine tissue integrity over one week of culture, histological observations were performed on H&E-stained tissue sections at day 0, 3, and 7. The appearance of spongiosis, necrosis, parakeratosis, epidermal/dermal separation, hyperplasia, removal of stratum corneum or vacuoles are all structural features indicating skin viability.[27-29] All these parameters were observed in skin sections to detect tissue damage. Representative images of donor 1 hematoxylin and eosin-stained tissue over time are shown in **Figure 2.18**. Compared with control skin at day 0, cultured skin shows no evidence of spongiosis, necrosis, and parakeratosis over the course of seven days of culture. A slight increase in epidermal thickness is observed over the 7 days. The stratum corneum remains attached to the epidermis except sometimes due to preparation artifacts. There is no sign of epidermal/dermal separation. On day 7, pyknosis was observed on the upper layers of keratinocytes. It is characterized by contracted and intensely stained nuclei leaving an empty space around them.[27] This is the typical structure of cells undergoing necrosis and apoptosis.[30] This phenomenon has not been observed on all skin sections, it represents about 50% of the samples and may depend on the donor. The integrity of the basal cell layer is still good and proliferation can still occur, but the cornification process does not seem to occur because the cells undergo death by necrosis or apoptosis. Therefore, the tissue is still viable because there is no sign of necrosis but it starts to deteriorate after 1 week of culture. This observation has already been made in other skin culture studies.[29,31-32] 7 days of culture seems to be a good compromise to have time to test the different treatments or perform an infection.
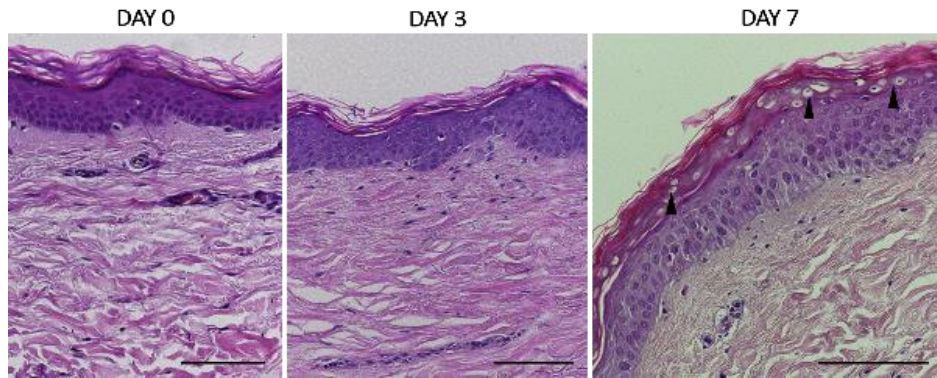
Figure 2.18 : *Characteristic images of histological structures observed upon ex vivo human skin at day 0, 3 and 7 of culture. Magnification 20 x. Black triangles indicate pyknosis. The length of the scale bars is 100 μm.*

2.2.2 Wound closure kinetic

An incisional wound was applied to *ex vivo* human skin explants with a 2-mm biopsy punch. Macroscopic observation of the skin during culture is shown in **Figure 2.19**. On the day of collection, the skin has a pink color. When the wound is made, redness is observed at the wound caused by the blood capillaries present in the skin without actually creating bleeding. Over time, the specimens lose their reddish color and become white due to the lack of blood flow. White is the normal color of non-vascularized but still viable tissue. The sign of dead tissue is a gray color that turns black due to necrotic tissue.
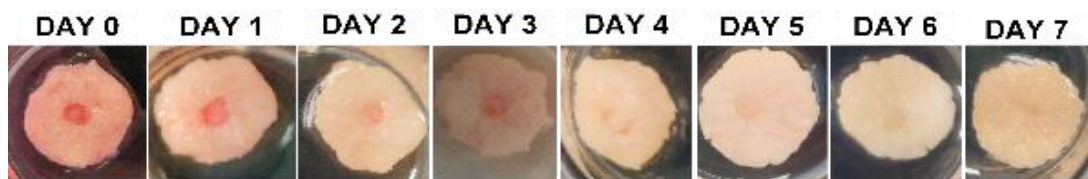
Figure 2.19 : *Macroscopic visualization of wounded skin over the days of one week.*

The investigation of re-epithelialization in our experimental skin wound model was performed by H&E staining. Serial histological analyses were performed on lesioned skin explants on days 0, 3, and 7 after wounding. Qualitative analysis of microscopic events was performed at magnification 4x to visualize the entire wound (**Figure 2.20**). At day 0, the clean cut of the wound edge is visible. By day 3, the wound healing process has begun to occur, as evidenced by the observation of the healing tongue structure. This shape of the wound edge shows that the keratinocytes at the margins of the wound have proliferative and migratory activity for re-epithelialization. After 7 days of culture, the entire wounded area was progressively colonized by a monolayer of proliferating keratinocytes until it covered the

wound bed. In parallel, the area beyond the wound edge showed an intact skin morphology with the epidermis attached to the dermis throughout the 7 days of culture.
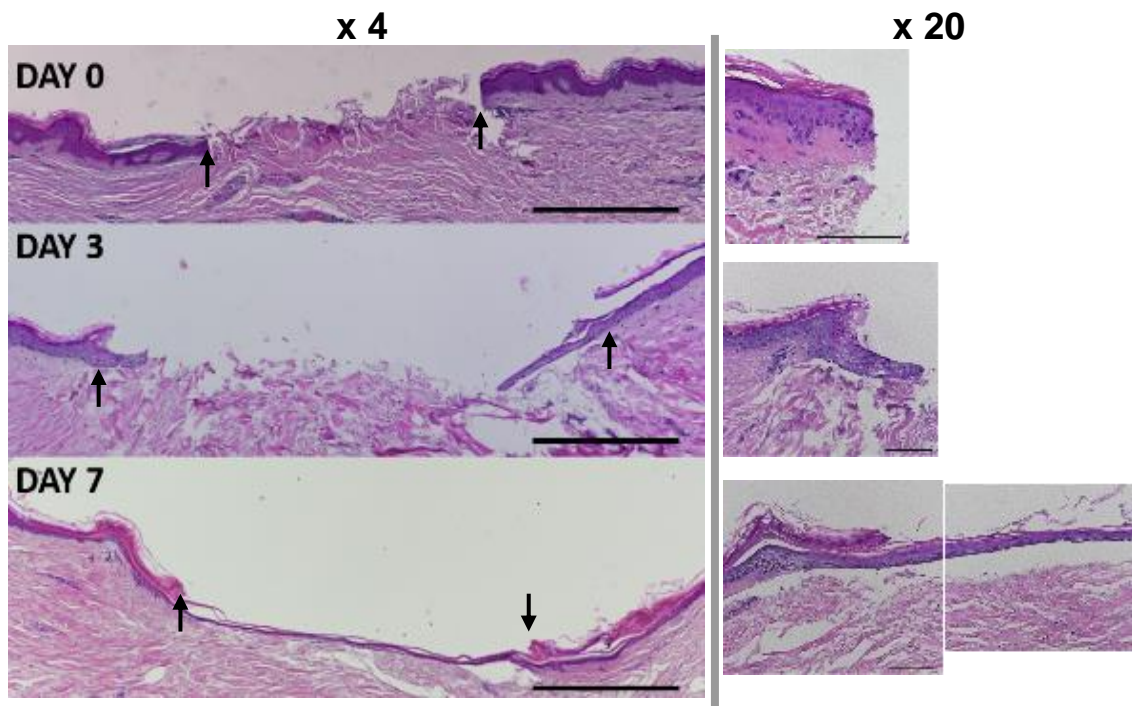
Figure 2.20 : *Kinetics of Re-Epithelialization in Human Skin Explants by H&E staining at day 0, 3 and 7 in culture. **Left.** Magnification 4 x. Black arrows indicated the original incision areas. The length of the scale bars is 500 μm. **Right.** Zoom on healing tongue structure. Magnification 20 x. The length of the scale bars is 100 μm.*

2.2.3 Medium study

In order to modulate the skin culture conditions, several media were tested. As a standard medium, we chose the commonly used DMEM, supplemented with fetal bovine serum (FBS) and a mixture of antibiotics. The serum was added to stimulate cell activity and optimize skin viability and the antibiotics to limit contamination. Fetal bovine serum is obtained from the blood of healthy bovine fetuses.[33] Because the healing process is different in the fetus and the adult[34], a newborn calf serum (NCS) was chosen to observe the difference in skin structure and healing. NCS is the liquid component of coagulated blood from healthy, slaughtered bovine calves less than 20 days old.[33] For the second medium tested, we explored the possibility of adapting the model to diabetic conditions. The standard DMEM contains 4.5 g/L of glucose required for growth culture. In the case of a diabetic study, DMEM with a low glucose concentration can be used to mimic the clinical condition of the diabetic patient. In our case, we test DMEM with 1g/L glucose supplemented with FBS serum and antibiotics. Finally, to

fit our infected wound model, we chose a medium without antibiotics for the fourth condition. During culture, the explants did not show any signs of contamination or decreased viability compared to explants cultured with antibiotics.

First, the skin structure was observed by H&E staining to identify damage according to culture conditions (**Figure 2.21**).
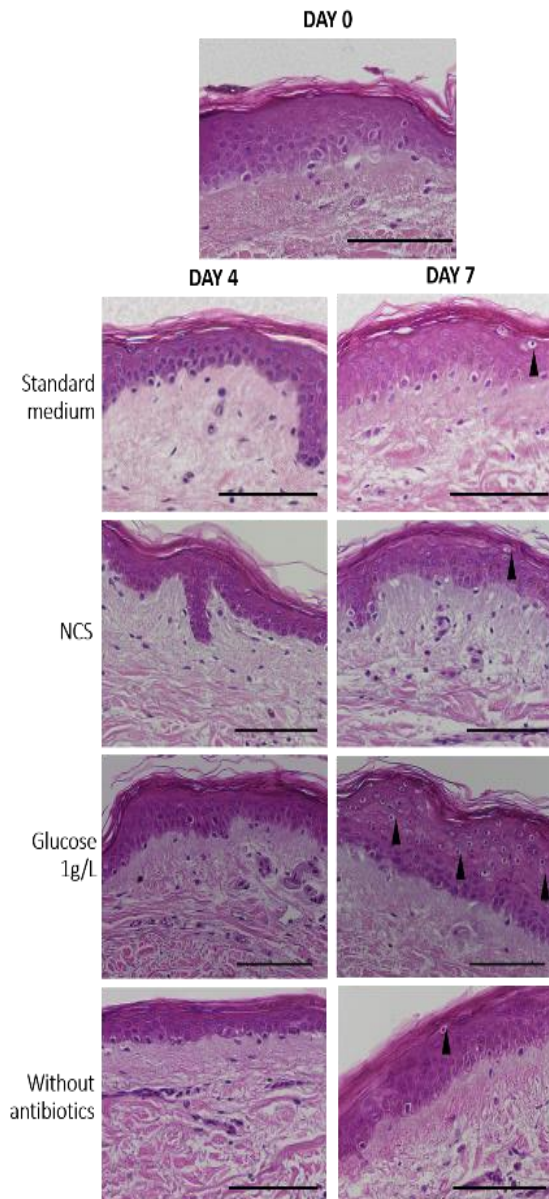
Figure 2.21 : *Characteristic images of histological structures observed upon ex vivo human skin at day 0, 4 and 7 of culture with several medium composition. Magnification x20. The length of the scale bars is 100 μm.*

After 4 days, no difference in epidermal structure for the 4 media tested have been detected. The epidermis remained attached to the dermis and there was no evidence of spongiosis, necrosis, parakeratosis or massive keratinocyte death. The epidermis was still

attached to the dermis. After 7 days, skin cultured with standard medium showed good skin integrity with only a few pyknosis compared to **Figure 2.18**. The two types of serum and the use of antibiotics did not seem to influence the structure of the skin after 7 days of culture. However, the low-glucose culture shows skin damage at day 7 compared to the culture with standard medium. The outer layers of the epidermis show pyknosis with only 1 or 2 layers of viable keratinocytes. Thus, glucose is important in the integrity of the skin structure during culture and would not only impact wound healing. Skin culture under low glucose diabetic conditions should be done differently or only over 4 days.

Then, the kinetics of re-epithelialization with the 4 tested media were performed by serial histological analysis on days 0, 4 and 7 (**Figure 2.22**). No significant differences in wound healing have been observed between the two serums. In correlation with the skin structure results, the wound healing process with low level of glucose culture looked to stop during the process and the healing tongue is shorter than with the standard medium. The culture without antibiotics didn't show any influence on wound healing. The healing tongue extends progressively through the wound bed.
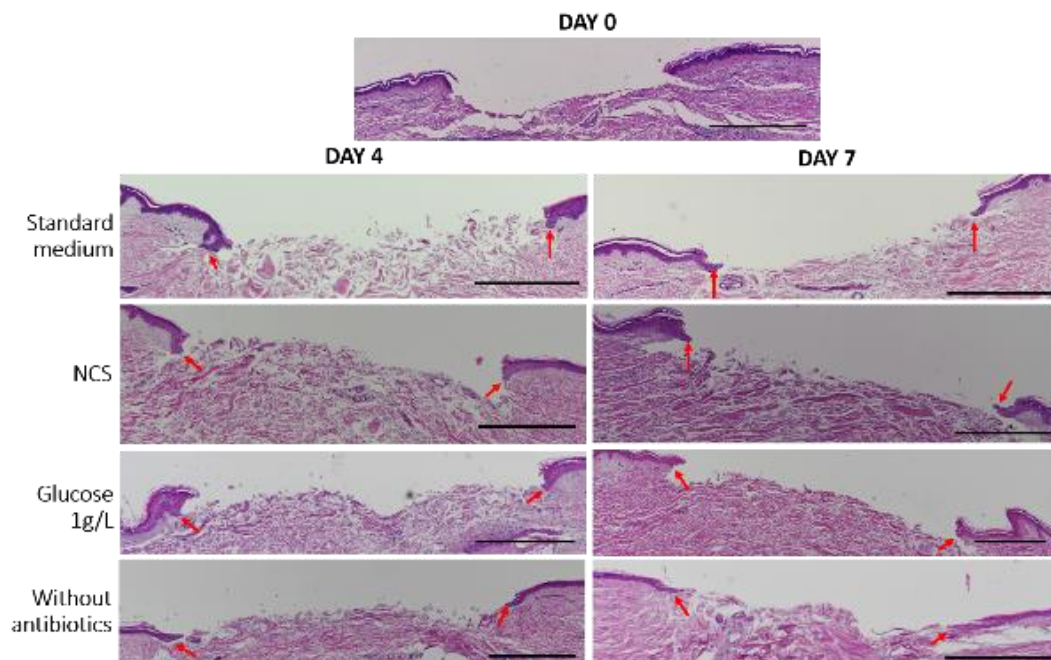

Figure 2.22 : *Kinetics of Re-Epithelialization in Human Skin Explants by H&E staining at day 0, 4 and 7 in culture with several medium compositions. Magnification 4 x. The length of the scale bars is 500 μm.*

The development of the *ex vivo* skin model allows various study purposes. The understanding of this experimental model is crucial to translate the results. This part had the

objectives to decipher the skin structure to well establish the model. The histological analysis of skin over time has shown a good viability with low signs of skin damages. In order to deepen skin characterization, the analysis of the metabolic activity of the epidermal layers could be performed. The skin section analysis by immunohistological staining allows the detection of cell activity. For example, the detection of filaggrin, loricrin, involucrin, keratin 10 and keratin 14 can be a great combination of biomarkers to demonstrate that the *ex vivo* human models in culture present a good viability.[35-36] In addition, the re-epithelialization process could also be characterized. For instance, numeration of Ki67+ proliferating keratinocytes using immunohistological staining of the skin section is a common technique used for wound healing study.[37-38]

The modulation of culture conditions is one of the advantages of this model. Many different types of media have been used to make skin cultures. The choice of media depends on the nature of the study and laboratory practices. DMEM is commonly used in the majority of cell experiments and tissue culture. Addition of serum to a culture medium is commonly used for cell proliferation enhancement, however the serum is composed of several growth factors and its exact composition varies. With a no well-defined medium composition the reproducibility can be impacted. Some studies think that culture medium without addition of serum is efficient to maintain the skin integrity in culture.[39] Other culture parameters such as temperature and light can be modified in order to better reproduce the culture conditions. Indeed, 37°C is traditionally used for tissue culture but does not reproduce clinical conditions. The temperature of the skin should be close to 32°C on the surface.

The possibility to modulate the medium without risk of reducing the viability allows us the opportunity to implement new clinical conditions like infected wounds as previously described in part 1 with the Genoskin model. The difficulty of obtaining skin samples at the hospital due to the limitation of surgical interventions constrained us in the development of the model. The dependence on surgeries is one of the shortcomings of the model and can lead to a limitation in the experimentation due to a lack of supply.

REFERENCES

1.   Fryberg, R.; Banks, J., Challenges in the Treatment of Chronic Wounds. Ad. Wound care **2015,** 4, 560.

2.   Dinh, T.; Tecilazich, F.; Kafanas, A.; Doupis, J.; Gnardellis, C.; Leal, E.; Tellechea, A.; Pradhan, L.; Lyons, T. E.; Giurini, J. M.; Veves, A., Mechanisms involved in the development and healing of diabetic foot ulceration. . Diabetes **2012,** 61, , 2937.

3.   Dalton, T.; Dowd, S.; Wolcott, R.; Sun, Y.; Watters, C.; A Griswold, J.; Rumbaugh, K. An *In Vivo* Polymicrobial Biofilm Wound Infection Model to Study Interspecies Interactions. PloS one **2011**, 6, e27317.

4.   Piaggesi, A.; Låuchli, S.; Bassetto, F.; Biedermann, T.; Marques, A.; Najafi, B.; Palla, I.; Scarpa, C.; Seimetz, D.; Triulzi, I.; Turchetti, G.; Vaggelas, A., Advanced Therapies in Wound Management. J. Wound Care **2018,** 27, 52.

5.   Altinbasak, I.; Jijie, R.; Barras, A.; Golba, B.; Sanyal, R.; Bouckaert, J.; Drider, D.; Bilyy, R.; Dumych, T.; Paryzhak, S.; Vovk, V.; Boukherroub, R.; Sanyal, A.; Szunerits, S., Reduced Graphene-Oxide-Embedded Polymeric Nanofiber Mats: An "On-Demand" Photothermally Triggered Antibiotic Release Platform. ACS Appl. Mater. Interfaces **2018,** 48, 41098-41106.

6.   Li, C.; Ye, R.; Bouckaert, J.; Zurutuza, A.; Drider, D.; Dumych, T.; Paryzhak, S.; Vovk, V.; Bilyy, R. O.; Melinte, S.; Li, M.; Boukherroub, R.; Szunerits, S., Flexible Nanoholey Patches for Antibiotic-Free Treatments of Skin Infections. ACS Appl. Mater. Interfaces **2017,** 9, 36665-36674.

7.   Trøstrup, H.; Thomsen, K.; Calum, H.; Høiby, N.; Moser, C., Animal models of chronic wound care: the application of biofilms in clinical research. . Chronic Wound Care Management and Research **2016,** 3, 123—132.

8.   Zomer, H. D.; Trentin, A. G. Skin Wound Healing in Humans and Mice: Challenges in Translational Research. Journal of Dermatological Science **2018**, 90 (1), 3–12.

9.   Plastic   Surgery   Statistics | Global   Plastic   Surgery   Statistics https://www.isaps.org/medical-professionals/isaps-global-statistics/ (accessed May 28, 2021).

10.   Xu, W.; Hong, S. J.; Jia, S.; Zhao, Y.; Galiano , R. D.; Mustoe, T. A., Application of a partial-thickness human *ex vivo* skin culture model in cutaneous wound healing study. Lab. Investig. **2012,** 99, 584–599

11.   Mendoza-Garcia, J.; Sebastian, A.; Alonso-Rasgado, T.; Bayat, A. Optimization of an *Ex Vivo* Wound Healing Model in the Adult Human Skin: Functional Evaluation Using Photodynamic Therapy. Wound Repair and Regeneration **2015**, 23 (5), 685–702.

12.   Schaudinn, C.; Dittmann, C.; Jurisch, J.; Laue, M.; Günday-Türeli, N.; Blume-Peytavi, U.; Vogt, A.; Rancan, F., Development, standardization and testing of a bacterial wound infection model based on *ex vivo* human skin. . PLoS ONE **2017,** 12, e0186946.

13.   Yoon, D. J.; Fregoso, D. R.; Nguyen, D.; Chen, V.; Strbo, N.; Fuentes, J. J.; Tomic-Canic, M.; Crawford, R.; Pasta, I.; Isseroff, R. R., A tractable, simplified *ex vivo* human skin model of wound infection. . Wound Repair Regen. **2019,** 27, 421-425.

14.   Corzo-Leon, D. M. C. A.; MacCallum, D. M., An *ex vivo* human skin model to study superficial fungal infections. . Front. Microbiol. **2019,** 10, 1172.

15.   Steinstraesser, L.; Sorkin, M.; Niederbichler, A. D.; Becerikli, M.; Stupka, J.; Daigeler, A.; Kesting, M. R.; Stricker, I.; Jcobsen, F.; Schulte, M., A novel human skin chamber model to study wound infection *ex vivo*. Arch. Dermatol. Res. **2010,** 302, 357-365.

16.   *Ex Vivo* Model of Human Skin (HOSEC) as Alternative to Animal Use for Cosmetic Tests. Procedia Engineering **2015**, 110, 67–73.

17.   *Ex vivo* human skin models from donated human skin https://www.genoskin.com/ (accessed Jun 4, 2021).

18.   Pages, E.; Pastore, M.; Rosselle, L.; Barras, A.; Skandrani, N.; Cantelmo, A.; Boukherroub, R.; Merle, E.; Descargues, P.; Szunerits, S. LB1138 An *Ex Vivo* Human Skin Model for Healing of Infected Wounds. Journal of Investigative Dermatology **2019**, 139 (9), B24.

19.   Oates, A.; Bowling, F. L.; Boulton, A. J. M.; Bowler, P. G.; Metcalf, D. G.; McBain, A. J. The Visualization of Biofilms in Chronic Diabetic Foot Wounds Using Routine Diagnostic Microscopy Methods. Journal of Diabetes Research **2014**, 2014, e153586.

20.   Hochstim, C. J.; Choi, J. Y.; Lowe, D.; Masood, R.; Rice, D. H. Biofilm Detection With Hematoxylin-Eosin Staining. Arch Otolaryngol Head Neck Surg **2010**, 136 (5), 453.

21.   Hong, S. D.; Dhong, H.-J.; Chung, S.-K.; Kim, H. Y.; Park, J.; Ha, S. Y. Hematoxylin and Eosin Staining for Detecting Biofilms: Practical and Cost-Effective Methods for Predicting Worse Outcomes After Endoscopic Sinus Surgery. Clin Exp Otorhinolaryngol **2014**, 7 (3), 193–197.

22.   Tandara, A.; Mustoe, T., Oxygen in Wound Healing—More than a Nutrient. World J. Surg. **2004,** 28, 294.

23.   Bowler, P. G.; Duerden, B. I.; Armstrong, D. G. Wound Microbiology and Associated Approaches to Wound Management. Clin Microbiol Rev **2001**, 14 (2), 244–269.

24.   Hurlow, J.; Blanz, E.; Gaddy, J. A. Clinical Investigation of Biofilm in Non-Healing Wounds by High Resolution Microscopy Techniques. J Wound Care **2016**, 25 (Suppl 9), S11–S22.

25.   Hammond, M. E.; Lapointe, G. R.; Feucht, P. H.; Hilt, S.; Gallegos, C. A.; Gordon, C. A.; Giedlin, M. A.; Mullenbach, G.; Tekamp-Olson, P., IL-8 induces neutrophil chemotaxis predominantly via type I IL-8 receptors. J. Immunol. **1995,** 155, 1428-1433

26.   Sharma, A.; Zakka, L. R.; Mihm, M. C. Anatomy of the Human Skin and Wound Healing. In Bioengineering in Wound Healing; Frontiers in Nanobiomedical Research; World Scientific, 2016; Vol. Volume 8, pp 27–57. https://doi.org/10.1142/9789813144583_0002.

27.   Matarrese, P.; Beauchef, G.; Peno-Mazzarino, L.; Lati, E.; Fitoussi, R.; Vié, K. Assessment of an *Ex Vivo* Irritation Test Performed on Human Skin Explants and Comparison of Its Results with Those of a 24-/48-h Human Patch Test for the Evaluation of Cosmetics. Toxicology *in Vitro* **2021**, 70, 105030. https://doi.org/10.1016/j.tiv.2020.105030.

28.   Moll, I.; Houdek, P.; Schmidt, H.; Moll, R. Characterization of Epidermal Wound Healing in a Human Skin Organ Culture Model: Acceleration by Transplanted Keratinocytes1. Journal of Investigative Dermatology **1998**, 111 (2), 251–258. https://doi.org/10.1046/j.1523-1747.1998.00265.x.

29.   Neil, J. E.; Brown, M. B.; Williams, A. C. Human Skin Explant Model for the Investigation of Topical Therapeutics. Sci Rep **2020**, 10 (1), 21192. https://doi.org/10.1038/s41598-020-78292-4.

30.   Kroemer, G.; Galluzzi, L.; Vandenabeele, P.; Abrams, J.; Alnemri, E.; Baehrecke, E.; Blagosklonny, M.; El-Deiry, W.; Golstein, P.; Green, D.; Hengartner, M.; Knight, R.; Kumar, S.; Lipton, S.; Malorni, W.; Nuñez, G.; Peter, M.; Tschopp, J.; Yuan, J.; Piacentini, M.; Zhivotovsky, B.; Melino, G. Classification of Cell Death. Cell Death Differ 2009, 16 (1), 3–11. https://doi.org/10.1038/cdd.2008.150.

31.   Xu, W.; Hong, S. J.; Jia, S.; Zhao, Y.; Galiano, R. D.; Mustoe, T. A. Application of a Partial-Thickness Human *Ex Vivo* Skin Culture Model in Cutaneous Wound Healing Study. *Laboratory Investigation* **2012**, *92* (4), 584–599. https://doi.org/10.1038/labinvest.2011.184.

32.   Frade, M. A. C.; Andrade, T. A. M. de; Aguiar, A. F. C. L.; Guedes, F. A.; Leite, M. N.; Passos, W. R.; Coelho, E. B.; Das, P. K. Prolonged Viability of Human Organotypic Skin Explant in Culture Method (HOSEC). *Anais Brasileiros de Dermatologia* **2015**, *90* (3), 347–350. https://doi.org/10.1590/abd1806-4841.20153645.

33.   Pirnia, A.; Assadollahi, V.; Alasvand, M.; Moghadam, A.; Gholami, M. R. A Comparison of the Effects of Fetal Bovine Serum and Newborn Calf Serum on Cell Growth and Maintenance of Cryopreserved Mouse Spermatogonial Stem Cells. *Mol Biol Rep* **2020**, *47* (12), 9609–9614. https://doi.org/10.1007/s11033-020-06004-2.

34.   Ulrich, M. M. W. Fetal Wound Healing. In *Textbook on Scar Management: State of the Art Management and Emerging Technologies*; Téot, L., Mustoe, T. A., Middelkoop, E., Gauglitz, G. G., Eds.; Springer International Publishing: Cham, 2020; pp 3–9. https://doi.org/10.1007/978-3-030-44766-3_1.

35.   Danso, M. O.; Berkers, T.; Mieremet, A.; Hausil, F.; Bouwstra, J. A. An *Ex Vivo* Human Skin Model for Studying Skin Barrier Repair. *Experimental Dermatology* **2015**, *24* (1), 48–54. https://doi.org/10.1111/exd.12579.

36.   Eberlin, S.; Silva, M. S. da; Facchini, G.; Silva, G. H. da; Pinheiro, A. L. T. A.; Eberlin, S.; Pinheiro, A. da S. The *Ex Vivo* Skin Model as an Alternative Tool for the Efficacy and

Safety Evaluation of Topical Products. *Altern Lab Anim* **2020**, *48* (1), 10–22. https://doi.org/10.1177/0261192920914193.

37.   Bhora, F. Y.; Dunkin, B. J.; Batzri, S.; Aly, H. M.; Bass, B. L.; Sidawy, A. N.; Harmon, J. W. Effect of Growth Factors on Cell Proliferation and Epithelialization in Human Skin. *Journal of Surgical Research* **1995**, *59* (2), 236–244. https://doi.org/10.1006/jsre.1995.1160.

38.   Onuma, H.; Mastui, C.; Morohashi, M. Quantitative Analysis of the Proliferation of Epidermal Cells Using a Human Skin Organ Culture System and the Effect of DbcAMP Using Markers of Proliferation (BrdU, Ki-67, PCNA). *Archives of Dermatological Research* **2001**, *293* (3), 133–138. https://doi.org/10.1007/s004030000195.

39.   Lebonvallet, N.; Jeanmaire, C.; Danoux, L.; Sibille, P.; Pauly, G.; Misery, L. The Evolution and Use of Skin Explants: Potential and Limitations for Dermatological Research. *Eur J Dermatol* **2010**, *20* (6), 671–684. https://doi.org/10.1684/ejd.2010.1054.

CHAPTER 3 : APPLICATIONS OF *EX VIVO* SKIN MODELS : SKIN IRRITATION TO INFLUENCE OF ANTIBIOTICS ON INFECTED SKIN

3.1 Skin irritation - Influence of temperature on skin structure

The toxicity assay, or irritancy test, consists of confirming that a product does not have any bad effect on human or animal tissues.[1] It provides information about the tolerance and dose-dependent effect of the product. In the cosmetic field, many efforts have been employed to stop animal experimentation for toxicity assay.[2-4] One of the alternative methods that has been proposed is the use of *ex vivo* human skin. A lot of research about the viability of the *ex vivo* model of human skin in culture has been carried out and shows a good skin viability for several days in culture.[5-7] Skin irritancy induced by a chemical product can be tested at concentrations that are close to real exposure conditions.[8-9] Different versions of this model have been proposed to observe the skin viability after other stimulation than chemical produced.[10-12] Thus, *ex vivo* human skin models are also of interest for other skin barrier disruptors such as physical stimulation. Skin viability after stimulation such as laser irradiation[13], electrochemical stimulation[14] or mechanical injury[15] can be assessed by histologic observation or molecular and functional assays.

In transdermal drug delivery systems, the application of a physical stimulation[16], such as photothermal activaiton[17], ultrasound pulses[18] or mechanical skin penetration[19], on the top of the skin can lead to skin barrier disruption or injury if it's not well controlled.[20] The skin irritancy assay is a convenient model to establish the reliability of the system. The appropriate model must (i) remain viable during treatment and for several days afterwards, (ii) present an air/skin interface to receive topical products directly, (iii) have the stratum corneum at the top of the skin to represent the skin permeability and (iv) the 3D organization of the skin layers with epidermal and dermal cellular types.[21] The human *ex vivo* model remains the faster and less expensive *in vitro* model as well as the most representative *in vitro* model of human skin.[22]

Several technologies have been proposed over the years to modify the barrier properties of the *stratum corneum* (SC) and to deliver therapeutics.[23] While the use of chemical skin enhancers (e. g. azone, peptides and more lately ionic liquids)[24-27] has allowed in some cases to increase passive diffusion of small molecules, significant efforts have been spent in the last years on the development of physical technologies to modify the barrier properties of the SC and to allow a broader class of drugs to be delivered into the skin.[16,23] Heat, in the form of thermal ablation, has been already considered as possible strategy.[28-31] The creation of local

heat leads to cell ablation and transient creation of microchannels or pores typically 50-100 µm in diameter. This technology enables the transdermal delivery of a wide range of drugs.[32]

An example of the use of an *ex vivo* skin model to analyze skin irritation is shown in the following.[33] A drug loaded hydrogels was studied as a controlled-release system (**Figure 3.1**). Indeed, our group investigated lately the formulation of a heat active hydrogels by mixing graphene oxide (GO) or carboxyl enriched reduced graphene oxide (rGO-COOH) with metformin hydrochloride, an insulin sensitizer drug currently used as first line therapy to treat patients with type 2 diabetes. The driving forces of the gelation process between the graphene-based nanomaterial and metformin are hydrogen bonding and electrostatic interactions, weakened at elevated temperature. Using the excellent photothermal properties of the graphene matrixes, it could be demonstrate that these supramolecular drug reservoirs can be photothermally activated for transdermal metformin delivery
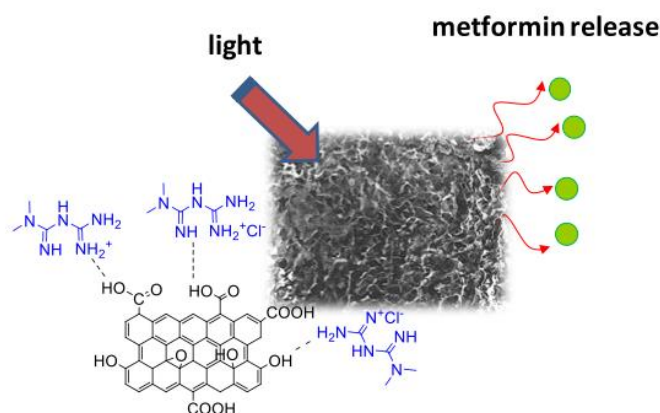

Figure 3.1*: Schematic representation of the near-infrared light activatable hydrogels for metformin delivery.[33]*

Taking advantage of the availability of the bandage, the thermal damage to the skin tissue caused by laser irradiation was evaluated in my thesis. When skin is exposed to temperatures above the physiological temperature over an extended period of time, skin tissue damage can occur.[34] It has been recently demonstrated that heating rGO loaded hydrogels in contact with a skin at a laser power density of up to 5 W cm^{-2} did not induce any significant histological changes to the skin.[35] **Figure 3.2** shows the histological analysis of human skin in contact with rGO-COOH/metformin gel before and after laser irradiation (10 min, 0.5-1.0 W cm^{-2}) using conventional hematoxylin and eosin (H&E) staining. At a laser power density up to 0.7 W cm^{-2} (corresponding to 52°C) normal dermis characteristics are observed. The

epidermis as well as the dermis are unaffected. These results are in agreement with reports by others using Cu7S4 loaded microneedles, where tissue necrosis in the dermis could be visualized after NIR irradiation for 3 min and 1 min, respectively.[36] Application of ≥ 1 W cm^{-2} laser power results however in skin damage.
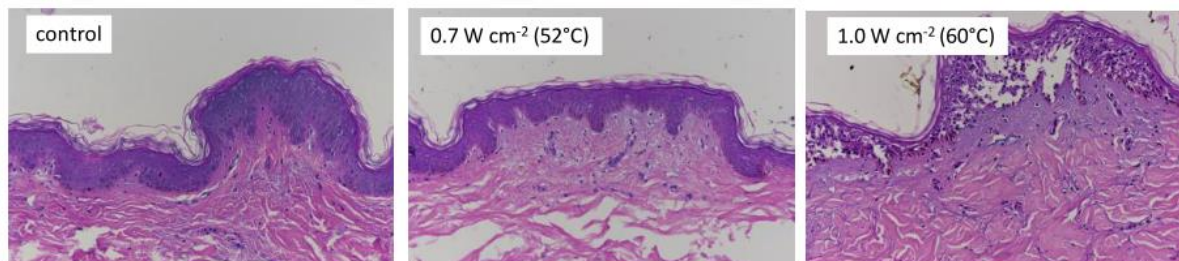

Figure 3.2 : *Bright-field micrograph of histological section of an ex vivo human skin model before (control) and after 10 min laser irradiation at 0.7 W cm^{-2} and 1 W cm^{-2}.*

In conclusion, explants used in our experiments are surplus tissues from plastic surgeries. The purpose of this model is to evaluate the effect of our technologies in a clinical environment and to confirm the non-toxicity of the system. As a starting point, we tested the use of *ex vivo* skin explants as a tool to validate the effect of the laser on the skin structure for a new drug delivery system. Indeed, the delivery of an antidiabetic drug was proposed by switching on and off cycles of near-infrared light, which increased the release in the on state of the laser.[33] With this test, we determined the best temperature that can be used for drug delivery. The use of human skin as a test system has proven to be an important tool that allows direct testing of the impact on human skin instead of using the animal model.

3.2 Topical Wound healing treatment Skin irritation

When developing new treatments, it is extremely important to consider the safety and the efficiency of the treatment. *Ex vivo* models have been largely used for wound care treatment like topical ointment or dressing as the air/skin interface lends itself well to the study of local treatments.[7,37-38] The objective of this part of the thesis is to describe our first line results with the *ex vivo* human skin model and to illustrate the applicability of this tool for the evaluation of topical products in wound healing treatment. We tested 6 products: ethanol 70%, PBS at pH 5,5, curcumin (diluted in ethanol), platelet extract, hydrogel polyvinyl alcohol (PVA) and a commercial healing cream (Cicatryl®). 10µl of each solution were added onto the top of the wound. The PVA hydrogels were made in 96 well plates to obtain 5mm diameter and can be

placed directly on the wound. The cream was applied with a sterile swab. The control consisted of 10 µl PBS.

The histological observation of wound skin was performed to identify the skin and wound structure (**Figure 3.3**). Wound healing was analyzed on day 0, 4 and 7 days. The control showed a poor healing rate with a short healing tong at day 7. This can be explained by the variability of donors. Indeed, in **Figure 2.20**, the epidermal outgrowth evolved more quickly over the wound bed. However, the analysis of the wound healing can be performed because the same donor is used for control and treatment conditions. The comparison between wound with PBS and skin with product allows to determine the wound healing enhancement or inhibition.
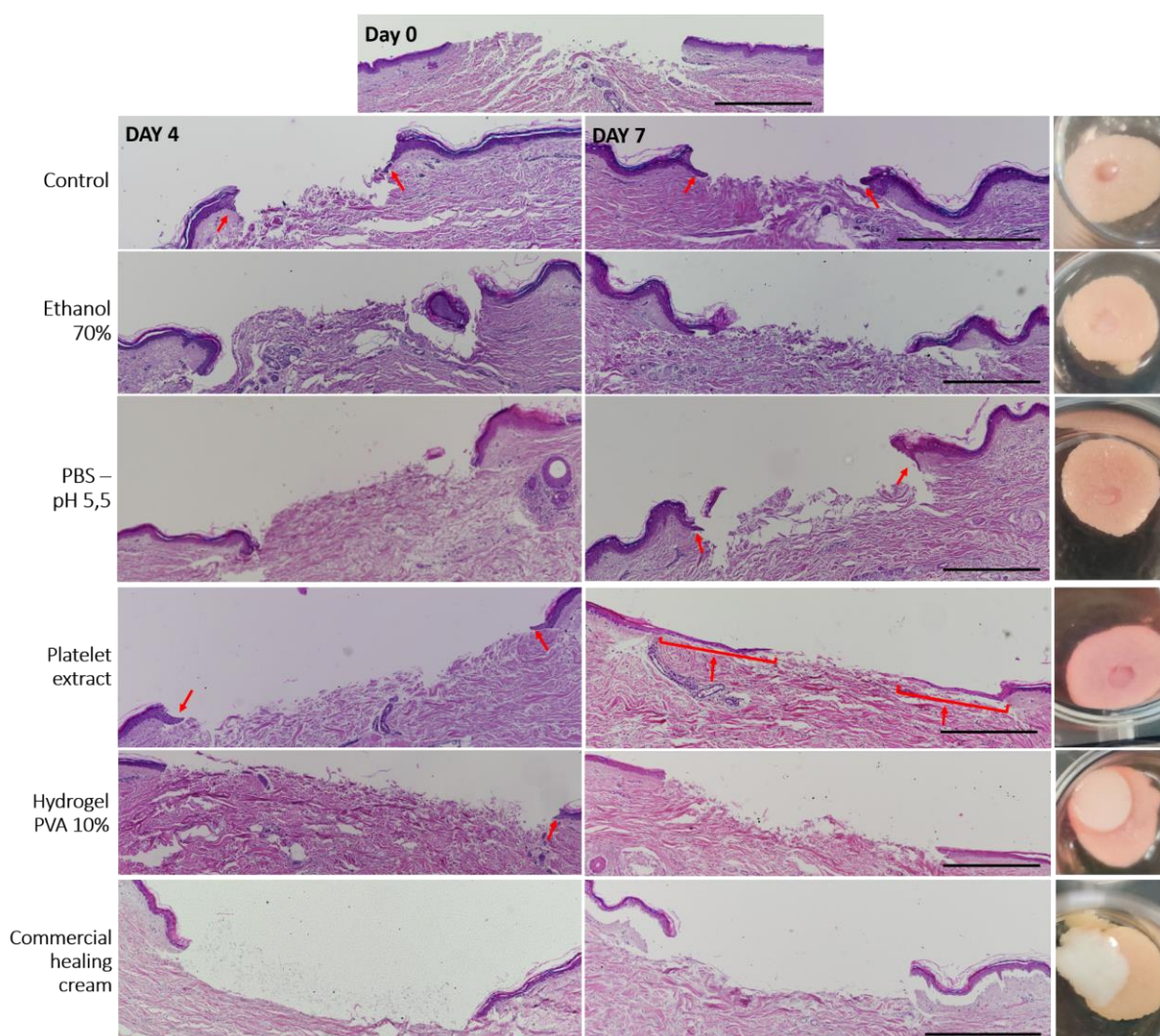

Figure 3.3 : *Representative images of hematoxylin and eosin staining of ex vivo wounds treated with several products. Macroscopic pictures of ex vivo skin models with the treatment are shown on the right.*

Ethanol 70% was used as a negative control of wound healing. Indeed, the observation of the wound edge showed that no epidermal tongue is visible when the skin is treated with the chemical product. Thus, Ethanol 70% seems to have a harmful effect on the cicatrization by stopping it. PBS at pH 5.5 was selected following the hypothesis that pH affects wound healing. Indeed, chronic wounds have been analyzed to be at a pH around 8 while a wound that has a good healing process would have a pH closer to the physiological pH, around 7-7.5.[39-40] The pH 5.5 corresponds to the physiological pH of the skin, which allows for barrier properties. The histological observation of this experiment has shown that the acidic pH does not seem to have a beneficial effect on healing. Indeed, the beginning of the healing tongue is well observed but the growth is delayed, it is only observed on the histological sections of day 7. The control is the PBS used in a standard way at pH 7.4 and seems to be more adapted in our experiment. The comparison with skin without liquid deposition showed that PBS at pH 7,4 doesn't have properties that activate healing (data not shown).

The third product tested was a platelet extract. It consists of a platelet lysate that contains a large amount of proteins such as numerous growth factors known to activate healing.[41-42] Indeed, the first step of classical wound healing is the formation of a blood clot containing a large quantity of platelets. This phenomenon allows the release of numerous molecules that regulate healing. Platelet extract is known to be a promising treatment for chronic wounds. The histological observation of the wound in our *ex vivo* skin model treated with the platelet extract shows a significant increase in the size of the epidermal outgrowth at the wound edge. On day 7, the healing tongue was 3 times longer than on the control sample without treatment. This also shows us that even though healing is slower with this donor skin, we are still able to study treatments that can improve healing.

Recently, much hope has been placed on PVA hydrogel for biomedical use.[43-46] This polymer is capable of being physically cross-linked implying that there is no use of toxic chemicals for hydrogel cross-linking.[47-49] In addition, all the long washing steps are not necessary for the hydrogel preparation. Consequently, the biocompatibility of the hydrogel is very satisfactory because there is no risk of chemical residue. However, spontaneous cross-linking can occur during the hydrogel stockage that makes long-term conservation difficult for the moment and optimizations are needed. The hydrogel is an innermost material. On its own it does not provide elements that will allow the cellular mechanisms to be activated, it only provides a protection that protects and preserves a moist environment. As we can observe in

our *ex vivo* models, results of this patch on the skin do not show very obvious healing properties. However, we can see that the structure of the skin seems very clean, the epidermis is attached to the dermis and the edge of the wound remains straight compared to the treatment with solution or cream. Moreover, the beginning of healing is still observed on day 7. Thus, the hydrogel combined with healing molecules could be tested for safety and efficiency with our *ex vivo* skin model. However, it is important to ensure that the hydrogel does not inhibit healing.

The last product tested is a commercialized healing cream: Cicatryl®. The results obtained with H&E staining do not show very convincing healing properties. Indeed, the humid environment provided by the deposit of cream for several days leads to the detachment of the epithelium. In the manufacturer's instructions, it is indicated to apply the cream abundantly and to cover it with a bandage. The application of the cream for several hours up to 24 hours surely allows time for the healing molecule to penetrate the wound. However, during the experiment, the cream was left on the skin for 7 days to avoid the risk of contamination when cleaning the explant. The overly humid environment therefore does not seem to be adequate for wound healing in our model. The use of the *ex vivo* skin model for the treatment with cream or ointment requires some optimizations to avoid this kind of problem.

In conclusion, it is important to determine the treatment conditions that you want to study. The use of a hydrogel dressing for 1 week without decreasing the viability of the samples showed good feasibility, but the test of a cream for a long time is not recommended. Based on these results, the use of a hydrogel containing platelet extract appears to be an encouraging option for establishing a treatment for chronic wound healing. Despite the risk of mixing the medium with the treatment, we chose the culture of explants directly in the medium which is simpler to implement.[22] A system of delineation of the surface area of the skin could be considered to better mimic clinical conditions. For example, it is possible to mount the tissue in diffusion cells with the medium under the skin, and thus avoid lateral migration of the drug into the medium.[50-51] The possibility to use a gelose is also a good option to stabilize the sample or using a ring around the wound to stop the liquid migration.[52]

3.3 **Effect of an antibiotics on the *ex vivo* infected skin model**

In order to explore the wound model potential as a test system for local antimicrobial treatment, *S. aureus* infected wounds were treated with two different concentrations of cefepime (8 and 30 µg mL^{-1}) by placing the solution on the top of the infected wound at day 4 and incubate for additional 24 h at 37 °C and 5% CO_2 (**Figure 3.4**).
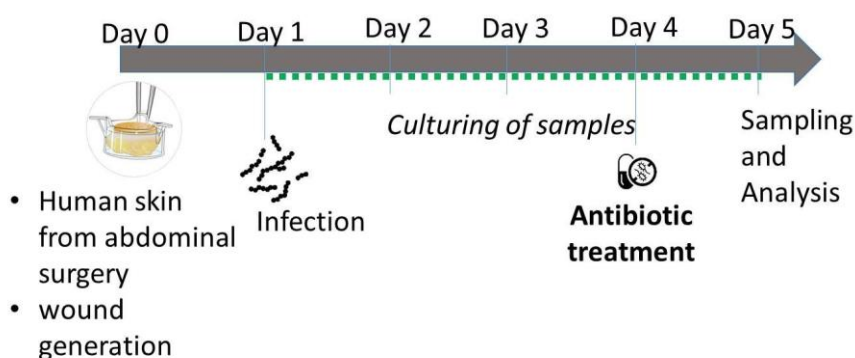
Figure 3.4: *Effect of cefepime on the ex vivo infected skin model. Experimental work flow of antibiotic treatment of the infected wounds.*

Cefepime, a fourth-generation cephalosporin antibiotic, was selected for its antibacterial efficiency against *S. aureus* strains.[53-54] For *S. aureus* a minimum inhibitory concentration (MIC) value of 3±0.3 µg mL^{-1} was obtained with cefepime (**Figure 3.5**).
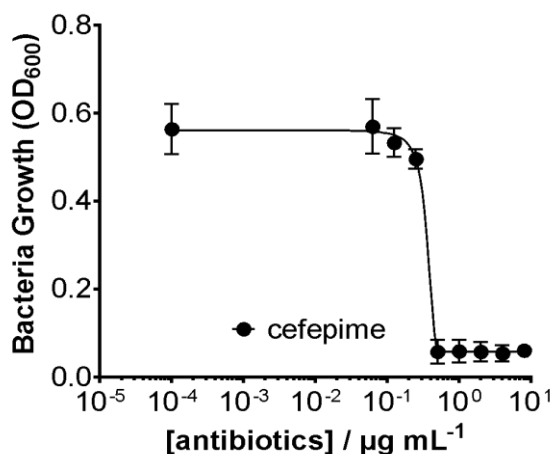

Figure 3.5: *Effect of cefepime on the ex vivo infected skin model. Determination of MIC value of cefepime for S. aureus used in this study;*

The pro-inflammatory responses after 24 h of antibiotic treatment of the infected wounds are shown in **Figure 3.6**. The cytokine expression profile showed progressive restoration of pro-inflammatory cytokines level in the samples treated with the antibiotic. The expression levels of IL-6 levels, as well as IFN-1α and IFN-β, decreased in a concentration dependent manner, reaching the basal levels of uninfected skin upon 30 µg mL^{-1} cefepime. In the case of TNF-α, the lower antibiotic concentration was already sufficient to decrease the expression levels. The mRNA levels of IL-8, on the other hand, did not significantly change even with higher antibiotic concentrations. As discussed above, in our model we detected small IL-8 induction in response to the infection, which is not altered by antibiotic treatment. Amongst the different cytokines, IL-1 was the most affected by cefepime. As shown in **Figure 3.6,** both antibiotic concentrations reduced the expression of IL-1 to undetected levels.
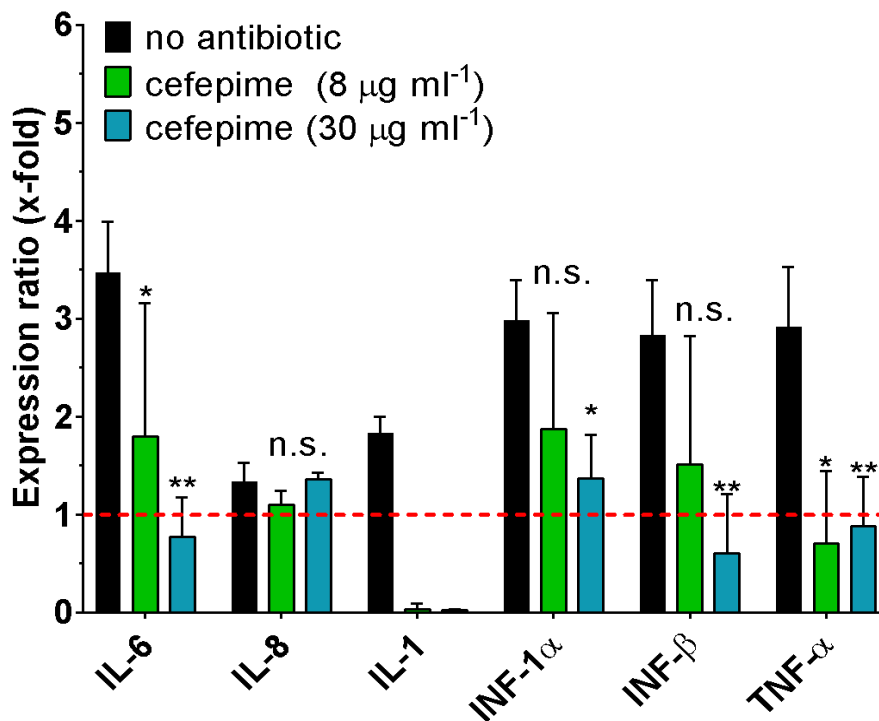
Figure 3.6: *Effect of cefepime on the ex vivo infected skin model. Pro-inflammatory responses upon bacterial challenge with S. aureus (1× 10^7 CFU mL^{-1}) (black bars as in Figure 3) following treatment with cefepime (8 µg mL^{-1}) (green bars) and cefepime (30 µg mL^{-1}) (blue bars) for 24h. Values are displayed as mean ±SEM (* p<0.1,** p<0.01, *** p<0.001; n=2-6). Both treated groups were normalized to the untreated infected group. Dotted line: expression level in untreated infected skins.*

Visualization of the deeper layers of the skin after cefepime (30 µg mL^{-1}) using SEM (**Figure 3.7**), showed a significant decrease in the population of *S. aureus* compared to the infected skins, confirming the efficacy of the treatment.
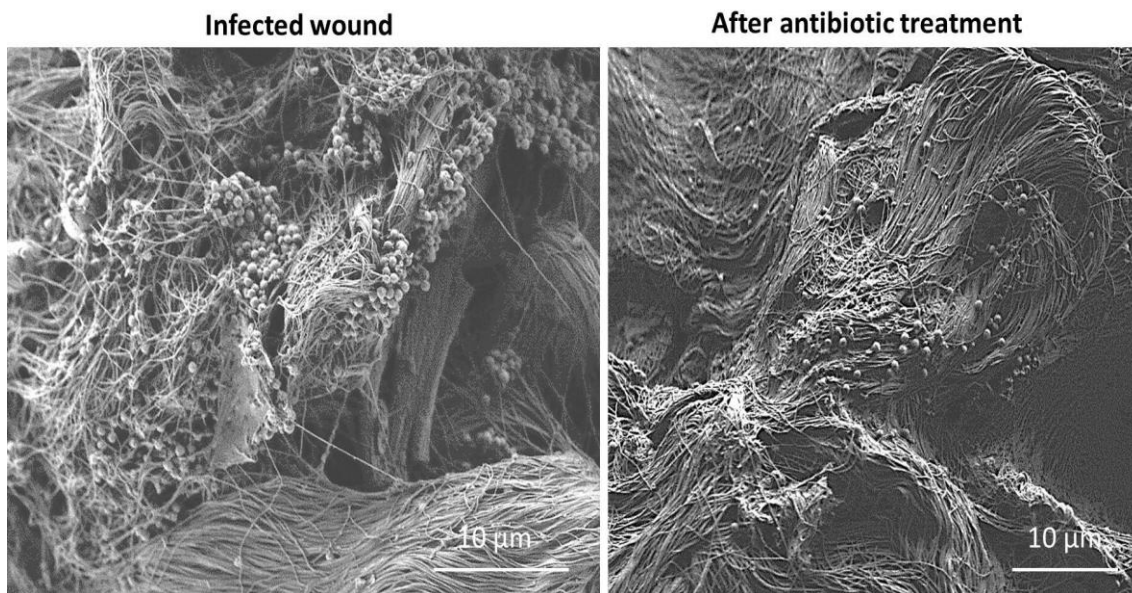

Figure 3.7 : Effect of cefepime on the ex vivo infected skin model. SEM images of skin infected with S. aureus (1× 10^7 CFU mL^{-1}) before and after treatment with cefepime (30 µg mL^{-1}).

In conclusion, it was shown that the administration of a treatment on the infected wound model has an impact on the host immune response. Indeed, analysis of cytokine expression showed a significant reduction in pro-inflammatory responses in infected wound explants treated with the antibiotic compared to vehicles. Single application of cefepime over 24 h resulted in an effective antimicrobial agent against *S. aureus*-infected wound skin. Thus, the *ex vivo* infected skin model is capable of generating a quantifiable bacterial infection and immune response. Furthermore, it has proven to be a useful test system for topical antimicrobial treatment of acute wound infections. However, several studies have shown that topical administration of antibiotics is not effective in disrupting biofilm structure.[55-57] Here, the concentrations of cefepime used are very high, e.g. 8 µg/ml is almost 3 times the MIC value on S aureus strains. The use of new antibacterial treatments through the development of new technologies is proposed in the following sections.

REFERENCES

1.   Draize, J. H.; Woodard, G.; Calvery, H. O. Methods for the Study of Irritation and Toxicity of Substances Applied Topically to the Skin and Mucous Membranes. *J Pharmacol Exp Ther* **1944**, *82* (3), 377–390.

2.   *Ex Vivo* Model of Human Skin (HOSEC) as Alternative to Animal Use for Cosmetic Tests. *Procedia Engineering* **2015**, *110*, 67–73. https://doi.org/10.1016/j.proeng.2015.07.011.

3.   Skin Organ Culture for the Study of Skin Irritancy. *Toxicology in Vitro* **1990**, *4* (4–5), 293–301. https://doi.org/10.1016/0887-2333(90)90067-4.

4.   Reus, A. A.; Usta, M.; Krul, C. A. M. The Use of *Ex Vivo* Human Skin Tissue for Genotoxicity Testing. *Toxicology and Applied Pharmacology* **2012**, *261* (2), 154–163. https://doi.org/10.1016/j.taap.2012.03.019.

5.   Frade, M. A. C.; Andrade, T. A. M. de; Aguiar, A. F. C. L.; Guedes, F. A.; Leite, M. N.; Passos, W. R.; Coelho, E. B.; Das, P. K. Prolonged Viability of Human Organotypic Skin Explant in Culture Method (HOSEC). *Anais Brasileiros de Dermatologia* **2015**, *90* (3), 347–350. https://doi.org/10.1590/abd1806-4841.20153645.

6.   Xu, W.; Hong, S. J.; Jia, S.; Zhao, Y.; Galiano, R. D.; Mustoe, T. A. Application of a Partial-Thickness Human *Ex Vivo* Skin Culture Model in Cutaneous Wound Healing Study. *Laboratory Investigation* **2012**, *92* (4), 584–599. https://doi.org/10.1038/labinvest.2011.184.

7.   Neil, J. E.; Brown, M. B.; Williams, A. C. Human Skin Explant Model for the Investigation of Topical Therapeutics. *Sci Rep* **2020**, *10* (1), 21192. https://doi.org/10.1038/s41598-020-78292-4.

8.   Matarrese, P.; Beauchef, G.; Peno-Mazzarino, L.; Lati, E.; Fitoussi, R.; Vié, K. Assessment of an *Ex Vivo* Irritation Test Performed on Human Skin Explants and Comparison of Its Results with Those of a 24-/48-h Human Patch Test for the Evaluation of Cosmetics. *Toxicology in Vitro* **2021**, *70*, 105030. https://doi.org/10.1016/j.tiv.2020.105030.

9.   Hwang, J.; Jeong, H.; Lee, N.; Hur, S.; Lee, N.; Han, J. J.; Jang, H. W.; Choi, W. K.; Nam, K. T.; Lim, K.-M. *Ex Vivo* Live Full-Thickness Porcine Skin Model as a Versatile *In Vitro* Testing Method for Skin Barrier Research. *International Journal of Molecular Sciences* **2021**, *22* (2), 657. https://doi.org/10.3390/ijms22020657.

10.   Danso, M. O.; Berkers, T.; Mieremet, A.; Hausil, F.; Bouwstra, J. A. An *Ex Vivo* Human Skin Model for Studying Skin Barrier Repair. *Experimental Dermatology* **2015**, *24* (1), 48–54. https://doi.org/10.1111/exd.12579.

11.   Hofmann, E.; Fink, J.; Eberl, A.; Prugger, E.-M.; Kolb, D.; Luze, H.; Schwingenschuh, S.; Birngruber, T.; Magnes, C.; Mautner, S. I.; Kamolz, L.-P.; Kotzbeck, P. A Novel Human *Ex Vivo* Skin Model to Study Early Local Responses to Burn Injuries. *Sci Rep* **2021**, *11* (1), 364. https://doi.org/10.1038/s41598-020-79683-3.

12.   Park, J.-H.; Lim, S.-D.; Oh, S. H.; Lee, J. H.; Yeo, U. C. High-Intensity Focused Ultrasound Treatment for Skin: *Ex Vivo* Evaluation. *Skin Research and Technology* **2017**, *23* (3), 384–391. https://doi.org/10.1111/srt.12347.

13.   Cho, H.; Won, C. H.; Chang, S. E.; Lee, M. W.; Park, and G.-H. Usefulness and Limitations of Skin Explants to Assess Laser Treatment. *Medical Lasers* **2013**, *2* (2), 58–63. https://doi.org/10.25289/ML.2013.2.2.58.

14.   Hutchison, D. M.; Hakimi, A. A.; Wijayaweera, A.; Seo, S.; Hong, E. M.; Pham, T. T.; Bircan, M.; Sivoraphonh, R.; Dunn, B.; Kobayashi, M. R.; Kim, S.; Wong, B. J. Electrochemical Treatment of *Ex Vivo* Human Abdominal Skin and Potential Use in Scar Management: A Pilot Study. *Scars, Burns & Healing* **2021**, *7*, 2059513120988532. https://doi.org/10.1177/2059513120988532.

15.   Verhoeven, M.; Bystrova, S.; Winnubst, L.; Qureshi, H.; de Gruijl, T. D.; Scheper, R. J.; Luttge, R. Applying Ceramic Nanoporous Microneedle Arrays as a Transport Interface in Egg Plants and an Ex-Vivo Human Skin Model. *Microelectronic Engineering* **2012**, *98*, 659–662. https://doi.org/10.1016/j.mee.2012.07.022.

16.   Gratieri, T.; Alberti, I.; Lapteva, M.; Kalia, Y. N. Next Generation Intra- and Transdermal Therapeutic Systems: Using Non- and Minimally-Invasive Technologies to Increase Drug Delivery into and across the Skin. *European Journal of Pharmaceutical Sciences* **2013**, *50* (5), 609–622. https://doi.org/10.1016/j.ejps.2013.03.019.

17.   Teodorescu, F.; Oz, Y.; Quéniat, G.; Abderrahmani, A.; Foulon, C.; Lecoeur, M.; Sanyal, R.; Sanyal, A.; Boukherroub, R.; Szunerits, S. Photothermally Triggered On-Demand Insulin Release from Reduced Graphene Oxide Modified Hydrogels. *Journal of Controlled Release* **2017**, *246* (Supplement C), 164–173. https://doi.org/10.1016/j.jconrel.2016.10.028.

18.   Zorec, B.; Jelenc, J.; Miklavčič, D.; Pavšelj, N. Ultrasound and Electric Pulses for Transdermal Drug Delivery Enhancement: *Ex Vivo* Assessment of Methods with *in Vivo* Oriented Experimental Protocols. *International Journal of Pharmaceutics* **2015**, *490* (1), 65–73. https://doi.org/10.1016/j.ijpharm.2015.05.035.

19.   Waghule, T.; Singhvi, G.; Dubey, S. K.; Pandey, M. M.; Gupta, G.; Singh, M.; Dua, K. Microneedles: A Smart Approach and Increasing Potential for Transdermal Drug Delivery System. *Biomedicine & Pharmacotherapy* **2019**, *109*, 1249–1258. https://doi.org/10.1016/j.biopha.2018.10.078.

20.   Paudel, K. S.; Milewski, M.; Swadley, C. L.; Brogden, N. K.; Ghosh, P.; Stinchcomb, A. L. Challenges and Opportunities in Dermal/Transdermal Delivery. *Ther Deliv* **2010**, *1* (1), 109–131.

21.   Abd, E.; Yousef, S. A.; Pastore, M. N.; Telaprolu, K.; Mohammed, Y. H.; Namjoshi, S.; Grice, J. E.; Roberts, M. S. Skin Models for the Testing of Transdermal Drugs. *Clin Pharmacol* **2016**, *8*, 163–176. https://doi.org/10.2147/CPAA.S64788.

22.   Lebonvallet, N.; Jeanmaire, C.; Danoux, L.; Sibille, P.; Pauly, G.; Misery, L. The Evolution and Use of Skin Explants: Potential and Limitations for Dermatological Research. *Eur J Dermatol* **2010**, *20* (6), 671–684. https://doi.org/10.1684/ejd.2010.1054.

23.   Akhtar, N.; Singh, V.; Yusuf, M.; Khan, R. A. Non-Invasive Drug Delivery Technology: Development and Current Status of Transdermal Drug Delivery Devices, Techniques and Biomedical Applications. *Biomedical Engineering / Biomedizinische Technik* **2020**, *65* (3), 243–272. https://doi.org/10.1515/bmt-2019-0019.

24.   Zakrewsky, M.; Lovejoy, K. S.; Kern, T. L.; Miller, T. E.; Le, V.; Nagy, A.; Goumas, A. M.; Iyer, R. S.; Sesto, R. E. D.; Koppisch, A. T.; Fox, D. T.; Mitragotri, S. Ionic Liquids as a Class of Materials for Transdermal Delivery and Pathogen Neutralization. *PNAS* **2014**, *111* (37), 13313–13318. https://doi.org/10.1073/pnas.1403995111.

25.   Som, I.; Bhatia, K.; Yasir, Mohd. Status of Surfactants as Penetration Enhancers in Transdermal Drug Delivery. *J Pharm Bioallied Sci* **2012**, *4* (1), 2–9. https://doi.org/10.4103/0975-7406.92724.

26.   Kim, Y.-C.; Ludovice, P. J.; Prausnitz, M. R. Transdermal Delivery Enhanced by Magainin Pore-Forming Peptide. *Journal of Controlled Release* **2007**, *122* (3), 375–383. https://doi.org/10.1016/j.jconrel.2007.05.031.

27.   Chen, Y.; Shen, Y.; Guo, X.; Zhang, C.; Yang, W.; Ma, M.; Liu, S.; Zhang, M.; Wen, L.-P. Transdermal Protein Delivery by a Coadministered Peptide Identified via Phage Display. *Nat Biotechnol* **2006**, *24* (4), 455–460. https://doi.org/10.1038/nbt1193.

28.   Lee, J. W.; Gadiraju, P.; Park, J.-H.; Allen, M. G.; Prausnitz, M. R. Microsecond Thermal Ablation of Skin for Transdermal Drug Delivery. *J Control Release* **2011**, *154* (1), 58–68. https://doi.org/10.1016/j.jconrel.2011.05.003.

29.   Levin, G.; Gershonowitz, A.; Sacks, H.; Stern, M.; Sherman, A.; Rudaev, S.; Zivin, I.; Phillip, M. Transdermal Delivery of Human Growth Hormone Through RF-Microchannels. *Pharm Res* **2005**, *22* (4), 550–555. https://doi.org/10.1007/s11095-005-2498-6.

30.   Ramadan, S.; Guo, L.; Li, Y.; Yan, B.; Lu, W. Hollow Copper Sulfide Nanoparticle-Mediated Transdermal Drug Delivery. *Small* **2012**, *8* (20), 3143–3150. https://doi.org/10.1002/smll.201200783.

31.   Wang, D.; Dong, H.; Li, M.; Meng, X.; Cao, Y.; Zhang, K.; Dai, W.; Wang, C.; Zhang, X. Hyaluronic Acid Encapsulated CuS Gel-Mediated Near-Infrared Laser-Induced Controllable Transdermal Drug Delivery for Sustained Therapy. *ACS Sustainable Chem. Eng.* **2017**, *5* (8), 6786–6794. https://doi.org/10.1021/acssuschemeng.7b01035.

32.   Szunerits, S.; Boukherroub, R. Heat: A Highly Efficient Skin Enhancer for Transdermal Drug Delivery. *Frontiers in Bioengineering and Biotechnology* **2018**, *6*, 15. https://doi.org/10.3389/fbioe.2018.00015.

33.   Chengnan, L.; Pagneux, Q.; Voronova, A.; Barras, A.; Abderrahmani, A.; Plaisance, V.; Pawlowski, V.; Hennuyer, N.; Staels, B.; Rosselle, L.; Skandrani, N.; Li, M.; Boukherroub, R.; Szunerits, S. Near-Infrared Light Activatable Hydrogels for Metformin Delivery. *Nanoscale* **2019**, *11* (34), 15810–15820. https://doi.org/10.1039/C9NR02707F.

34.   Im, I.-T.; Youn, S. B.; Kim, K. Numerical Study on the Temperature Profiles and Degree of Burns in Human Skin Tissue During Combined Thermal Therapy. *Numerical Heat Transfer, Part A: Applications* **2015**, *67* (9), 921–933. https://doi.org/10.1080/10407782.2014.955338.

35.   Teodorescu, F.; Quéniat, G.; Foulon, C.; Lecoeur, M.; Barras, A.; Boulahneche, S.; Medjram, M. S.; Hubert, T.; Abderrahmani, A.; Boukherroub, R.; Szunerits, S. Transdermal Skin Patch Based on Reduced Graphene Oxide: A New Approach for Photothermal Triggered Permeation of Ondansetron across Porcine Skin. *Journal of Controlled Release* **2017**, *245*, 137–146. https://doi.org/10.1016/j.jconrel.2016.11.029.

36.   Zhang, Y.; Wang, D.; Gao, M.; Xu, B.; Zhu, J.; Yu, W.; Liu, D.; Jiang, G. Separable Microneedles for Near-Infrared Light-Triggered Transdermal Delivery of Metformin in Diabetic Rats. *ACS Biomater. Sci. Eng.* **2018**, *4* (8), 2879–2888. https://doi.org/10.1021/acsbiomaterials.8b00642.

37.   Eberlin, S.; Silva, M. S. da; Facchini, G.; Silva, G. H. da; Pinheiro, A. L. T. A.; Eberlin, S.; Pinheiro, A. da S. The *Ex Vivo* Skin Model as an Alternative Tool for the Efficacy and Safety Evaluation of Topical Products. *Altern Lab Anim* **2020**, *48* (1), 10–22. https://doi.org/10.1177/0261192920914193.

38.   Skindersø, M. E.; Hansen, J. L. *An Alternative to Animal Experiments: Development of an in Vitro Human Skin Model for Evaluation of Topical Antimicrobial Compounds*; Project funded by the Danish 3R-Center; Rigshospitalet, Department of Clinical Microbiology: Danemark, 2017; p 42.

39.   Schneider, L. A.; Korber, A.; Grabbe, S.; Dissemond, J. Influence of PH on Wound-Healing: A New Perspective for Wound-Therapy? *Arch Dermatol Res* **2007**, *298* (9), 413–420. https://doi.org/10.1007/s00403-006-0713-x.

40.   Percival, S. L.; McCarty, S.; Hunt, J. A.; Woods, E. J. The Effects of PH on Wound Healing, Biofilms, and Antimicrobial Efficacy. *Wound Repair and Regeneration* **2014**, *22* (2), 174–186. https://doi.org/10.1111/wrr.12125.

41.   Demidova-Rice, T. N.; Wolf, L.; Deckenback, J.; Hamblin, M. R.; Herman, I. M. Human Platelet-Rich Plasma- and Extracellular Matrix-Derived Peptides Promote Impaired Cutaneous Wound Healing *In Vivo*. *PLOS ONE* **2012**, *7* (2), e32146. https://doi.org/10.1371/journal.pone.0032146.

42.   Chicharro-Alcántara, D.; Rubio-Zaragoza, M.; Damiá-Giménez, E.; Carrillo-Poveda, J.; Cuervo-Serrato, B.; Peláez-Gorrea, P.; Sopena-Juncosa, J. Platelet Rich Plasma: New Insights for Cutaneous Wound Healing Management. *JFB* **2018**, *9* (1), 10. https://doi.org/10.3390/jfb9010010.

43.   Oliveira, R. N.; Rouzé, R.; Quilty, B.; Alves, G. G.; Soares, G. D. A.; Thiré, R. M. S. M.; McGuinness, G. B. Mechanical Properties and *in Vitro* Characterization of Polyvinyl Alcohol-Nano-Silver Hydrogel Wound Dressings. *Interface Focus* **2014**, *4* (1), 20130049. https://doi.org/10.1098/rsfs.2013.0049.

44.   Physically Crosslinked Poly(Vinyl Alcohol)-Hydroxyethyl Starch Blend Hydrogel Membranes: Synthesis and Characterization for Biomedical Applications - ScienceDirect.

45.   Kamoun, E. A.; Kenawy, E.-R. S.; Tamer, T. M.; El-Meligy, M. A.; Mohy Eldin, M. S. Poly (Vinyl Alcohol)-Alginate Physically Crosslinked Hydrogel Membranes for Wound Dressing Applications: Characterization and Bio-Evaluation. *Arabian Journal of Chemistry* **2015**, *8* (1), 38–47. https://doi.org/10.1016/j.arabjc.2013.12.003.

46.   Poly Vinyl Alcohol Hydrogel and Its Pharmaceutical and Biomedical Applications: A Review.

47.   Holloway, J. L.; Lowman, A. M.; Palmese, G. R. The Role of Crystallization and Phase Separation in the Formation of Physically Cross-Linked PVA Hydrogels. *Soft Matter* **2012**, *9* (3), 826–833. https://doi.org/10.1039/C2SM26763B.

48.   Investigation of a Novel Freeze-Thaw Process for the Production of Drug Delivery Hydrogels | SpringerLink.

49.   Hassan, C. M.; Peppas, N. A. Structure and Morphology of Freeze/Thawed PVA Hydrogels. *Macromolecules* **2000**, *33* (7), 2472–2479. https://doi.org/10.1021/ma9907587.

50.   Steinstraesser, L.; Sorkin, M.; Niederbichler, A. D.; Becerikli, M.; Stupka, J.; Daigeler, A.; Kesting, M. R.; Stricker, I.; Jacobsen, F.; Schulte, M. A Novel Human Skin Chamber Model to Study Wound Infection *Ex Vivo*. *Arch Dermatol Res* **2010**, *302* (5), 357–365. https://doi.org/10.1007/s00403-009-1009-8.

51.   Zhang, N.; Wu, Y.; Xing, R.; Xu, B.; Guoliang, D.; Wang, P. Effect of Ultrasound-Enhanced Transdermal Drug Delivery Efficiency of Nanoparticles and Brucine. *Biomed Res Int* **2017**, *2017*, 3273816. https://doi.org/10.1155/2017/3273816.

52.   Maboni, G.; Davenport, R.; Sessford, K.; Baiker, K.; Jensen, T. K.; Blanchard, A. M.; Wattegedera, S.; Entrican, G.; Tötemeyer, S. A Novel 3D Skin Explant Model to Study Anaerobic Bacterial Infection. *Front Cell Infect Microbiol* **2017**, *7*. https://doi.org/10.3389/fcimb.2017.00404.

53.   Chapman, T. M.; Perry, C. M. Cefepime. *Am J Respir Med* **2003**, *2* (1), 75–107. https://doi.org/10.1007/BF03256641.

54.   Gentry, L. O.; Rodriguez-Gomez, G. Randomized Comparison of Cefepime and Ceftazidime for Treatment of Skin, Surgical Wound, and Complicated Urinary Tract Infections in Hospitalized Subjects. *Antimicrobial Agents and Chemotherapy* **1991**, *35* (11), 2371–2374. https://doi.org/10.1128/AAC.35.11.2371.

55.   Chadha, T. Bacterial Biofilms: Survival Mechanisms and Antibiotic Resistance. *Journal of Bacteriology & Parasitology* **2014**, *05* (03). https://doi.org/10.4172/2155-9597.1000190.

56.   Bessa, L. J.; Fazii, P.; Di Giulio, M.; Cellini, L. Bacterial Isolates from Infected Wounds and Their Antibiotic Susceptibility Pattern: Some Remarks about Wound Infection. *International Wound Journal* **2015**, *12* (1), 47–52. https://doi.org/10.1111/iwj.12049.

57.   Wu, H.; Moser, C.; Wang, H.-Z.; Høiby, N.; Song, Z.-J. Strategies for Combating Bacterial Biofilm Infections. *International Journal of Oral Science* **2015**, *7* (1), 1–7. https://doi.org/10.1038/ijos.2014.65.

CHAPTER 4 : PHOTOTHERMAL ACTIVATABLE CRYOGEL LOADED WITH ANTIMICROBIAL AGENTS

4.1 Phothothermal activable cryogel loaded with antibiotics

Most bacterial diseases can be treated with antibiotics, although antibiotic-resistant strains are starting to emerge.[1] In chronic wound infection, the biofilm organization of bacteria makes the use of systemic antibiotics ineffective. Local application of antibacterial agents seems unavoidable for wound care, however passive antibacterial dressings have not shown sufficient efficacy.[2-3] The enhancement of antibiotic action must be incorporated into the therapy.

Cryogel has been recently investigated as a potential material for wound care products.[4] While hydrogels have been extensively evaluated as depots for drug cargo and their delivery, and various antibacterial hydrogels have been proposed,[5-7] in recent years cryogels (CGs) have emerged as an attractive alternative.[8-10] The higher porosity of cryogels compared to traditional hydrogels result in improved gel swellability and consequently enhanced drug storage and release. In a recent study, it was demonstrated the superior performance of cryogels over traditional hydrogels for conjugation and release of anti-cancer drugs.[11] In this part, the efficiency of a NIR-activable on-demand antibiotic releasing cryogel patch (**Figure 4.1**) was demonstrated with the *ex vivo* infected wound model. [12]
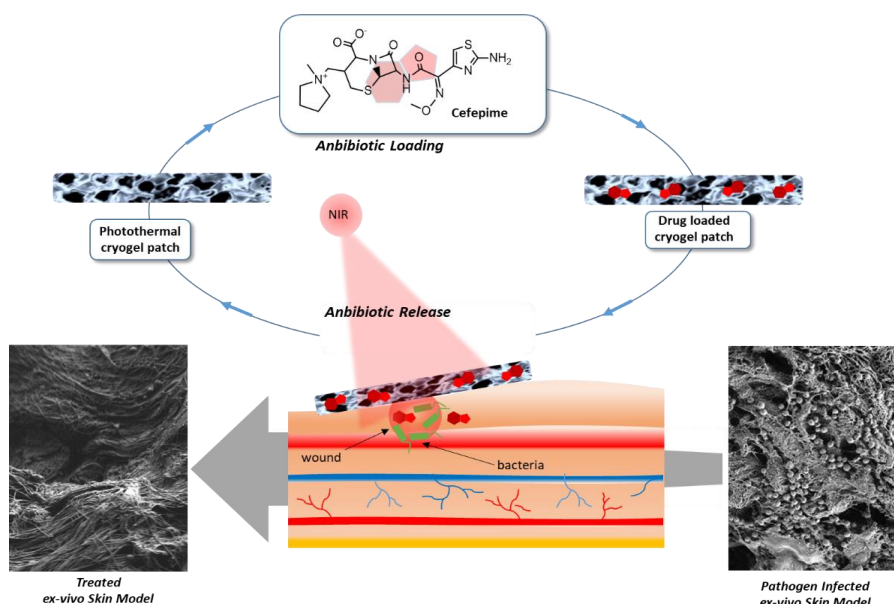

Figure 4.1: *A reduced graphene oxide (rGO) based cryogel bandage: Loading of the cryogel due to gel swelling, 'on-demand' antibiotic release upon light activation, treatment of S. aureus infected ex vivo skin model.[12]*

The cryogel matrix is composed of butyl methacrylate (BuMA), poly(ethylene glycol) methyl ether methacrylate (PEGMEMA) and poly(ethylene glycol) dimethacrylate (PEGDMA), where reduced graphene oxide (rGO) is incorporated during the fabrication process. The PEG based components provide the required hydrophilicity to the gel, while the hydrophobic BuMA and rGO elements are required for a controlled release of cefepime, the antibiotic used in this study.

4.1.1 Effect of antibiotic-loaded cryogels

The importance of temperature in the wound–healing process and as antibiotic alternative for the effective killing of pathogens, has been recognized as a novel way to treat wound infections.[13-14] In this work we investigated the antibacterial effects of a reduced graphene oxide (rGO)-loaded cryogel. A butyl methacrylate based cryogel was synthesized by mixing poly(ethylene glycol) methyl ether methacrylate (PEGMEMA) and butyl methacrylate (BuMA) in a molar percentage of 80:20, with 0.8 wt. % rGO (**Figure 4.2**). This part of work was done in collaboration with Amitav Sanyal from Boğaziçi University of Turkey, Department of Chemistry.
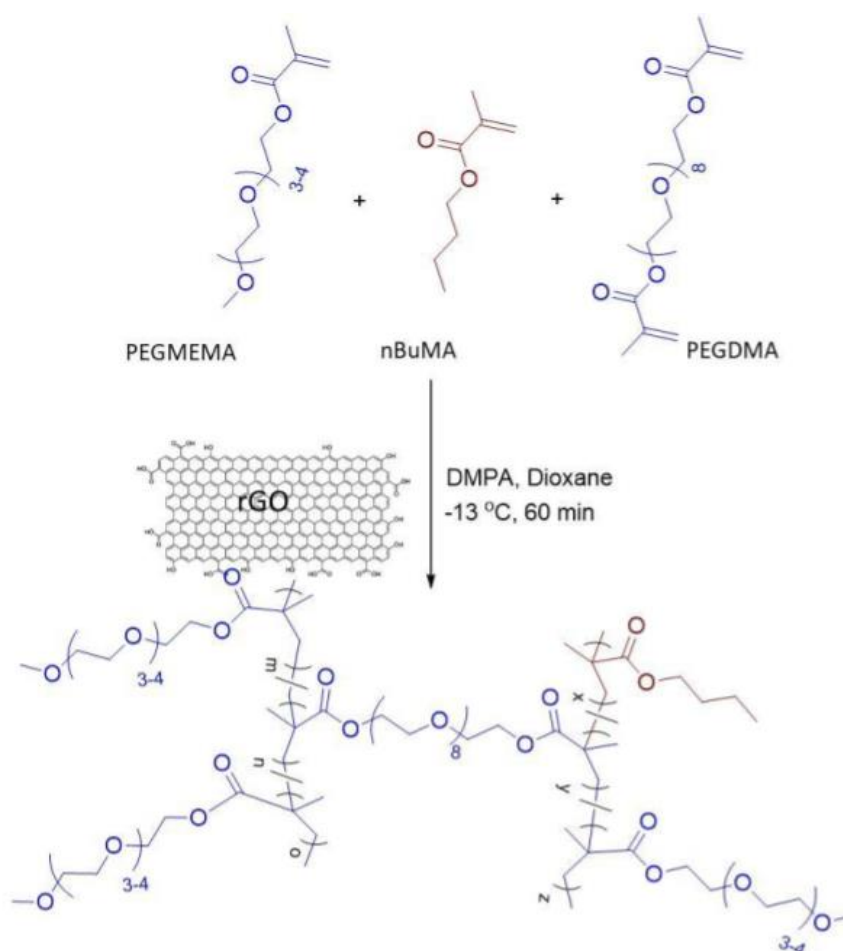
Figure 4.2: *Synthesis and characteristics of rGO-loaded butyl methacrylate-based cryogels: Schematics of synthesis of rGO-containing NIR-responsive butyl methacrylate based cryogels.*

The use of PEG based PEGMEMA starting materials and PEGDMA as crosslinker provided hydrophilicity to the gel, important to provide a hydrated environment to the wound and which allows in addition the absorption of eventual any formed wound fluid. The hydrophobic BuMA will allow tuneable release of antibiotics, while the photothermal properties of rGO will be used for swelling the gel and release of drugs. It is thus expected that such porous hydrophilic structures undergo rapid swelling when immersed or in contact with water, helping the release of drugs on demand. **Figure 4.3** shows the sponge-like morphology of the cryogel used in this work. The incorporation of rGO changes significantly the physical appearance of the cryogel: while hydrogels without rGO (noted in the following as CG) had cotton like appearance, incorporation of rGO results in a dark cryogel (rGO-CG).
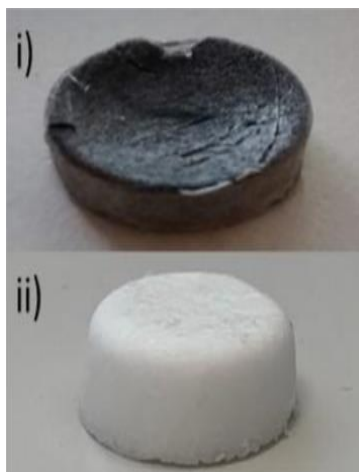

Figure 4.3: *Synthesis and characteristics of rGO-loaded butyl methacrylate-based cryogels: Optical images of cryogels with (i) rGO, and (ii) without rGO.*

The morphologies of the obtained cryogels were determined using SEM (**Figure 4.4**). A highly macroporous structure was evident in both cryogels. This macroporous structure develops due to the frozen solvent domains around which the monomers polymerize and crosslink during the cryogelation. As expected, the cryogels undergo rapid swelling when immersed in water. The rGO-containing cryogel possesses low swelling and water take capacity when compared to the cryogel without rGO (**Figure 4.4.**). This could be expected due to the large aromatic structure of hydrophobic rGO. PEG-based materials are generally soft

matrixes with poor mechanical properties. Addition of rGO provides these cryogels with a certain level of mechanical integrity that will ensure their durability while maintaining enough softness to enable conformal contact with skin.
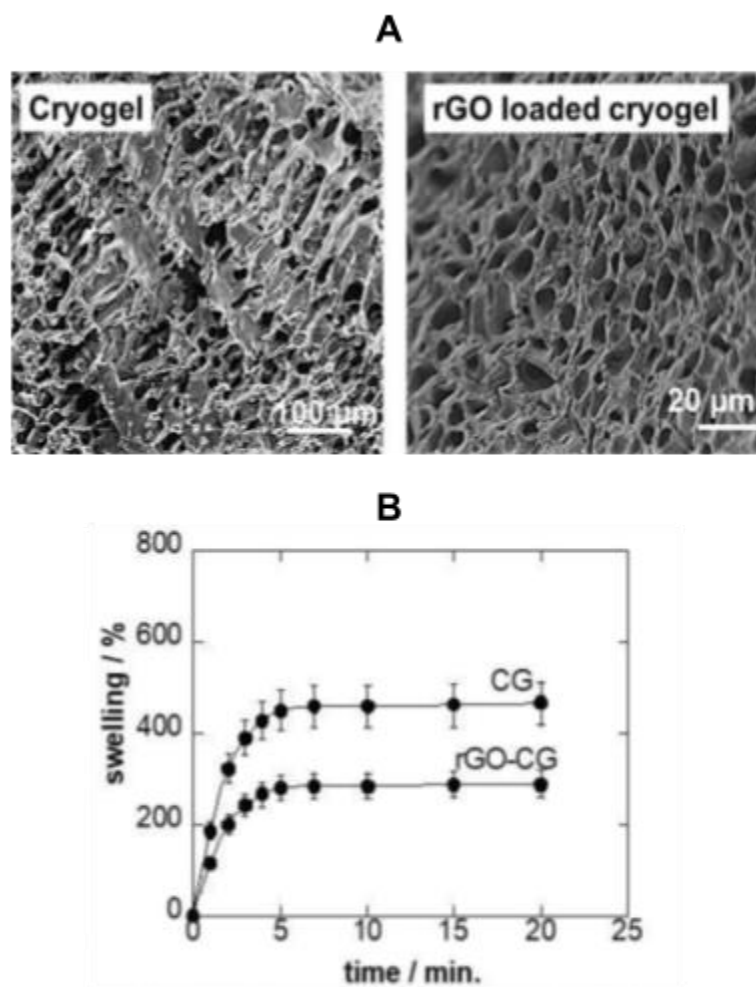

Figure 4.4: *Synthesis and characteristics of rGO-loaded butyl methacrylate-based cryogels. **A.** SEM micrographs showing the porous morphologies of CG (Left) and rGO-CG (Right). **B.** Equilibrium swelling of CG and rGO-CG cryogels from PEGMEMA/BuMA (80/20) with 0.8 wt. % rGO.*

4.1.2 Loading and passive drug release from CG and rGO-CG

Cryogels have found to be promising polymeric materials for drug delivery due to their generally high drug loading capability and tuneable release profiles.[11] The macroporous structure of rGO-together with their high swelling ability due to the presence of large voids, is expected to facilitate drug transport. Cefepime, a fourth-generation cephalosporin antibiotic,

was selected for its antibacterial efficiency against *S. aureus* strains.[15] For *S. aureus* a minimum inhibitory concentration (MIC) value of 3 ± 0.3 µg mL^{-1} was obtained with cefepime (**Figure 4.5A**).
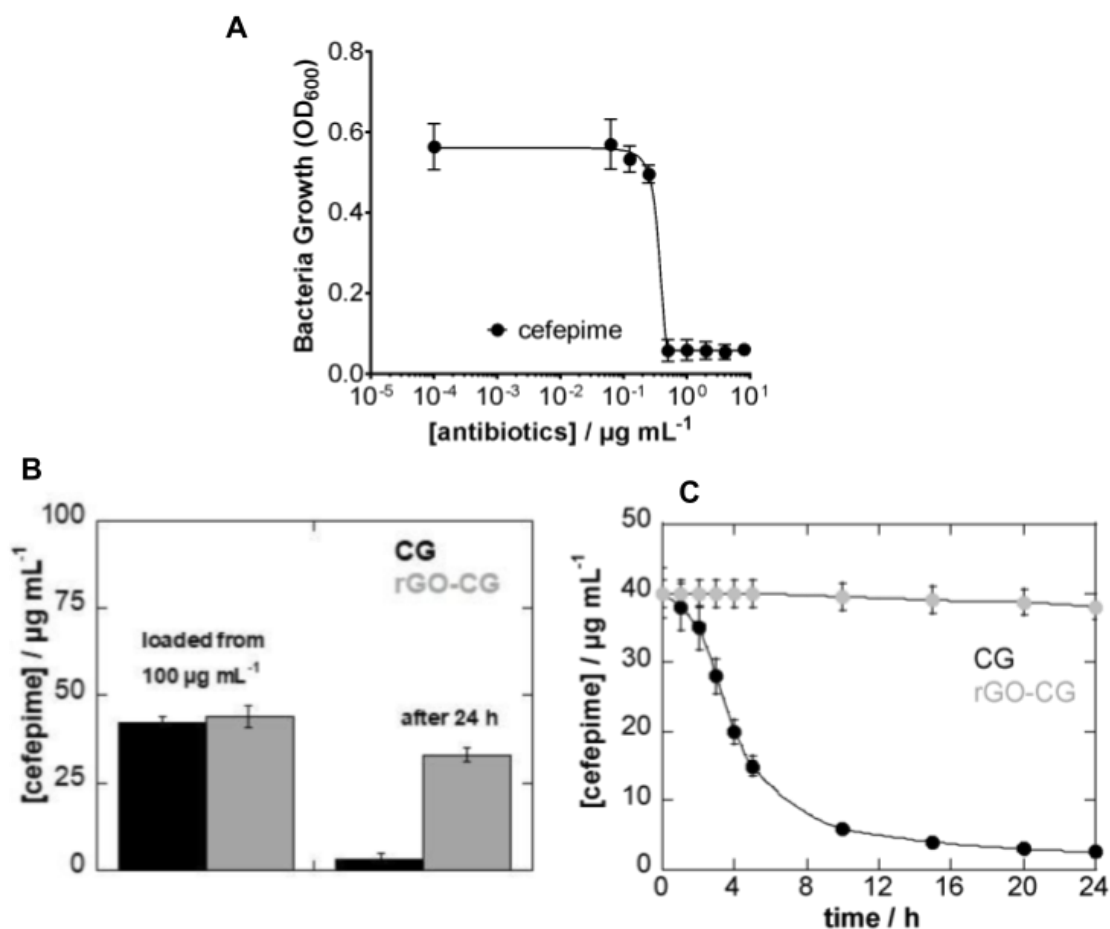

Figure 4.5: *Antibiotic loaded cryogels. **A.** Determination of MIC value of cefepime for S. aureus used in this study.**B**. Loading of 50 mg CG and rGO-CG with 100 µg mL^{-1} cefepime followed by washing for three times 5 min in water and immersion for 24 h in water to evaluate the passive release characteristic. **C.** Passive release profile of cefepime loaded CG and rGO-CG gels into water over a period of 24h.*

From a solution of 100 µg mL^{-1} cefepime, about 45 µg was incorporated into CG and rGO-CG (**Figure 4.5B**). While loading capacity is comparable, a large difference is seen in the passive release characteristics when immersed in water. Indeed, before photothermal activation, the passive release characteristics of the gels have to be established. After 24h almost all cefepime integrated into CG was released (**Figure 4.5B**). This differs to the rGO-CG bandage, where only a fraction of cefepime was released passively in a time span of 24h (**Figure 4.5C**) and about 38 µg remained attached in rGO-CG most likely due to pi-pi stacking

interactions between the rGO matrix and the antibiotic, as previously shown for other matrices,[15-16] which accounts for 0.72 µg cefepime/ µg gel.

4.1.3 Photothermal triggered drug release from rGO-CG

The possibility to release the remaining cefepime from rGO-CG using the photothermal heating properties of rGO was further determined. Indeed, light irradiation of the rGO-loaded cryogels when immersed in water in the near infrared (980 nm) at 1.0 W cm^{-2} results in temperature increase to about 75°C within few minutes and remained constant thereafter (**Figure 4.6A**). Lowering the power density to 0.5 W cm^{-2} resulted in a heating up to 50°C. The CG without rGO integration shows no temperature variations upon light irradiation.
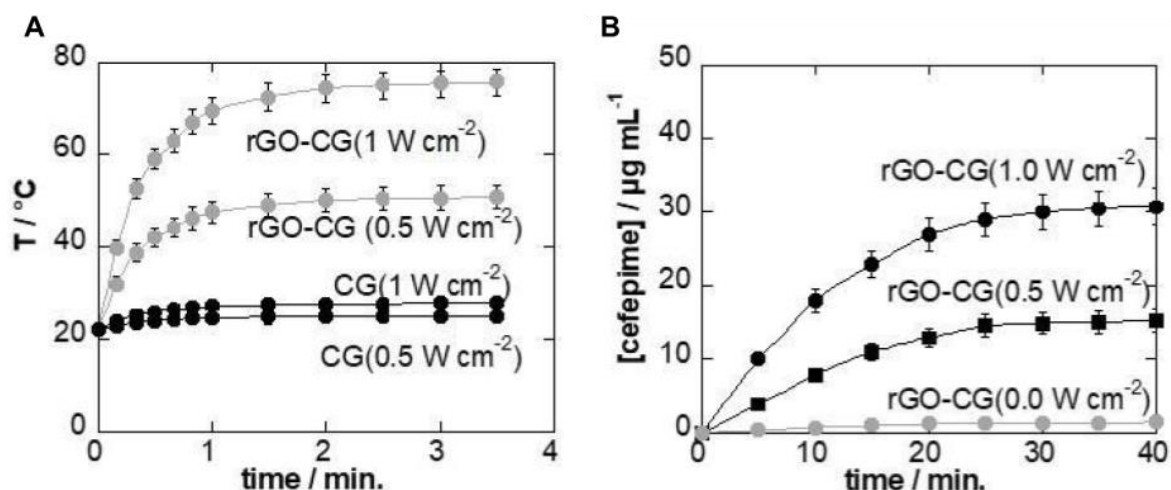

Figure 4.6 : *Photothermal drug release from rGO-CG:* ***A.*** *Photothermal heating curves of the CG (black) and rGO-CG (grey) when illuminated at 980 nm for 4 min with a laser power of 0.5 and 1.0 W cm^{-2}.* ***B.*** *Drug release upon photothermal activation for 40 min with a laser power of 0.0 (grey points; control group: no NIR activation), 0.5 (black squares) and 1.0 W cm^{-2} (black points).*

As expected, the laser power used has also an influence on the active release profile of the antibiotic. A total amount of 30 µg of antibiotic was released from the cryogel at 1.0 W cm^{-2} over a time span of 40 min, whereas, about 15 µg was released when the laser power was half in value (**Figure 4.6B**). The passive release quantity did account for only 1 µg mL^{-1}. The morphology of the cryogel was not altered after post swelling and cefepime release (**Figure 4.7**). Also, no observable change in the porous morphology of the cryogels were observed upon photothermal heating, as determined from SEM analysis.
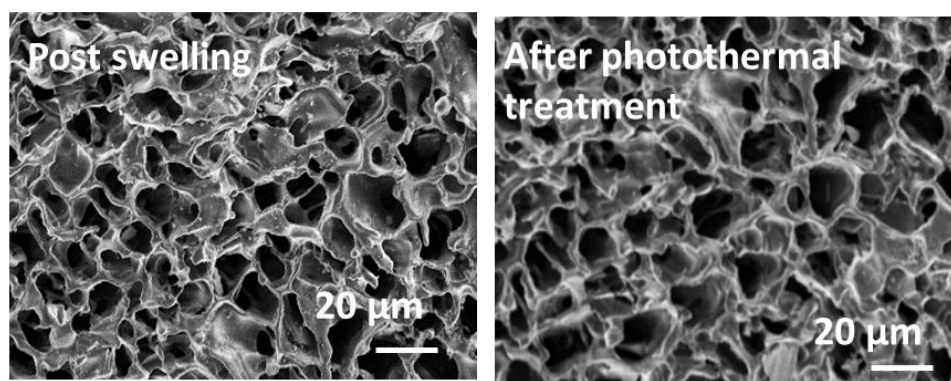
Figure 4.7: *Photothermal drug release from rGO-CG: SEM images showing the cryogel morphology before (left) and after heating (right).*

In order to demonstrate "on-demand" release of cefepime from the gel, multiple cycles of stimulations with a fixed interval for cooling down were performed (**Figure 4.8A**).
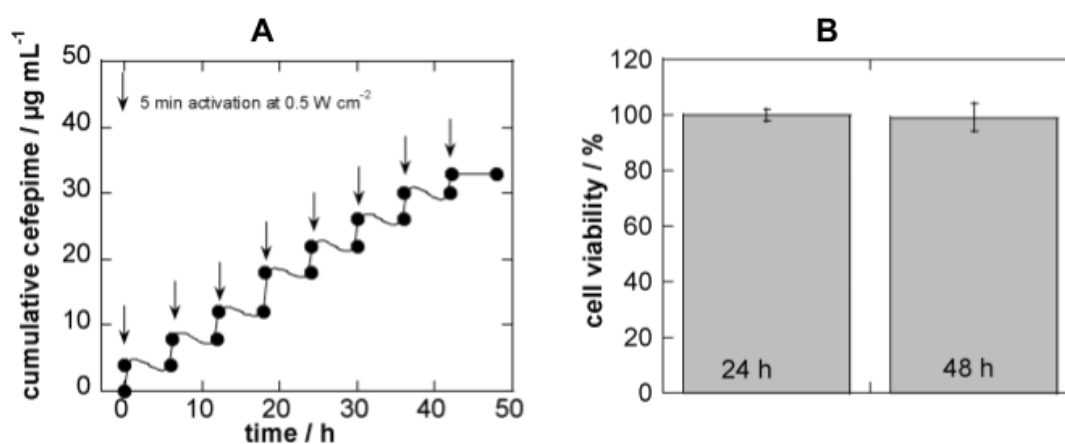
Figure 4.8: *On-demand release of cefepime over a time period of 2 days: **A.** light activation for 5 min at 0.5 W cm^{-2} followed by 6h rest. HeLa cell viability after 24 and 48h incubation with rGO-CG.*

We opted for activation for 5 min which corresponds to a release of about 4 µg ml^{-1} cefepime, close to the MIC value of *S. aureus* (**Figure 4.8A**). 5 min activation for the first 40 h results in a reproducible release of about 4 µg ml^{-1}; after 40h, the rGO-GC was almost deprived of cefepime and the release decreased to 2 µg ml^{-1}. Additionally, the cell biocompatibility of the rGO-CG was assessed on HeLa cell line (**Figure 4.8.B**). No cell viability loss was observed after 48h when in contact with the bandage.

4.1.4 Validation on an *ex vivo* infected skin model

Ex vivo models of infected human skin wounds were performed to validate the performance of the cryogels to treat skin infection **(Figure 4.9)**. Following human skin collection and injury, the wound area was infected with *S. aureus*. After 4 days of infection, part of the sample was used for analysis while the other part was treated with rGO-CG gels loaded with cefepime and cefepime solutions.
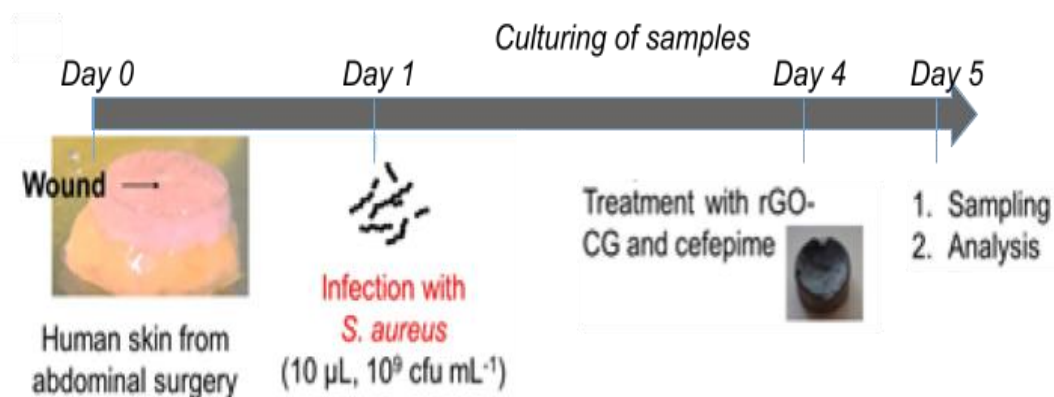
Figure 4.9: *Wound production and infection of Woundskin® model together with immunobiological analysis: Experimental workflow: Representative image of the wound skin model, showing the superficial epidermis layer, the dermis, and the underneath adipose tissue. Arrow indicates the wound region. Wound skin models were collected at day 0 and freshly shipped. Bacterial infection was performed upon reception by dropping S. aureus solutions on the wound region and keeping the skin in culture medium without antibiotics at 37 °C for 5 days.*

The *S. aureus* infected skin model was treated with cefepime (20 µg) as well as cefepime loaded rGO-CGs. The first indication of a healing effect is seen in the change of the wound color from yellow to light pink (**Figure 4.10A**).

Figure 4.10 : *Effect of wound healing of rGO-CG bandages loaded with cefepime: **A.** Optical images of infected wound skin and after treatment with cefepime (20 µg mL^{-1}) for 24 h and rGO-CG+cefepime bandages activated for 10 min at 980 nm (1 W cm^{-1}). **B.** Bacterial counts per gram skin tissue as determined from infected skin before and after treatment. All the values are displayed as means ± SEM.*

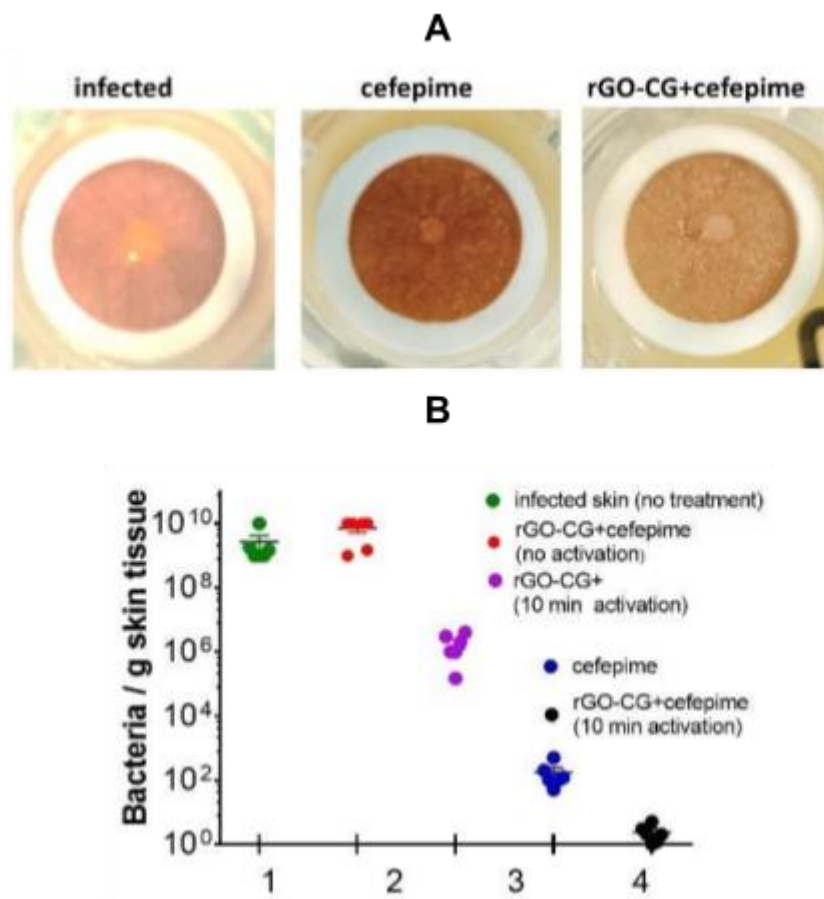To quantify the infection, the number of viable bacteria in the skin tissue was determined (**Figure 4.10B**). A considerable decrease was observed after treatment of the infected wound for 24h with cefepime as well as with a rGO-CG bandage loaded with cefepime and light activated for 10 min, which results in a release of about 20 µg of antibiotic. No decrease in the number of viable bacteria was observed using the same rGO-CG bandage loaded with cefepime without light activation. This confirms indeed that no passive release of the antibiotics occurs over a time of 24h. The slightly better bacterial ablation with the rGO-CG is most likely due to the increased temperature under light illumination.

Scanning electron microscopy (SEM) of vertically cut skin confirms in addition the ablation of *S. aureus* using the rGO-CG bandage under light activation (**Figure 4.11A**). A high number of bacteria are interwoven in the collagen bundles of infected skin and appear

physically attached to the collagen fibers. The appearance of the individual bacteria in the dermis coincides with the hallmarks of an acute wound model.[18] Treatment with the cefepime loaded rGO-CG bandage under light activation results in ablation of a large number of bacteria in the skin.
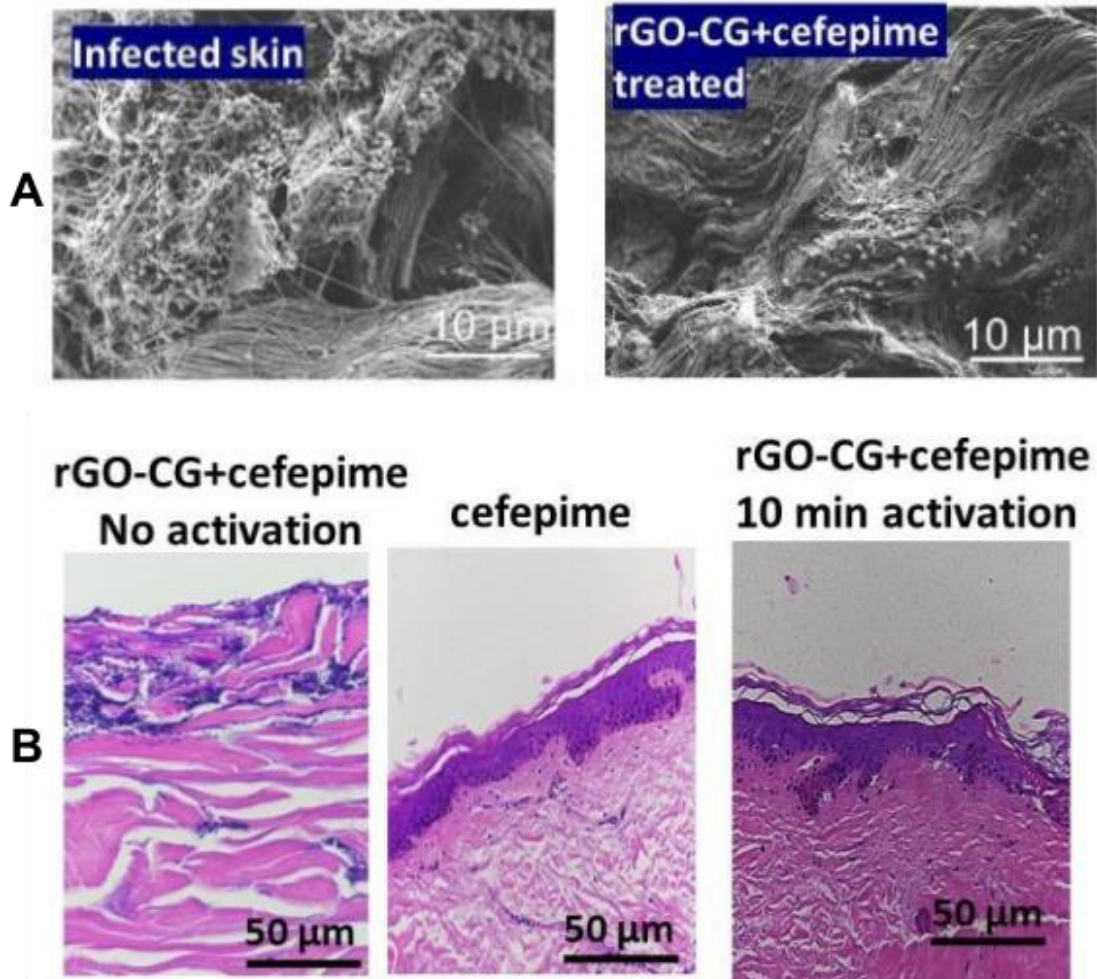
Figure 4.11 : *Effect of wound healing of rGO-CG bandages loaded with cefepime: **A**. SEM images of infected wound and after treatment with rGO-CG+cefepime bandages activated for 10 min at 980 nm (1 W cm^{-1}). **B**. H&E staining of S. aureus (1× 10^7 CFU mL^{-1}) infected skin (Left) after treatment with cefepime loaded rGO-CG with light activation (right) as well as with cefepime (middle).*

H&E staining after skin treatment (**Figure 4.11B**) was further used to evaluate the effect of releasing antibiotics in healing. While non-treated skin clearly shows bacteria infiltration, rGO-CG loaded with cefepime under light activation indicates the recovery of the skin structure.

Finally, the effect on resident inflammatory cells was determined through the quantification of *S. aureus*-induced cytokines before and after treatment. As shown in **Figure 4.12**, the cytokine expression profile shows progressive restoration of pro-inflammatory cytokines level in the skin samples after treatment. A significant increase in the levels of Il-6, IFN-1α, IFN-β and TNF-α is observed after *S. aureus* infection of the skin for 5 days (green lines. The level of IL-8 remained unchanged. IL-8 is mainly produced by macrophages with its primary function being to induce chemotaxis of target cells, such as neutrophils and granulocytes.[19] The low level of IL-8 in response to the infection might indicate that no severe inflammation was installed in the skin. After treatment with cefepime (blue line) as well as the bandage under light activation (black), the levels of IL-6, IL-1, IFN-1α and TNF-α are reduced, an indication that tissue damage and bacterial infection are reduced. In the case of the NIR active rGO-CG, the level of IL-1 and IFN-1α dropped below that of the wounded skin. This might indicate a complete skin recovery.
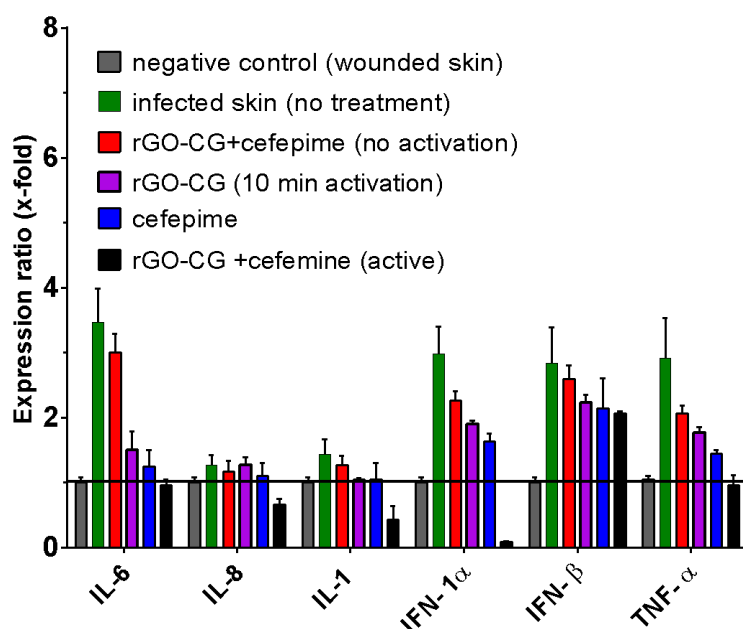
Figure 4.12: *Pro-inflammatory cytokines analysis determined by qPCR: wounded skin (grey). Wounded and infected skin with S. aureus (1×10^7 CFU mL^{-1}) (green). rGO-CG loaded with cefepime but not activated (red). rGO-CG and light activated for 10 min (violet). infected issue treated with cefepime ($20\,\mu g$ mL^{-1}) (blue). Cefepime loaded rGO-CG activated for 10 min at 0.5 W cm^{-2} for one time (black). Values are displayed as mean $\pm$SEM (* p<0.1, ** p<0.001; *** p<0.0001; n=6).*

In conclusion, the model proved to generate a quantifiable bacterial infection and immune response. Moreover, it resulted to be a useful test system for topical antimicrobial treatment of acute wound infections. Single application of cefepime over 24 h resulted in an

effective antimicrobial agent against *S. aureus*-infected wound skin. Furthermore, we tested the performance of the infected *ex-vivo* model on innovative bandages, such as cefepime loaded rGO-cryogels with "on-demand" release under photothermal activation. The scaffold exhibits minimal passive release and a rapid active release response, presumably due to aromatic stacking of cefepime to rGO and thermally promoted release from rGO under light activation. As antibiotic resistance is widely increasing, new antimicrobial approaches are needed. Short-term heat exposure inhibited infection-induced inflammation most likely by abrogating recruitment of inflammatory cells. Although *ex vivo* human skin has been previously used as a model to study skin wound processes and drug delivery, our study is the first one reporting the efficacy of a novel antibiotic formulation. For future work, it would be interesting to investigate the biological interactions of the different bacteria biofilms with chronic wounds, as well as compare the effects of different antimicrobial agents.

4.2 Photothermal active Cryogel loaded with antibacterial peptides

Peptide-containing biomaterials find widespread applications ranging from therapeutics, tissue engineering to wound healing.[20-23] Indeed, despite the large panel of antibiotics available for the treatment of infectious diseases, the increasing prevalence of bacteria strains that are resistant to conventional antibiotics makes research for alternative therapeutic options timely.[24] Administration or delivery of peptides has been generally undertaken through encapsulation or conjugation to polymeric materials or using them as building blocks to furnish self-assembled scaffolds. In particular, peptide-based hydrogels have attracted much attention as biological scaffolds for the sustained release of drugs for tissue engineering and wound healing applications.[22,25-26]

The incorporation of biologically active peptides into synthetic polymer scaffolds might be one way to combine the biocompatible nature of the peptide with that of the mechanical rigidity of the loading scaffold. The issues to consider when constructing peptide-loaded chemically derived scaffolds are to have a gel support, which allows facile incorporation of the biologically active peptides. At the same time, the design should be such that passive and/or burst release is restricted, while preferably, a triggered "on-demand" release can be achieved.[27]

While hydrogels are great platforms as drug cargos and delivery, the focus has shifted in the recent years to utilization of the macroporous member of the hydrogel family, often referred to as cryogels (CGs).[28-30] The higher porosity of CGs addresses several challenges encountered in traditional hydrogels. Compared to hydrogels, CGs exhibit enhanced drug release due to their higher porosity and swellability. In a recent study, the superior performance of CGs over traditional hydrogels for conjugation and release of anticancer drugs have been demonstrated.[11] In that work, drug release was achieved through cleavage of chemically conjugated therapeutics in a highly acidic environment. While pH-change-triggered release has been widely employed, it is generally slow and relies on the pH of the environment. External triggers such as light and heat have emerged as attractive alternatives to trigger release of therapeutic agents in an on-demand and controlled fashion like already discussed in other chapters of the thesis.[16,31-33]

In this part of the work, the fabrication of a layered device that utilizes a furanyl-functionalized CG is outlined. On-demand release of antimicrobial peptides was achieved by firmly attaching the CG to a Kapton/ rGO interface to conduct thermal stimulation for peptide release (**Figure 4.13**). Indeed, the good photothermal properties of rGO allowed increasing the temperature of the attached CGs, which are composed of hydrophilic PEG groups along with furfuryl units. The furfuryl units provide covalent linkage sites for the attachment of maleimide-modified peptides at room temperature using the Diels−Alder (DA) cycloaddition reaction through formation of the thermally labile endo-cycloadduct. Heat activation of the thermally labile furan/maleimide bond using the photothermal properties of an externally attached Kapton/rGO matrix, upon a 980 nm laser irradiation, results in a retro DA reaction and controlled peptide release. The peptide chosen in this study is a maleimide-modified cationic peptide, maleimide−RWRWRWC−NH2 targeting the bacterial membrane of Gram-positive bacteria.[34-35] Apart from efficient thermally controlled release and bactericidal killing, selective ablation of *S. aureus* in a mixture of bacteria is demonstrated as well as the patch efficiency in the infected wound environment through the *ex vivo* infected skin model.[36]
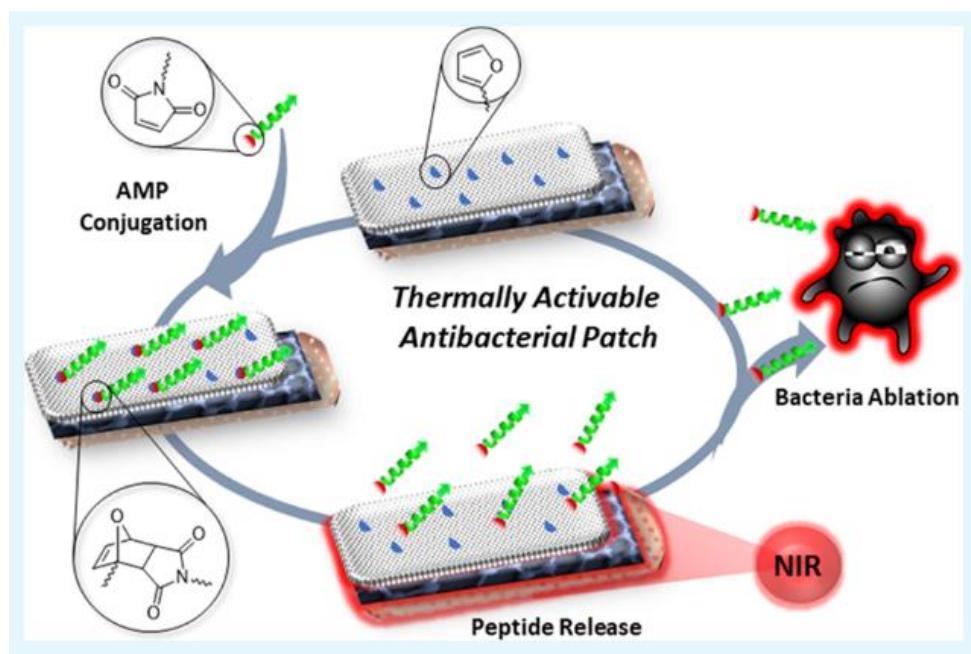
Figure 4.13 *: Action of heat on the furan-containing CG device for controlled drug delivery: (a) covalent linkage of maleimide-modified antibacterial peptide via DA reaction at room temperature. (b) Release of maleimide-modified antibacterial peptide at T >40 °C. © Antibacterial action of the peptide against Gram-positive S. aureus. A rGO/Kapton interface was applied as an external heating source.[91]*

4.2.1 Furanyl-Based Cryogel

A furanyl based cryogel (CG) was synthesized by mixing PEG methyl ether methacrylate (PEGMEMA) and furfuryl methacrylate (FuMA) monomers (**Figure 4.14**). This CG containing 40% FuMA (CG-40) was studied as a potential dressing material. This part of the work was done in collaboration with Amitav Sanyal from Boğaziçi University of Turkey, Department of Chemistry.

Figure 4.14 *: Synthetic route for the fabrication of furan-containing CGs.*

Analysis of morphology by scanning electron microscopy (SEM) shows the mesh structure of the cryogel with the visible porosity (**Figure 4.15A**). The analysis of swelling properties shows that gel reached swelling equilibrium within a few minutes, which ensured rapid transport of therapeutic materials through the matrix (**Figure 4.15B**). These two characteristics make it a good candidate for the drug delivery system.

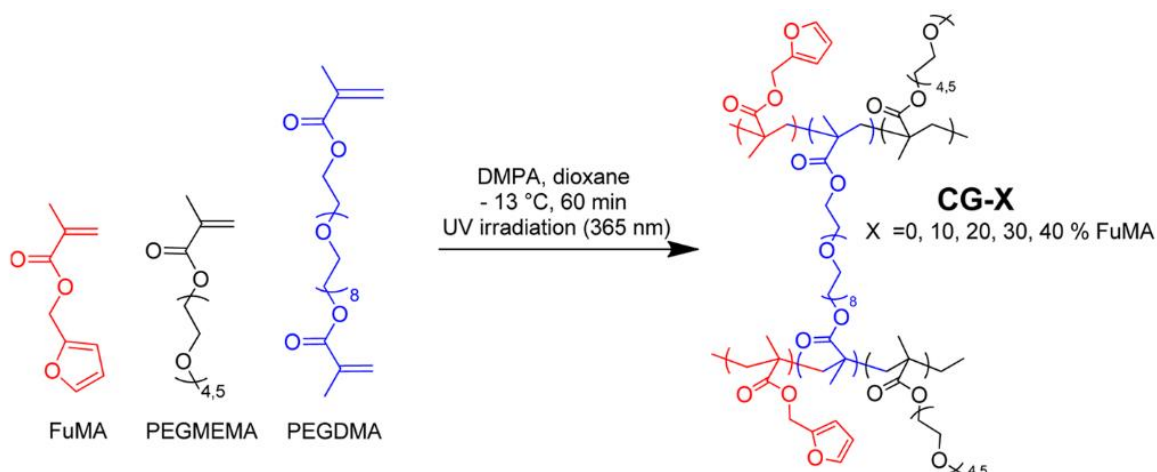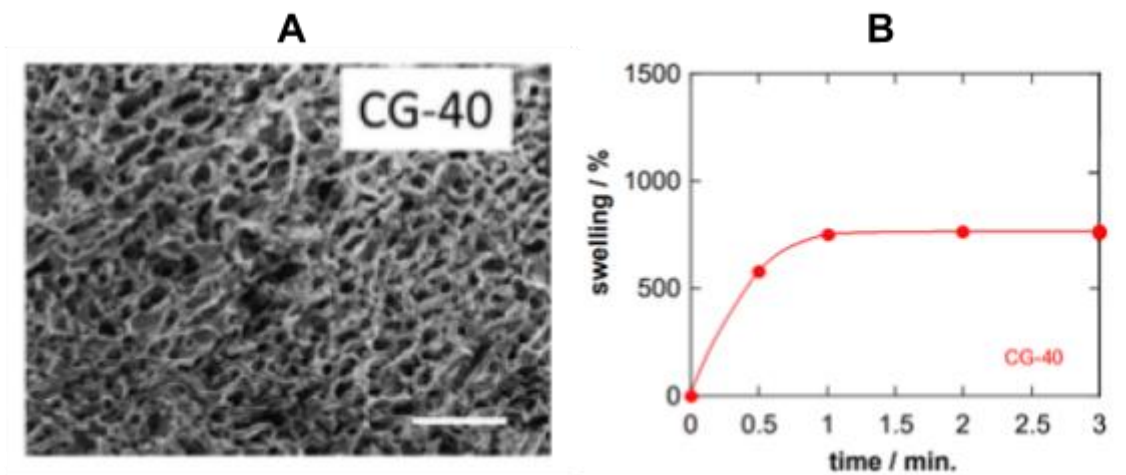*Figure 4.15 : Cryogels properties. **A**. SEM images of the formed furan-containing CG40; scale bar = 100 μm. **B**. Swelling behavior of CG-40: Water uptake of different cryogels at 24 °C.*

The furfuryl-containing CG is able to conjugate maleimide-containing molecules through the Diels−Alder (DA) cycloaddition reaction. This reaction offers a reversible covalent conjugation−deconjugation handle for attachment and release of therapeutic agents.[37-38] While this reaction has been extensively explored to fabricate crosslinked hydrogel materials,[39-43] utilization of furan units as a handle to chemical conjugate is not widespread.[44-47] For instance, maleimide-containing hydrogels have been appended with therapeutic agents and released upon heating by Bowman and co-workers.[44-45] Likewise, Vieyres *et al*. reported furan group-containing dendrimers, where lipoic acid-modified drugs were conjugated and released upon heating.[46] In the schema below (**Figure 4.16**), N-(5-fluoresceinyl)maleimide, a green fluorescent dye, was used as a model molecule to validate the loading mechanism. Incubation of CG-40 at room temperature for 24 h with N-(5-fluoresceinyl)maleimide resulted in the formation of a fluorescent gel, with a loading efficiency of 40 ±2%.[36]
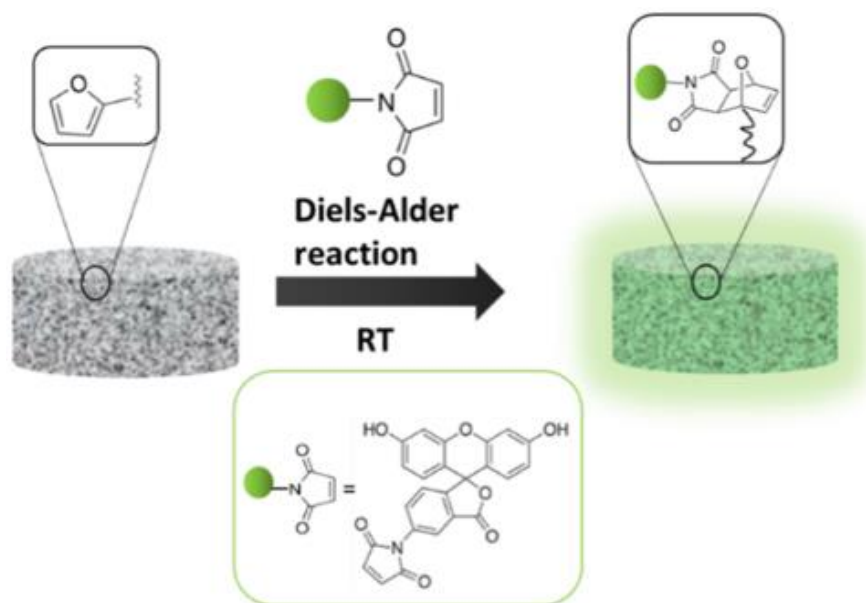
Figure 4.16 *: Schematic illustration of furfuryl-containing CG-40 before and after loading with N-(5-fluoresceinyl)maleimide via DA cycloaddition.*

The equilibrium of the DA cycloaddition reaction is thermally governed. While elevated temperatures induce the reverse reaction (retro-DA cyclo-reversion), that is leading to the reformation of maleimide and furan fragments, lower temperatures favor formation of the cycloadduct. Thus, subjecting the polymer networks to increased temperatures should drive the reactions in favor of cyclo-reversion and thus result in a controlled release of the cargo.

Temperature-guided delivery systems for peptides using photothermal active materials such as reduced graphene oxide (rGO),[16,48-53] molybdenum disulfide (MoS2),[54-55] and others[56-57] have been widely used over the years. The synergistic effect through the combination of antibacterial agents and heat on the antibacterial performance and biofilm disruption properties has also been demonstrated in several papers.[39,58-59] To increase the temperature, the CG was heated by a photothermal active heating patch, as schematically outlined in Figure **4.17A**. The photothermal patch consists of a Kapton substrate coated with a rGO layer (Kapton/rGO).[50] The irradiation of the Kapton/rGO surface with a near-infrared laser activates the photothermal activity of the rGO. The heat generated is sufficient to increase the temperature of the CG when immersed into water to a temperature as high as 70 °C (**Figure 4.17B**), leading to a heat-triggered release of N-(5-fluoresceinyl)maleimide.
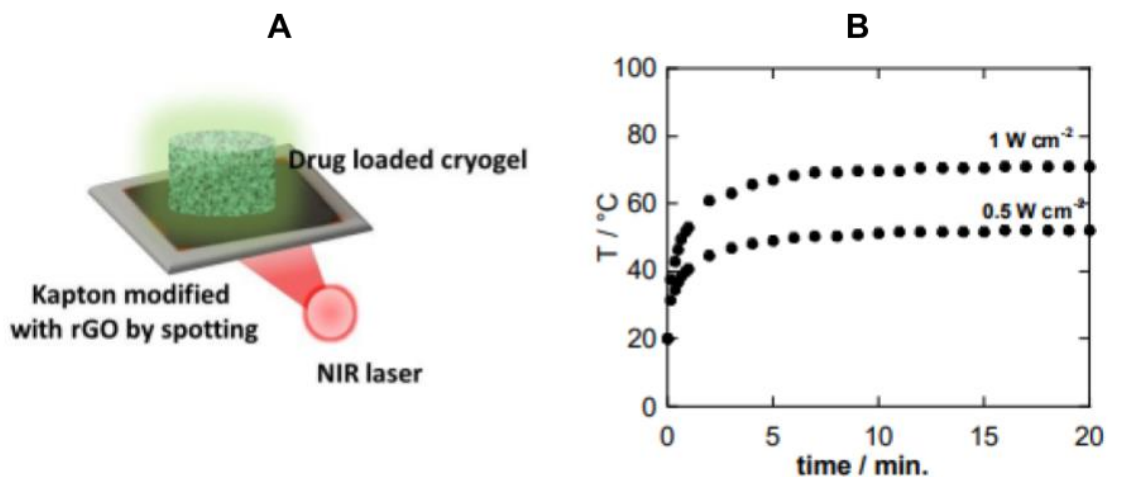
Figure 4.17*: **A**. Schematic illustration of the local heating of the drug loaded cryogel to release drugs. **B**. Photothermal heating curves of the CG-40 using Kapton/rGO nanoheater in water, following exposure to laser light of 980 nm at a power density of 0.5 or 1W cm^{-2}.*

We opted here for a distinct approach for achieving thermal-guided release by placing a CG loaded with antimicrobial peptides in close contact to a flexible Kapton substrate coated with rGO, as previously developed for the electrochemical delivery ofinsulin.[60] This approach proved to be highly efficient for the release of the maleimide-modified antibacterial peptide from the CG. Indeed, incorporating rGO into the gel has shown large peptide retention due to π−π stacking and other interactions of the peptide with the incorporated rGO sheets. In addition, no direct contact of rGO with the infected skin occurs, and cytotoxicity issues can be ruled out. Moreover, this technique can be applied for any type of hydrogel/CG without the need to incorporate any heating-responsive component within their structure.

4.2.2 Loading and Release of an Antimicrobial Peptide from CG-40.

Motivated by the possibility to load and photothermally release a maleimide-functional dye from a CG-40 gel, the efficacy of the CG for loading and releasing of a maleimide-modified antibacterial peptide (**Figure 4.18**) was pursued.
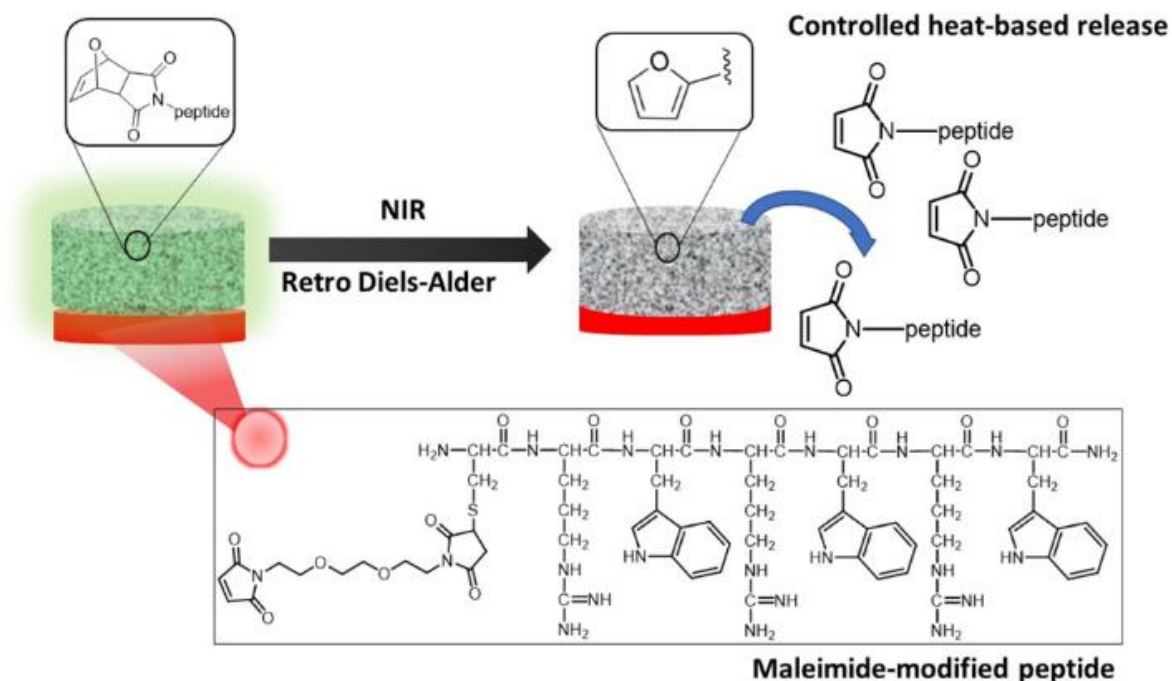
Figure 4.18*: Schematic representation of maleimide-modified antimicrobial peptide release through retro-DA based cleavage at temperature >40 °C.*

The antimicrobial peptide investigated is a maleimide-modified cationic peptide containing three tryptophan and three arginine units (Maleimide-RWRWRWC-NH$_2$). The principle of conjugation is illustrated in **Figure 4.19**.
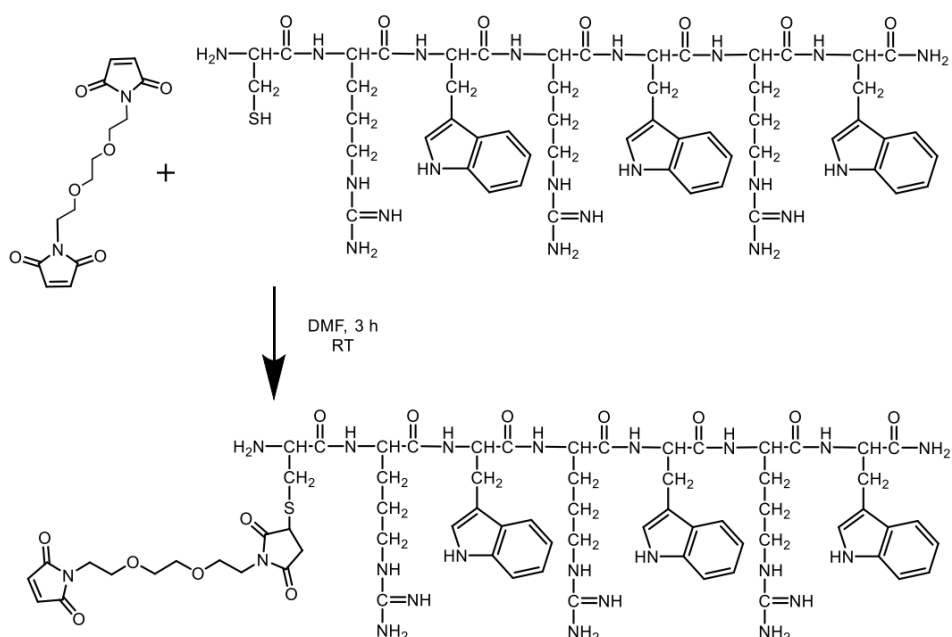
Figure 4.19*: Formation and structure of the maleimide-conjugated antimicrobial peptide*

This small peptide targets the bacterial membrane and inhibits cellular respiration and cell wall synthesis.[34-35] The maleimide-modified peptide has a preferential antibacterial effect on Gram-positive bacteria with a smaller minimum inhibition (MIC) value for methicillin-resistant *Staphylococcus aureus* ATCC 43300 but only affecting moderately Gram-negative bacteria strains (**Table 4.1**).

antibacterial drug	*E. coli* DCM 30083 (μg mL^{-1})	*S. aureus* ATCC 43300 (μg mL^{-1})
RWRWRWC–NH$_2$	33.0	17.3
maleimide–RWRWRWC–NH$_2$	57.2	34.7

Table 4.1: *Minimal inhibitory concentration (MIC) of RWRWRWC-NH₂ and Maleimide modified RWRWRWC-NH₂ on Gram-négative and Gram-positive bacteria strains.*

Peptide loading onto the CG-40 was achieved by immersion at room temperature in an aqueous solution of the peptide (300 μg mL^{-1}). After 5 h incubation, followed by washing with water to remove unbound maleimide-modified peptide, HPLC analysis of the remaining peptide in solution indicated that about 195 μg mL^{-1} (65%) of the peptide was chemically integrated into the CG (**Figure 4.20**). Compared to other literature reports,[16,61] the loading time and amount of maleimide-modified antimicrobial peptide into CG-40 are comparable to that of insulin loading into a PEG-based hydrogel where after 4 h, 88% of insulin was integrated.
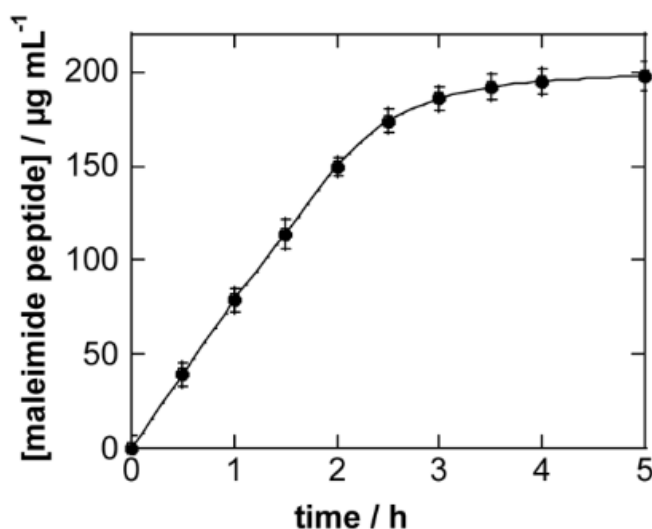
Figure 4.20: *Loading kinetics of maleimide-modified antimicrobial peptide onto CG-40.*

Photothermal activation of the CG between 37 and 60 °C resulted in the antibacterial peptide release (**Figure 4.21A**) in a temperature-dependent manner. After 10 min, the peptide

amount released at 52 °C accounts for about 33 μg mL^{-1} (**Figure 4.21B**) close to the MIC value of *S. aureus* ATCC43300 (**Table 4.1**).
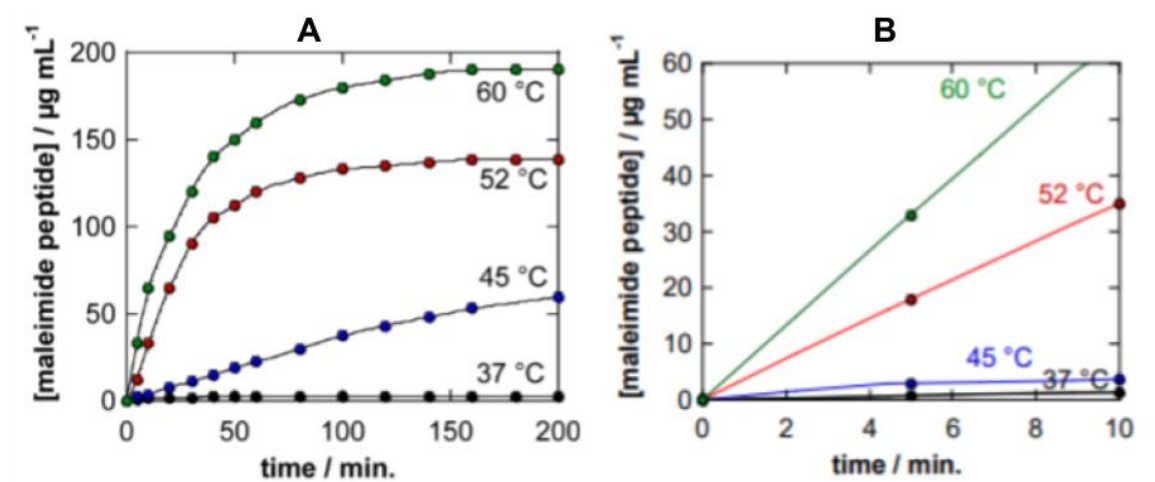
Figure 4.21*: Release kinetics at 37 °C (black), 45 °C (blue), 52 °C (red), and 60 °C (green) of maleimide-modified antimicrobial peptide.**A**. For 3 hours. **B**. For the first 10 min.*

The enhanced release rate, observed at higher temperatures, correlates with the increased rate of the retro-DA reaction. Most importantly, insignificant release was observed at 37 °C due to the chemical linkage between the peptide and the CG. The release can be explained by the excellent light-to-heat conversion performance of the external Kapton/rGO matrix (**Figure 4.22**).
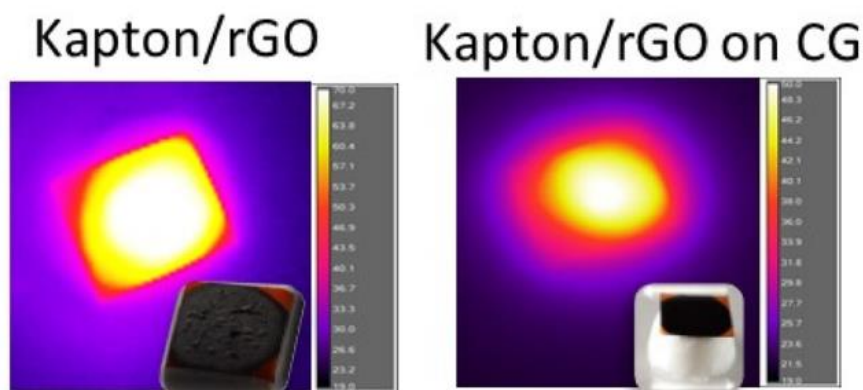
Figure 4.22*: Thermal images captured by an infrared (IR) camera (Thermovision A40) of the Kapton/rGO substrate without and with a CG upon NIR illumination at 1 W cm^{-1}.*

The temperature image of the Kapton/rGO matrix shows a homogeneous heat distribution with a temperature increase to 52 °C upon laser irradiation at 980 nm at a power

density of 0.5 Wcm^{-2} for 10 min. In the case of the Kapton/rGO with attached CG-40, a temperature of 52 °C was only reached when a laser power of 1.0 W cm^{-1} was applied. The thermal damage to an *ex vivo* skin tissue was evaluated as skin exposure to temperatures above the physiological temperature over an extended period of time can result in skin tissue damage.[49] **Figure 4.23** depicts the histological analysis of human skin in contact with the CG-40 before and after heat activation for 10 min using conventional hematoxylin and eosin (H&E) staining. Heating up to 52 °C for 10 min, normal dermis characteristics are observed and epidermis as well as dermis are unaffected. Increasing the temperature to 60 °C led, however, to skin damage and was not used in subsequent experiments.
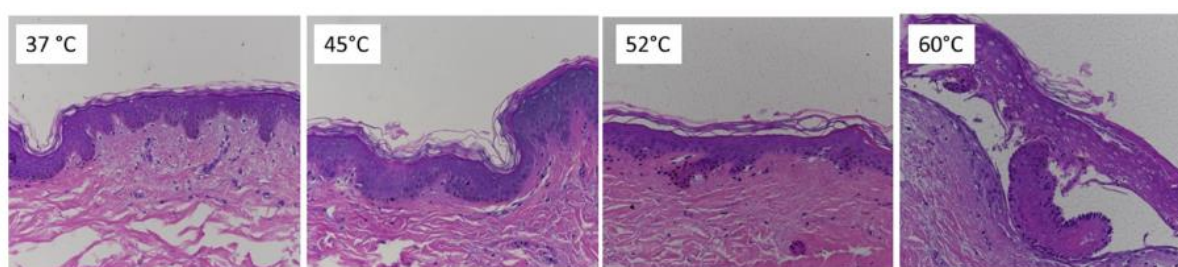
***Figure 4.23**: Bright-field micrographs of a histological section of an ex vivo human skin model thermally activated for 10 min to different final temperatures with a CG-40 loaded with antimicrobial peptide in contact with Kapton/rGO.*

The activity of the released antibacterial peptide was assessed on planktonic *S. aureus* using a standard colony forming unit (CFU) counting test. **Figure 4.24A** clearly shows that the amount of the released peptide at 37 °C was not sufficient to induce *S. aureus* ablation. Heating the CG up to 45 and 52 °C resulted in a time-dependent release of the peptide. Twenty minutes were required in the case of heating at 45 °C to reach 30 μg mL^{-1} (close to the MIC value) of the released peptide (**Table 4.1**), while increasing the activation temperature to 52 °C revealed a complete bacterial ablation at around 20 min. In the case of *Escherichia coli* (*E. coli*) (**Figure 4.24B**), a comparable trend as for *S. aureus* was observed. Due to the larger MIC values, higher peptide concentrations were needed and the antibacterial effect was thus shifted on the time scale.

In a control experiment, a CG-40 without the antimicrobial peptide was irradiated under the same conditions (**Figure 4.24C**). The absence of antimicrobial peptide in the CG-40 achieved a decrease in the bacteria concentration of only 1 × log at 52 °C, while no change was recorded at 45 °C. The decrease of 1 × log at 52°C was most likely due to the photothermal heating effect.[15,62]
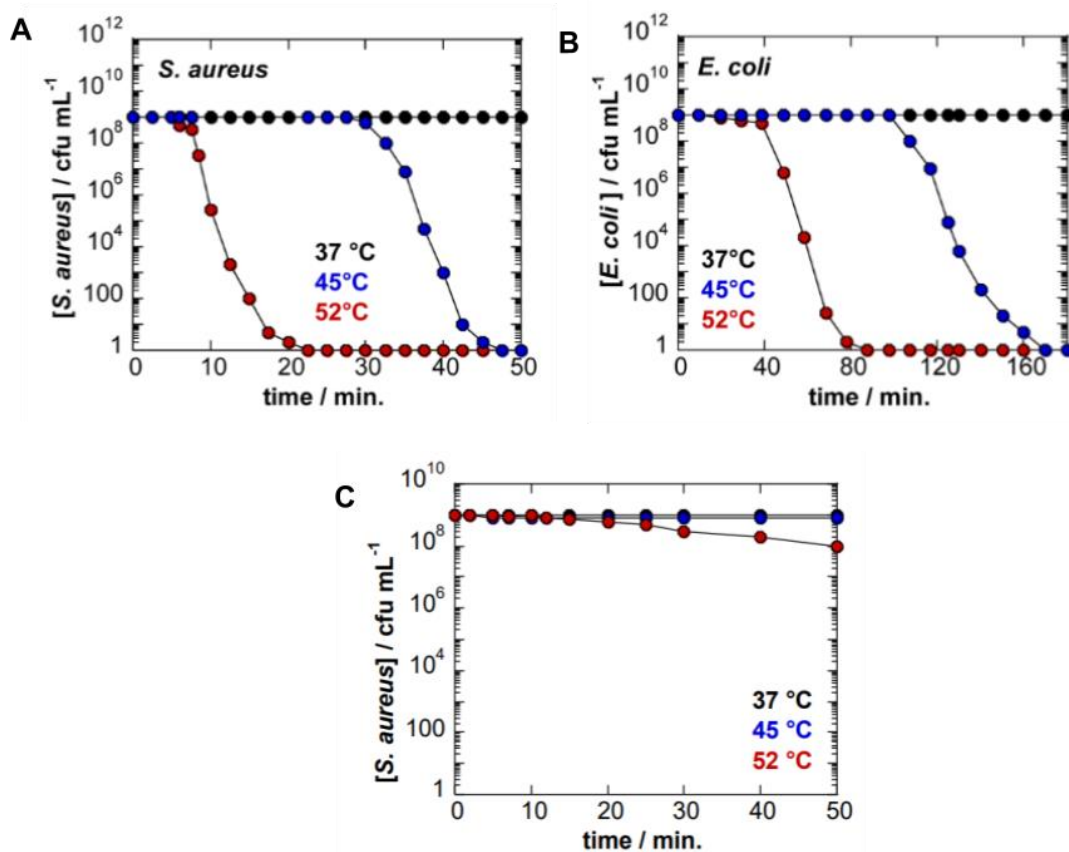
Figure 4.24: *Ablation of S. aureus and E. coli and a mixture of both pathogens: change in the bacteria concentration as a function of time and applied temperature of CG-40 loaded with 197 µg mL⁻¹ maleimide-modified antimicrobial peptide for **A.** S. aureus ATCC 4330 and **B.** E. coli DCM 30083. **C.** Change in bacteria concentration as a function of time and applied temperature to CG-40.*

We took advantage of the difference in MIC values for *S. aureus* and *E. coli* and checked if our approach would allow for selective pathogen ablation. **Figure 4.25** depicts the scanning electron microscopy (SEM) images obtained from a solution containing *S. aureus* and *E. coli* before and after treatment with a CG-40 loaded with the maleimide-modified antimicrobial peptide for 40 min at 52 °C. One can clearly see the presence of both pathogens in the initial suspension. Thereafter, only *E. coli* strains remained, indicating that S. aureus was completely ablated under these conditions.
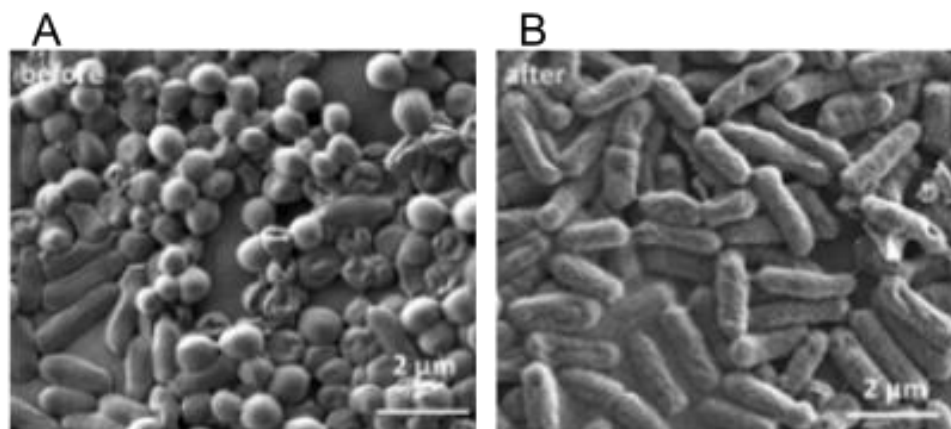
Figure 4.25: *SEM images of a mixture of S. aureus and E. coli (each 5 × 105 CFU mL−1) before and after treatment with a CG-40 loaded with maleimide-modified antimicrobial peptide and activated at 52 °C.*

This visual examination was further consolidated by cell growth measurements (**Figure 4.26A**) and by bacteria plating (**Figure 4.26B**) to quantify the number of viable bacteria cells by spotting the bacteria solution on selective agar plates, Chapman and MacConkey, respectively.
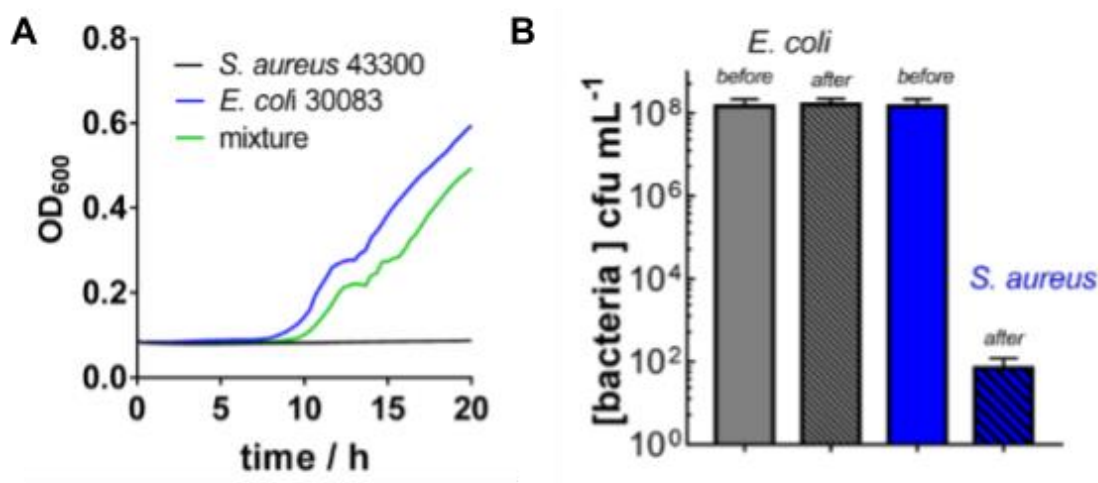
Figure 4.26: **A**. *Bacteria cell growth measurements of S. aureus, E. coli, and a bacteria mixture in the presence of 35 µgmL−1 maleimide-modified antimicrobial peptide.* **B**. *Amounts of viable bacteria of a mixture of S. aureus (blue) and E. coli (black) before and after treatment with a CG-40 loaded with maleimide-modified antimicrobial peptide and activated at 52 °C for 10 min.*

Bacteria cell growth measurements of *S. aureus*, *E. coli*, and a bacteria mixture in the presence of 35 µg mL^{-1} maleimide-modified antimicrobial peptide revealed complete *S. aureus*

cell growth inhibition, in contrast to *E. coli* exponential cell growth after 10 h of incubation (**Figure 4.5A**). The mixture exhibited a growth profile comparable to the *E. coli* bacteria growth curve, with an overall decreased optical density, indicating lower bacteria present, as expected. Viable cell determination also indicated that, in the case of *S. aureus*, a significant decrease in bacterial cell viability was achieved, while no effect was observed on *E. coli*.

To make this approach closer to reality, the biocompatibility of CG-40 and peptide-loaded CG-40 was assessed on HeLa cell line derived from cervical carcinoma from a 31 years old female (**Figure 4.27**). No loss in cell viability was observed upon incubation of HeLa cells for 24 and 48 h with CG-40 and CG-40 loaded with maleimide-modified antimicrobial peptide. This can be expected due to the benign nature of the CG components toward cells. Also, lack of toxicity suggests that no residual monomers, which could lead to potential cytotoxicity, are present in the CG matrix. Furthermore, eventual detrimental effects of thermal activation of the peptide-loaded CG-40 on cell viability were determined. Thermal activation of the CG for 10 min at 52 °C did not induce any change in cell viability.
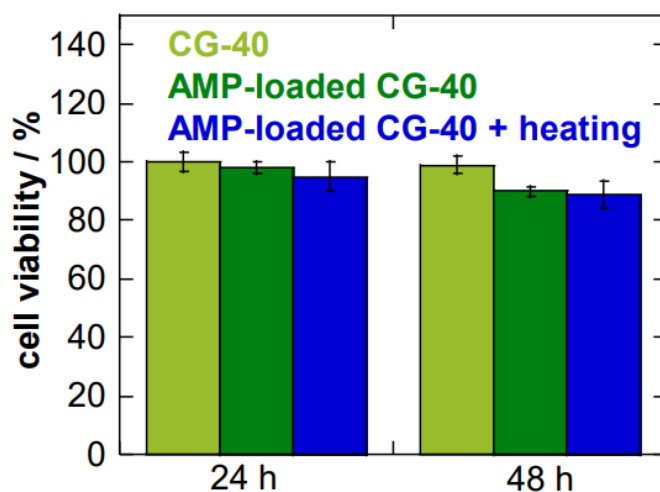
Figure 4.27: *Cell viability for 24 h and 48 h of CG-40, CG-40 loaded with antimicrobial peptide without and with heat activation at 52°C for 10 min.*

Finally, to provide a first demonstration on how this technology can be applied, an *ex vivo* wound skin (**Figure 4.28A**) was infected with *S. aureus* (**Figure 4.28B**) and the wound texture was investigated after treatment with a peptide-loaded CG-40 activated at 52 °C for 10 min. Infection with *S. aureus* was performed in the wound region of the skin for 3 days and then treated with the peptide-loaded CG-40 via light activation at 52°C for 10 min. The success of the treatment was followed by a visual inspection of the skin, displaying changes in the color

upon infection. On day 3, the wound area appeared yellow and had a strong wet aspect, one of the indications of infection. After treatment with only the CG-40 (**Figure 4.28C**), no improvement of the aspect of the wound was observed. Heat treatment (**Figure 4.28D**) did somehow change the wound appearance showing a drier aspect. Peptide-loaded CGs but not activated (**Figure 4.28**) also indicated no wound healing effect. However, heat activated and peptide-loaded CG-40 (**Figure 4.28F**) resulted in *ex vivo* skin showing a comparatively dry aspect. These results, though preliminary, suggest that sufficient peptide release occurs to eradicate bacterial infection.
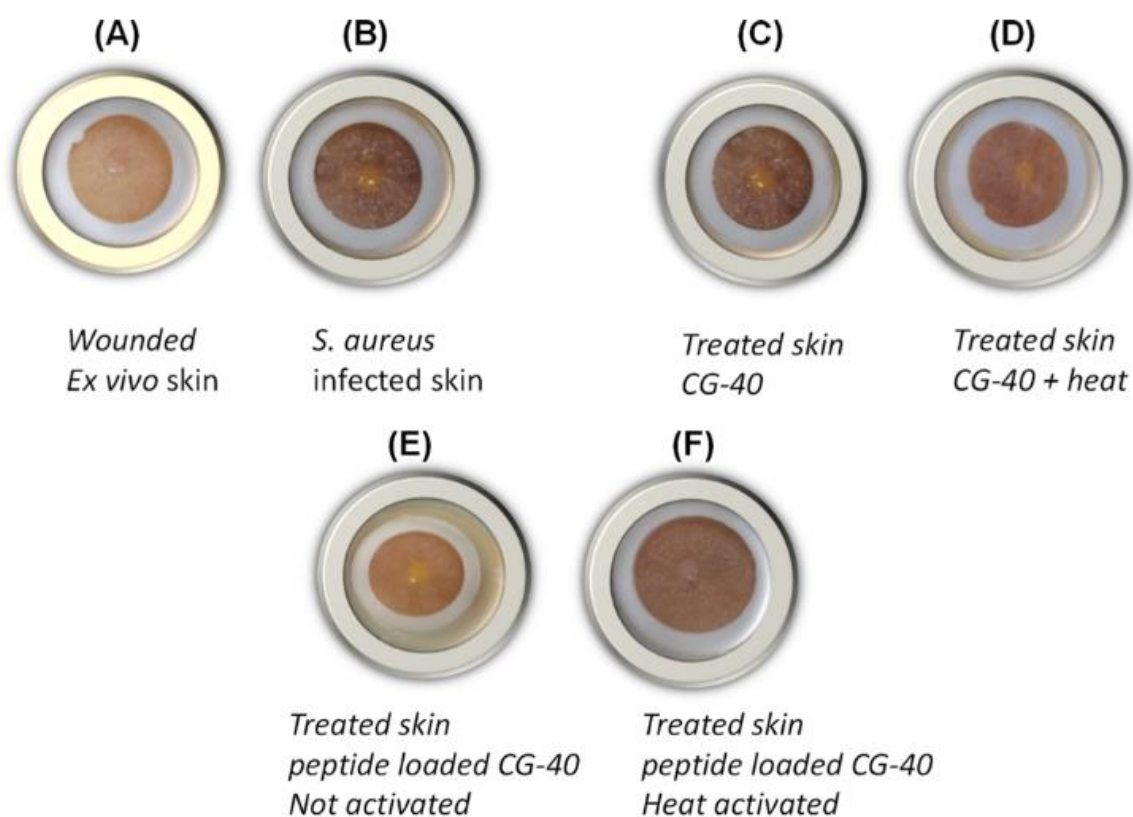
Figure 4.28 : *Optical images of (**A**) wounded ex vivo skin, (**B**) wounded and infected ex vivo skin, and (**C−F**) wounded and infected ex vivo skin after treatment: (**C**) treated skin with CG-40, (**D**) treated skin with CG-40 and heat activate (52 °C for 10 min). (**E**) peptide-loaded CG-40 but not activated. (**F**) peptide-loaded CG-40 and heat activated (52 °C for 10 min).*

In conclusion, a layered device for an on-demand release of an antimicrobial peptide was successfully applied to efficiently kill specific bacteria upon photothermal activation by a drug delivery system. A FuMa-containing CG matrix allows covalent conjugation of a maleimide-containing bioactive peptide through the DA reaction. An underlying rGO layer coated on Kapton enables photothermal heating of the construct upon exposure to NIR

irradiation, which releases the conjugated bioactive agent through the retro DA reaction. Application of this device for on-demand killing of bacteria was achieved through conjugation of a maleimide-containing antimicrobial peptide. Photothermal release of the peptide from the CG results in the bactericidal effect with selectivity for the Gram-positive *S. aureus*, while no significant effect was observed for the Gram-negative *E. coli* strain. In addition, this photothermally active cryogel device could be used as wound care product for wound infection treatment. With recent advances in fabrication and assembly of highly porous cryogel for drug delivery and wound dressings, this may contribute to wound management. Our *ex vivo* human model provides a first demonstration of treatment efficiency and confirms the medical application of the patch. Further experimental and clinical validation needs to be extended to make the patch more suitable for wound size and the wound care conditions, with a possibility of home treatment.

REFERENCES

1.   Thornton Spann, C.; Taylor, S. C.; Weinberg, J. M. Topical Antimicrobial Agents in Dermatology. *Clinics in Dermatology* **2003**, *21* (1), 70–77. https://doi.org/10.1016/S0738-081X(02)00320-6.

2.   Brouillard, C.; Bursztejn, A.-C.; Latarche, C.; Cuny, J.-F.; Truchetet, F.; Goullé, J.-P.; Schmutz, J.-L. Silver Absorption and Toxicity Evaluation of Silver Wound Dressings in 40 Patients with Chronic Wounds. *Journal of the European Academy of Dermatology and Venereology* **2018**, *32* (12), 2295–2299. https://doi.org/10.1111/jdv.15055.

3.   Lipsky, B. A.; Hoey, C. Topical Antimicrobial Therapy for Treating Chronic Wounds. *Clinical Infectious Diseases* **2009**, *49* (10), 1541–1549. https://doi.org/10.1086/644732.

4.   Shiekh, P. A.; Andrabi, S. M.; Singh, A.; Majumder, S.; Kumar, A. Designing Cryogels through Cryostructuring of Polymeric Matrices for Biomedical Applications. *European Polymer Journal* **2021**, *144*, 110234. https://doi.org/10.1016/j.eurpolymj.2020.110234.

5.   Li, S.; Dong, S.; Xu, W.; Tu, S.; Yan, L.; Zhao, C.; Ding, J.; Chen, X. Antibacterial Hydrogels. *Advanced Science* **2018**, *5* (5), 1700527. https://doi.org/10.1002/advs.201700527.

6.   Yang, K.; Han, Q.; Chen, B.; Zheng, Y.; Zhang, K.; Li, Q.; Wang, J. Antimicrobial Hydrogels: Promising Materials for Medical Application. *IJN* **2018**, *13*, 2217–2263. https://doi.org/10.2147/IJN.S154748.

7.   Hoque, J.; Bhattacharjee, B.; Prakash, R. G.; Paramanandham, K.; Haldar, J. Dual Function Injectable Hydrogel for Controlled Release of Antibiotic and Local Antibacterial Therapy. *Biomacromolecules* **2018**, *19* (2), 267–278. https://doi.org/10.1021/acs.biomac.7b00979.

8.   Zhao, X.; Guo, B.; Wu, H.; Liang, Y.; Ma, P. X. Injectable Antibacterial Conductive Nanocomposite Cryogels with Rapid Shape Recovery for Noncompressible Hemorrhage and Wound Healing. *Nat Commun* **2018**, *9* (1), 2784. https://doi.org/10.1038/s41467-018-04998-9.

9.   Li, P.; Jia, Z.; Wang, Q.; Tang, P.; Wang, M.; Wang, K.; Fang, J.; Zhao, C.; Ren, F.; Ge, X.; Lu, X. A Resilient and Flexible Chitosan/Silk Cryogel Incorporated Ag/Sr Co-Doped Nanoscale Hydroxyapatite for Osteoinductivity and Antibacterial Properties. *J. Mater. Chem. B* **2018**, *6* (45), 7427–7438. https://doi.org/10.1039/C8TB01672K.

10.   Han, L.; Li, P.; Tang, P.; Wang, X.; Zhou, T.; Wang, K.; Ren, F.; Guo, T.; Lu, X. Mussel-Inspired Cryogels for Promoting Wound Regeneration through Photobiostimulation, Modulating Inflammatory Responses and Suppressing Bacterial Invasion. *Nanoscale* **2019**, *11* (34), 15846–15861. https://doi.org/10.1039/C9NR03095F.

11.   Aydin, D.; Arslan, M.; Sanyal, A.; Sanyal, R. Hooked on Cryogels: A Carbamate Linker Based Depot for Slow Drug Release. *Bioconjugate Chem.* **2017**, *28* (5), 1443–1451. https://doi.org/10.1021/acs.bioconjchem.7b00140.

12.   Rosselle, L.; Cantelmo, A. R.; Barras, A.; Skandrani, N.; Pastore, M.; Aydin, D.; Chambre, L.; Sanyal, R.; Sanyal, A.; Boukherroub, R.; Szunerits, S. An 'on-Demand' Photothermal Antibiotic Release Cryogel Patch: Evaluation of Efficacy on an *Ex Vivo* Model for Skin Wound Infection. *Biomater. Sci.* **2020**, *8* (21), 5911–5919. https://doi.org/10.1039/D0BM01535K.

13.   Guo, J.; Chang, C.; Li, W. The Role of Secreted Heat Shock Protein-90 (Hsp90) in Wound Healing - How Could It Shape Future Therapeutics? *Expert Rev Proteomics* **2017**, *14* (8), 665–675. https://doi.org/10.1080/14789450.2017.1355244.

14.   Khan, A. A.; Banwell, P. E.; Bakker, M. C.; Gillespie, P. G.; McGrouther, D. A.; Roberts, A. H. Topical Radiant Heating in Wound Healing: An Experimental Study in a Donor Site Wound Model*. *International Wound Journal* **2004**, *1* (4), 233–240. https://doi.org/10.1111/j.1742-4801.2004.00065.x.

15.   Altinbasak, I.; Jijie, R.; Barras, A.; Golba, B.; Sanyal, R.; Bouckaert, J.; Drider, D.; Bilyy, R.; Dumych, T.; Paryzhak, S.; Vovk, V.; Boukherroub, R.; Sanyal, A.; Szunerits, S. Reduced Graphene-Oxide-Embedded Polymeric Nanofiber Mats: An "On-Demand" Photothermally Triggered Antibiotic Release Platform. *ACS Appl. Mater. Interfaces* **2018**, *10* (48), 41098–41106. https://doi.org/10.1021/acsami.8b14784.

16.   Teodorescu, F.; Oz, Y.; Quéniat, G.; Abderrahmani, A.; Foulon, C.; Lecoeur, M.; Sanyal, R.; Sanyal, A.; Boukherroub, R.; Szunerits, S. Photothermally Triggered On-Demand Insulin Release from Reduced Graphene Oxide Modified Hydrogels. *Journal of Controlled Release* **2017**, *246* (Supplement C), 164–173. https://doi.org/10.1016/j.jconrel.2016.10.028.

18.   Schaudinn, C.; Dittmann, C.; Jurisch, J.; Laue, M.; Günday-Türeli, N.; Blume-Peytavi, U.; Vogt, A.; Rancan, F. Development, Standardization and Testing of a Bacterial Wound Infection Model Based on *Ex Vivo* Human Skin. *PLOS ONE* **2017**, *12* (11), e0186946. https://doi.org/10.1371/journal.pone.0186946.

19.   Hammond, M. E.; Lapointe, G. R.; Feucht, P. H.; Hilt, S.; Gallegos, C. A.; Gordon, C. A.; Giedlin, M. A.; Mullenbach, G.; Tekamp-Olson, P. IL-8 Induces Neutrophil Chemotaxis Predominantly via Type I IL-8 Receptors. *The Journal of Immunology* **1995**, *155* (3), 1428–1433.

20.   Hosoyama, K.; Lazurko, C.; Muñoz, M.; McTiernan, C. D.; Alarcon, E. I. Peptide-Based Functional Biomaterials for Soft-Tissue Repair. *Front. Bioeng. Biotechnol.* **2019**, *7*, 205, DOI: 10.3389/fbioe.2019.00205

21.   Hamley, I. W. Small Bioactive Peptides for Biomaterials Design and Therapeutics. *Chem. Rev.* **2017**, *117*, 14015– 14041, DOI: 10.1021/acs.chemrev.7b00522

22.   Yadav, N.; Chauhan, M. K.; Chauhan, V. S. Short To Ultrashort Peptide-Based Hydrogels As A Platform For Biomedical Applications. *Biomater. Sci.* **2020**, *8*, 84– 100, DOI: 10.1039/c9bm01304k

23.   Zong, J.; Cobb, S. L.; Cameron, N. R. Peptide-Functionalized Gold Nanoparticles: Versatile Biomaterials For Diagnostic And Therapeutic Applications. *Biomater. Sci.* **2017**, *5*,872– 886, DOI: 10.1039/c7bm00006e

24.   Fox, J. L. Antimicrobial Peptides Stage A Comeback. *Nat. Biotechnol.* **2013**, *31*, 379–382, DOI: 10.1038/nbt.2572

25.   Li, J.; Xing, R.; Bai, S.; Yan, X. Recent Advances Of Self-Assembling Peptide-Based Hydrogels For Biomedical Applications. *Soft Matter* **2019**, *15*, 1704– 1715, DOI: 10.1039/c8sm02573h

26.   Jiang, L.; Xu, D.; Sellati, T. J.; Dong, H. Self-Assemblyt Of Cationic Multidomaine Peptide Hydrogels: Supermolecualr Nanostructure And Theological Properties Dicated Antimicrobial Activity. *Nanoscale* **2015**, *7*, 19160– 19169, DOI: 10.1039/c5nr05233e

27.   Liu, J.; Detrembleur, C.; Mornet, S.; Jérôme, C.; Duguet, E. Design Of Hybrid Nanovehicles For Remotely Triggered Drug Release: An Overview. *J. Mater. Chem. B* **2015**, *3*, 6117– 6147, DOI: 10.1039/c5tb00664c

28.   Hoare, T. R.; Kohane, D. S. Hydrogels In Drug Delivery: Progress And Challenges. *Polymer* **2008**, *49*, 1993– 2007, DOI: 10.1016/j.polymer.2008.01.027

29.   Henderson, T. M. A.; Ladewig, K.; Haylock, D. N.; McLean, K. M.; O'Connor, A. J. Cryogels For Biomedical Applications. *J. Mater. Chem. B* **2013**, *1*, 2682, DOI: 10.1039/c3tb20280a

30.   Plieva, F. M.; Galaev, I. Y.; Noppe, W.; Mattiasson, B. Cryogel Applications In Microbiology. *Trends Microbiol.* **2008**, *16*, 543– 551, DOI: 10.1016/j.tim.2008.08.005

31.   Wang, Y.; Shim, M. S.; Levinson, N. S.; Sung, H.-W.; Xia, Y. Stimuli-Responsive Materials for Controlled Release of Theranostic Agents. *Adv. Funct. Mater.* **2014**, *24*, 4206– 4220, DOI: 10.1002/adfm.201400279

32.   Linsley, C. S.; Wu, B. M. Recent Advances In Light-Responsive On-Demand Drug-Delivery Systems. *Ther. Delivery* **2017**, *8*, 89– 107, DOI: 10.4155/tde-2016-0060

33.   Karimi, M.; Sahandi Zangabad, P.; Ghasemi, A.; Amiri, M.; Bahrami, M.; Malekzad, H.; Ghahramanzadeh Asl, H.; Mahdieh, Z.; Bozorgomid, M.; Ghasemi, A.; Rahmani Taji Boyuk, M. R.; Hamblin, M. R. Temperature-Responsive Smart Nanocarriers for Delivery Of Therapeutic Agents: Applications and Recent Advances. *ACS Appl. Mater. Interfaces* **2016**, *8*, 21107– 21133, DOI: 10.1021/acsami.6b00371

34.   Wenzel, M.; Chiriac, A. I.; Otto, A.; Zweytick, D.; May, C.; Schumacher, C.; Gust, R.; Albada, H. B.; Penkova, M.; Kramer, U.; Erdmann, R.; Metzler-Nolte, N.; Straus, S. K.; Bremer, E.; Becher, D.; Brotz-Oesterhelt, H.; Sahl, H.-G.; Bandow, J. E. Small Cationic Antimicrobial Peptides Delocalized Peripheral Membrane Proteins. *Proc. Natl. Acad. Sci. U. S. A.* **2014**, *111*, E1409– E1418, DOI: 10.1073/pnas.1319900111

35.   Wenzel, M.; Prochonow, P.; Mowbray, C.; Vuong, C.; Hoxtermann, S.; Stepanek, J. J.; Albada, H. B.; Hall, J.; Metzler-Nolte, N.; Bandow, J. E. Toards Profiles and Resistance Development and Toxicity for the small cationic hexapeptide RWRWRW-NH2. *Front. Cell Dev. Biol.* **2016**, *4*, 86, DOI: 10.3389/fcell.2016.00086

36.   Chambre, L.; Rosselle, L.; Barras, A.; Aydin, D.; Loczechin, A.; Gunbay, S.; Sanyal, R.; Skandrani, N.; Metzler-Nolte, N.; Bandow, J. E.; Boukherroub, R.; Szunerits, S.; Sanyal, A. Photothermally Active Cryogel Devices for Effective Release of Antimicrobial Peptides: On-Demand Treatment of Infections. *ACS Appl. Mater. Interfaces* **2020**, *12* (51), 56805– 56814. https://doi.org/10.1021/acsami.0c17633.

37.   Liu, Y.-L.; Chuo, T.-W. Self-healing polymers based on thermally reversible Diels-Alder chemistry. *Polym. Chem.* **2013**, *4*, 2194– 2205, DOI: 10.1039/c2py20957h

38.   Schütz, M. B.; Lê, K.; Ilyas, S.; Mathur, S. Reversible Covalent Assembly of Nanoparticles through On-Surface Diels–Alder Reaction. *Langmuir* **2020**, *36*, 1552– 1558, DOI: 10.1021/acs.langmuir.9b02261

39.   Altinbasak, I.; Sanyal, R.; Sanyal, A. Best Of Both Worlds: Diels–Alder Chemistry Towards Fabrication Of Redox-Responsive Degradable Hydrogels For Protein Release. *RSC Adv.* **2016**, *6*, 74757– 74764, DOI: 10.1039/c6ra16126j

40.   Chen, X.; Dam, M. A.; Ono, K.; Mal, A.; Shen, H.; Nutt, S. R.; Sheran, K.; Wudl, F. A Thermally Re-Mendable Cross-Linked Polymeric Material. *Science* **2002**, *295*, 1698– 1702, DOI: 10.1126/science.1065879

41.   Ma, T.; Gao, X.; Dong, H.; He, H.; Cao, X. High-Throughput Generation Of Hyaluronic Acid Microgels Viamicrofluidics-Assisted Enzymatic Crosslinking And/Or Diels–Alder Click Chemistryfor Cell Encapsulation And Delivery. *Appl. Mater. Today* **2017**, *9*, 49– 59, DOI: 10.1016/j.apmt.2017.01.007

42.   Nimmo, C. M.; Owen, S. C.; Shoichet, M. S. Diels–Alder Click Cross-Linked Hyaluronic Acid Hydrogels for Tissue Engineering. *Biomacromolecules* **2011**, *12*, 824– 830, DOI: 10.1021/bm101446k

43.   Wei, H.-L.; Yang, J.; Chu, H.-J.; Yang, Z.; Ma, C.-C.; Yao, K. Diels–Alder Reaction In Water For The Straightforward Preparation Of Thermoresponsive Hydrogels. *Appl. Polym. Sci.* **2011**, *120*, 974– 980, DOI: 10.1002/app.33116

44.   Koehler, K. C.; Anseth, K. S.; Bowman, C. N. Diels–Alder Mediated Controlled Release from a Poly(ethylene glycol) Based Hydrogel. *Biomacromolecules* **2013**, *14*, 538– 547, DOI: 10.1021/bm301789d

45.   Koehler, K. C.; Alge, D. L.; Anseth, K. S.; Bowman, C. N. A Diels-Alder modulated approach to control and sustain the release of dexamethasone and induce osteogenic differentiation of human mesenchymal stem cells. *Biomaterials* **2013**, *34*, 4150– 4158, DOI: 10.1016/j.biomaterials.2013.02.020

46.   Vieyers, A.; Lam, T.; Guillet, R.; France, G.; Castonguay, A.; Kakkar, A. Combined CuI-Catalysed Alkyne-Azide Cycloaddition and Furan-Maleimide Diels-Alder "Click" Chemistry Approach to Thermoresponsive Dendrimers. *Chem. Commun.* **2010**, *46*, 1875– 1877, DOI: 10.1039/B924888A

47.   Yamashita, S.; Fukushima, H.; Niidome, Y.; Mori, T.; Katayama, Y.; Niidome, T. Controlled-Release System Mediated by a Retro Diels–Alder Reaction Induced by the

Photothermal Effect of Gold Nanorods. *Langmuir* **2011**, *27*, 14621– 14626, DOI: 10.1021/la2036746

48.   Chengnan, L.; Pagneux, Q.; Voronova, A.; Barras, A.; Abderrahmani, A.; Plaisance, V.; Pawlowski, V.; Hennuyer, N.; Staels, B.; Rosselle, L.; Skandrani, N.; Li, M.; Boukherroub, R.; Szunerits, S. Near-Infrared Light Activatable Hydrogels for Metformin Delivery. *Nanoscale* **2019**, *11* (34), 15810–15820. https://doi.org/10.1039/C9NR02707F.

49.   Im, I.-T.; Youn, S. B.; Kim, K. Numerical Study on the Temperature Profiles and Degree of Burns in Human Skin Tissue During Combined Thermal Therapy. *Numerical Heat Transfer, Part A: Applications* **2015**, *67* (9), 921–933. https://doi.org/10.1080/10407782.2014.955338.

50.   Teodorescu, F.; Quéniat, G.; Foulon, C.; Lecoeur, M.; Barras, A.; Boulahneche, S.; Medjram, M. S.; Hubert, T.; Abderrahmani, A.; Boukherroub, R.; Szunerits, S. Transdermal Skin Patch Based on Reduced Graphene Oxide: A New Approach for Photothermal Triggered Permeation of Ondansetron across Porcine Skin. *Journal of Controlled Release* **2017**, *245*, 137–146. https://doi.org/10.1016/j.jconrel.2016.11.029.

51.   Chen, Y. C.; Lin, K. Y. A.; Lin, C. C.; Lu, T. Y.; Lin, Y. H.; Lin, C. H.; Chen, K. F. Photoinduced Antibacterial Activity Of Nrc03 Peptide-Conjugated Dopamine/Nano-Reduced Graphene Oxide Against *Staphylococcus Aureus*. *Photochem. Photobiol. Sci.* **2019**, *18*, 2442–2448, DOI: 10.1039/c9pp00202b

52.   Oz, Y.; Barras, A.; Sanyal, R.; Boukherroub, R.; Szunerits, S.; Sanyal, A. Functionalization of Reduced Graphene Oxide via Thiol–Maleimide "Click" Chemistry: Facile Fabrication of Targeted Drug Delivery Vehicles. *ACS Appl. Mater. Interfaces* **2017**, *9*, 34194–34203, DOI: 10.1021/acsami.7b08433

53.   Otari, S. V.; Kumar, M.; Anwar, M. Z.; Thorat, N. D.; Patel, S. K. S.; Lee, D.; Lee, J. H.; Lee, J.-K.; Kang, J. C.; Zhang, L. Rapid Synthesis And Decoration Of Reduced Graphene Oxide With Gold Nanoparticles By Thermostable Peptides For Memory Device And Photothermal Applications. *Sci. Rep.* **2017**, *7*, 10980, DOI: 10.1038/s41598-017-10777-1

54.   Yadav, V.; Roy, S.; Singh, P.; Khan, Z.; Jaiswal, A. 2D MoS2-Based Nanomaterials for Therapeutic, Bioimaging, and Biosensing Applications. *Small* **2019**, *15*, 1803706, DOI: 10.1002/smll.201803706

55.   Shi, J.; Li, J.; Wang, Y.; Cheng, J.; Zhang, C. Y. Recent Advances In Mos2-Based Photothermal Therapy For Cancer And Infectious Disease Treatment. *J. Mater. Chem. B* **2020**, *8*, 5793– 5807, DOI: 10.1039/d0tb01018a

56.   Zou, Q.; Abbas, M.; Zhao, L.; Li, S.; Shen, G.; Yan, X. Biological Photothermal Nanodots Based on Self-Assembly of Peptide–Porphyrin Conjugates for Antitumor Therapy. *J. Am. Chem. Soc.* **2017**, *139*, 1921– 1927, DOI: 10.1021/jacs.6b11382

57.   Chen, G.; Ma, B.; Xie, R.; Li, C.; Dou, K.; Gong, S. CuS-Based Theranostic Micelles for NIR-Controlled Combination Chemotherapy and Photothermal Therapy and Photoacoustic Imaging. *ACS Appl. Mater. Interfaces* **2017**, *9*, 41700– 41711, DOI: 10.1021/acsami.7b14083

58.	Teirlinck, E.; Barras, A.; Liu, J.; Fraire, J. C.; Lajunen, T.; Xiong, R.; Forier, K.; Li, C.; Urtti, A.; Boukherroub, R.; Szunerits, S.; De Smedt, S. C.; Coenye, T.; Braeckmans, K. Exploring Light-Sensitive Nanocarriers for Simultaneous Triggered Antibiotic Release and Disruption of Biofilms Upon Generation of Laser-Induced Vapor Nanobubbles. *Pharmaceutics* **2019**, *11*, 201, DOI: 10.3390/pharmaceutics11050201

59.	Ahmed, W.; Zhai, Z.; Gao, C. Adaptive Antibacterial Biomaterial Surfaces And Their Applications. *Mater. Today Bio* **2019**, *2*, 100017, DOI: 10.1016/j.mtbio.2019.100017

60.	Teodorescu, F.; Rolland, L.; Ramarao, V.; Abderrahmani, A.; Mandler, D.; Boukherroub, R.; Szunerits, S. Electrochemically Triggered Release Of Human Insulin From An Insulin-Impregnated Reduced Graphene Oxide Modified Electrode. *Chem. Commun.* **2015**, *51*, 14167– 14170, DOI: 10.1039/c5cc05539c

61.	Vermonden, T.; Censi, R.; Hennink, W. E. Hydrogels for Protein Delivery. *Chem. Rev.* **2012**, *112*, 2853– 2888, DOI: 10.1021/cr200157d

62.	Li, C.; Ye, R.; Bouckaert, J.; Zurutuza, A.; Drider, D.; Dumych, T.; Paryzhak, S.; Vovk, V.; Bilyy, R. O.; Melinte, S.; Li, M.; Boukherroub, R.; Szunerits, S. Flexible Nanoholey Patches for Antibiotic-Free Treatments of Skin Infections. *ACS Appl. Mater. Interfaces* **2017**, *9*, 36665– 36674, DOI: 10.1021/acsami.7b12949

CHAPTER 5 : CONCLUSIONS AND PERSPECTIVES

Chronic wounds are a major public health issue because of the high cost of their management. This thesis work focused on the development of *ex vivo* skin models for the study of chronic wounds with a particular interest in infected wounds. These *ex vivo* human study models were proposed to simplify the research compared to the complex *in vivo* process which requires specialized facilities, authorizations and also represents a high cost. These models have been developed to test the efficiency of a wide variety of treatments from therapeutic molecules to dressings as well as physical stimuli. The viability of the skin samples allows us to test treatments over a period of 7 days. Chronic wounds are often associated with infection, the infected model also allowed us to test various antibacterial treatments successfully. This underlines that the developed and used *ex vivo* model is not only a simple but robust research tool. In addition, the use of *ex vivo* models using human material allows to reproduce as closely as possible human wound healing mechanisms and all the characteristics of human skin with all cell types. However, it is important to have a good understanding of the model, especially in terms of the histological structure as well as the complications that may be encountered, in order to be able to translate the results in a meaningful way. For this reason, it is necessary to delimit the study and to take into account the characteristics that the treatments may have in order to properly analyze their effects. A myriad of biomarkers is available to make the studies completer and more robust before undertaking *in vivo* tests.[1-2]

In this work the focus of the *ex vivo* skin model was mainly on testing the efficacy of an antibacterial treatment. On-demand drug delivery systems for the treatment of chronic wounds was investigated with this model. It could he shown that the release of drugs locally on the wound allows to increasing the effectiveness of treatments compared to systemic drug delivery. These approaches seem to be adapted to overcome current developments in local passive therapies that have shown nonsignificant efficacy.[3] Transdermal delivery technologies provide a stimulation that aims to penetrate deeper into the skin and thus into the wound.[4] Here, an innovative material has been used to release drugs on demand; a cryogel. With recent advances in fabrication and assembly of highly porous cryogel for drug delivery and wound dressings, this may contribute to wound management. The incorporation of nanomaterials, such as rGO, or the use of coated surfaces with nanomaterials enable photothermal heating of the dressing upon exposure to NIR irradiation which releases the conjugated bioactive agent on the wound. Our *ex vivo* human model provides a first demonstration of treatment efficiency and confirms the medical application of the patch. Further experimental and clinical validation

needs to be extended to make the patch more suitable for wound size and the wound care conditions, with a possibility of home treatment.

In the future, the *ex vivo* models presented will be very useful for testing the efficacy and risks in various projects on the treatment of chronic wounds using biocompatible materials, nanomaterials and other healing compounds. In addition, we are able to modulate the model to adapt to other uses like diagnostic tests. Indeed, physiological sensors are increasingly developed for wound monitoring and also need to be tested with wound models.[5]

What are the future aspects of this work ? During the last year of the thesis, several approaches have been undertaken to make studies of wound healing, infection or drug delivery more robust. A 2-D cellular model has been developed in order to test therapeutic molecules or nanomaterials for the treatment of chronic. In order to test the ability of novel therapeutics to improve wound healing, a wound assay was set up in the laboratory using fluorescent fibroblasts (**Figure 5.1**).[7]
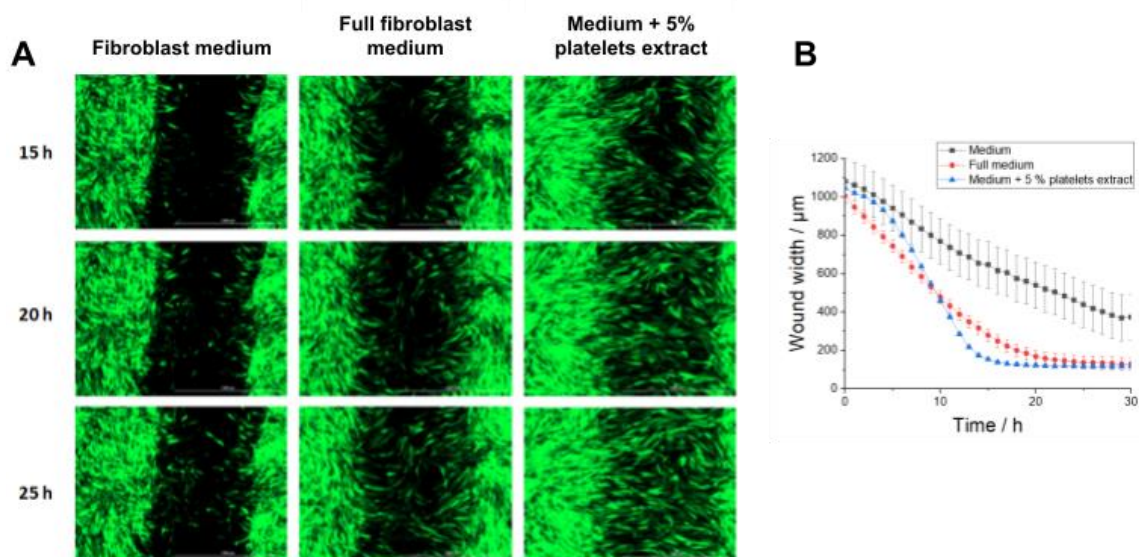
Figure 5.1 : *Analysis of GFP-human dermal fibroblasts cells (GFP-HDFCs) migration by in vitro scratch assay.* ***A.*** *Representative time-lapse images were acquired at day 15, 20 and 25h.* ***B.*** *Kinetic of wound width showing the wound closure over 30h of culture.*

The influence of molecules at the cellular level is studied with a scratching model which consists in making an artificial gap using a tip on a confluent cell monolayer.[8] The overtime observation of the wound closure allowed us to study the migration of fibroblasts under the effect of a therapeutic. For this, we used mitomycin C to stop the proliferation of cells.

Fibroblast cells were cultured in a chemical medium specially designed for the culture of fibroblasts (Fibroblast Medium). The manufacturer proposes a cocktail of growth factors to add to the medium in order to optimize the growth of fibroblasts, we then obtain the Full Fibroblast Medium. These two media were used as negative and positive controls. The addition of platelet extract to the culture medium showed a clear improvement in wound closure by fibroblast migration, as shown in **Figure 5.1**. The platelet extract has promising properties and further investigations and optimization are needed in order to develop a new treatment for chronic wounds by combining different technologies.

New transdermal drug delivery technologies can be implemented in the future such as the use of ultrasound for drug delivery (**Figure 5.2**.) and microneedles (**Figure 5.3**.). Ultrasound for transdermal delivery of therapeutics is one of the techniques that has been investigated in order to cross the stratum corneum barrier. Several researches on sonophoresis have been developed in order to apply this technique to various drugs delivery.[9] In order to deepen this point, we collaborated with the company Sinaptec® and the possibility to improve skin penetration with sonication probes. The first results (**Figure 5.2**) were obtained from a probe at low frequency ultrasound (107 KHz) which appears to be more effective to increase skin permeability.[10]

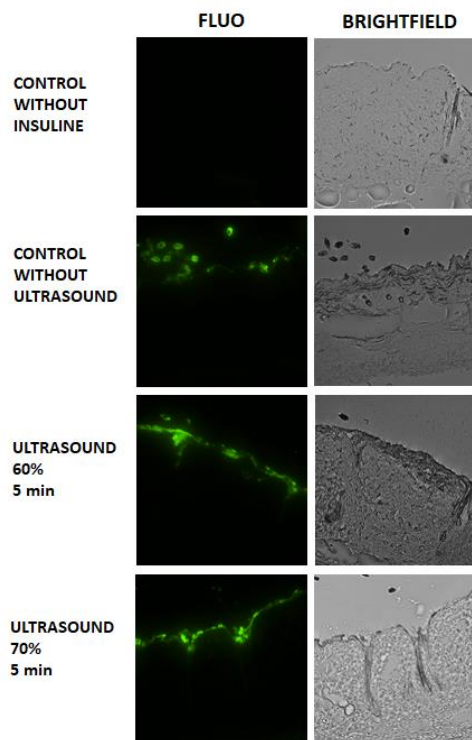***Figure 5.2 :** Penetration study through excised human skin by fluorescent microscopy. The samples were illuminated at 450 nm to excite the FITC conjugated to insulin. Normal untreated control skin doesn't show any fluorescence at this wavelength. The control of treated skin with Insulin-FITC without ultrasound stimulation shows a low fluorescence caused by fluorescent structures not bonded to the skin. Treated skin with Insulin-FITC and stimulated by ultrasonic vibration for 5min at 60 and 70% of amplitude show fluorescence in the stratum corneum and in the hair follicles.*

The ultrasonic vibrations are delivered through a cylindrical metal rod whose tip is placed on the top of the skin. Mouse skin was used for the permeability study. Insulin labeled with a fluorescent dye, fluorescein isothiocyanate (FITC), was used to visualize the drug in the skin. The amplitude of vibration was estimated to 10µm/A. Fluorescent observation of skin sections showed that the fluorescence is localized in the stratum corneum and hair follicles regardless of the ultrasound power used (**Figure 5.2**) and the application time. In comparison with the control, insulin-FITC remains fixed at the stratum corneum, whereas in ultrasound stimulation insulin-FITC is removed during washing. It seems interesting to use a probe with ultrasound that penetrates deeper into the skin to optimize the phenomenon of skin permeabilization.

On the other hand, microneedle patches are gaining increased attention a tool for transdermal drug delivery. While degradable microneedle (MN) arrays are widely employed, the use of non-dissolving MN patches remains a challenge to overcome. A cross-linking gelatin methacrylate with polyethylene glycol diacrylate (PEGDA) showed good properties for engineering non-dissolving MN arrays and was prepared by Bilal Demil, post-doctoral student in our team together with CEA Grenoble. Incorporation of MoS_2 nanosheets as a photothermal component into the MN hydrogels results in MNs featuring on-demand release properties: The microneedle array formed using 500 µg/mL of MoS_2 possessed in addition sufficient mechanical strength to penetrate mouse skin (**Figure 5.3a**) under compression (**Figure 5.3b**) without causing damage to the microneedles. SEM images indicated that the microneedles maintained their conical shape and sharp tips after removal from the mouse skin (**Figures 5.3c, d**). Hematoxylin and eosin (H&E) staining of the mouse skin tissue further confirmed that the microneedles had penetrated the stratum corneum and perforated into the epidermal layer (**Figure 5.3e**). The objective of this study was the development of a microneedle patch for the activatable delivery of insulin and might be a potential approach for the delivery of other proteins. Furthermore, this patch with non-dissolvable microneedles has promising properties

for treating chronic diseases. Indeed, stimulation by heating is supposed to stimulate healing mechanisms. No human skin samples were available to further investigate the hypothesis with our *ex vivo* model. Nevertheless, this patch could be tested for stimulation of wound healing in combination with drug delivery systems. The microneedles allow for deeper heating of the skin tissue which could stimulate dermal remodeling compared to the top dressing.
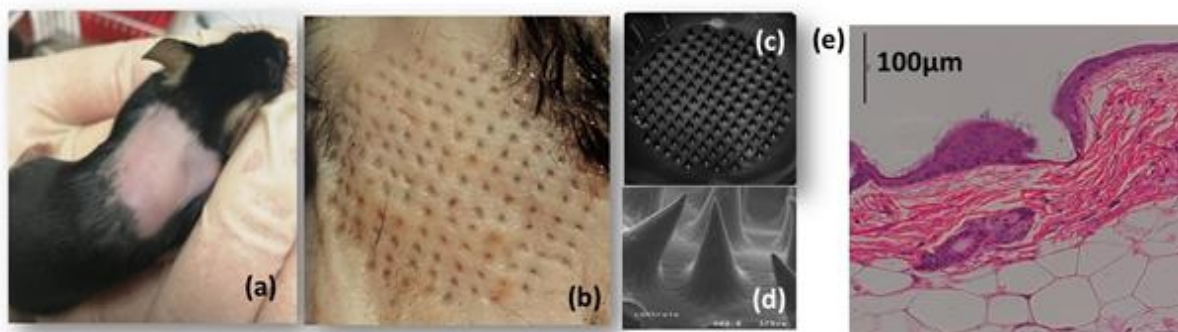
*Figure 5.3: Biophysical Properties of the MoS2-MNs Patch (**a**) Microscopic images of mouse back shaved before application of MoS$_2$-MNs array formed from hydrogel cocktails containing 500 µg mL^{-1} of MoS$_2$. (**b**) Image of relevant skin transcutaneously- treated with the MoS$_2$-MNs array patch. (**c,d**) SEM images of MoS$_2$-MNs array after skin penetration. (**e**) H&E stained section of the mouse skin penetrated by one MoS$_2$-MNs array patch.*

To investigate the efficiency of the MoS$_2$-MNs arrays to lowering blood glucose level (BGL), MoS$_2$-MNs arrays as well as MoS$_2$-MNs arrays loaded with 100 µg mL^{-1} (2.88 Insulin units) of insulin were applied on the back of C57BL/6 mice with a homemade applicator and removed after 10 min. The change in BGL measured over a period of 1h after application is shown in **Figure 5.4a**. Mice treated with a blank MoS$_2$-MNs patch (not loaded with insulin) but activated for 10 min. was used as a control. As expected, mice treated with this patch showed no BGL decline even after 1h. The same was observed for insulin-loaded MoS$_2$-MNs arrays without light activation. Indeed, the high molecular weight and hydrophilic character of insulin restricted the passive skin permeation. The BGL followed almost the same trend as the blank, indicating that insulin was not released passively. This was different to mice treated with an insulin-loaded MoS$_2$-MNs array -photothermally-activated for 10 min, where a steady drop in BGL was observed after 15 min, by which it had dropped by 30% from its initial value. These results confirmed that the biological activity of released insulin remained intact after light exposure. Important observation was also the time evolution of the marks left by microneedles on the skin of the treated mice. After 30 min, the marks on the skin have

completely faded, indicating that the array did not permanently destroy the skin of the mouse (**Figure 5.4b**).

To complete the results, we took the opportunity of using pancreatectomized Gottingen minipig as a valuable model of insulin-dependent diabetes.[11] Of particular relevance, diabetic minipigs share many similarities with humans with regard to pharmacokinetics of compounds after subcutaneous administration, structure and function of the gastrointestinal tract, morphology of the pancreas, and the overall metabolic status of the two species.[12-13] Application of a MoS_2-MNs array loaded with human insulin on the ear of the minipig resulted in a reduction of the BGL after 30 min from the start of the patch application. The decrease of the BGL coincides with a peak in the plasma insulin concentration, confirming the hypoglycemic effect of insulin released from the patch (**Figure 5.4c**).
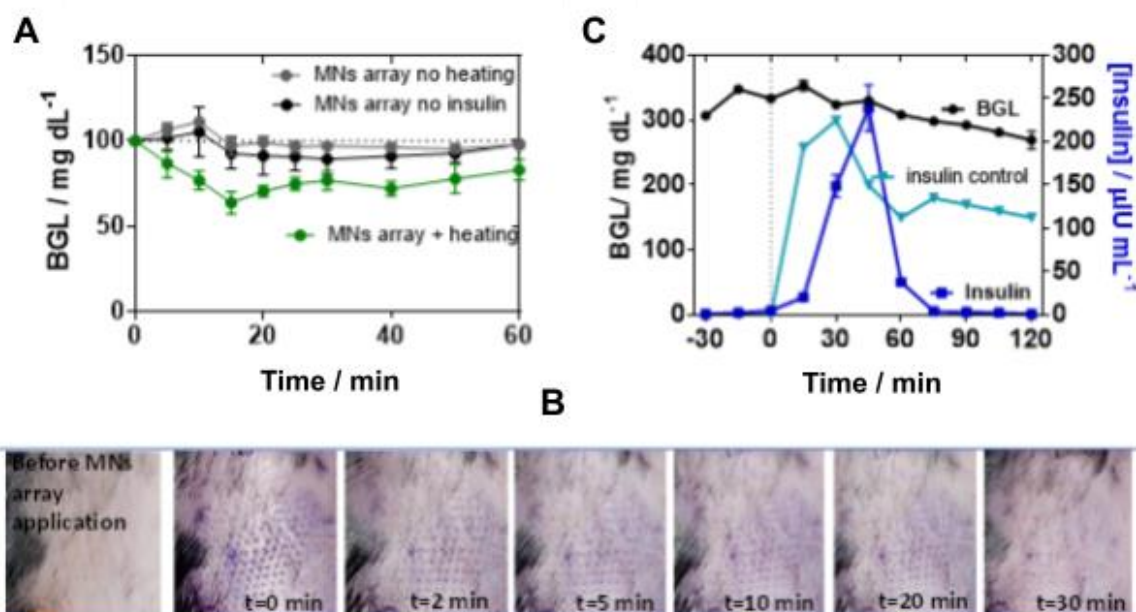
Figure 5.4: *In Vivo Permeation Study in Mice and Mini-Pigs:* ***A.*** *Effect of insulin (2.88 IU) loaded onto MoS_2-MNs (MNs) arrays on mouse blood glucose level (BGL) over time.* ***B.*** *Photographic images of mouse skin before and after application of MoS_2-MNs arrays.* ***C.*** *Measurement overtime of blood insulin (dark blue line) and blood glucose level (BGL, black line) in minipig carrying MoS_2-MNs arrays (MNs) patch loaded with human insulin (2.88 IU). In a control experiment (bright blue), insulin was injected subcutaneously (2.88 IU) and blood insulin was dosed over time.*

REFERENCES

1.   Lindley, L. E.; Stojadinovic, O.; Pastar, I.; Tomic-Canic, M. Biology and Biomarkers for Wound Healing. *Plast Reconstr Surg* **2016**, *138* (3), 18S-28S. https://doi.org/10.1097/PRS.0000000000002682.

2.   Agyare, C.; Osafo, N.; Boakye, Y. D. *Biomarkers of Wound Healing*; IntechOpen, 2018. https://doi.org/10.5772/intechopen.80222.

3.   Brouillard, C.; Bursztejn, A.-C.; Latarche, C.; Cuny, J.-F.; Truchetet, F.; Goullé, J.-P.; Schmutz, J.-L. Silver Absorption and Toxicity Evaluation of Silver Wound Dressings in 40 Patients with Chronic Wounds. *Journal of the European Academy of Dermatology and Venereology* **2018**, *32* (12), 2295–2299. https://doi.org/10.1111/jdv.15055.

4.   Prausnitz, M. R.; Langer, R. Transdermal Drug Delivery. *Nature Biotechnology* **2008**, *26* (11), 1261–1268. https://doi.org/10.1038/nbt.1504.

5.   Brown, M. S.; Ashley, B.; Koh, A. Wearable Technology for Chronic Wound Monitoring: Current Dressings, Advancements, and Future Prospects. *Front. Bioeng. Biotechnol.* **2018**, *6*. https://doi.org/10.3389/fbioe.2018.00047.

6.   Gupta, S.; Andersen, C.; Black, J.; de Leon, J.; Fife, C.; Lantis Ii, J. C.; Niezgoda, J.; Snyder, R.; Sumpio, B.; Tettelbach, W.; Treadwell, T.; Weir, D.; Silverman, R. P. Management of Chronic Wounds: Diagnosis, Preparation, Treatment, and Follow-Up. *Wounds* **2017**, *29* (9), S19–S36.

7.   Sami, D. G.; Heiba, H. H.; Abdellatif, A. Wound Healing Models: A Systematic Review of Animal and Non-Animal Models. *Wound Medicine* **2019**, *24* (1), 8–17. https://doi.org/10.1016/j.wndm.2018.12.001.

8.   Liang, C.-C.; Park, A. Y.; Guan, J.-L. *In Vitro* Scratch Assay: A Convenient and Inexpensive Method for Analysis of Cell Migration *in Vitro*. *Nat Protoc* **2007**, *2* (2), 329–333. https://doi.org/10.1038/nprot.2007.30.

9.   Seah, B. C.-Q.; Teo, B. M. Recent Advances in Ultrasound-Based Transdermal Drug Delivery. *Int J Nanomedicine* **2018**, *13*, 7749–7763. https://doi.org/10.2147/IJN.S174759.

10.   Park, D.; Park, H.; Seo, J.; Lee, S. Sonophoresis in Transdermal Drug Deliverys. *Ultrasonics* **2014**, *54* (1), 56–65. https://doi.org/10.1016/j.ultras.2013.07.007.
11.   Larsen, M. O.; Rolin, B. Use of the Göttingen Minipig as a Model of Diabetes, with Special Focus on Type 1 Diabetes Research. *ILAR Journal* **2004**, *45* (3), 303–313. https://doi.org/10.1093/ilar.45.3.303.

12.   Yu, J.; Wang, J.; Zhang, Y.; Chen, G.; Mao, W.; Ye, Y.; Kahkoska, A. R.; Buse, J. B.; Langer, R.; Gu, Z. Glucose-Responsive Insulin Patch for the Regulation of Blood Glucose in Mice and Minipigs. *Nat Biomed Eng* **2020**, *4* (5), 499–506. https://doi.org/10.1038/s41551-019-0508-y.

13.   Sterkers, A.; Hubert, T.; Gmyr, V.; Torres, F.; Baud, G.; Delalleau, N.; Vantyghem, M. C.; Kerr-Conte, J.; Caiazzo, R.; Pattou, F. Islet Survival and Function Following Intramuscular

Autotransplantation in the Minipig. *American Journal of Transplantation* **2013**, *13* (4), 891–898. https://doi.org/10.1111/ajt.12136.

LIST OF PUBLICATIONS

1. Chengnan, L.; Pagneux, Q.; Voronova, A.; Barras, A.; Abderrahmani, A.; Plaisance, V.; Pawlowski, V.; Hennuyer, N.; Staels, B.; **Rosselle, L**.; Skandrani, N.; Li, M.; Boukherroub, R.; Szunerits, S. Near-Infrared Light Activatable Hydrogels for Metformin Delivery. *Nanoscale* **2019**, *11* (34), 15810–15820. https://doi.org/10.1039/C9NR02707F.
   - **Cover page**

2. Pages, E.; Pastore, M.; Rosselle, L.; Barras, A.; Skandrani, N.; Cantelmo, A.; Boukherroub, R.; Merle, E.; Descargues, P.; Szunerits, S. LB1138 An Ex Vivo Human Skin Model for Healing of Infected Wounds. Journal of Investigative Dermatology **2019**, 139 (9), B24.

3. **Rosselle, L.**; Cantelmo, A. R.; Barras, A.; Skandrani, N.; Pastore, M.; Aydin, D.; Chambre, L.; Sanyal, R.; Sanyal, A.; Boukherroub, R.; Szunerits, S. An 'on-Demand' Photothermal Antibiotic Release Cryogel Patch: Evaluation of Efficacy on an Ex Vivo Model for Skin Wound Infection. *Biomater. Sci.* **2020**, *8* (21), 5911–5919. https://doi.org/10.1039/D0BM01535K.
   - **Cover page**

4. Chambre, L.; **Rosselle, L**.; Barras, A.; Aydin, D.; Loczechin, A.; Gunbay, S.; Sanyal, R.; Skandrani, N.; Metzler-Nolte, N.; Bandow, J. E.; Boukherroub, R.; Szunerits, S.; Sanyal, A. Photothermally Active Cryogel Devices for Effective Release of Antimicrobial Peptides: On-Demand Treatment of Infections. *ACS Appl. Mater. Interfaces* **2020**, *12* (51), 56805–56814. https://doi.org/10.1021/acsami.0c17633.

5. Andrei, C.-C.; Moraillon, A.; Larquet, E.; Potara, M.; Astilean, S.; Jakab, E.; Bouckaert, J.; **Rosselle, L.**; Skandrani, N.; Boukherroub, R.; Ozanam, F.; Szunerits, S.; Gouget-Laemmel, A. C. SERS Characterization of Aggregated and Isolated Bacteria Deposited on Silver-Based Substrates. *Anal Bioanal Chem* **2021**, *413* (5), 1417–1428. https://doi.org/10.1007/s00216-020-03106-5.

6. Demir, B; Rosselle, L; Voronova, A; Pagneux, Q; Quenon, A; Gmyr,V; Jary, D; Skandrani, N; Hennuyer,N; Staels, B; Hubert, T; Abderrahmani, A;Plaisance, V; Pawlowski, V; Boukherroub, R;Vignoud, S; Szunerits, S. Innovative transdermal delivery of insulin using Gelatin Methacrylate-based Microneedle Patches in Mice and Mini-Pigs. *Nanoscale horizons* **2021**.
   - ***Reviewing***

APPENDIX 1 : EXPERIMENTAL SECTION

S1. Skin processing

S1.1   Sampling and process GENOSKIN model

Ready-to-use *ex vivo* human skin samples were provided by Genoskin (France). The model used was the HypoSkin® model (surface of 0.5 cm²). Full thickness human skin with epidermis, dermis and hypodermis was collected from abdominal surgery with the informed consent of the individual donors, in full respect of the Declaration of Helsinki. The skin explant was embedded in a gel-like matrix with the epidermal surface left in direct contact with the air (Figure XX). The matrix and the culture medium allow maintaining the skin alive for at least 7 days.

To generate a wound (2 mm in diameter), a defect of a controlled diameter was performed to remove all the epidermis and upper part of the dermis. A silicon ring was adhered on the skin surface to prevent lateral bacteria leakage. The system was mounted into cell culture inserts and maintained in standard cell culture conditions.
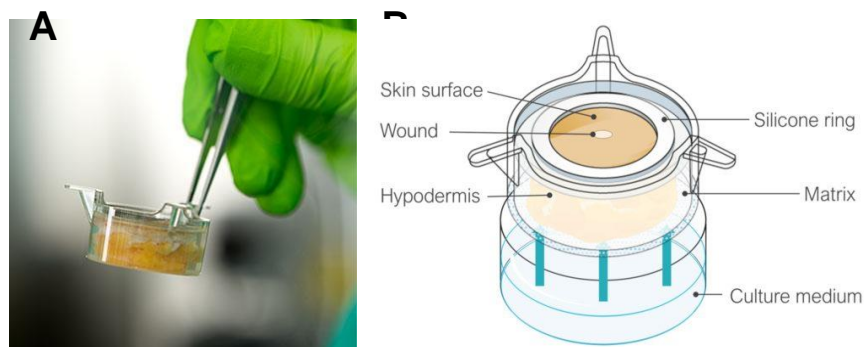

Figure 1: HypoSkin model. A. B. Histology confirmation. C.

Samples were delivered in the gel-matrix at room temperature. All samples were provided in a suitable culture plate to allow the culture in sterile condition and wound evolution observation of each sample.

S1.2 Sampling and process skin from surgery

S1.3 Tissue culture

The day of the receipt, fresh medium pre-heated at 37°C was added to each well and skin samples were incubated at 37°C and 5% CO2. Each culture day, the medium was renewed according to manufacturer instruction (Figure).

The HypoSkin® model was modified to allow the infection to occur by removing the antibiotics from culture medium and gel-matrix.

S.2 Infection

S2.1 Bacteria strains and culture condition

Staphylococcus aureus (ATCC® 43300™) and *Pseudomonas aeruginosa* (strain PAO1) were used to infect wounds. Before the wound infection, *S. aureus* was cultured in Brain Heart Infusion broth for 5h and *P. aeruginosa* in Luria-Bertani-Lennox broth overnight. Bacteria were incubated at 37°C under stirring (150 revolutions per minute) in aerobic condition. At the end of the incubation, bacteria were washed with medium and centrifuged. The pellets were resuspended in an appropriate medium and diluted to obtain the desired concentration (between 1x10^6 and 1x10^9 CFU/ml).

S2.2 Skin infection

10µl of bacteria suspension at 1x10^9 CFU/ml or 1x10^6 were added on the surface of skins. Thus, each skin was infected with 10^7 or 10^4 CFU. PBS was used as control for non-infected wound skin. Skins were cultured for 3 days at 37°C for the wound colonization. The culture media were refreshed every day for each skin sample. For control skins (with and without infection), the infection was proceeded during 3 days and for treated skins, the infection was proceeded for 2 days and the treatment was performed for 24h before the collecte. **(Figure 2)**
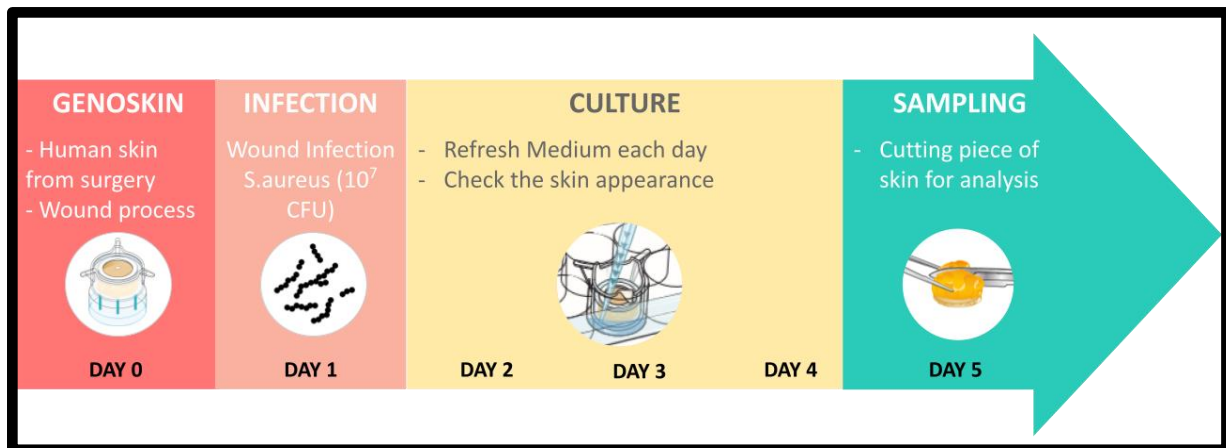
Figure 2 : *Skin infection experiment workflow from the preparation to the collect*

S3. Sample Collection

After five days of culture, skin samples were collected and cut in several parts to perform analysis. All steps were performed on sterile conditions. Briefly, the cell culture insert containing the skin sample was put in a sterile petri dish. With a forcep, the silicone ring is detached from the surface of the skin. The porous membrane under the gelose was removed and the skin sample pushed gently with a forcep to remove it from the insert. To avoid the biofilm and wound damage, the skin was kept right side up and the gelose matrix was mildly detached from the sample using a forcep. Then, the whole sample was weighting. Finally, five pieces were cut from each sample in order to perform all the necessary experiments:

 - A half part for the histology was cut in the middle of the wound

 - A quart part was cut for the RNA extraction and directly flash freezed after the weighting.

 - A quart part was cut for the bacteria counting. The piece was weighted to allow the calculation of CFU/g tissue.

 - A thin slice was cut for the SEM preparation

Each part contained a part of the wound. Then, all pieces were prepared according to protocols explained below.

S4. Skin analysis

S4.1 Macroscopic analysis: sample viability detection

Each culture day, skin samples were observed. We were able to detect skin infection development or not and healthy, damaged or dead skin. In healthy skin, the surface is clear pink and the wound appears whiter. The wound edge should appear clearly. In infected skin, *S. aureus* makes yellow pigment that allows us to easily detect a biofilm formation on the skin. *P. aeruginosa* produces a green pigment that can be detected on the skin. In damaged samples, the epidermis may change color and become gray, which means that the sample is no longer viable. If the wound contours become imprecise, it may mean that the epidermis is detaching and degrading rapidly.

Healthy tissue
No macroscopic sign
of infection

Macroscopic sign of
infection : Yellow
biofilm
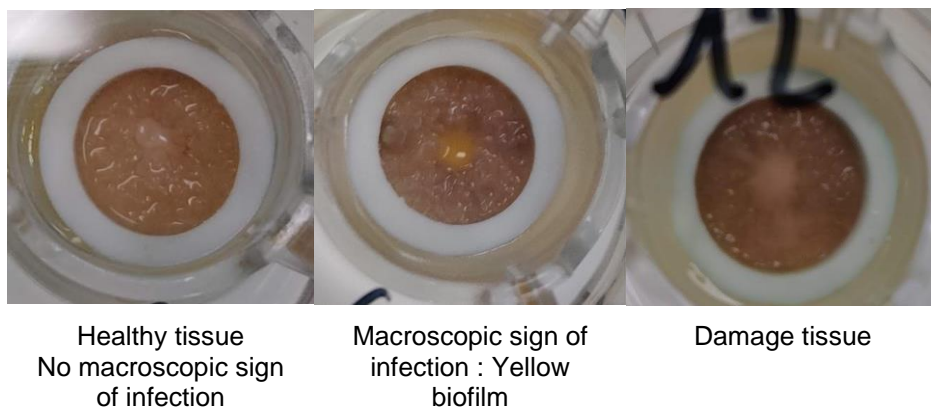
Damage tissue

Figure 3 : *Macroscopic images of representative appearance of skin samples*

Damage tissue can also be detected during the collect. Each sample was weighed before cutting to notice the modulation due to the infection and potentially damage skin. The epithelium should be attached to the dermis if the skin is healthy but can separate if the skin is seriously affected.

S.4.2 Sterility check

To detect the passage of bacteria through the skin, the 1ml medium contained in each well was put in an agar plate to confirm the sterility. As the culture is done without antibiotics, the risk of contamination becomes higher. We can detect any contamination both from the culture and the skin. 50µl of skin culture medium was spread on a BHI agar plate and incubated 24h at

37°C. The day after, the culture plate was analysed to determine the growth of colonies indicating the presence of cultured microorganisms in the sample. Contamination by known bacteria used for the infection (*S. aureus* and *P. aeruginosa*) can be easily dertermine by the characteristic shapes and colors of colonies. *S. aureus* presente Yellow colonies (**Figure 4A**) and *P. aeruginosa* green colonies (**Figure 4B**)

S. aureus streaked on agar plate   **P. aeruginosa streaked on agar plate**

Yellow, round, regular colonies   Green, round, spread colonies
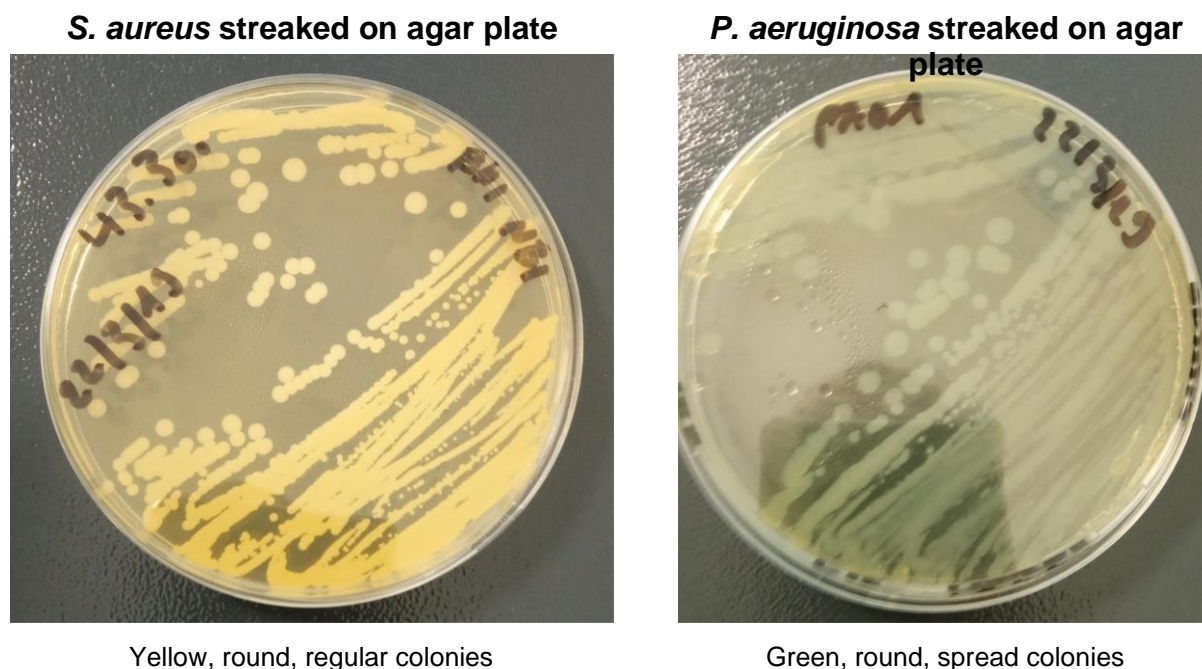
Figure 4 : Appearance of colonies obtain with S. aureus (Left) and P. aeruginosa

Additionally, contamination by unknown microorganisms can occur. The phenomenon is normal considering the natural presence of commensal flora on the skin. Some colonies can appear on the gelose. In the example presented in **Figure 5**, we can observe white and spread colonies that can correspond to Bacillus subtilis colony's shape. We can easily do the difference between the yellow colonies of *S. aureus* and other contamination.

In addition, contamination with unknown microorganisms can occur. This is normal given the natural presence of commensal flora on the skin. Consequently, some colonies may therefore appear on the agar. In the example presented in **Figure 5**, we can observe white and spread out colonies that may correspond to a *Bacillus subtilis* colony. We can easily distinguish between yellow colonies of *S. aureus* and other contaminants.

Samples with contamination

Samples without contamination

Samples with *S. aureus* infection (yellow colonies)
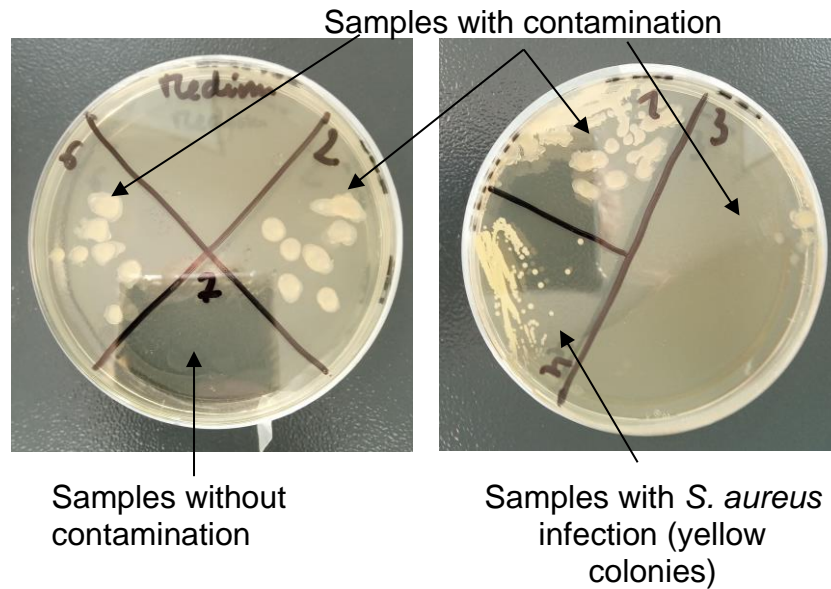
Figure 5 : *Example of sterility test of the liquid skin culture medium*

S4.3 Bacteria counting

To assess the number of viable bacteria in skin tissue, skin samples were cut in several pieces, homogenized in 1 ml PBS (to mix the tissue), sonicated 10 min at 40 kHz (Weff=20%) (to detach bacteria from the tissue) and serially diluted for colony counting. 50µl of diluted homogenate was plated on BHI agar plate or LB-Lennox agar plate depending on the bacteria strain. The plates were incubated overnight at 37°C. Finally, a number of colonies were counted to determine the colony forming unit (CFU)/ml in the homogenate and determine the CFU/g tissue.

S4.4 Histology

Solvents for histological analysis were purchased from Merck and used as received without further purification unless otherwise noted.

Half of the skin explants were washed and fixed immediately in 4% paraformaldehyde solution for 48h. In order to maintain the flat shape of the skin and to avoid folding, the piece was placed in an embedding cassette with foam. Sterile paper was added to avoid absorption of biofilm into the foam. The samples had to be held without being crushed, so depending on the thickness of the skin we adapted the amount of foam used. (**Figure 6**)
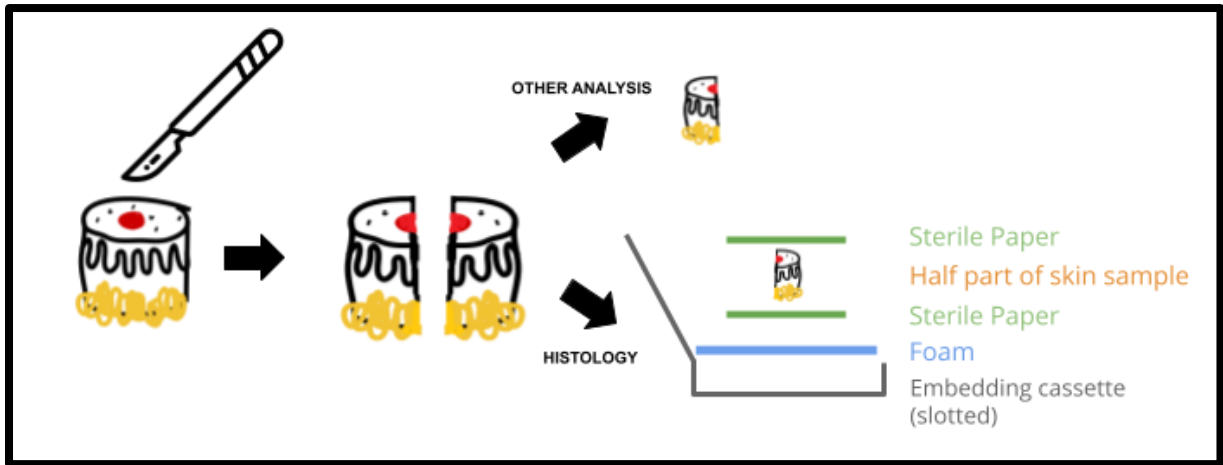
Figure 6 : *Sample preparation for fixative step*

After the fixation time, the samples were placed in a dehydration automate which consists in passing samples in several solvent baths to allow the good dehydration. Each step is listed in **Table 1** with the appropriate time incubation.

Table 1: Steps for automated tissue processing

Step	Solution	Temperature	Time
1	Fixation	RT	24 - 36h
2	70% Ethanol	RT	45 min
3	70% Ethanol	RT	45 min
4	90% Ethanol	RT	45 min
5	90% Ethanol	RT	45 min
6	100% Ethanol	RT	45 min
7	100% Ethanol	RT	45 min
8	100% Ethanol	RT	45 min
9	Xylene	RT	45 min
10	Xylene	RT	45 min

| 11 | Paraffin | 60°C | 45 min |
| 12 | Paraffin | 60°C | until embedding |

Then, samples are embedded in paraffin with the embedding station Leica EG1160. Next, each sample was sectioned with 5µm thickness using a rotary microtome Leica RM2145. Prior to staining, samples must be dewaxed and rehydrated to allow stain penetration. This consists in passing the samples in the same solvents as the dehydration step but in the reverse order. Each step is listed in **Table 2** with the appropriate time incubation.

Table 2: Steps for Deparaffinization and Rehydration sections

Step	Solution	Time
1	Xylene	5 min
2	Xylene	5 min
3	100% Ethanol	5 min
4	100% Ethanol	5 min
5	96% Ethanol	5 min
6	Eau osmosée	Until staining

Finally, tissue sections were stained with different methods described below.

S4.4.1   **Histological Staining (Hematoxylin & Eosin)**

For hematoxylin & eosin (H&E) staining of paraffin sections, the sections were first deparaffinized and rehydrated by transferring them through a series of two times xylene, two times 100% ethanol, one time 90% ethanol, and deionized water (5 minutes for each step). From the deionized water, the sections were then transferred to a solution of Gill's haematoxylin (Sigma-Aldrich) for 5 minutes before being blued in 2 baths of deionized water for 1 minute each. After the blueing the sections were submerged in eosin Y (Sigma-Aldrich) for 2min. Subsequently, the sections underwent a dehydration series before being mounted with non-aqueous mounting medium. Each step is listed in T**able XX** with the appropriate time incubation.

Table 3: Steps for H&E tissue staining

Step	Solution	Time
1	Hematoxylin Gill	5 min
2	osmose H2O	30 sec
3	osmose H2O	30 sec
4	Eosine Y	2 min
5	100% Ethanol	10 sec
6	100% Ethanol	6 min
7	Xylene	Until mounting
8	Mounting with ….	X

S4.4.2 GRAM staining

We use the kit Thermo Scientific™ Richard-Allan Scientific™ Gram Stain (Tissue) to identify gram-positive and gram-negative bacteria in tissue sections:

- Gram-positive organisms stain blue to blue-black
- Gram-negative organisms stain red
- Tartrazine provides a yellow background stain

Table 4: Steps for Gram tissue staining

N°	Steps	Time
1	Deparaffinize and hydrate sections to deionized water.	Follow steps in table XX
2	Stain sections in Crystal Violet Solution	1 minute
3	Rinse sections in running water	1 minute

4	Place sections in Gram's Iodine Solution	5 minutes
5	Rinse sections in running water	30 seconds
6	Differentiate sections in Decolorizing Solution.	1 minute
7	Rinse sections in running water	30 seconds
8	Stain sections in Safranin O Stain Solution	30 seconds
9	Rinse sections in running water	30 seconds
10	Stain sections in Tartrazine Stain Solution	20 seconds
11	Dehydrate sections in two changes of anhydrous alcohol; 10 dips each ensuring Tartrazine is retained on section.	30 seconds
12	Clear sections in three changes of clearing reagent for 1 minute each and mount	3 x 1 minute
13	Mounting	X

S4.5 Fluorescence

S4.5.1   Bacteria fixation

In order to set up the staining of bacteria in tissue section, a pre-test was needed on bacteria suspension. The preparation of bacteria smear was performed with the methanol fixation method described by Levin *et al*. with some modification. Briefly, 1ml of bacteria suspension was dropped into 10ml ice cold 80% methanol. The mix was let stand at room temperature for 1 hour before to add 800µl of 4% formaldéhyde (Alfa Aesar). The mix was let stand at room temperature for 5min and spin down at relatively low speed (4000 RPM in a Eppendorf centrifuge) for 10min. Bacteria were resuspend gently in 1ml of ice cold 80% methanol. The fixated bacteria were keep at 4°C maximum 1 week before microscopic analysis. 10µl of fixed bacteria were dropped on glass slide coated with 0.1% poly-L-lysine and let stand 2 minutes before washing in PBS bath. Then, slides are staining by following protocole of Immunofluorescence Anticorps anti-*S. aureus* on tissue section.

S.4.5.2   **Immunofluorescence Anticorps anti-*S. aureus* on tissue section**

After deparaffinization of the skin samples, the slides were incubated overnight at 4 °C with rabbit polyclonal anti-S. aureus antibodies (OriGene Technologies, USA) at a dilution of 1 : 100, rinsed with PBS (pH 7.4, 0.01 M) three times, followed by 1 h incubation with anti-rabbit IgG Alexa Fluor 488 conjugated antibody (ThermoScientific, France) at room temperature. After washing several times with PBS, the slides were covered with VECTASHIELD mounting medium containing DAPI (Vector Laboratories, France). Fluorescence images were captured using an ORCA-Flash4.0 LT PLUS fluorescent microscope camera (Hamamatsu, France) and analysed by NIS-ElementsMicroscope Imaging Software.

S.4.6 Gene expression: Pro-inflammatory reaction

S.4.6.1   **RNA isolation**

Skin pieces for RNA analysis were flash frozen in liquid nitrogen directly after the collection and stored at -80°C until further processing. For total RNA extraction, 130 mg were homogenized in 1 ml trizol with a tissue homogenizer (Precellys, France). RNA was then obtained by chloroform separation (200 µL) under manual shaking and centrifugation (13500 rpm, MiniSpin®, Eppendorf, France). The upper aqueous phase was recovered and RNA isolated and purified using the RNeasy Midi Kit (Quiagen, France). RNA was eluted in RNase-free H_2O (40 µL) and the concentration determined with NanoDrop One (Thermoscientific, France). RNA was stored at -80°C until cDNA conversion.

S.4.6.2   **Reverse transcription**

cDNA was synthesized from 200 ng RNA using iScript cDNA synthesis kit (Biorad, France) following the manufacturer's instructions and stored at -20°C until real-time PCR analysis.

S.4.6.3   **Real-time PCR (qPCR)**

Real-time PCR was performed using the SsoFast EvaGreen Supermix (Biorad, France) by following the manufacturer's instructions. The qPCR reactions were performed with 2µL of cDNA at a dilution of 1:10. The expression of the following pro-inflammatory cytokines was analysed: interleukin-6 (IL-6), interleukin-8 (IL-8), interferon- α1 (IFN-α1), interleukin-1 (IL-1α) and tumor necrosis factor- α (TNF-α). The primer sequences were designed according to ref.[12] and provided by Eurogentec (France) (see sequences in **Tables 5)**

Table 5 : Primer sequences

TARGET GENE	SEQUENCE 5' → 3'
18S	f: gaaactgcgaatggctcattaaa r: cacagttatccaagtaggagagg
IL-6	f: caatgaggagacttgcctgg r: gcacagctctggcttgttcc
IL-8	f: tctgcagctctgtgtgaagg r: aatttctgtgttggcgcagt
IL-1	f: aatgacgccctcaatcaaag r: tgggtatctcaggcatctcc
IFN-α1	f: acccacagcctggataacag r: ctctcctcctgcatcacaca
IFN-β	f: actgcctcaaggacaggatg r: agccaggaggttctcaacaa
TNFα	f: aacctcctctctgccatcaa r: ggaagacccctcccagatag

f: Forward primer; r: Reverse primer

The qPCR reaction was performed with a CFX96 Real-Time System C1000 Thermal Cycler (Biorad, France) with standard cycling conditions as following: 95 °C 3 min, (95 °C 10 s, 61 °C, 30 s, 95 °C 30 s) × 40 cycles, followed by a cooling phase. Relative quantification of mRNA for pro-inflammatory cytokines was calculated using the housekeeping genes 18S and normalized to the uninfected or untreated control (x-fold expression) depending on the conditions.

S.4.7 Morphological investigations using scanning electron microscopy

Skin samples were fixed in paraformaldehyde (4%) and glutaraldehyde (0.5%) in PBS (pH 7.4, 0.01 M) for 48 h at room temperature. The samples were then washed with Milli-Q water (3 × 5 min), followed by an incubation step in 1% osmium tetroxide for 1 h in the dark. The samples were dehydrated by a 15 min immersion in increasing ethanol concentration solutions consisting of 50%, 70%, 90% and 2 × 100%. Finally, the samples were air-dried with hexamethyldisilazane. Samples were then imaged under high vacuum at 1 kV by a secondary electron detector using a Zeiss Merlin Compact VP SEM (Zeiss, France).

S.4.8 Statistics.

For the ex vivo experiments, the data in the figures represent means ± SE of individual skins pooled from four to six independent experiments. For in vitro experiments, the data in the figures represent means ± SE of involving at least three technical replicates. Unless otherwise stated, statistical significance was calculated by standard two-sided t test (Prism v6.0f). P values of less than 0.05 were considered significant.

S.5 Synthesis

S.5.1 Materials

2-Dimethoxy-2-phenylacetophenone (DMPA), butyl methacrylate (BuMA), poly(ethylene glycol) methyl ether methacrylate (PEGMEMA, $Mn = 300$ g mol^{-1}), poly(ethylene glycol) dimethacrylate (PEGDMA, $Mn = 550$ g mol^{-1}), dioxane, cefepime, furfuryl methacrylate (FuMA), N-(5- fluoresceinyl) maleimide, trifluoroacetic acid (TFA), acetone, isopropanol (IPA), dichloromethane (DCM), diethyl ether (Et2O), hexane, acetonitrile (MeCN), dimethyl sulfoxide (DMSO), dimethylformamide (DMF), 1,2-ethanedithiol (EDT), and triisopropylsilane (TIS) were purchased from Sigma-Aldrich (France). Graphene oxide (GO) was purchased from Graphenea (Spain). PEGDMA and FuMA were purified by passing through activated aluminum oxide column prior to use. 1,8-bismaleimidodiethyleneglycol (BM(PEG)2) was obtained from Thermofisher. Solvents were procured from Merck and used as received. All gelation reactions were performed using a UV Lamp (365 nm, 100 W), and

samples were exposed from a distance of 10 cm. Kapton® HN polyimide foils (125 µm thick) were obtained from DuPontTM.

S.5.2 Reduced graphene oxide (rGO) loaded BuMA cryogels (rGO-CG)

GO aqueous suspension (150 mg, 3 mg mL−1) was prepared by sonication and hydrazine hydrate (50 µL, 1.03 mmol) was added to this suspension. The mixture was heated in an oil bath at 100 °C for 24 h over which the reduced GO gradually precipitated out the solution. The product was isolated by filtration over a PVDF membrane with a 0.45 µm pore size, washed copiously with water (5 × 20 mL) and methanol (5 × 20 mL), and dried in an oven. A mixture of BuMA (20 mol%), PEGMeMA (80 mol%), PEGDMA (80 mol%), DMPA (5 mol%), and rGO (0.8 wt%) was prepared in 1,4-dioxane (0.3 M) and sonicated to obtain maximal homogeneity before gelation. The mixture was poured into a glass vial and purged with nitrogen to remove dissolved oxygen. Cryogel formation was undertaken at −13 °C using UV irradiation exposure (100 W, 10 cm distance to source). After 1 h of UV-irradiation, cryogels were thawed at room temperature and washed with 1,4-dioxane, followed by water to remove unreacted monomers. The cryogels were dried in vacuo to yield black sponge like materials. Identical procedures were followed for obtaining cryogels without rGO and for cryogels with different amounts of butyl methacrylate monomer. Cryogels without rGO were obtained as white spongy materials.

S.5.3 FuMA Cryogel

S.5.3.1   Fabrication of Furfuryl-Containing CGs

For the synthesis of 10% FuMA-containing CGs (CG-10), a mixture of PEGMEMA (61.9 mg, 0.206 mmol), FuMA (8.6 mg, 0.052 mmol), PEGDMA (141.7 mg, 0.258 mmol), and DMPA (3.3 mg, 0.01296 mmol) was added to 1,4-dioxane (1.5 mL) in a small vial. The mixture was sonicated for 45 s to ensure mixing. Then, the vial was cooled to −13 °C using a cryostat. The cooled reaction mixture was exposed to UV irradiation for 60 min. The vial was removed from the cryostat and warmed naturally to room temperature. The obtained CGs were rinsed with 1,4-dioxane (three times) and water to remove all unreacted materials. The other CGs (CG-20, CG-30, and CG-40) were prepared in the same manner by only changing the ratio of

FuMA/PEGMEMA. The CGs were vacuum dried to yield white cylindrical CGs of 1.5 cm in diameter and 4–5 mm in thickness. For fabrication of the sample of rGO-incorporated furfuryl-containing CG, the exact same procedure was followed in the presence of 2 wt % rGO in the polymerization mixture.

S.5.4 Synthesis of Maleimide-Modified Peptides

S.5.4.1   Synthesis of RWRWRWC–NH₂

The peptide RWRWRWC–NH$_2$ was synthesized manually by means of the Fmoc/*t*Bu protocol on an Fmoc-Rink amide resin (0.74 mmol/g) yielding C-terminal amide after cleavage. Solid-supported reactions were undertaken in plastic syringes (10 mL) with a porous polypropylene disc filter. The resin was swollen for 1 h in DMF, and the Fmoc protecting group was removed by adding 20% solution of piperidine in DMF (3 mL, 2×10 min). After removal of the solution, the resin was washed with DMF (3×2 min, 3 mL), IPA (3×2 min, 3 mL), and DCM (3×2 min, 3 mL), and the successful deprotection was confirmed by the Keiser test. Coupling of each amino acid (4 equiv) was achieved by addition of 2-(1*H*-benzotriazole-1-yl)-1,1,3,3-tetramethylaminium tetrafluoroborate (TBTU, 4 equiv), 1-hydroxybenzotriazole hydrate (HOBt, 4 equiv), and *N*,*N*-diisopropylethylamine (DiPEA, 8 equiv) in DMF (3 mL) to the resin. The suspension was shaken at room temperature for 90 min. Solvents and reagents were removed by filtration, and the resin was washed with DMF, IPA, and DCM. The successful coupling was confirmed by the Keiser test (in case of incompletion of the reaction, the coupling was repeated). The Fmoc protecting group was cleaved in order to enable attachment of the next amino acid. Subsequently, the cycle of washing, deprotection was repeated. After the sequence was finished, the Fmoc protecting group was removed, and resin was washed and dried *in vacuo*. Amino acids used during the synthesis were side chain protected with the BOC group (for the Trp), Pbf (in the case of Arg), and Trt (for Cys). The protecting groups were removed during cleavage of the peptide from the resin with a treatment of TFA/TIS/EDT (95:2,5:2,5 v/v/v, 2 mL $\times$ 3 h). The peptide was precipitated in a mixture of cold Et$_2$O/hexane (20 mL, 1:1 v/v). The supernatant was removed, and the peptide was washed several times with Et$_2$O/hexane to be further dispersed in water with the addition of acetonitrile, lyophilized, and purified by a semi-preparative HPLC system with a photo diode arrays (PDA) detector using NUCLEODUR 100–5 C18ec reversed phase column (125×10 mm) using buffer A (H$_2$O/TFA 100:0.1 v/v) and buffer B (MeCN/TFA 100:0.1 v/v) as the mobile phase. The flow rate was set

up at 5 mL/min. Electron spray ionization mass spectra were obtained on an Esquire 6000 mass spectrometer (Bruker). LC–MS analysis confirmed peptide formation ($m/z = 525.0$).

S.5.4.2 Functionalization of RWRWRWC–NH₂ Peptide with Maleimide Function

To a small vial containing 100 μL of DMF, BM(PEG)$_2$ (0.81 mg, 2.62 μmol) and peptide RWRWRWC–NH$_2$ (1 mg, 0.871 μmol) are mixed together. The reaction mixture was stirred overnight at 24 °C. The next day, the solution was precipitated in cold ether and centrifuged at 13,000 rpm for 5 min to obtain the desired peptide–maleimide (73%). LCMS analysis revealed the successful conjugation ($m/z = 727.0$) ([Figure S6](#)).

S.5.5 Conjugation of Furan–CCG with Maleimide Ligands

S.5.5.1 Conjugation of *N*-(5-Fluoresceinyl) Maleimide

A solution of *N*-(5-fluoresceinyl) maleimide in PBS (30 μg mL^{-1}) was loaded into the CG (30 mg) and allowed to react for 24 h at room temperature. Any unbound dye was washed with PBS. Solution of PBS was analyzed by fluorescence to ensure total removal of the dye.

S.5.5.2 Conjugation of Maleimide-Functionalized Antibacterial Peptides

Maleimide-modified peptide (1 μL, 500 μg mL^{-1} in water) was loaded into CG-40 (30 mg) for 24 h at room temperature. Any unbound peptide was washed with water. Solution of water was analyzed by UV to ensure total removal of free peptide.

S.6 Swelling, loading and release of Cryogels

S6.1 Equilibrium swelling of cryogels

Swelling experiments were undertaken with a circular piece of dried cryogel immersed in distilled/deionized water at room temperature. The increase in mass of cryogel sample was recorded at predetermined intervals after removing the sample from water. . Prior to weighing, any surface adhered water was removed with a tissue paper. The percentage of water uptake was calculated using the equation:

percentage of swelling $(\%) = (W_{wet} - W_{dry})/W_{dry} \times 100$

where W_{wet} and W_{dry} denote the hydrogels weights in their wet and dry state, respectively.

S6.2 Quantification of Loading and Release

S6.2.1   High-Performance Liquid Chromatography (HPLC)

The concentration of peptide loaded onto CGs was determined by HPLC (Shimadzu, Tokyo, Japan) equipped with a 5 μm C4 QS Uptisphere® 300 Å, 250 mm × 4.6 mm column (Interchim, Montluçon, France) heated to 40 °C. The mobile phase consisted of a mixture of eluent A (0.1% trifluoroacetic acid in water) and eluent B (0.1% trifluoroacetic acid in acetonitrile) at a flow rate of 1 mL/min. The samples were injected at a volume of 40 μL and the detection wavelength was 227 nm. First, a calibration curve of a series of peptide solutions of different concentrations was generated. The concentration of the peptide remaining in the supernatant solution used for loading was measured, allowing the determination of the peptide concentration loaded onto CG. The concentration of aliquots removed at different time intervals during the photothermal and passive releases were measured using the same parameters as above to determine the amount and % of peptide released.

S6.2.2 Fluorescent Plate Reader for Quantification of Dye Loading and Release

The concentration of N-(5-fluoresceinyl) maleimide loaded onto CG (30 mg) was determined by a Cytation™ 5 Cell Imaging Multi-Mode Reader from Biotek plate reader. A calibration curve was obtained using a series of dye solutions at different concentrations. The concentrations of dye remaining in the supernatant used for loading and wash solutions were measured, allowing the determination of the dye concentration loaded on CG. The concentrations of aliquots removed at different time intervals during the photothermal and passive releases were measured using the same parameters as above to determine the amount and % of dye released.

S.6.3 Loading of BuMA rGO-CG with cefepime

rGO-GC cryogel (50 mg) was loaded with cefepime by immersing the cryogel for 24 h in an aqueous solution of the antibiotic (100 µg mL−1) at 37 °C followed by rinsing with water (three times) and immersion for 24 h in water to wash off loosely bound and/or surface absorbed cefepime. The loading efficiency was estimated from HPLC analysis of the solution after loading. The difference in the amount of cefepime present before and after gel immersion was linked to the loading efficiency. High performance liquid chromatography (HPLC) analysis was carried out on a Shimadzu LC2010-HT (Shimadzu, Tokyo, Japan) using a 5 µm C4 QS Uptisphere® 300 Å, 250 × 4.6 mm column (Interchim, Montluçon, France) heated to 40 °C. The mobile phase consists of a mixture of eluent A (trifluoroacetic acid 0.05% in H2O) and eluent B (trifluoroacetic acid 0.045% in CH3CN) at a flow rate of 1 mL min−1. The isocratic flow (eluent A) was for 5 min, the linear gradient was 0 to 80% of eluent B in 10 min and further 80% of eluent B for 5 min. The detection was performed at 254 nm. Solutions were analyzed directly without dilution by injecting of 40 µL into the HPLC column.

S6.4 Release of cefepime from BuMA rGO-CG

Release experiments were performed into 1 mL PBS buffer. The rGO-cryogel was irradiated with a continuous mode laser (Gbox model, Fournier Medical Solution) with an output light at 980 nm (1 W cm−2) for various time intervals (1–60 min). Thermal images were captured by an Infrared Camera (Thermovision A40) and treated using ThermaCam Researcher Pro 2.9 software. The amount of antibiotic released was evaluated by HPLC.

S.6.5 Photothermal Release og FuMA cryogel

S6.5.1   Preparation of Photothermal Heating Kapton/rGO Substrates

Kapton foils (10 × 10 mm^2) were sequentially cleaned in an ultrasonic water bath, first with acetone (30 min), followed with isopropanol (10 min) and then dried under a gentle flow of nitrogen. Thereafter, the Kapton foils were coated with rGO by drop-casting (100 µL) three times. Samples were left for drying at room temperature for several hours before use.

S6.5.2   Photothermal Release Conditions

Release experiments were undertaken in PBS buffer (1 mL). The CG was irradiated with a continuous mode laser (Gbox model, Fournier Medical solution) with an output light at 980 nm (1 W cm^{-2}) for various time intervals (1–60 min). An IR camera (Thermovision A40) was used to capture the thermal images and processed using ThermaCam Researcher Pro 2.9 software. The amount of antibiotic released was determined by HPLC. The quantity of *N*-(5-fluoresceinyl) maleimide released was evaluated by fluorescence spectroscopy.

S.7 Cytotoxicity assay

HeLa cells, derived from cervical carcinoma from a 31 years old female [ATCC® CCL-2TM, ECACC, Sigma Aldrich, Saint-Quentin Fallavier, France], were cultured and maintained in Dulbecco's Modified Eagle's medium (DMEM, Gibco®) supplemented with 10% fetal bovine serum (FBS, Gibco®) and 1% penicillin–streptomycin (Gibco®) in a humidified incubator at 37 °C and 5% CO2. Cells were seeded at a density of 105 cells per well in a 24-well plate and grown for 24 h before assay. The culture medium was replaced with a fresh medium that contains the cryogels (10 mg). After 24 h, the old medium was removed and cells were washed with PBS. The cell viability was evaluated using resazurin cell viability method. Briefly, 1 mL of the resazurin solution (11 μg mL−1) in complete medium were added to each well and the plate was incubated for 4 h in the humidified incubator. The fluorescence emission of each well was measured at 593 nm (20 nm bandwidth) with an excitation at 554 nm (18 nm bandwidth) using a CytationTM 5 Cell Imaging Multi-Mode Reader (BioTek Instruments SAS, France). Each condition was replicated three times and the mean fluorescence value of non-exposed cells was taken as 100% cellular viability.

S.8 Bacteria assay

S.8.1 Bacteria

E. coli DSM 30083 and *S. aureus* ATCC 43300 were used in this work. Three to five morphologically similar colonies from fresh agar plates were transferred into a sterile tube containing sterile broth. The bacteria were incubated overnight at 37 °C. The next day, OD$_{600}$ of the overnight culture was adjusted to an OD$_{600}$ of 0.1 and was grown to a mid-log phase. After

preparing the inoculum at a concentration of 5×10^5 CFU/mL, the bacterial suspension was used within 30 min to avoid greater changes in cell concentrations.

S.8.2 Determination of Minimal Inhibitory Concentration

The minimal inhibitory concentration (MIC) values against *E. coli* DSM 30083 and *S. aureus* ATCC 43300 were assessed. MIC values were determined in a microdilution assay. Briefly, the peptide and the peptide conjugate were dissolved in DMSO at a concentration of 10 mg/mL. Serial dilutions were prepared in Mueller–Hinton broth, inoculated with 5×10^5 CFU/mL and incubated for 16 h at 37 °C. Inoculated medium without peptide or conjugate served as a growth control, and uninoculated medium served as sterile control. The lowest concentration that prevented visible growth was reported as MIC value.

S.8.3 Determination of Bacterial Cell Viability

The antibacterial activity of released antibacterial peptide was evaluated using *E. coli* and *S. aureus* strains by cell growth measurements based on the optical density at 600 nm and by plating methods to quantify the viable cell number. Briefly, the bacterial cells were inoculated in LB broth (*E. coli*) and Mueller–Hinton broth (*S. aureus*) in the presence of different concentrations of released peptide at 37 °C for 6 h and the growth was monitored by measuring the absorbance at 600 nm. A 10-fold serial dilution of the bacterial solutions in medium was spotted in 10 μL aliquots on LB-agar (*E. coli*) and Mueller–Hinton agar (*S. aureus*). Colony counting after overnight incubation at 37 °C allowed reading out the initial and final concentrations of viable bacteria in cfu mL^{-1}. All experiments were performed in triplicate.

S.8.4 Selective Pathogen Ablation

The selectivity of maleimide-conjugated peptide was evaluated using *S. aureus* 43300 and *E. coli* DSM 30083 strains by SEM imaging, cell growth measurements based on the optical density at 600 nm, and by plating methods to quantify the viable cell number. Briefly, the bacterial cells (5×10^5 CFU mL^{-1}) were inoculated in Mueller–Hinton broth in the presence of the maleimide-conjugated peptide (32 μg mL^{-1}) at 37 °C for 20 h and the growth was monitored by measuring the absorbance at 600 nm. A 10-fold serial dilution of the bacterial solutions in

medium was spotted in 10 μL aliquots on selective agar plates (Chapman and Mac Conkey). Cfu mL^{-1} were determined after overnight incubation at 37 °C.